EXPERIMENTAL AND ANALYTICAL ASSESSMENT OF INTERNAL AND PANEL-TO-

FLOOR CONNECTORS FOR CROSS LAMINATED TIMBER (CLT) BALLOON-STYLE

CONSTRUCTION

A Thesis

by

BENJAMIN N. HAYES

Submitted to the Graduate and Professional School of
Texas A&M University
in partial fulfillment of the requirements for the degree of

MASTER OF SCIENCE

Chair of Committee,	Maria Koliou
Committee Members,	Matthew Yarnold
	Amir Behzadan
Head of Department,	Robin Autenrieth

December 2021

Major Subject: Civil Engineering

ABSTRACT

Cross-Laminated Timber (CLT) is an innovative building material that has become increasingly popular in mid-rise building construction for its quick assembly capability, its environmental friendliness, and its beneficial strength-to-weight ratio. Currently, CLT balloon-style construction is not allowed in areas of high seismicity. The goal of this research was to study the behavior of CLT balloon-style construction connections, characterize their behavior through fitting the cyclic data to hysteretic models, doing further investigation with finite element analysis, and to understand the biaxial response of CLT shear walls. Ten different connection configurations were tested in this study – six panel-to-panel connections and four wall-to-floor connections. The experimental data was used to calibrate two different connector hysteretic models. In-depth finite element analysis was completed on these configurations and the response was compared to the experimental data. Lastly, a full-scale CLT shear wall test was done with biaxial loading protocol to characterize connection and system response to loading in two directions.

The experimental test program provided insight into the benefits of using angled fasteners, namely that they provided good stiffness and good ductility, and an initial look at the behavior of wall-to-floor configurations. The numerical modeling that was completed demonstrated that the Pinching4 hysteretic model is preferable to the CUREE-SAWS model for the connections that were tested. The finite element models that were developed were validated and their assumptions can be used for parameter studies and further investigation into CLT behavior. Finally, the biaxial wall test provided good insight into the behavior of CLT shear walls, demonstrating that sliding-rocking behavior is beneficial to overall system behavior even when loaded in two directions.

DEDICATION

I dedicate this thesis first to my Lord and Savior, Jesus Christ. He created me in His image, and all my work is done with the goal of honoring God and bringing glory to His name. I strive to fulfill the command given in Colossians 3:23 (NKJV) – "And whatever you do, do it heartily, as to the Lord and not to men."

I would also like to dedicate my work to my loving wife, Taylor. She has worked many long, hard years putting me through school and she deserves the world. None of this is possible without her unending support.

Lastly, I would like to dedicate this this work to my parents who pushed me to attend graduate school – and specifically at Texas A&M. I am grateful for their support and encouragement.

ACKNOWLEDGEMENTS

CONTRIBUTORS AND FUNDING SOURCES

TABLE OF CONTENTS

LIST OF FIGURES

xv

LIST OF TABLES

1. INTRODUCTION

Throughout most of the 20th century, the most popular and widely-used building material was concrete because it was economical, much was known about its properties, and it could be cast into virtually any form (Brandner, Flatscher et al. 2016). Timber was only used in lightweight construction, for example, residential building construction using dimension lumber for framing. The idea for Cross-Laminated Timber (CLT) is similar to plywood or even to three-layer solid wood board, but leverages the difference in the wood's mechanical properties parallel to the grain and perpendicular to the grain by alternating the orientation of the layers (Brandner, Flatscher et al. 2016). Cross-laminated timber, also referred to as X-lam, was originally used as the web of a solid-web girder for a bridge deck in 1989, and began to be more widely used for wall panels and floor systems in the 1990s as the saw mill industry was looking to find a higher value for side boards (Brandner, Flatscher et al. 2016).

CLT is an engineered wood product that is becoming increasingly popular in building construction nowadays. It consists of dimension lumber glue-laminated together with alternating layers being oriented at 90 degrees to the previous layer (see Figure 1.1). To be qualified as cross-laminated timber, the panel must consist of at least three glued boards, with consecutive layers oriented opposite the previous layer; but, CLT is not limited to only three boards and can often consist of up to seven or nine boards (Karacabeyli and Douglas 2013). Additionally, when a panel has at least five layers, the outermost layers can be placed in the same direction giving a double layer and taking advantage of the strength of wood in tension/compression parallel to the grain. The CLT panels can have dimensions varying between 4 inches thick and 20 inches thick which is the maximum allowable thickness per the National Design Specifications (NDS) for Wood Construction (2018). CLT is a versatile building material because it can be manufactured

and prefabricated to fit nearly any dimension, with the larger dimension often being limited to the width of the press that is used (Pei, Lindt et al. 2016). It is manufactured by selecting the lumber to be used, sanding the lumber so it is flat on top and bottom, cutting all the members for all layers to size, and applying adhesive between individual boards and between the layers. The panel is then pressed while side pressure is applied, then the panel is taken to be machined flat and kiln dried (Karacabeyli and Douglas 2013). The advantage of cross-laminated timber is to allow for greater dimensional stability which can lead to longer spans for floor slabs, greater dimensions for wall panels, and even allows for the possibility of balloon-framed construction (Karacabeyli and Douglas 2013).

Figure 1.1. Photo of CLT Cross-Section

The advantage of using CLT for residential multi-story building construction is that it lends itself to quick erection even in the absence of highly skilled labor. CLT also provides significantly greater load carrying capacity when compared to typical sawn lumber construction. Additionally, it provides good thermal insulation and relatively good resistance to fire (Popovski and Karacabeyli 2012). It offers a solution to fire resistance as it self-protects by developing a charring layer on the surface when exposed to the fire (Aghayere and Vigil 2017). It has also been found that CLT mid-rise buildings tend to cost less to construct when compared to concrete

and/or steel midrise buildings, along with the fact that it is a renewable material – leaving less of an environmental footprint (Aghayere and Vigil 2017).

Along with many of the benefits that CLT can provide for residential and mid-rise commercial construction is the fact that it is often more of an environmentally friendly building material. Using a life-cycle assessment, CLT and glulam products used in building construction leave less of an environmental footprint than typical building materials (Robertson, Lam et al. 2012). A study conducted in Canada (Canadian Wood Council and the University of British Columbia) studied the life cycle assessment of a mid-rise office building in order to determine what building material was more environmentally friendly. The materials included in this study were CLT/glulam products, reinforced concrete and structural steel. Because the construction and operation of buildings is responsible for over 40% of global energy consumption, it is imperative that countries use the building material that is the most energy efficient while requiring the least energy to be constructed (Robertson, Lam et al. 2012). The study considered three qualitative and three quantitative measures to evaluate the findings and identify which of the studied building materials leaves the least environmental impact. The three quantitative measures considered were material extraction, material manufacturing/processing, and intermediary material transportation effects. The three qualitative measures, which were determined based on case studies and literature reviews, were on-site building construction, on-site transportation as well end-of-life demolition and disposal of the material. CLT/glulam performed better than traditional building materials (concrete and steel) in every category but one, processing and manufacturing the CLT panels and glulam beams, which took nearly 80% more energy than the production of traditional cast-in-place concrete (Robertson, Lam et al. 2012). The study concluded that CLT mid-rise buildings generally use less energy to build, less

3

energy to take down at end-of-life, and generally leave less of a negative impact on the environment (Robertson, Lam et al. 2012).

CLT is beginning to be used more and more in the United States, but it has already been used for midrise buildings throughout Europe and Canada over the past 20 years. Due to more restrictive and stringent building codes in the United States, cross laminated timber is just now making its way into the midrise building construction in the U.S. There are many midrise CLT buildings in Europe, Canada, and Australia that have already been constructed. The tallest CLT/mass timber hybrid building to date was finished in Vancouver, British Columbia in 2017 at the University of British Columbia – Brock Commons Tallwood House. It is an 18 story CLT hybrid building that was constructed out of 17 stories of CLT wood panel floors and walls supported by glulam columns, all on top of a reinforced concrete podium first floor. This project was finished only 70 days after the CLT panels and glulam columns arrived on-site. The tallest contemporary CLT building to date, the Forte building, in Melbourne, Australia, is a 10-story apartment complex and was finished in 2012.

While many CLT low-rise and mid-rise building have already been constructed outside the United States, it has not become as popular in the U.S. However, with the economic, environmental, and constructability benefits inherent in CLT building designs, it is inevitable that more cross-laminated timber buildings will begin to appear in the United States.

2. LITERATURE REVIEW

2.1. Balloon-Frame Construction

Balloon frame construction has been around since the middle of the 1800's and was originally named as such because people remarked that building residential houses in such a way made them look like they would easily blow away (Cavanagh 1997). Balloon frame construction is usually contrasted with platform construction, as they are the two predominate methods for constructing buildings out of timber with sizes ranging from residential housing to midrise commercial buildings. The difference between platform construction and balloon frame construction is how each floor of the building is constructed, which ultimately changes the load path for gravity loads and for lateral loads.

Platform construction involves framing the walls for each floor of the building separately and building each floor on top of the next, using the previous floor as a "platform" for the subsequent floor. On the other hand, balloon frame construction involves framing the walls for each floor as one continuous wall for the entire height of the building and framing the floors into the wall at each prescribed height using angle brackets, the use of a wooden ledger to provide continuous bearing, or other connection method. When framing with dimension lumber and/or structural timber, platform-framed construction is much more economical and used more widely, but balloon frame construction lends itself well to use with CLT (Aghayere and Vigil 2017). Balloon framing with CLT can be a very efficient construction process because CLT wall panels can be prefabricated to nearly any size, only limited by press and shipping dimensions. Balloon framing with CLT is faster and more cost-effective than platform framing with CLT. However, balloon framing limits the total height of building as CLT panels are limited in length; because of this, balloon construction is often used in low-rise, commercial or industrial buildings

5

(Karacabeyli and Douglas 2013). Balloon frame construction is less popular with materials other than CLT because it complicates the design of connections and determination of the load path. However, balloon framing can be beneficial to use with CLT because of the constructability benefits as discussed previously.

The use of CLT shear walls in platform construction has been recognized in Canada and the United States alike, but its application in balloon-style construction has not received enough attention (Daneshvar, Niederwestberg et al. 2019). Researchers at the University of Alberta have begun looking at base shear, base hold-down, and panel-to-panel shear connections for CLT shear walls in balloon construction, but more research is needed in order for balloon style construction to be a viable building method in high seismic areas (Daneshvar, Niederwestberg et al. 2019). For balloon framed CLT construction to be further applicable in the United States, there is a need to understand the behavior of this type of construction as well as its performance under seismic loads. Experimental and analytical studies focusing on component behavior (such as wall panels, roofs, and connections) as well as building performance are needed.

2.2. Experimental Studies on CLT Structures

Research on CLT over the past 20 years began in Europe under Dujic et al., beginning in 2004, at the University of Ljubljana in Slovenia as researchers worked to determine what boundary conditions would be applicable for CLT walls in design for earthquakes (Dujic, Aicher et al. 2006). Lateral seismic design research was advanced under the SOFIE project in Italy beginning in 2006 as the project worked to accomplish connection tests, shear wall tests, and even full-scale shake table tests being the culmination of the project (Ceccotti, Sandhaas et al. 2013). CLT research made its way to Canada in 2010 where FPInnovations funded projects

6

investigated CLT shear walls (Popovski, Gavric et al. 2014) as well as wall connectors and brackets for application in seismically active regions in Canada (Joyce, Ballerini et al. 2011).

A significant portion of the existing research has focused on evaluating the performance of connections in CLT structures. Connections are main components with inelastic response in wood construction, while it is a more systematic way of minimizing uncertainties in computational modeling given that the feasibility of performing many full-scale shake table tests is very low. Additionally, the conducted full-scale shake table tests did not produce a complete collapse of a tall CLT building which led researchers to find that significant uplift is produced during seismic events. A performance-based design should be used in seismic design of CLT buildings and the connections should be sufficiently ductile in order to ensure accelerations at higher levels of the building can be limited (Pei, Lindt et al. 2016).

2.3.   Introduction to Connection Testing

Designing Cross-laminated timber wall and floor panels for gravity loads is relatively straightforward because for residential and even commercial building construction there are often plenty of wall lines in the floor plan and CLT panels have a high strength-to-weight ratio. The difficulty in using CLT panels for walls and floors comes when designing for lateral loads, and more specifically, seismic loads. Compared to light-frame wood buildings, CLT buildings are much stiffer, and therefore, are unable to achieve the same levels of lateral deflection that lead to effective energy dissipation. Because CLT panels are so stiff and are able to carry seismic loads with a relatively low level of lateral deflection, even in midrise building construction, the engineer must pay special attention to the design of the connections (Pei, Lindt et al. 2016). When a CLT building design lacks the proper amount of ductility in its connections, and they fail in a brittle manner, it leads to overall higher acceleration amplifications under seismic conditions

– and thus, excessive global overturning demands (Pei, Lindt et al. 2016). All relevant research on CLT panel behavior under seismic loads concludes that the panels behave rigidly and that the critical path to an effective design begins and ends with efficiently ductile connections (Dujic, Aicher et al. 2006, Joyce, Ballerini et al. 2011, Popovski and Karacabeyli 2012, Ceccotti, Sandhaas et al. 2013, Rinaldin, Amadio et al. 2013, Popovski, Gavric et al. 2014, Flatscher and Schickhofer 2015, Izzi, Polastri et al. 2018).

With research moving toward connection testing, panel-to-panel connectors, wall-to-wall, and floor-to-wall connections needed to be tested, modeled, and evaluated. Some of the first research on CLT connections came out of the SOFIE project, beginning in 2005. This first study, done by Gavric, Fragiamoco, and Ceccotti, recognized the importance of understanding the cyclic behavior of CLT connections (Gavric, Fragiacomo et al. 2012). The test program undertook testing of wall-to-wall parallel connections, wall-to-wall perpendicular connections, wall-to-floor connections, and floor-to-floor connections. The results of the test found that step joint connections exhibited a higher stiffness than spline LVL connections, but that spline joints could resist higher forces with higher displacements (Gavric, Fragiacomo et al. 2012). Additionally, the withdrawal tests showed that the critical failure mechanism for screws was head penetration rather than withdrawal of the full screw from the panel (Gavric, Fragiacomo et al. 2012).

While testing connections and different connection configurations, it became apparent there was a need to calibrate a hysteresis model for the cyclic and monotonic loading of CLT connections. Researchers at the University of British Columbia began comparing the Pinching4 model (Figure 2.2) with the CUREE SAWS model (Figure 2.1). The SAWS model is a combination of an exponential functions and a descent linear line, while the Pinching4 model is a

8

piecewise function made up of parameters (that can be seen in Figure 2.2) that describe the

load/displacement curve. CLT wall panels are relatively stiff and, therefore, their performance

under seismic loading conditions is controlled by their connections. This study looked at various

connectors and two different hysteresis models (SAWS and Pinching4 models). The three

controlling factors that were investigated for each connector were pinching behavior, strength,

and stiffness degradation. The study found that the Pinching4 model showed more representative

performance because it was easier at fitting the actual curve, while it accounts for rapid

degradation of reloading stiffness and unloading stiffness more accurately (Shen, Schneider et al.

2013).
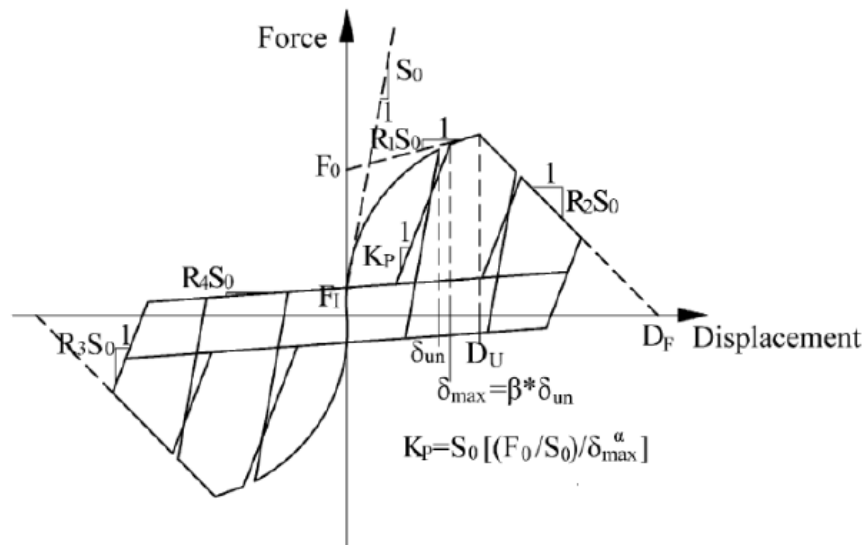
$F_0 = intercept\ of\ strength\ for\ asymptotic\ line\ to\ envelope\ curve$
$D_F = Failure\ Displacement$
$D_U = Displacement\ at\ Peak\ Load$
$S_0 = initial\ stiffness\ of\ hysteretic\ curve$
$R_1 = stiffness\ ratio\ of\ asymptotic\ line\ to\ envelope\ curve$
$R_2 = stiffness\ ratio\ of\ the\ descending\ segment\ of\ envelope\ curve$
$R_3 = stiffness\ ratio\ of\ unloading\ segment\ of\ envelope\ curve$
$R_4 = stiffness\ ratio\ of\ pinching\ part\ of\ hysteretic\ curve$
$\alpha, \beta\ control\ stiffness\ degredation\ and\ energy\ degradation$

Figure 2.1: SAWS Model (Shen, Schneider et al. 2013)

9
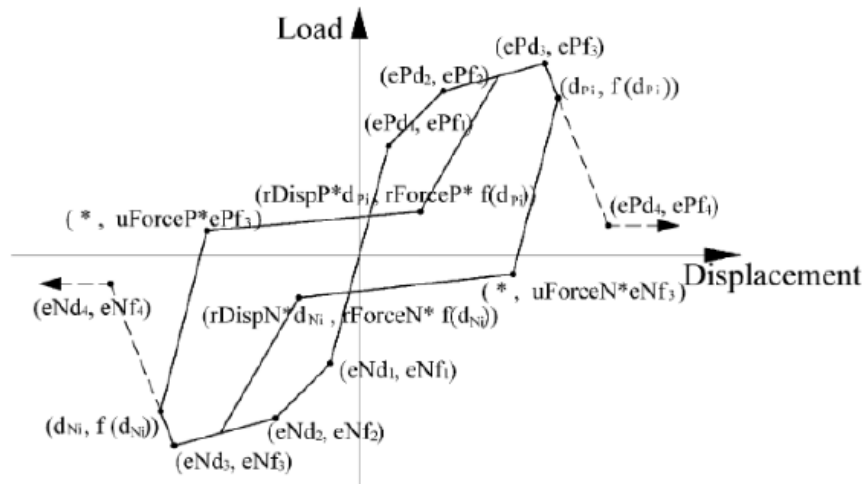
$ePf = defining\ force\ points\ on\ postive\ response\ envelope$
$ePd = defining\ deformation\ points\ on\ postive\ response\ envelope$
$eNf = defining\ force\ points\ on\ negative\ response\ envelope$
$eNd = defining\ deformation\ points\ on\ negative\ response\ envelope$
$rDispP = ratio\ of\ deformation\ at\ which\ reloadading\ occurs\ to\ the\ historic\ deformation\ demand$
$fForceP = ratio\ of\ the\ force\ when\ reloading\ begins\ to\ force\ corresponding\ to\ \max deformation$
$uForceP = ratio\ of\ strength\ developed\ upon\ unloading\ from\ negative\ load\ to\ \max monotonic\ load$
$rDispN = ratio\ of\ deformation\ at\ which\ reloading\ occurs\ to\ \min deformation$
$fForceN = ratrio\ of\ force\ where\ reloading\ begins\ to\ force\ at\ \min deformation$
$uForceN = ratior\ of\ strength\ developed\ upon\ unloading\ from\ negative\ load\ to\ \min monotonic\ load$
$gammaK = control\ cyclic\ degration\ model\ for\ unloading\ stiffness\ degradation$
$gammaD = control\ cyclic\ degradation\ model\ for\ reloading\ stiffness\ degradation$
$gammaF = control\ cyclic\ degradation\ model\ for\ strength\ degradation$
$gammaE = control\ maximum\ energy\ dissipation\ under\ cyclic\ loading$

Figure 2.2: Pinching4 Model (Shen, Schneider et al. 2013)

Other research focusing on hysteretic models was done in Italy by researchers at the

University of Sassari and the University of Trieste. This study presented a model to analyze CLT

buildings subjected to earthquake loads. Model was for single story wall/floor connections.

Strength and stiffness parameters for different connectors were found by testing the connectors

and comparting them to the numerical hysteresis model and repeating to minimize the total

energy difference between experimental and numerical. The hysteresis model was validated by

comparing calculations to a CLT building tested in Trento by CNR-IVALSA (Rinaldin, Amadio

et al. 2013).

10

2.4. Floor-to-Wall Connections Tests

There two main connection methods used when detailing a floor-to-wall connection in balloon frame construction. The simplest attachment method involves the use of a Structural Composite Lumber (SCL) continuous ledger to provide bearing support for the CLT floor panels. Self-tapping screws (STS) can be used to attach the SCL to the continuous CLT wall and to attached the CLT floor panel to the SCL ledger as well (Karacabeyli and Douglas 2013). The other method involves attaching the CLT floor panel to the continuous CLT wall panel by means of a steel L-shaped bracket and self-tapping screws (Karacabeyli and Douglas 2013).

CLT exhibits high in-plane stiffness when subjected to lateral loads and behaves linear-elastically and tends to fail in a brittle way. To combat this issue, floor-to-wall connectors must be designed to dissipate the energy excited in the structure during a seismic event. This means connections (both floor-to-wall and panel-to-panel) must behave in a ductile manner and failure similarly. In addition to designing connections to behave in a ductile manner, one must also consider the biaxial nature of loading floor-to-wall connections and the fact that the CLT behaves differently when loaded parallel to the grain or perpendicular to the grain.

The most relevant study done by researchers investigating floor-to-wall connections for CLT buildings was provided by NSERC, NEWBuildS and SSEF, in Canada, and tested floor-to-wall connection brackets (CLT wall to steel floor) under cyclic loading (Schneider, Karacabeyli et al. 2014). The study intended to quantify induced-damage and evaluate connections of three-ply CLT wall panels subjected to cyclic loading. Six connections were tested under earthquake loads that were comprised of two different brackets and five different fastener types. Wall to floor connections were made with L-shaped brackets, and the different fasteners that were tested were a spiral nail, two different ring shank nails, and two different screws. Two different test

11

setups were used (one to monitor displacement parallel to the grain and one perpendicular to the grain). Failure parallel to the grain was dominated by pullout (self-tapping screws often sheared off because they have a higher withdrawal resistance). Failure perpendicular to the grain included wood crushing through the entire depth of the top layer, but the brackets rotated about their center of gravity (c.g.) and demonstrated a high plastic deformation. Damage perpendicular to the grain was much greater than parallel to the grain. Plastic failure is preferable, so pullout failure is preferable if shearing of the connectors can be avoided (Schneider, Karacabeyli et al. 2014).

Schneider, Karacebeyli et al. (2014) provided a good assessment of damage accumulation first put forward by (Gosain, Brown et al. 1977), that is a way of assessing the damage as a means of energy absorption. This method makes damage a function of the force per cycle multiplied by the displacement during that cycle and divided by the yield force multiplied by the displacement at yield. The damage at each cycle is summed over all tests to get a ratio of the amount of damage taken by the connection, or the amount of energy absorbed.

A study on floor-to-wall connections by Izzi, Polastri et. al. (2018) focused on modelling different connection configurations and different bracket connectors to add ductility to the building system as a whole. The study showed that the combination of shear and tension in the floor-to-wall connection affects the stiffness of shear walls as a system and is able to dissipate energy more effectively (Izzi, Polastri et al. 2018). This numerical model focused on three failure mechanisms: withdrawal of the nails connected to the floor panel, pull-through of anchoring bolts, and tensile failure in the cross-section of the bracket. The simulation aimed at proposing a numerical model that predicts the behavior and failure mechanism of wall-to-floor connections in CLT-to-steel connections. Loading direction had a significant impact on failure mechanism, and

12

the study also found that it is necessary to consider group effect in nailed joints which reduces the capacity of each individual nail.

Some of the most recent and innovative research into CLT connections has been done by Polastri, Giongo, and Piazza (2017) (Polastri, Giongo et al. 2017) at the University of Trento, Italy. Their research has been centered around developing a new type of connector (called X-RAD) that is made up of a metal part surrounded by a hardwood insert that is screwed into the corners of CLT panels by doubly inclined self-tapping screws. The connection is versatile as it can be used in both platform and balloon-style construction. Not only is the X-RAD connector characterized by high stiffness and a strong capacity, but the experiment showed that it has adequate ductility and energy dissipation in seismic loading scenarios (Polastri, Giongo et al. 2017).

While much of the floor-to-wall connection testing is helpful, it is mostly applicable to platform-style construction. Schnieder et al. (2014) showed that connection failure mechanisms are much different parallel and perpendicular to the grain (in reference to the outermost layer of CLT) (Schneider, Karacabeyli et al. 2014). This principle can be applied to balloon style construction as well, but not everything from their study is perfectly applicable to this type of construction. The numerical model presented by Izzi, Polastri et al. (2018) can be used for balloon style construction as it models the hysteretic behavior of connectors. Table 2.1 provides a summary of the relevant research that was consulted for this thesis.

Table 2.1. Summary of Floor-to-Wall Connection Research

RESEARCHER/ SOURCE	TYPE OF TEST	CONNECTION DESCRIPTION	STUDY OBJECTIVES
Schnieder et al. (2014)	Monotonic/Cyclic	Wall-to-Floor, two different brackets, spiral nails, ring shank nails, screws	Assess damage of connections and understand failure perpendicular vs. parallel to grain
Izzi, Polastri et al. (2018)	Numerical	Wall-to-Floor, nailed steel-to-CLT	Improve mechanical performance of connections, understand failure mechanisms in floor-to-wall connections
Polastri, Giongo, and Piazza (2017)	Monotonic/Cyclic	X-RAD Wall-to-Floor, STS	Demonstrate the competency of the X-RAD connector for use under seismic loading conditions

2.5.   Panel-to-Panel Connection Tests

There are a variety of different methods used to connect CLT panels to one another. The first method is to connect CLT floor panels together using internal splines. Prefabricating of the panels is necessary to allow room for the internal SCL or plywood spline that is used to screw the two panels together (Karacabeyli and Douglas 2013). Splines can also be done on the surface of the CLT panels, either as single or double surface splines, with the double splines obviously being stronger as they are double shear connections. Another common method of attaching CLT floor panels together is by means of a half-lapped joint where each panel is milled to allow the panels to come together and bear on one another, being attached by self-tapping screws (Karacabeyli and Douglas 2013).

Initial panel-to-panel connection tests were performed as a part of the SOFIE project, with the goal of investigating lap and spline joints and their performance when loaded parallel and perpendicular to the joint (Gavric, Fragiacomo et al. 2012). All connections were made with 8x80mm screws (wall-to-wall) and 10x140 screws (floor-to-floor), and shear tests were conducted using a reverse cyclic procedure with predefined yield values (Gavric, Fragiacomo et

al. 2012). Additionally, some tests used panels with a lapped joint (50mm or 120mm overlap), and other tests used panels with a splined joint. The tests found no brittle failure modes to have occurred, with the failure method eventually being bending of the screws after the formation of a plastic hinge – however, embedding of the screws into the wood was noticed at higher displacement rates (Gavric, Fragiacomo et al. 2012). The lapped joints exhibited a 50% higher stiffness than the spline joints, and the spline joints' maximum displacement was 19% higher than that of the lapped joints (Gavric, Fragiacomo et al. 2012).

Joyce, Ballerini, and Smith (Joyce, Ballerini et al. 2011) tested two different types of panel-to-panel connections: a double external spline and inclined screws (45 degrees) used in a butt connection. The study tested both configurations under monotonic and cyclic loading, and both connections were made with self-tapping screws. The point of the study was to determine whether inclined screws could be a good alternative to making panel-to-panel connections with a double external spline (Joyce, Ballerini et al. 2011). The tension tests showed that using inclined screws in a butt connection is provide significantly more elastic stiffness, but they do not provide comparable ductility to a double spline connection (Joyce, Ballerini et al. 2011).

Gavric, Fragiacomo, and Ceccotti (2015) (Gavric, Fragiacomo et al. 2015) tested floor-to-floor and wall-to-wall internal connections. The study investigated both lap connections and single external spline connectors, both made with self-tapping screws. Both configurations were subjected to monotonic and cyclic loads. The lap connections exhibited higher stiffness than the splined connections, but the spline joints exhibited more displacement at failure – they were more ductile (Gavric, Fragiacomo et al. 2015). The main conclusion from the study was that for connections subjected to cyclic loading, spline LVL joints resisted greater forces at higher displacement (Gavric, Fragiacomo et al. 2015).

In order to investigate what internal connection method was most preferable, Hossain, Danzig, and Tannert (2016) (Hossain, Danzig et al. 2016) investigated half lapped, single surface spline, and STS butt connections under both monotonic and cyclic loads. The purpose of the study was to validate doubly inclined STS butt connections as a viable connection method when compared to half lapped and single surface spline connections. The study found validated the hypothesis that STS butt connections are a valid alternative to half-lapped or single surface spline connections when the self-tapping screws are doubly inclined (Hossain, Danzig et al. 2016). The benefit of using STS butt connections is that they are carry more load and undergo more displacement which means they dissipate more energy, and they are cheaper prescribe because no machining of the ends of the panels is required.

Research performed in Canada by MITCAS Canada through the Accelerate project investigated the behavior of panel-to-panel connections specifically with the goal of researching behavior of screws in withdrawal, screws in shear, and screws that experience both (Hossain, Popovski et al. 2018). CLT connections were evaluated in terms of load-carrying capacity, yield strength, ductility, deformation capacity, and stiffness. Half-lap joints with self-tapping screws (STS) loaded in either shear or withdrawal demonstrated that joints loaded in shear exhibit high ductility, but low stiffness and joints loaded in withdrawal are very stiff but brittle. Combining the two – loading STS that act in shear and loading STS that act in withdrawal gains the benefits of both – high stiffness and high ductility. All CLT assemblies, where the STS were loaded in shear, exhibited very large displacements and the failure mode was a combination of wood crushing and screw yielding. No screw withdrawal was observed in shear loading. When the STS were loaded in withdrawal, they exhibited small displacements and the failure mode was screw withdrawal (screws in tension being pulled in and the screws in compression being pushed out).

STS loaded at 45 degrees to the grain leads to stiffer joints with most of the load being carried by the withdrawal resistance (Hossain, Popovski et al. 2018).

For the STS that acted in shear and withdrawal, the failure mode was more complex. The specimen would seem to fail in withdrawal as the screws in compression would begin to push out and the screws in tension would begin to pull out, however the specimen maintained in load-carrying capacity even with increasing displacement. The final failure was wood crushing by the shear-carrying screws. The conclusion was that loading a connection with screws in shear and in withdrawal leads to a large load carrying capacity with a relatively ductile failure – high stiffness and high ductility (Hossain, Popovski et al. 2018). Table 2.2 provides a summary of the relevant research that was consulted.

Table 2.2. Summary of Panel-to-Panel Connection Research

RESEARCHER/ SOURCE	TYPE OF TEST	CONNECTION DESCRIPTION	STUDY OBJECTIVES
Gavric, Fragiacomo, Ceccotti (2012)	Monotonic/Cyclic	Wood Screws, Half-lapped, Single External Spline	Determine mechanical properties of connectors and governing failure mechanisms
Joyce, Ballerini, and Smith (2011)	Monotonic/Cyclic	Wood Screws, STS, Double External Spline, Inclined STS Butt	Compare external spline connections with inclined STS butt connections to find which exhibits more ductile behavior
Gavric, Fragiacomo, and Ceccotti (2015)	Monotonic/Cyclic	Wood Screws, STS, Single External Spline, Half-lapped	Compare connection methods – spline and lap connections
Hossain, Danzig, and Tannert (2016)	Monotonic/Cyclic	STS, Half-lapped, Single External Spline, Doubly-Inclined STS Butt	Establish Doubly-Inclined STS Butt Connections as valid connection method
Hossain, Popovski, Tannert (2018)	Monotonic/Cyclic	STS, Half-lapped, fasteners installed at both 45deg and 90deg	Determine behavior of fasteners in combination of shear and withdrawal

2.6.   Problem Statement and Tasks

While much research has been done on cross-laminated timber behavior under seismic loading and the behavior of CLT connections, more needs to be conducted in balloon-frame

construction. Many of the wall-to-floor connection set-ups that have been tested are only applicable to platform construction, so a test setup that is directly applicable to balloon-frame construction is needed. Beginning to look at designing CLT buildings that are balloon-framed, the most cost-effective way to begin research is to begin with connection testing. Once the connections are understood, some parameters have been calculated, and many configurations have been tested, the next logical step would be to move to panel tests. After panel testing, balloon-framed buildings could then be tested in full-scale shake table tests.

A rational design procedure needs to be developed to prescribe what types of connectors and configurations dissipate the energy excited in the system by seismic loads. The issue is that CLT is sufficiently stiff to resist earthquake loads, but it has no means of energy dissipation. Therefore, all the energy excited by the strong ground motion into the structure is directly felt by the people and objects inside. To combat this issue, the connections need to be designed with sufficient ductility to provide a means of energy dissipation through damping. In a balloon-framed system, this can be accomplished through ductility in the wall-to-floor connections and through ductility in the wall-to-wall connections in taller structures. Additionally, in even taller systems where the aspect ratio of the walls is on the order of 8:1, energy dissipation can come through deflection of the walls throughout the stories of the building – given that the walls are sufficiently held down to transfer the load into the foundation.

Given these rational considerations for how connections ought to be designed for a balloon framed CLT building, a test matrix was developed to test connections that have the highest likelihood of being adopted in real-world construction practices. This led to the development of a test matrix that emphasized the testing of two different self-tapping screw manufacturers in a variety of different connection orientations. Once the behavior of the screws

tested in this project is understood under cyclic loading, screw manufacturers can get their

screws approved to be used in designs by demonstrating that they meet the minimum

requirements of connection strength and ductility determined by this project. The objective of

testing a wide variety of connection configurations is to provide a standard by which to measure

the behavior of these connections under seismic loading.

The objective of the work of this research project is to complete four tasks that will help

aide in the understanding of balloon framed CLT buildings and the design methodology that

ought to be used when designing for seismic loads. The four tasks that were completed are

described in Table 2.3:

Table 2.3. Description of Tasks

Task 1	Experimental Testing – Connection Tests
Task 2	Fitting Experimental Data to Numerical Models
Task 3	Finite Element Modeling of Connections
Task 4	Experimental Testing – Biaxial Wall Test

Task 1: Experimental Testing – Connection Tests
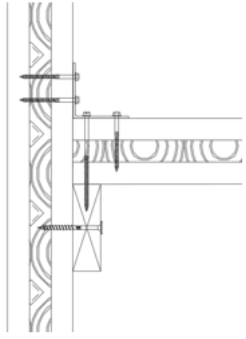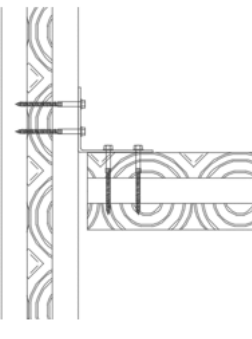
The test matrix for the panel-to-panel connections was developed to satisfy current

research gaps in inter-panel connectors, while also considering what will likely be used in real

wall-to-wall connections. The final panel-to-panel test matrix is shown in Table 2.4:

19

Table 2.4. Panel-to-Panel Test Matrix

Panel-to-Panel Connections (Wall-to-Wall)				
Configuration #	Connection Type	Connection Components	Fastener Angle and Spacing	Testing Protocol
1	Half-lapped	Screw A	90deg at 3in	2 monotonic, 10 cyclic
2		Screw B	90deg at 3in	2 monotonic, 10 cyclic
3		Screw A and Screw C	2 rows 90deg (A), 2 rows 45deg (C), at 4in	2 monotonic, 10 cyclic
4		Screw B and Screw D	2 rows 90deg (B), 2 rows 45deg (D), at 4in	2 monotonic, 10 cyclic
5	Single Surface Spline	Screw A	90deg at 6in	2 monotonic, 10 cyclic
6		Screw B	90deg at 6in	2 monotonic, 10 cyclic

The test matrix for the wall-to-floor connections was developed in order to determine how connections will likely be made in the design of load-bearing and non-load bearing CLT shear wall connections. After an in-depth literature review, and upon discussion with the project's expert panel, the following final wall-to-floor connection was determined to be as shown in Table 2.5.

Table 2.5. Wall-to-Floor Test Matrix

Wall-to-Floor Connections				
Configuration #	Connection Type	Connection Components	Connection Application	Testing Protocol
7	Load Bearing Shear Wall	Screw E, Screw F, Angle Bracket 1, LVL 2x4		2 monotonic, 10 cyclic
8		Screw G, Screw H, Angle Bracket 1, LVL 2x4		2 monotonic, 10 cyclic
9	Non-Load Bearing Shear Wall	Screw E, Angle Bracket 2		2 monotonic, 10 cyclic
10		Screw G, Angle Bracket 2		2 monotonic, 10 cyclic

All 120 connection tests were performed in order to simulate the behavior of the connection in the field and the behavior was fit to two different models in order to determine which is best. Monotonic tests were used as a reference to develop the cyclic loading curves that are unique to each different configuration. Ten cyclic tests were conducted to eleminate confounding variables that may have had any small effect on the consistency of the results (for example, imperfections in the CLT, manufacturing inconsistencies, and small dimensional variability of each specimen). Load was recorded, and displacement was recorded in a number of different locations on the specimen to ensure a pure shear test has been achieved. These were recorded through several different string potentiometers and controlled through a data acquisition system (DAQ). Load was measured from the load cell on the test frame. These measurements

were taken for each specimen and was plotted to determine the load-displacement curves necessary for comparison to numerical models.

Task 2: Fitting Experimental Data to Numerical Models

After the data was collected from the monotonic and cyclic experimental tests, force and displacement were plotted in order to obtain curves that can be fit to two different numerical models. The cyclic test data was fit to both the CUREE-SAWS and Pinching4 numerical models in order to determine which predicts more accurately the behavior of each connection. Once the parameters of each model were determined, this data will be further used for the numerical simulation of full-scale buildings subjected to seismic loads.

Task 3: Finite Element Modeling of Connections

In addition to the experimental test program, finite element models were developed for each connection test. The goal of using FEA to model tests that are done in the lab was to develop a model that can be validated by experimental data so that the model can be further used to glean even more useful information than what was determined in the lab. This finite element modelling was condcuted using the ABAQUS finite element software.

Task 4: Experimental Testing – Biaxial Wall Test

In addition to the connection tests, a full-scale biaxial wall test was performed to investigate the bahavior of wall-wall, and wall-foundation connections under a biaxial loading condition. Both a half-lap and a surface spline connection were tested with load and displacement being recorded at various different locations. A test like this has not been performed before, so the results are novel. The purpose of the test was to understand the behavior of a CLT wall under biaxial loads for balloon-framed systems.

3. EXPERIMENTAL TEST PROGRAM

3.1. Test Program Overview

Experimental testing presented in this chapter was performed at the Texas A&M University RELLIS Campus in the Structural and Materials Testing Laboratory (SMTL).

3.1.1. Overview

The test matrix was developed with the help of the expert panel on the project, which consisted of four members representing the wood industry and code council with an in-depth knowledge of CLT buildings, connections, and structural systems. They offered the advice necessary to develop the connection testing matrix that is representative of typical details that will eventually be adopted by the industry and construction sector. As determined from the literature review of relevant tests, the experimental test program consisted of panel-to-panel connections and floor-to-wall connections. Wall-to-foundation connections appear to be well understood, and their behavior will not significantly change when the structural system is changed to a balloon-framed style from platform type of construction. Additionally, wall-to-foundation connections are studied in the full-scale biaxial wall test (Section 6. BIAXIAL WALL TEST). With this information, the test matrix was developed which is further discussed in Section 3.1.3 Test Matrix.

3.1.2. Test Specimen and Fixture Design

The design and setup for the connection testing conducted in this project followed similar CLT connection tests that had been performed at the SMTL (Jalilifar 2021). Panel-to-panel connections were designed so that they could be tested on the fixture that had already been built, but a new fixture was designed and fabricated for the testing of all wall-to-floor balloon-style connections. While the specimens were designed to use the fixture that had already been built,

the connection type of the loading frame that was used was different from the original fixture. For this reason, another identical fixture was constructed, but with the connection type that was needed – a knife plate rather than a two-inch rod. A rendering of the fixture can be seen in Figure 3.1.
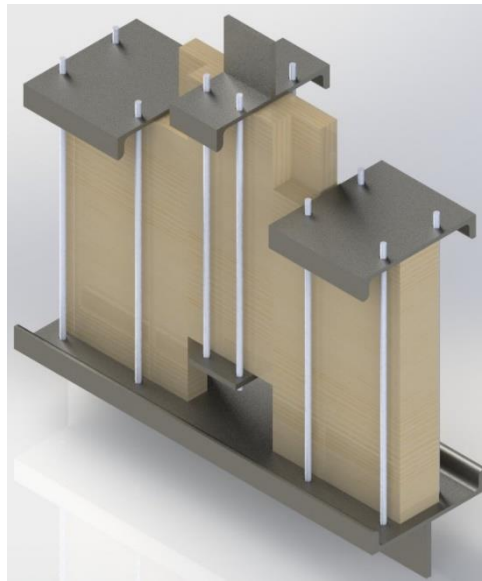
Figure 3.1. Panel-to-Panel Fixture

The design of the wall-to-floor fixture was limited by the capacity and dimensions of the testing machine on which it was to be used. An additional limitation that was considered during the design process was the slight amount of torsion that would be induced on the bottom fixture. Because there was about two inches of eccentricity between where the load was applied and where it was resisted by the connection (as can be seen in Figure 3.2), a small amount of torsion was induced on the fixture.
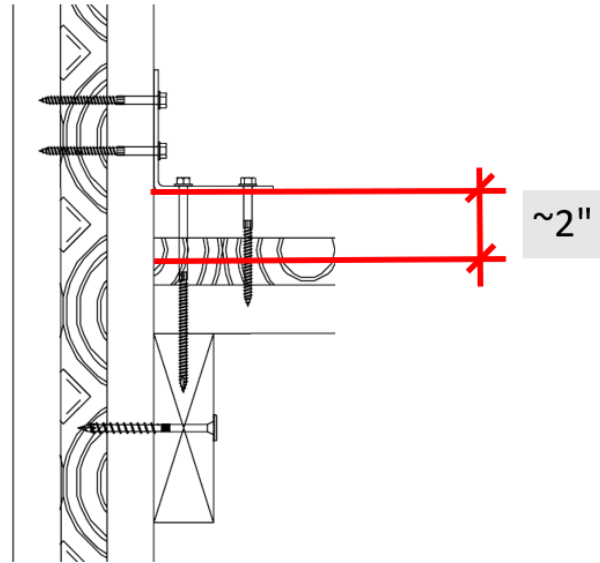
Figure 3.2. Wall-to-Floor Test Eccentricity

This torsional load was combatted by designing the wall-to-floor fixture for torsional stiffness, along with bending and shear strength. Adequate torsional stiffness was accomplished with the use of additional 6-inch-deep knife plates welded to the bottom of the H-fixture. Using half of the maximum capacity of the machine (full capacity is 100 kips), bolstered with predictions of the strength of the test specimens, a test fixture was designed for bending stress, shear stress, and, most importantly, deflection. A rendering of the fixture design can be seen in Figure 3.3.
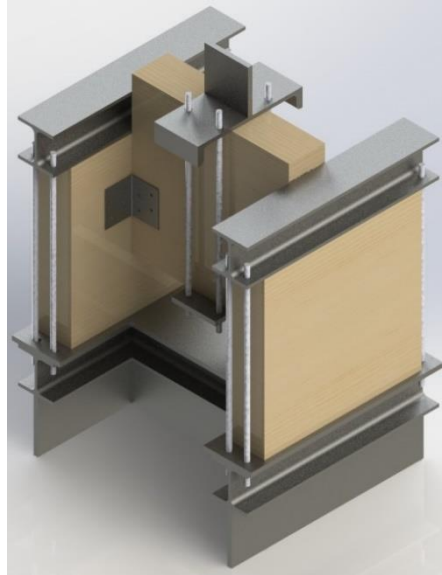
Figure 3.3. Wall-to-Floor Fixture

The bottom piece of the final wall-to-floor fixture that was built can be seen in Figure 3.4.

Figure 3.4. Wall-to-Floor Fixture (bottom piece)

The machine that was used to test all connection specimens listed in the test matrix was a 100-kip capacity axial precision material testing machine that applies tension/compression controlled by either force input or displacement input. A photo of the testing machine can be seen in Figure 3.5.
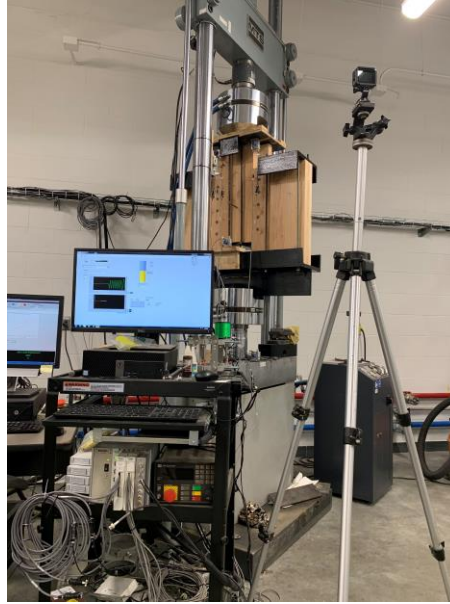
Figure 3.5. 100-kip Test Frame and Setup

Every test performed in the test matrix was conducted using an input displacement and measuring the corresponding force from a load cell. Other displacement measurements were recorded using string potentiometers placed at various locations on the specimen. All measurement outputs were managed by a data acquisition system (DAQ) and controlled by a LABVIEW program. The input displacement profile for monotonic tests was simply a constant displacement rate and the test was ended after the specimen had reached a peak load and then dropped below approximately 60% of that peak load. While this was used as a rule-of-thumb for all monotonic tests – some tests collected more data, and some tests collected less data. The input displacement profiles for the cyclic tests were developed from the results of the monotonic tests. More information on the specific loading protocol that was followed for the cyclic tests can be found in the testing section of this thesis (Section 3.4).

3.1.3. Test Matrix

The objective of the panel-to-panel test matrix (see Table 3.3) is to obtain results for a variety of different configurations and to investigate the viability of one novel connection layout.

27

Half-lap and single surface spline connections are well-studied (configurations 1, 2, 5, and 6), but for the purposes of this project results were obtained to calibrate numerical models and to create a standard by which to judge the behavior of all connections in balloon-frame systems going forward. The one panel-to-panel configuration that is not well understood is configuration 3 and 4. The purpose of those tests is to gain an understanding of the behavior of connection that includes fasteners installed at both 90 degrees and 45 degrees. For all three different configurations (half-lapped screws at 90 degrees, half-lapped screws at 90 and 45 degrees, and spline screws at 90 degrees), two different types of screws manufacturers were tested with the dimensions of each part of the screw being recorded. It was important for this project not to standardize a connection method around a single screw, but around a certain behavior that was favorable – therefore, different screw manufacturers were used to keep the results more standard. The dimensions and catalog numbers for each screw can be found in Table 3.1 and Table 3.2. A photo of each screw can be seen in Figure 3.6.

Table 3.1. Self-Tapping Screw Dimensions

	Manufacturer	Diameter	Shank Diameter	Root Diameter	Head Diameter	Length	Thread Length	Thread Pitch	F_{yb} (ksi)
Screw A	Simpson Strong-Tie	5/16	0.22	0.20	0.75	4	2.375	0.2	160
Screw B	MTC Solutions	5/16	0.228	0.209	0.87	4	2.75	0.22	150.2
Screw C	Simpson Strong-Tie	5/16	0.22	0.20	0.75	5	2.75	0.2	160
Screw D	MTC Solutions	5/16	0.228	0.209	0.87	5.5	3.125	0.22	150.2
Screw E	Simpson Strong-Tie	1/4	1/4	0.174	0.52	3.5	2.25	0.096	164
Screw F	Simpson Strong-Tie	1/4	1/4	0.174	0.52	6	3.25	0.095	164
Screw G	MTC Solutions	5/16	0.228	0.209	0.472	4	2.375	0.10	150.2
Screw H	MTC Solutions	5/16	0.228	0.209	0.472	6.25	3.125	0.10	150.2

all units are inches unless otherwise specified

Table 3.2. Catalog Number for All Screws

Legend	
Screw	Catalog Number
A	SDWS22400DB
B	(SK) 120080100000303
C	SDWS22500DB
D	(SK) 120080140000303
E	SDS25312SS
F	SDS25600
G	(Kombi) 130080100000103
H	(Kombi) 130080160000103
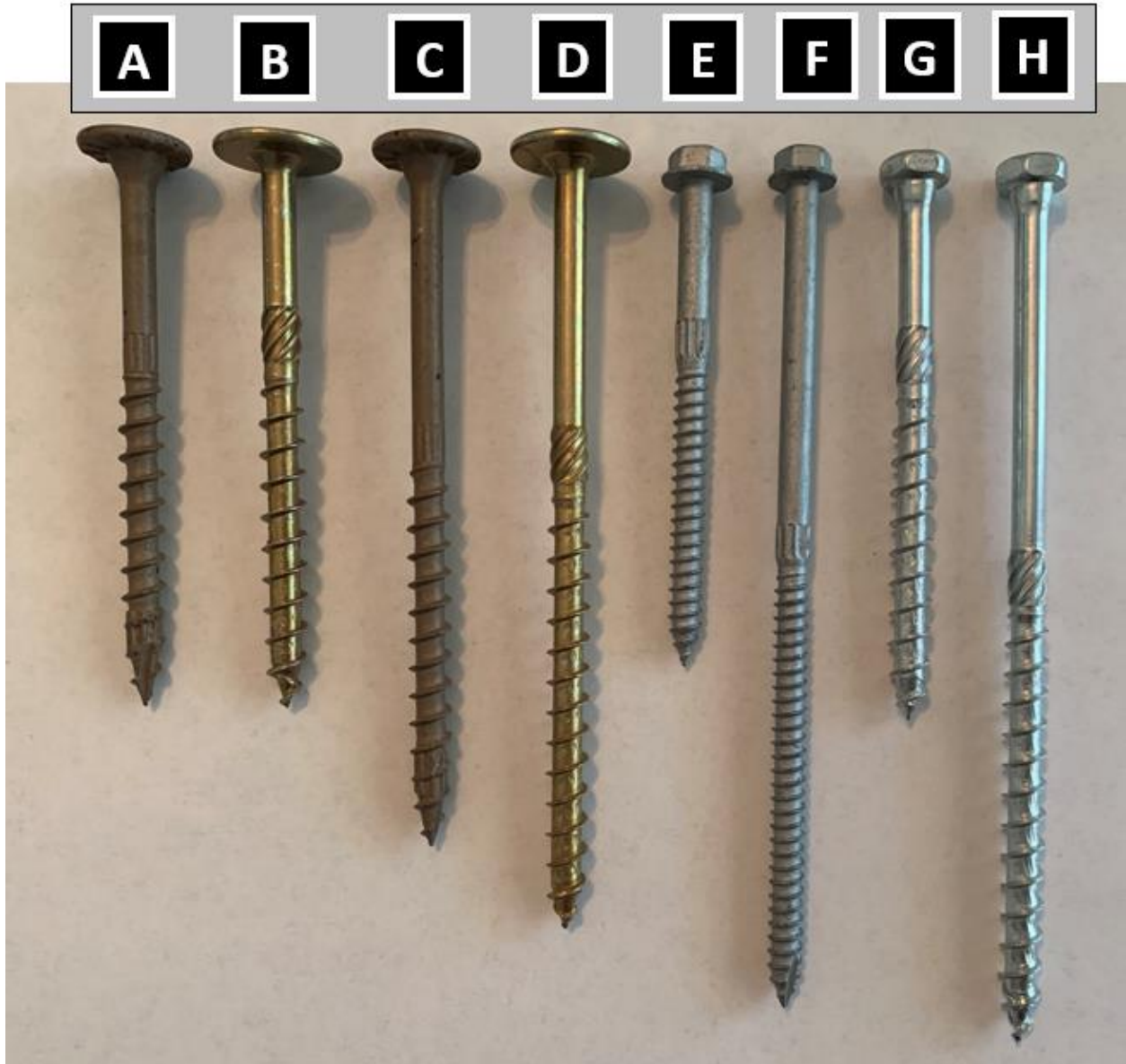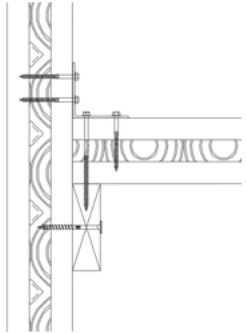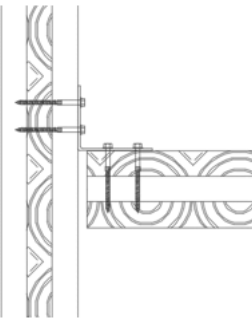
Figure 3.6. Self-Tapping Screws for Connection Tests

Table 3.3. Panel-to-Panel Test Matrix

Panel-to-Panel Connections (Wall-to-Wall)				
Configuration #	Connection Type	Connection Components	Fastener Angle and Spacing	Testing Protocol
1	Half-lapped	Screw A	90deg at 3in	2 monotonic, 10 cyclic
2		Screw B	90deg at 3in	2 monotonic, 10 cyclic
3		Screw A and Screw C	2 rows 90deg (A), 2 rows 45deg (C), at 4in	2 monotonic, 10 cyclic
4		Screw B and Screw D	2 rows 90deg (B), 2 rows 45deg (D), at 4in	2 monotonic, 10 cyclic
5	Single Surface Spline	Screw A	90deg at 6in	2 monotonic, 10 cyclic
6		Screw B	90deg at 6in	2 monotonic, 10 cyclic

Table 3.4. Wall-to-Floor Test Matrix

Wall-to-Floor Connections				
Configuration #	Connection Type	Connection Components	Connection Application	Testing Protocol
7	Load Bearing Shear Wall	Screw E, Screw F, Angle Bracket 1, LVL 2x4		2 monotonic, 10 cyclic
8		Screw G, Screw H, Angle Bracket 1, LVL 2x4		2 monotonic, 10 cyclic
9	Non-Load Bearing Shear Wall	Screw E, Angle Bracket 2		2 monotonic, 10 cyclic
10		Screw G, Angle Bracket 2		2 monotonic, 10 cyclic

The wall-to-floor tests (see Table 3.4) had the objective of replicating the actual size and spacing of connectors and connecting components that will be used in constructing balloon-

frame CLT buildings. It is projected that balloon-framed wall systems will be used to resist lateral loads in two different applications – load bearing and non-load bearing scenarios. The first scenario, load bearing, consists of a shear wall that is used to both carry lateral load (wind, seismic, etc.) and carry gravity loads (dead load, live load, etc.). This is observed by configurations 7 and 8 including a bearing component in the test setup. An LVL 2x4 is used as is typical in common CLT load bearing connections. The purpose of including this component in the connection testing program is to determine the behavior of a screw that is continuous through the floor and into the bearing component. The second scenario, non-load bearing, consists of a shear wall that is intended to only carry lateral loads and to support its own self-weight. Configurations 9 and 10 accomplish this goal by testing the floor panel in the opposite direction and by including vertical slots in the angle brackets where they are attached to the wall panel. The floor panel has layers tested in the opposite direction because the floor will be supported by a wall that is not part of the test setup. The vertical slots in the angle bracket aim to imitate the small amount of deflection allowance needed for the floor panel to keep from transferring gravity load into the wall.

3.1.4. Material Properties

The Cross-Laminated Timber for the project was specified to be Douglas-Fir and to obtain V1 stress-grade, per PRG 320-2018 requirements. All panels were 3-ply, with a thickness of 4.125 inches and a relative moisture content between 12%-15% at delivery. All panels were stored at a temperature of between 65- and 75-degrees Fahrenheit. Table 3.5 summarizes the modulus of elasticity, bending strength, and other values for the panels – stress grade V1.

Table 3.5. Specified Strengths and Moduli of Elasticity (Karacabeyli and Douglas 2013)

Stress Grade	Longitudinal Layers						Transverse Layers					
	f_b	E	f_t	f_c	f_s	f_{cp}	f_b	E	f_t	f_c	f_s	f_{cp}
E1	28.2	11700	15.4	19.3	0.50	5.3	7.0	9000	3.2	9.0	0.50	5.3
E2	23.9	10300	11.4	18.1	0.63	7.0	4.6	10000	2.1	7.3	0.63	7.0
E3	17.4	8300	6.7	15.1	0.43	3.5	4.5	6500	2.0	5.2	0.43	3.5
V1	10.0	11000	5.8	14.0	0.63	7.0	4.6	10000	2.1	7.3	0.63	7.0
V2	11.8	9500	5.5	11.5	0.50	5.3	7.0	9000	3.2	9.0	0.50	5.3

All self-tapping wood screws that were used in the experimental test program were either supplied by MTC or by Simpson StrongTie as described in Section Test Matrix 3.1.3. The allowable bending strength of all MTC fasteners was given as 169.5 ksi, while the allowable bending strength of all Simpson StrongTie fasteners was given as 160 ksi. All fasteners were steel with a modulus of elasticity of 29,000 ksi. The material properties of all LVL studs used in the test program are summarized in Table 3.6.

Table 3.6. LVL Material Properties

E (psi)	F_b (psi)	F_v (psi)	F_t (psi)	F_{cll} (psi)	F_c (psi)	SG
2.0	2800	285	1950	3000	750	0.5

3.2. Construction of Test Specimens

All specimens were constructed on-site, and the process is documented herein. A photo of every specimen configuration in its final form before testing can be found in Figure 3.7 and Figure 3.8 for panel-to-panel and wall-to-floor configurations, respectively.

Specimen 1   Specimen 2   Specimen 3

Specimen 4   Specimen 5   Specimen 6
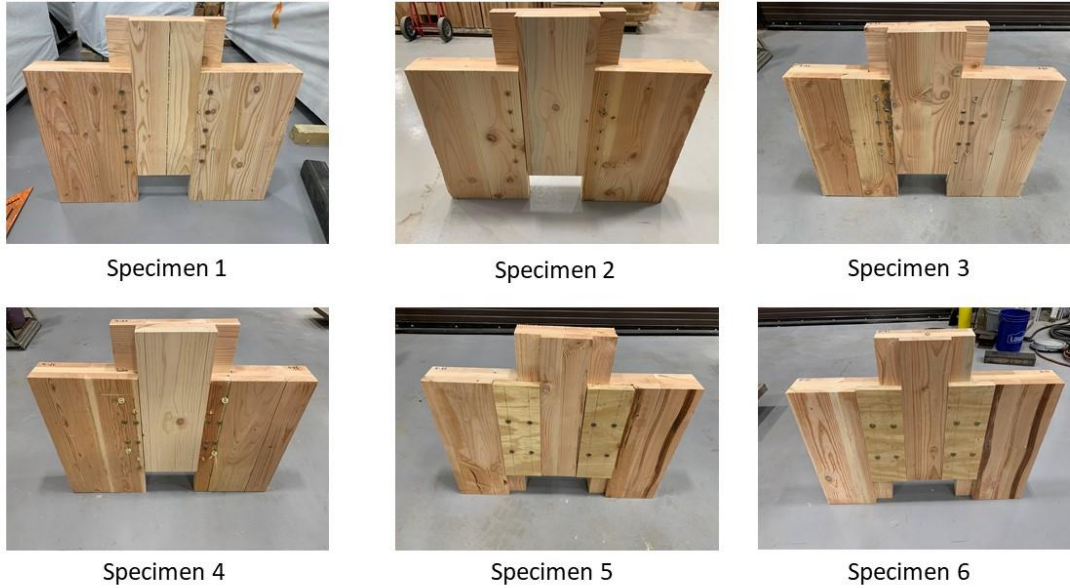
Figure 3.7. Photos of Panel-to-Panel Configurations

<div align="center">Specimen 7</div>

<div align="center">Specimen 8</div>

<div align="center">Specimen 9</div>

<div align="center">Specimen 10</div>

Figure 3.8. Photos of Wall-to-Floor Configurations

The connections were designed to fit the fixtures in which they were to be tested as described in Section 3.1.2. Additionally, they were designed to allow for up to six inches of displacement in one direction without bottoming out on the fixture during a test. Drawings were generated for each component for each specimen and the CLT manufacturer (DR Johnson) was able to manufacture each component of each specimen to the specification that was needed. This left the construction of the specimens to be relatively straightforward. An example of configuration 1 from drawing to construction is shown in Figure 3.9 and Figure 3.10, respectively.
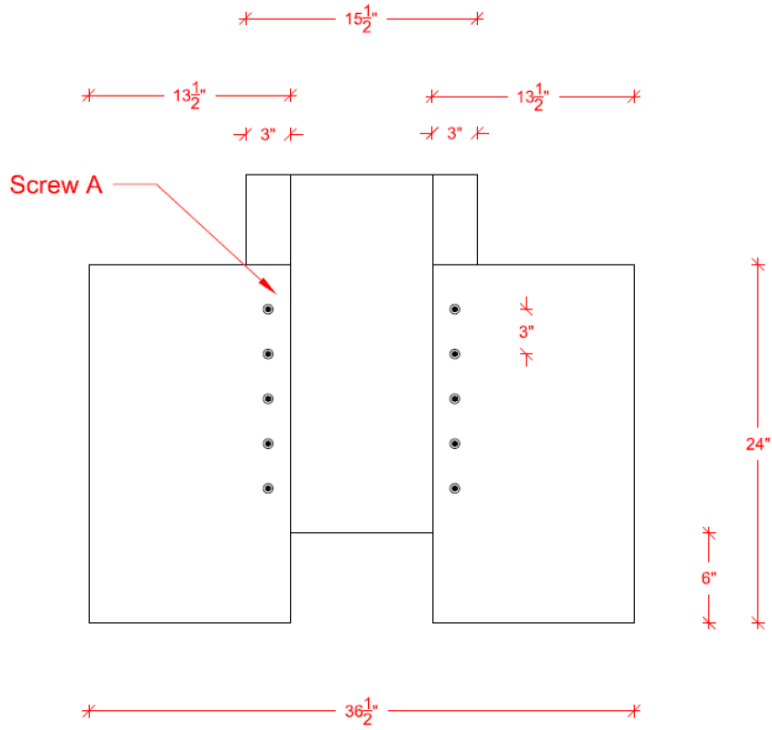
Figure 3.9. Configuration 1 Drawing
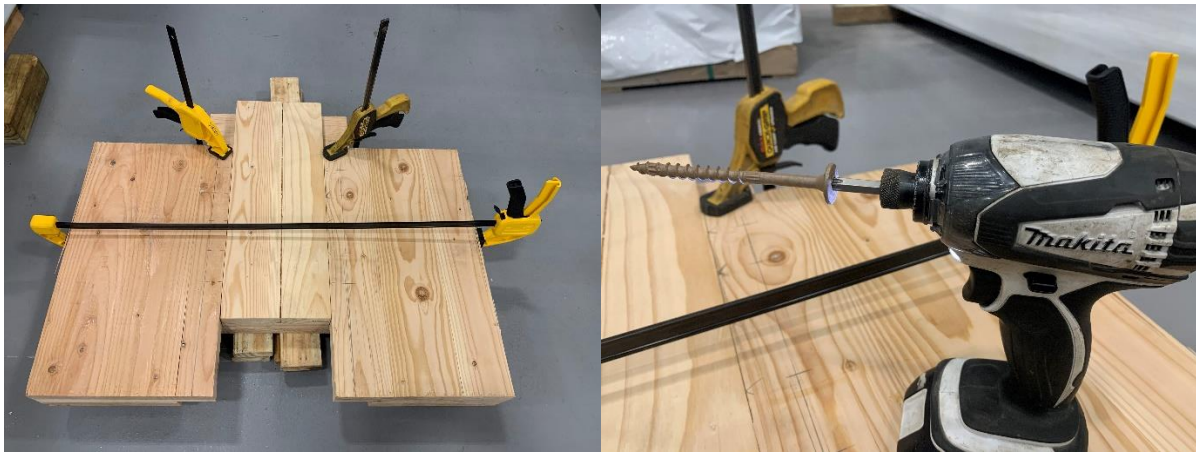
Figure 3.10. Construction of Specimen 1

The same method of construction was used for specimen 2, but with installing screw B instead of screw A. Drawings of this configuration can be found in APPENDIX A: CONNECTION TEST DRAWINGS. For configurations 3 and 4, the specimen was fixtured the same way, using wood clamps and the screw installation locations were laid out in a similar manner. To install the

screws at a 45-degree angle, a small pilot hole was started by installing a large 8d nail where the

nail would eventually go, and then removing the nail. This allowed for the screw to gain enough

traction when installed at an angle and not slip during the installation process. The drawing of

this configuration and a photo of the screws being installed at an angle can be seen in Figure 3.11

and Figure 3.12, respectively. Figure 3.13 shows which fasteners were installed at an angle and

which were installed at 90 degrees. Drawings for configuration 4 can be found in APPENDIX A:

CONNECTION TEST DRAWINGS.
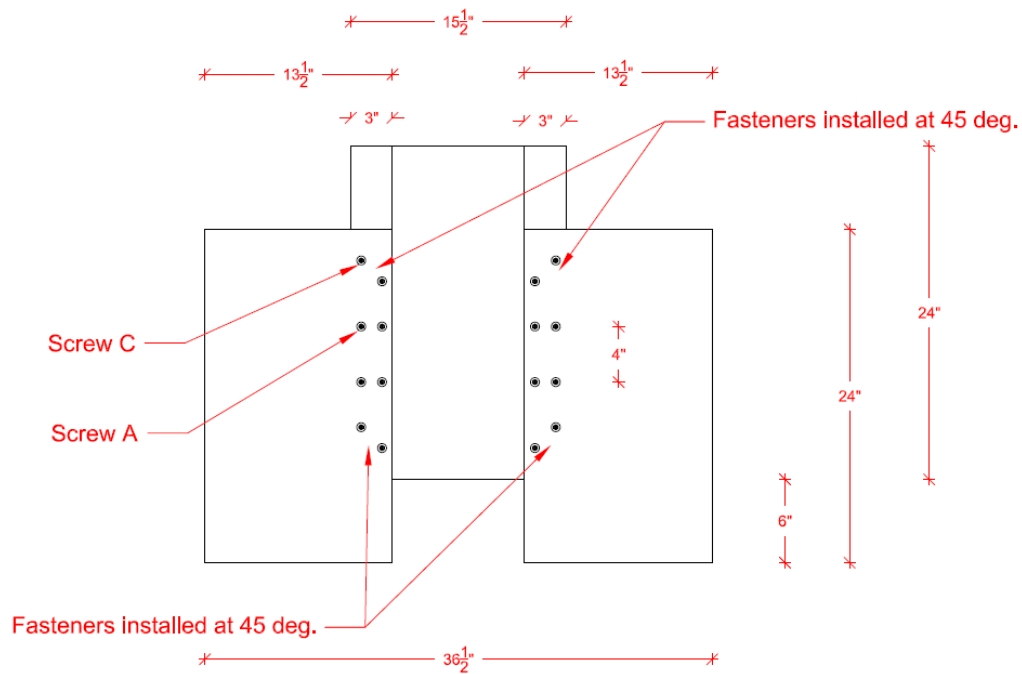
Figure 3.11. Specimen 3 Drawing

(a)   (b)

Figure 3.12. 45 Degree Fastener Installation
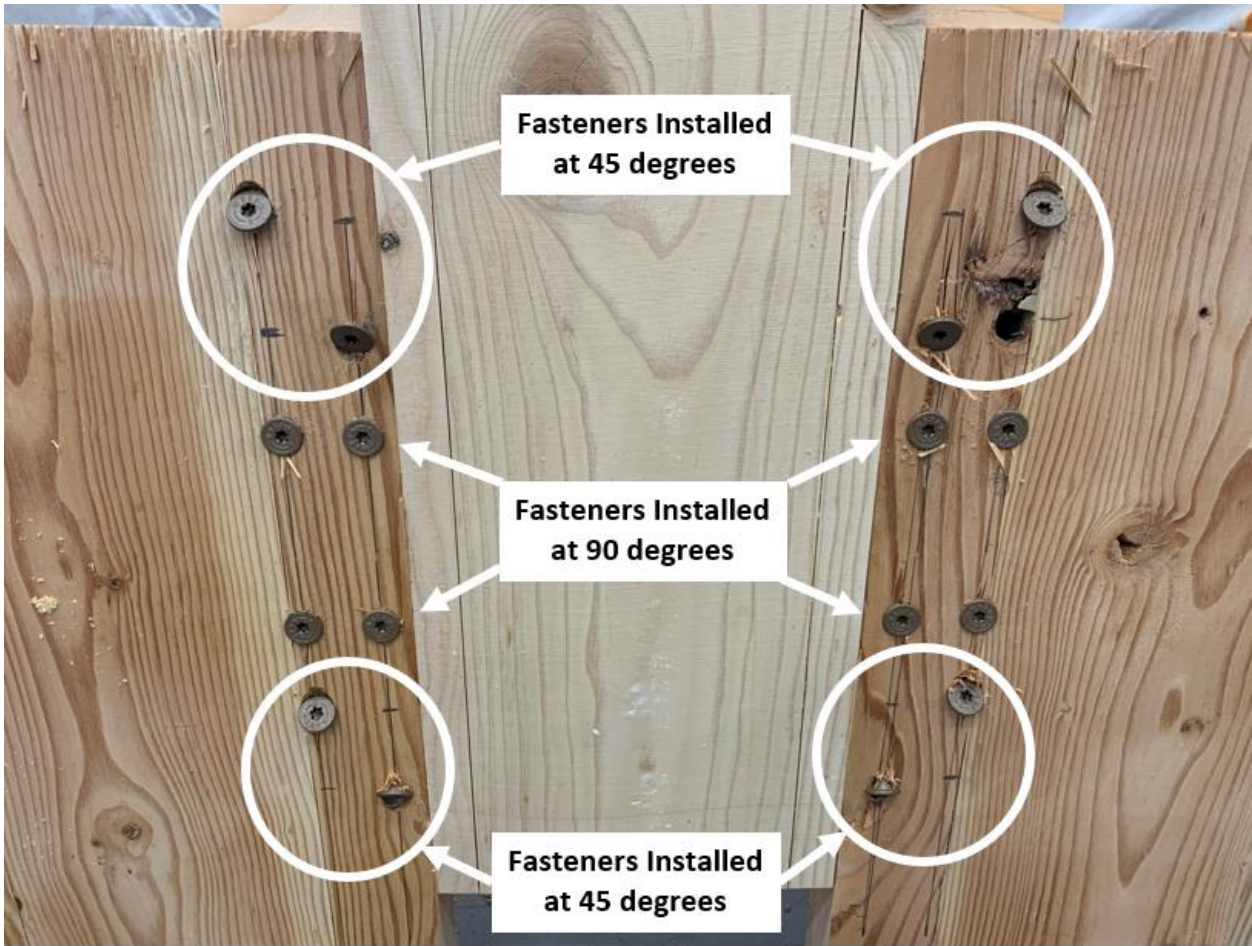
Figure 3.13. Photo of Specimen 3 Showing Angled Fasteners

Specimens 5 and 6 were constructed in a similar manner with the same fixturing using wood clamps. The splines were cut out of 1-1/8" structural plywood (pine). This was accomplished by using a circular saw to cut 24-inch strips off a 4'x 8' sheet and then using a table saw to cut the 24-inch strips into individual splines that are 6 inches wide. The specimens then had the screws installed in the same manner as all other specimens – using a drill/driver to drive the self-tapping screws through the spline and into the CLT. Photos of specimen configurations 5 and 6 can be seen in Figure 3.15. Drawings for specimen 6 can be found in APPENDIX A: CONNECTION TEST DRAWINGS.
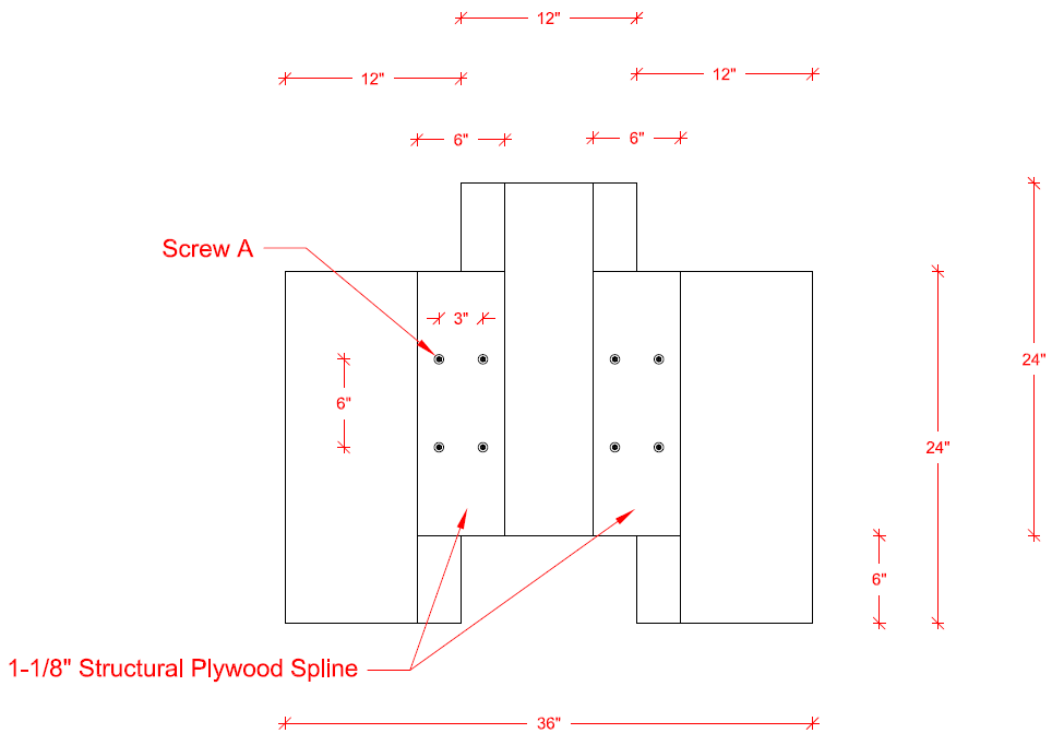
Figure 3.14. Specimen 5 Drawing
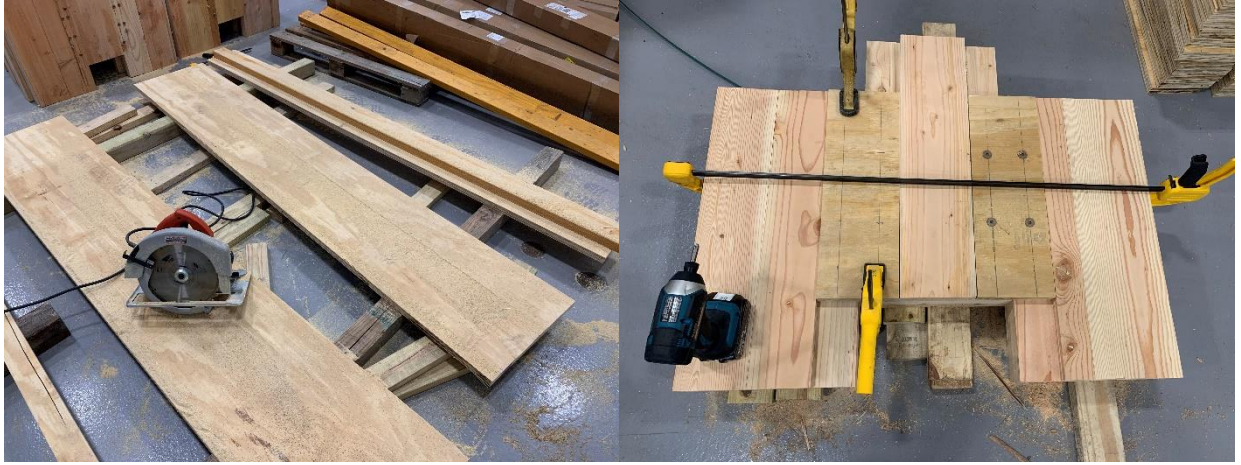
Figure 3.15. Specimen 5/6 Construction Photos

Specimens 7 and 8 were constructed in the same manner as one another, with their only difference being type of screw and dimension of the holes on the angle bracket. The LVL studs were cut to size using a miter saw and screwed to the CLT using self-tapping screws. The "floor" was then lined up on the LVL ledger on either side to provide the six-inch specified distance. The entire specimen was clamped together to ensure a tight fit-up and that wall and floor were at right angles. The angle brackets were centered on each side and secured using self-tapping wood screws specifically designed for steel-wood connections. A drawing of specimen 7 and a photo of its construction can be found in Figure 3.16 and Figure 3.17, respectively. Drawings of specimen 8 can be found in APPENDIX A: CONNECTION TEST DRAWINGS.
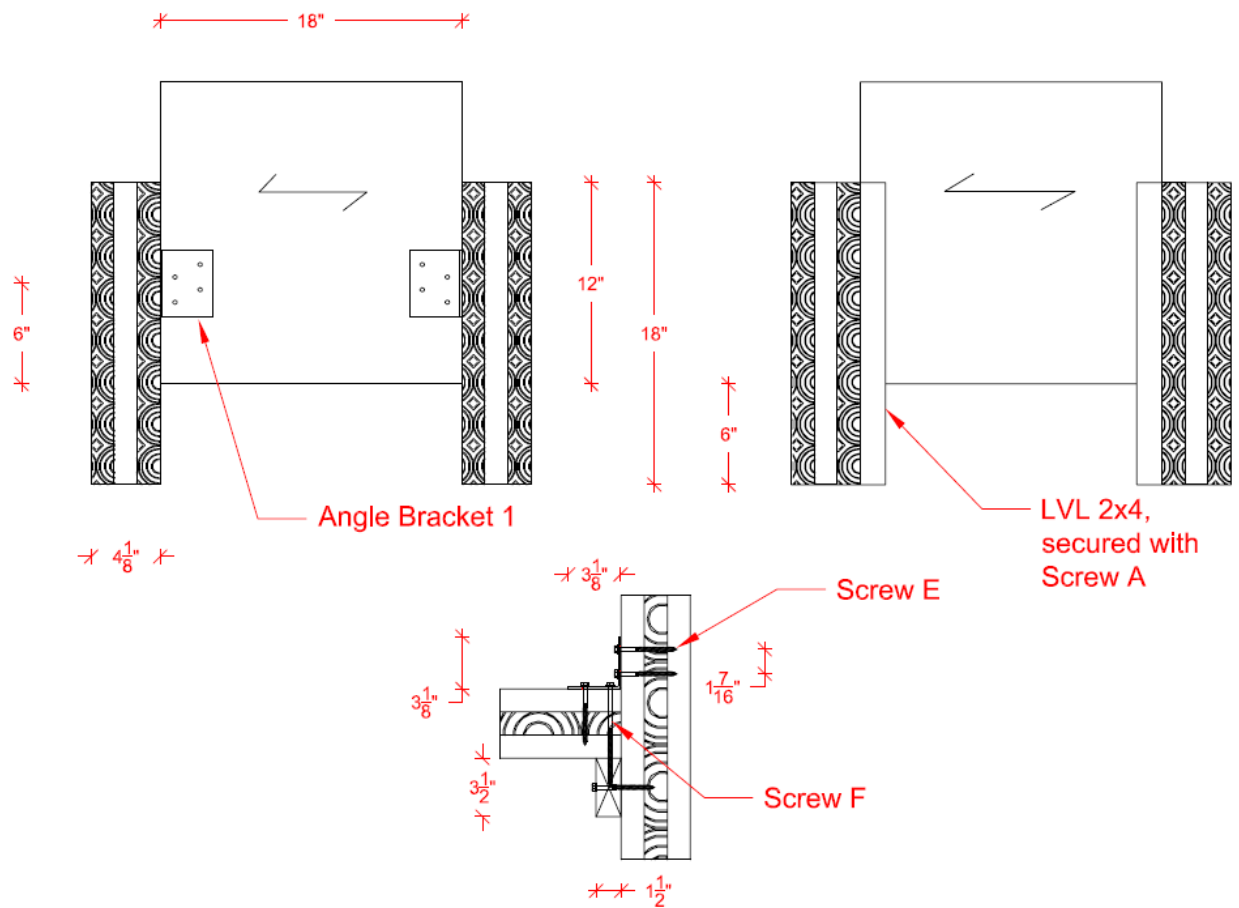
Figure 3.16. Specimen 7 Drawing

Figure 3.17. Construction of Specimen 7 and 8

Specimens 9 and 10 were constructed in a similar manner to specimens 7 and 8, but an accommodation was made to provide the half-inch gap specified between the wall and floor panels. To accomplish this gap, small half-inch shivs were fashioned and placed between the wall and floor before clamping the specimen together. The angle brackets were centered and installed using self-tapping screws and then the shivs were removed. A drawing of specimen 9 and construction photos can be found in Figure 3.18 and Figure 3.19, respectively. Drawings of specimen 10 can be found in APPENDIX A: CONNECTION TEST DRAWINGS.
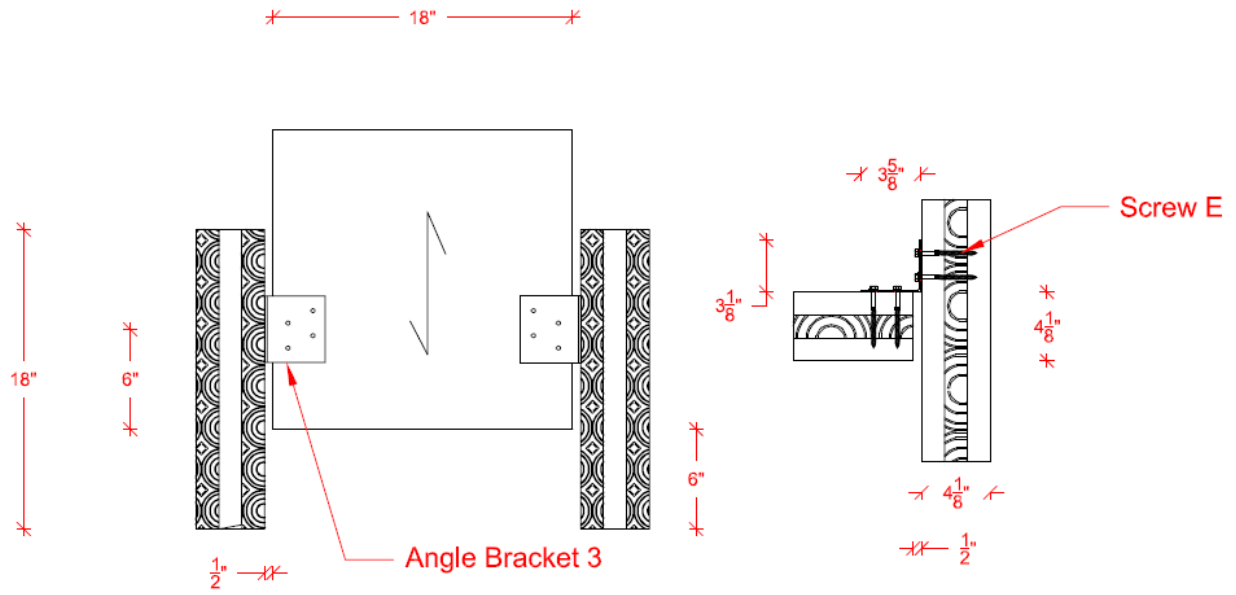
Figure 3.18. Specimen 9 Drawing
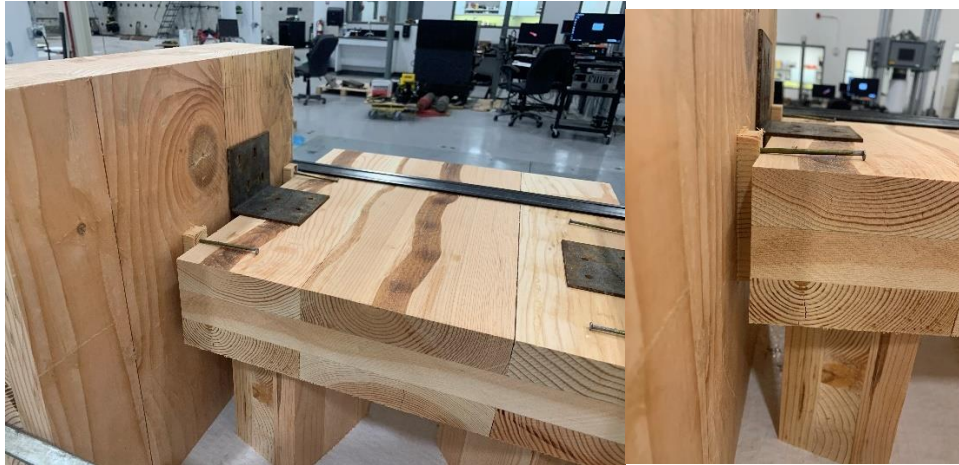
Figure 3.19. Construction of Specimen 9 and 10

3.3.   Instrumentation

The instrumentation plan for the connection tests centered around one main goal –

measuring force and total displacement of each connection. These were the two most important

measurements, with the displacement being the input file as well. The test had an input

displacement and the force that was generated was measured by the load cell. A few other

displacement measurements were taken but were extraneous to the data that was needed for

fitting to numerical models. Total displacement measurements were taken at the center of each

connection and at the center the of the specimen to ensure there was in-plane rotation happening

that could influence the quality of the results. A displacement measurement was taken at the

center of the specimen out-of-plane to ensure there was no rotation in that direction, which was

quickly determined that it was a non-issue. Both in-plane and out-of-plane rotation were

determined to be very small with respect to the magnitude of the total displacement.

The main displacement measurement was captured from the load frame to the bottom

fixture (this is the side of the specimen that moves as the top is fixed). All displacement

measurements were taken with 12-inch string potentiometers except for the out-of-plane

displacement measurement, which was taken with a 4-inch string potentiometer. The

instrumentation plan can be seen in Table 3.7 and Figure 3.20, while additional photos have been

included to show how the instrumentation plan was executed in the lab in Figure 3.21 and Figure

3.22.

Table 3.7. Instrumentation Summary

Channel	Device	Measurement
1	Load Cell	Force from load cell
2	Frame Displacement	Frame Displacement
3	SP-1 (12 in)	Displacement at center of specimen
4	SP-2 (12 in)	Displacement at right connection point
5	SP-3 (12 in)	Displacement at left connection point
6	SP-4 (12 in)	Displacement from frame to bottom fixture
7	SP-5 (4 in)	Out-of-Plane displacement
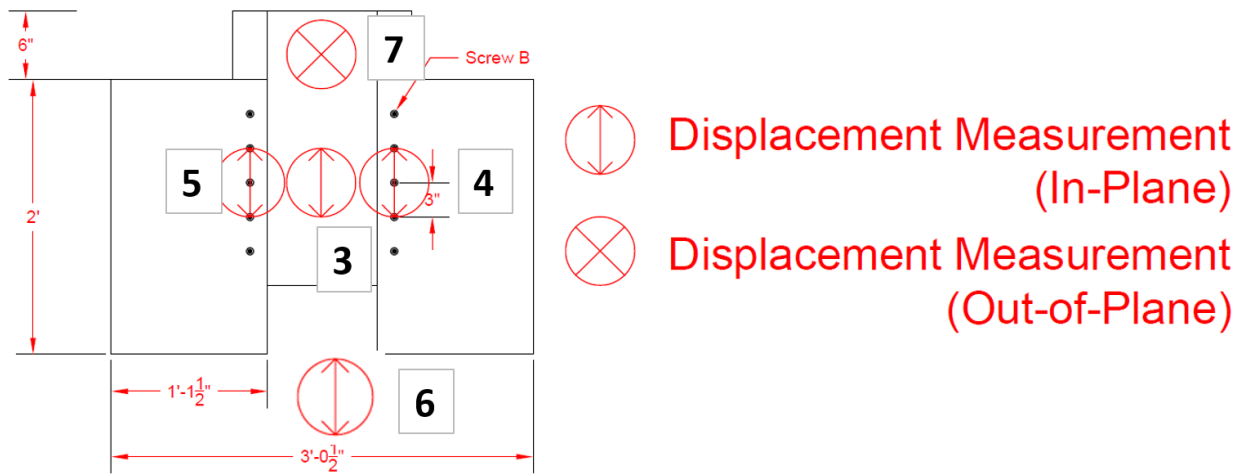
Figure 3.20. Instrumentation Locations on the Specimen
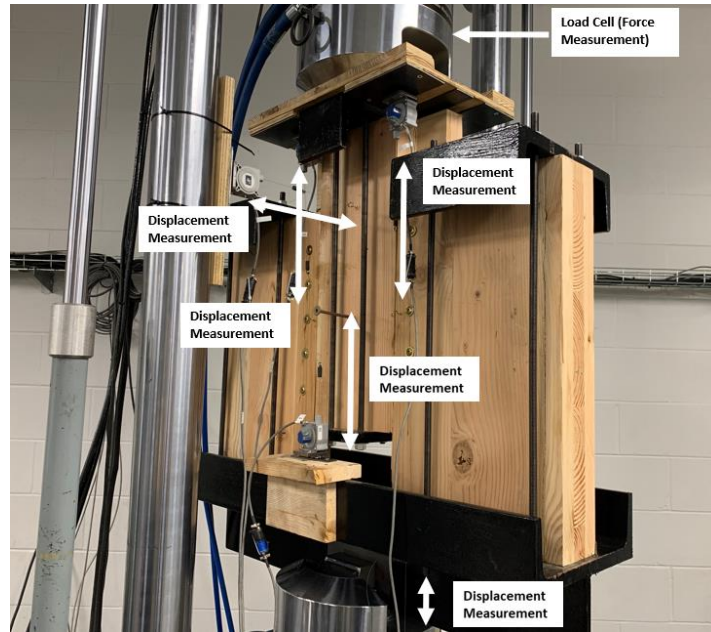
Figure 3.21. View of Panel-to-Panel Test Instrumentation
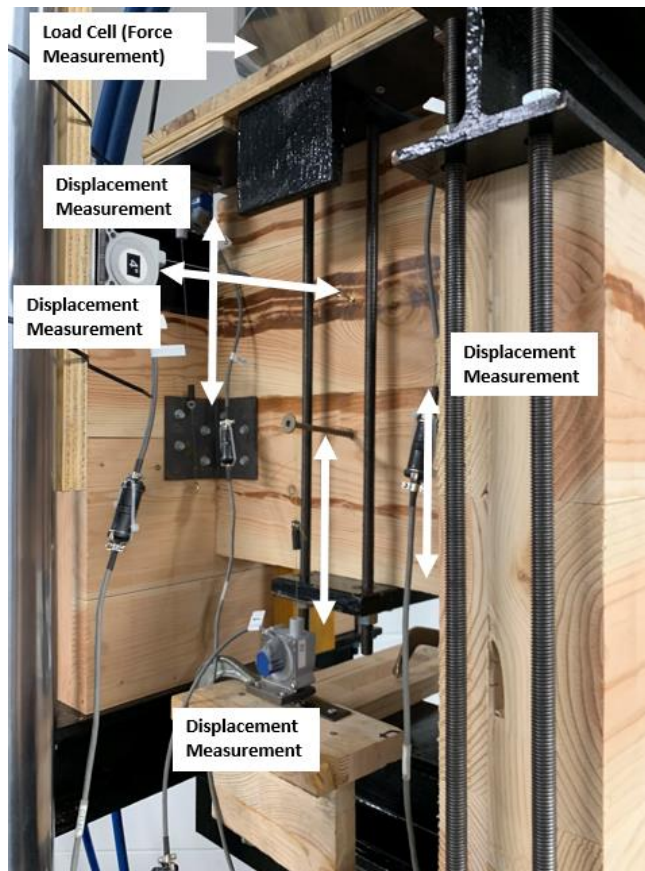
Figure 3.22. View of Wall-to-Floor Test Instrumentation

3.4. Testing

3.4.1. Loading Protocol

3.4.1.1. Monotonic Load Protocol

For monotonic application of load, a displacement-controlled test was chosen. The goal of the monotonic tests was for them to be quasi-static, so a relatively slow displacement rate was chosen. Each configuration was subject to the same monotonic load, with the displacement being controlled at 0.2 inches/minute. The test was run until it was observed that the specimen had reached a maximum load and then stopped at about 50% of its post-peak load. This gave the full load-displacement curve that was needed to develop the cyclic loading profiles.

3.4.1.2. Cyclic Load Protocol

The CUREE testing protocol was used for the cyclic tests which was developed by the CUREE-Caltech Wood-frame Project that was developed following the 1994 Northridge, California Earthquake. It was found after the Northridge earthquake that damage to wood frame construction was the predominate failure mechanism in nearly every category of loss – human life, property, and functionality (Krawinkler, Parisi et al. 2001). The objective of that project was to develop a design method for wood frame connections that was experimentally and theoretically validated and to make construction more efficient than before (Krawinkler, Parisi et al. 2001). This led to a standardization of connection testing protocol and input displacement profiles that could be used to ensure a given behavior that a connection exhibits is prohibitive to catastrophic failure during a major seismic event. The load protocol that came out of the project is a quasi-static, displacement controlled profile that seeks to imitate the damage caused by an earthquake whose probability of exceedance is 10% in 50 years (Krawinkler, Parisi et al. 2001).

47

The displacement-controlled input is defined by a reference deformation, Δ, that is determined by the monotonic test of the specimen taken to failure. To determine the reference deformation, the monotonic force-displacement curve was inspected. The reference deformation is given as 60% of the monotonic deformation capacity. The monotonic deformation capacity is defined as the first time when the applied load drops to 80% of the peak load reached during the test. Two monotonic tests were performed for each configuration to ensure the first test was not just an outlying data point.

Once the reference deformation is defined for the cyclic test, the displacement profile can be generated per the CUREE protocol. More specifically, the loading history consists of initiation cycles, primary cycles, and trailing cycles. The initiation cycles are the first six cycles that are very small, but just ensure that the leading equipment, measurement devices, etc. are working properly. A primary cycle is one that is larger than the preceding cycles and is then followed by smaller trailing cycles. A trailing cycle is defined as 75% of the magnitude of the preceding primary cycle. The displacement profile is defined as follows:

- Six initiation cycles with an amplitude of 0.05Δ

- A primary cycle with an amplitude of 0.075Δ

- Six trailing cycles

- A primary cycle with an amplitude of 0.1Δ

- Six trailing cycles

- A primary cycle with an amplitude of 0.2Δ

- Three trailing cycles

- A primary cycle with an amplitude of 0.3Δ

- Three trailing cycles

- A primary cycle with an amplitude of 0.4Δ

- Two trailing cycles

- A primary cycle with an amplitude of 0.7Δ

- Two trailing cycles

- A primary cycle with an amplitude of 1.0Δ

- Two trailing cycles (Krawinkler, Parisi et al. 2001)

All cyclic tests followed this protocol for the development of their loading profiles. The cyclic

loading profiles for all specimens with loading rate being 2.4 inches/minute can be seen in Figure

3.23.
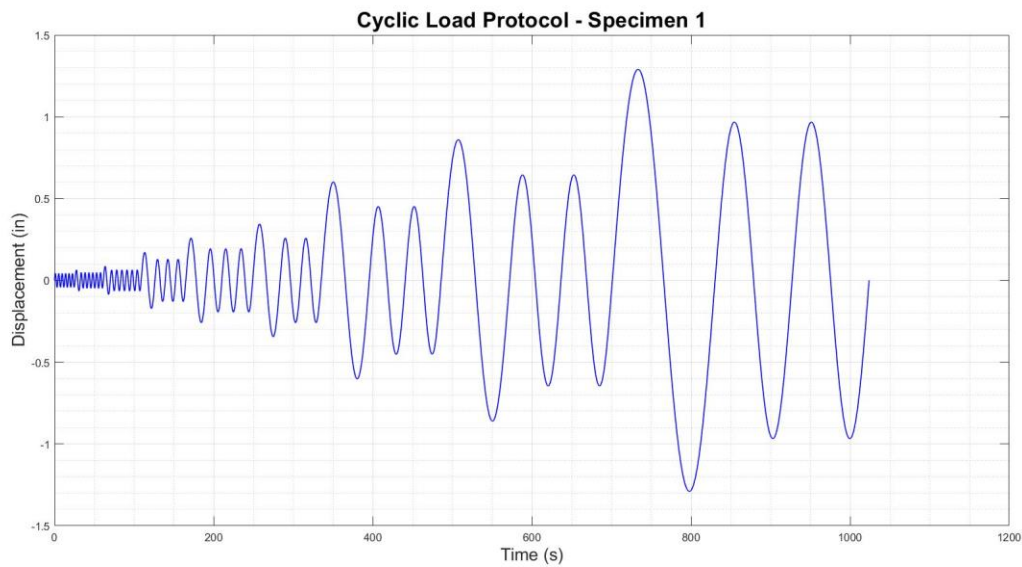
Figure 3.23. Specimen 1 Cyclic Loading Profile
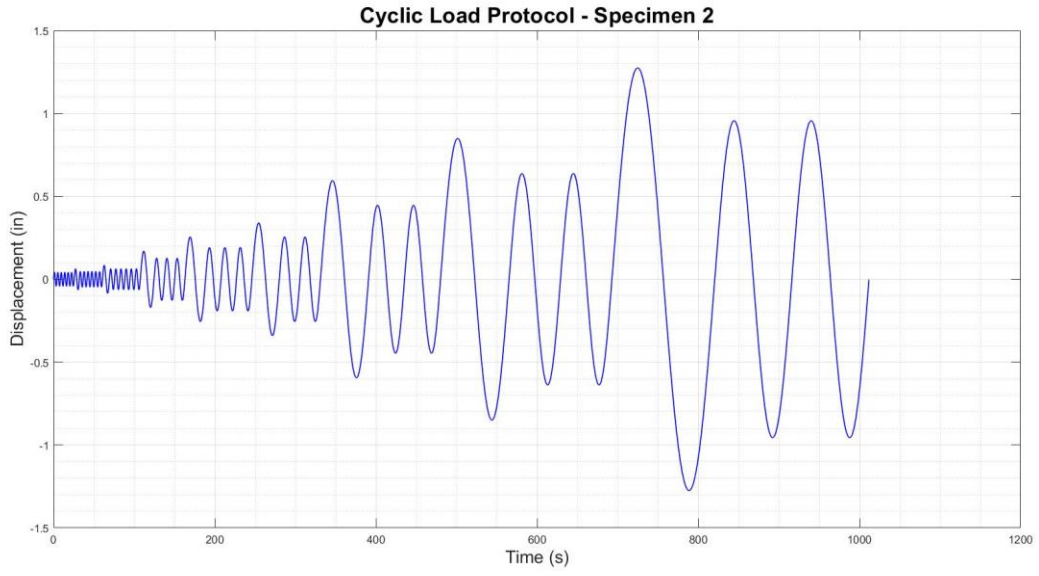
Figure 3.24. Specimen 2 Cyclic Loading Profile
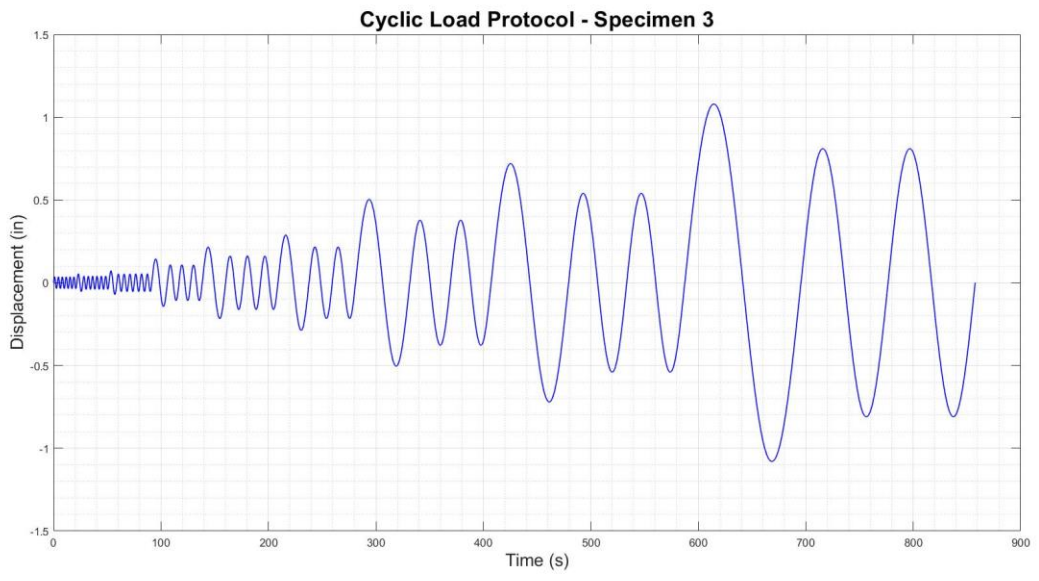
Figure 3.25. Specimen 3 Cyclic Loading Profile
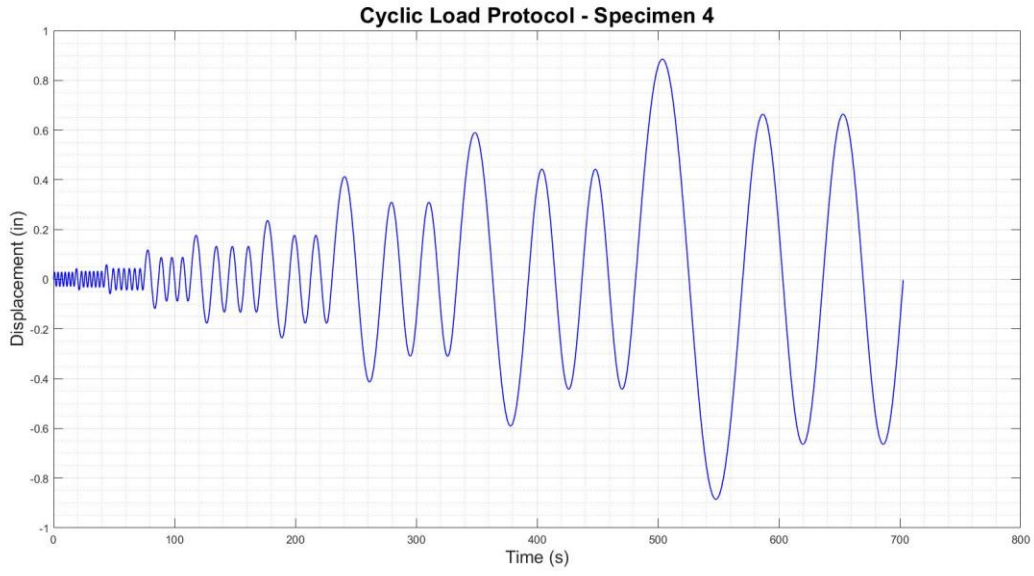
Figure 3.26. Specimen 4 Cyclic Loading Profile
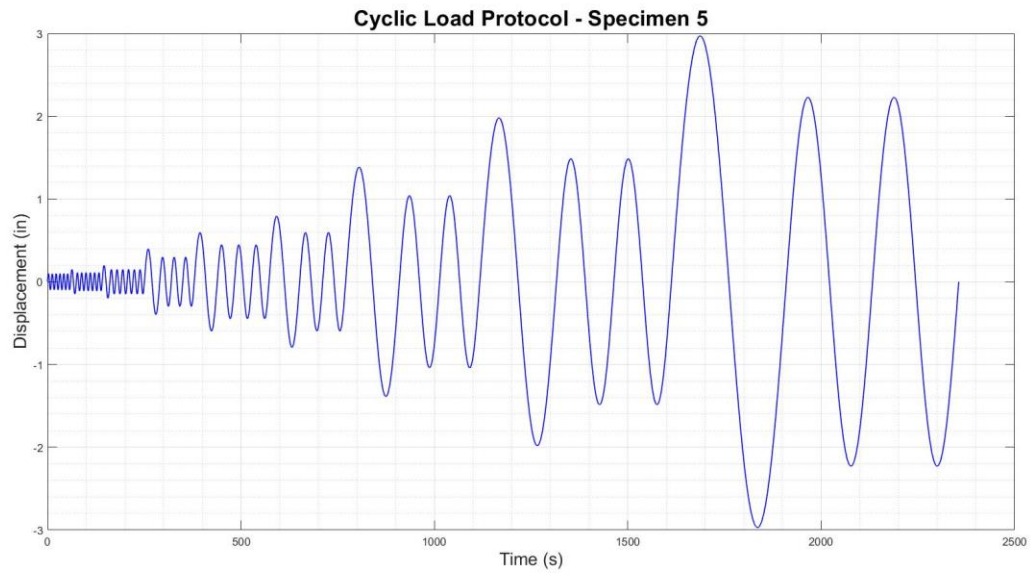
Figure 3.27. Specimen 5 Cyclic Loading Profile
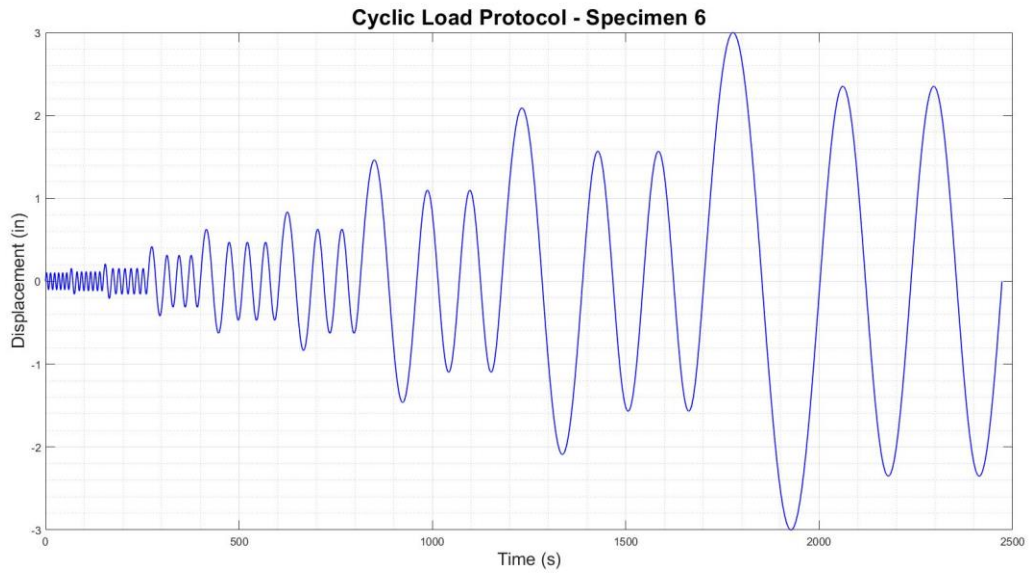
Figure 3.28. Specimen 6 Cyclic Loading Profile
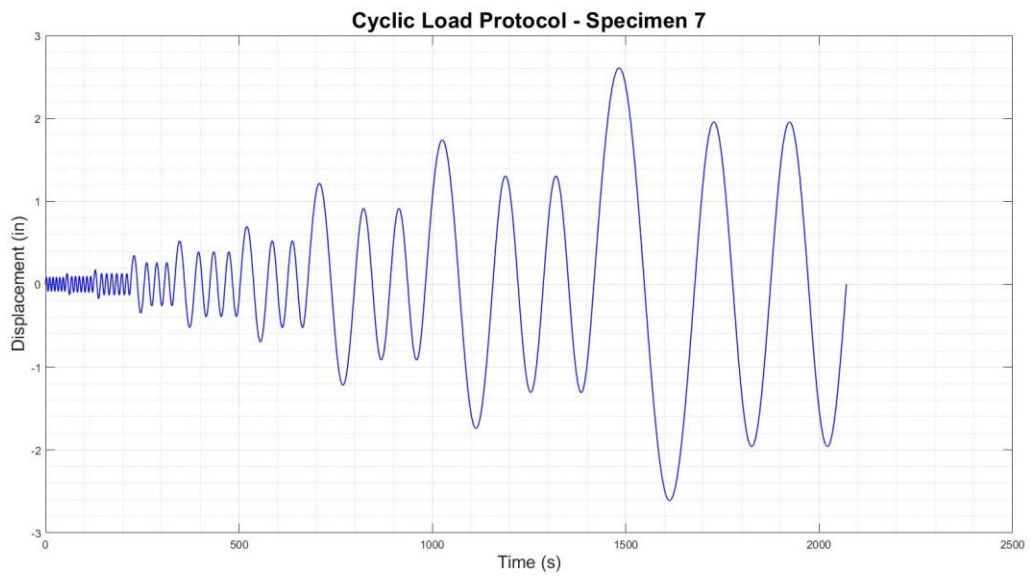
Figure 3.29. Specimen 7 Cyclic Loading Profile
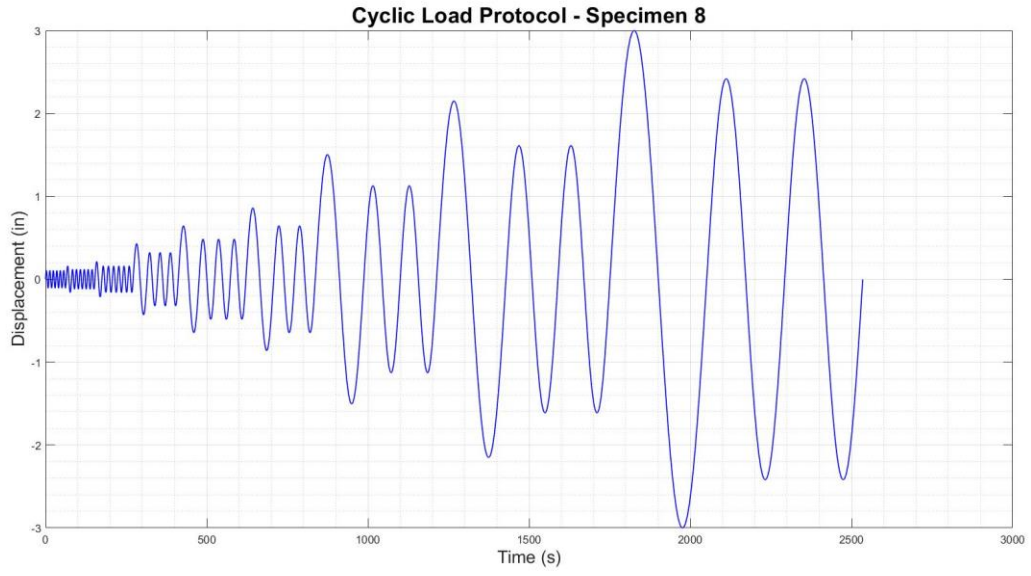
Figure 3.30. Specimen 8 Cyclic Loading Profile
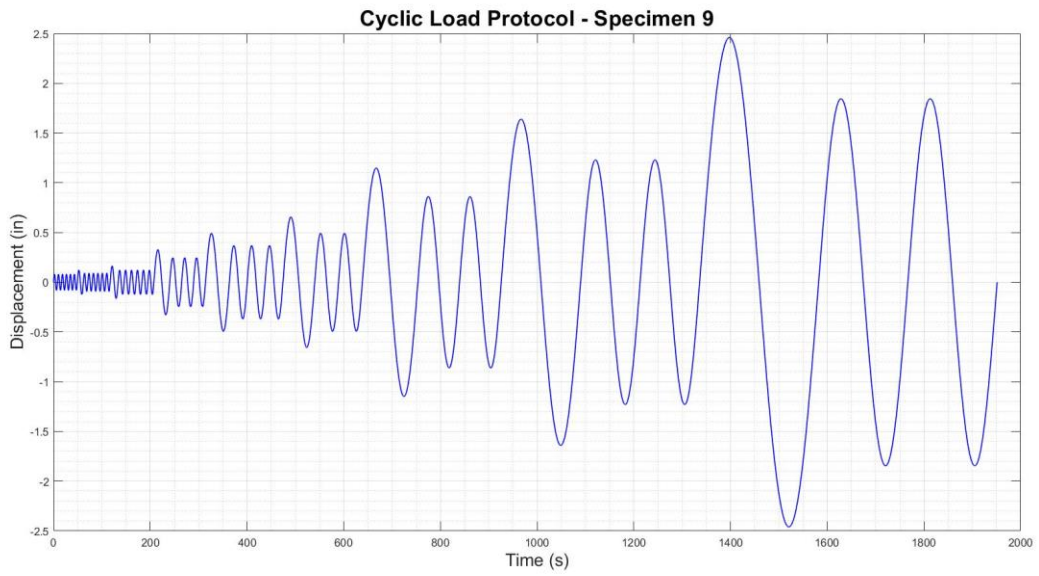
Figure 3.31. Specimen 9 Cyclic Loading Profile
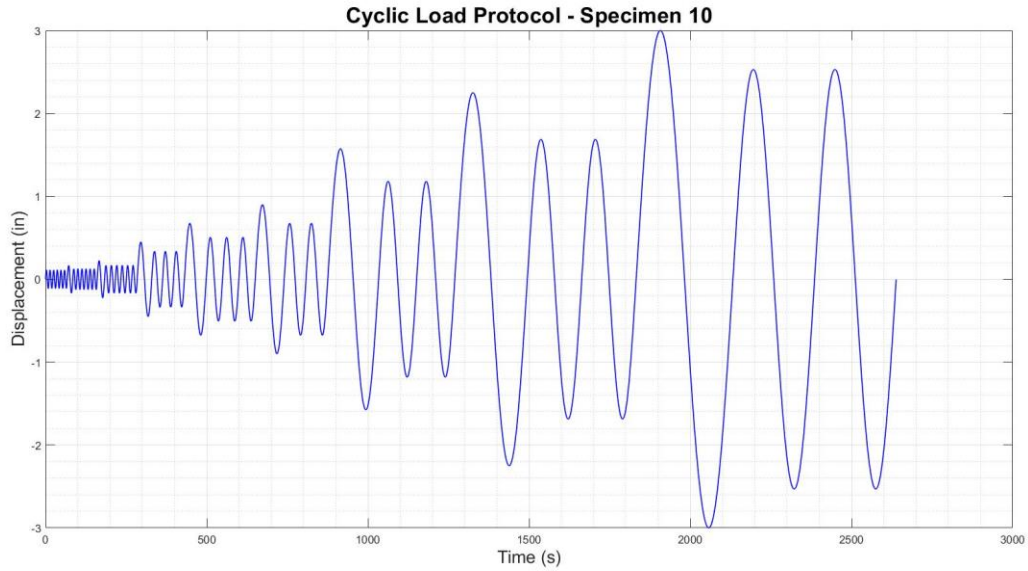
Figure 3.32. Specimen 10 Cyclic Loading Profile

3.4.2. Observed Failure Modes

All strength predictions were calculated per NDS and a failure mode was also predicted based on the dimensions of each connection method and fastener. This information is tabulated, along with the results of each test in

Table 3.8. In this table, the results for both monotonic and cyclic tests are compared with the predicted strength calculated using the LRFD design method to show an effective factor of safety that the design provides. The failure mode that is recorded from the experimental results was the failure observed during the monotonic tests, as this is best compared to what the code predicts.

Table 3.8. Summary of Test Results

| Specimen | Design | | | Experimental Result | | | Experimental to LRFD Design Ratio | |
| | Force Capacity (kip) | | Failure Mode | Force Capacity (kip) | | Failure Mode | | |
	ASD	LRFD		Monotonic	Cyclic		Monotonic	Cyclic
1	0.183	0.395	IV	1.839	1.296	IV	4.652	3.279
2	0.154	0.333	IV	1.991	1.611	IV	5.985	4.843
3	0.286	0.618	IV	1.650	1.239	IV	2.671	2.006
4	0.322	0.696	IV	1.574	1.358	IV	2.263	1.952
5	0.146	0.315	III_s	1.187	0.894	III_s	3.764	2.835
6	0.132	0.285	III_s	1.249	1.136	III_s	4.381	3.984
7	0.175	0.378	III_s	1.026	0.821	III_s	2.714	2.172
8	0.175	0.378	III_s	1.217	0.949	III_s	3.220	2.511
9	0.175	0.378	III_s	0.718	0.550	III_s	1.899	1.455
10	0.175	0.378	III_s	0.956	0.692	III_s	2.529	1.831

(all values are given per fastener)

As seen in Table 3.8, every configuration outperformed the design value, and often by a significant amount. This should be expected as there are many factors of safety inherent in the NDS design process. Additionally, the strength of every fastener is much greater when subjected to purely monotonic loading. Strength and stiffness degradation occurs when subjecting the fasteners to cyclic loads, but the amount to which effect is present and is highly dependent on the type of configuration that is tested.

The failure modes that occurred during monotonic tests and cyclic tests were markedly different, as would be expected. During monotonic loading, the primary mode of failure for configurations 1 and 2 were the formation of two plastic hinges in the fasteners with the screws eventually either pulling out of the wood or failing in shear (associated with NDS failure mode IV). This can be seen in Figure 3.33.

Figure 3.33. Monotonic Fastener Failure

For configurations 3 and 4, the predominate mode of failure during monotonic tests was the same

for fasteners installed at 90 degrees, but the fasteners that were installed at 45 degrees failed in

withdrawal. However, it should be noted that this configuration was observed to stay together

extremely well, even after failure. Once there was little strength left to be used in the specimen, it

would not come apart and even resisted further damage. A photo of one specimen that did fail

can be seen in Figure 3.34.
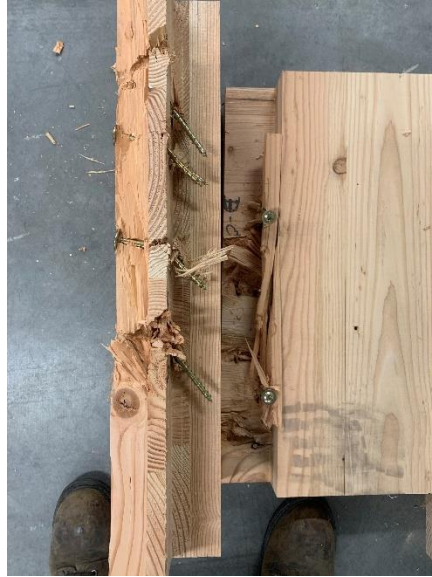
Figure 3.34. Fasteners Failing in Shear and Withdrawal

Configurations 5 and 6 had failures that were dominated by the fasteners forming a single plastic

hinge at the location of the spline (associated with NDS failure mode III_s). plastic hinge at this

location tore through much of the CLT during loading, but it eventually gave way to a

withdrawal failure from the CLT specimen, as shown in Figure 3.35Figure 3.35.
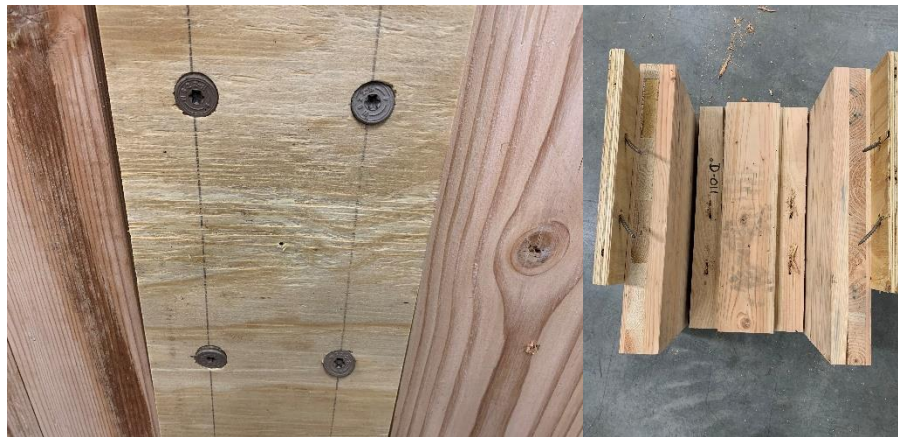
Figure 3.35. Failure of Fasteners at Spline

Configurations 7 and 8 failed in a way that involved the formation of a plastic hinge at the

interface of the steel angle bracket and the CLT, with crushing of the wood occurring (associated

with NDS failure mode III_s). Additionally, the angle bracket exhibited significant plastic

57

deformation, which only aided in prying the fasteners from the CLT and degrading the stiffness of the specimen even further. Failure of the fasteners and the angle bracket occurred almost simultaneously. Photos of this can be seen in Figure 3.36.
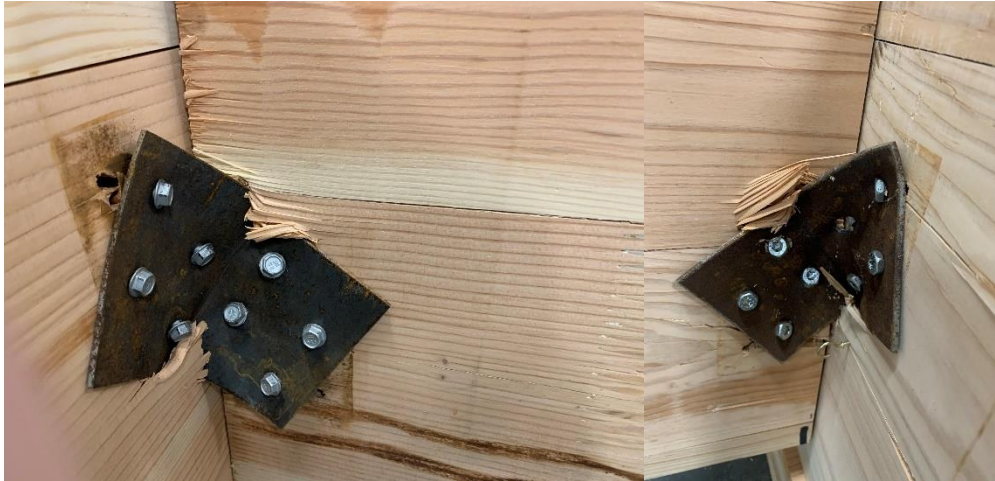
Figure 3.36. Load-Bearing Wall-to-Floor Monotonic Test Failure

Configurations 9 and 10 failed in a way that involved the formation of a plastic hinge at the interface of the steel angle bracket and the CLT, with significant crushing of the wood occurring (associated with NDS failure mode III_s). What added to the amount of deformation that occurred was the significant plastic deformation in the angle bracket as it yielded at the same time as the fasteners crushed the wood. The amount of plastic deformation in the angle bracket was greater for the non-load bearing tests (9 and 10) than it was for the load-bearing configurations (7 and 8) because there was a half-inch gap specified between the wall and the floor as will be typical for this type of construction in industry/practice. It was determined that when the angle bracket is allowed additional rotation and has a greater amount of moment applied because its attachment length is longer that more plastic deformation is inevitable. Photos of this can be seen in Figure 3.37.

Figure 3.37. Non-Load-Bearing Wall-to-Floor Monotonic Test Failure

During the cyclic tests, the failure modes were very similar to those observed in the monotonic tests, with the failure coming at smaller loads. However, in every instance, wood crushing was far more pronounced and caused many fasteners to rupture at the point of plastic hinge development. Photos of fasteners that failed during the cyclic test can be found in Figure 3.38.

| (a) | (b) |
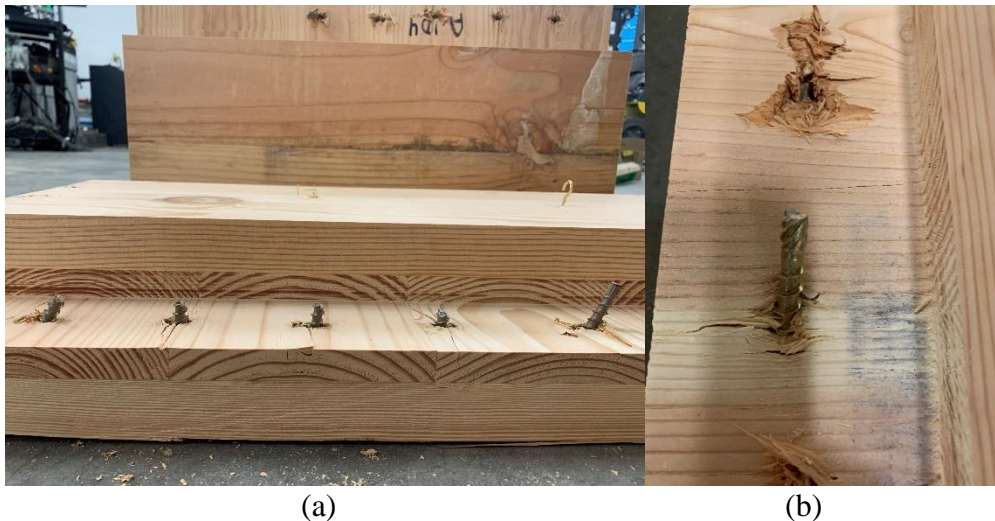
Figure 3.38. Half-Lapped, Specimen 1 (a) and 2 (b), Cyclic Test Failure

Specimens 3 and 4 had a unique quality that was demonstrated during cyclic testing. Because half of the fasteners were installed at 90 degrees and the other half installed at 45 degrees, the benefits of both installation angles were observed. The specimens exhibited high stiffness and high ductility. With the angled fasteners being installed in opposite directions, the load was

always resisted by a fastener in shear and withdrawal. This led to failure mainly in the crushing of wood as the screws had a difficult time pulling out of the specimen. Photos of this can be seen in Figure 3.39.

<div align="center">
(a)   (b)   (c)
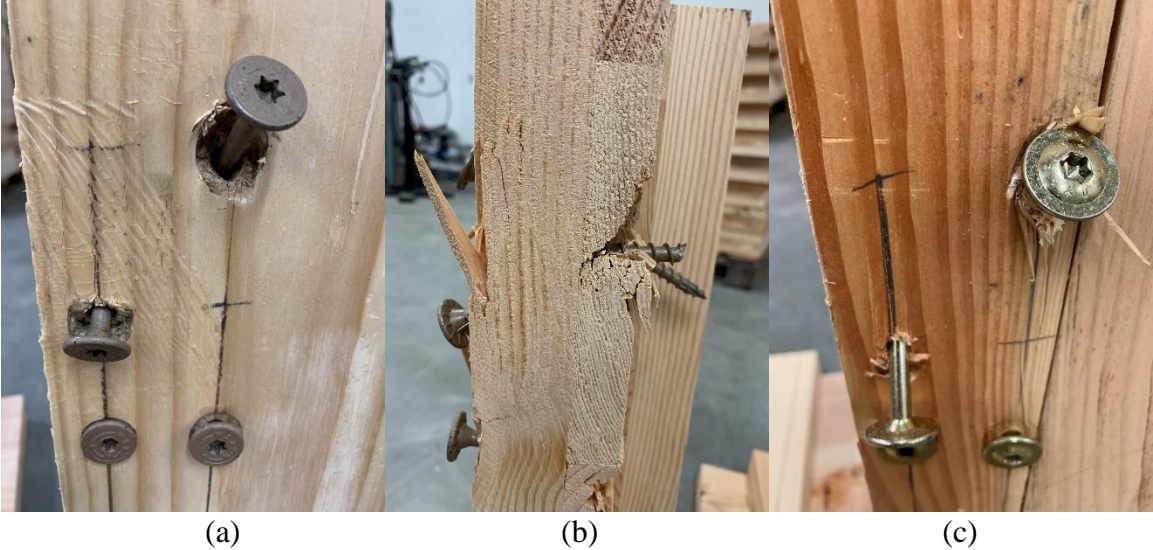
Figure 3.39. Half-Lapped, Specimen 3 (a)(b) and 4 (c), Cyclic Test Failure
</div>

Failure of specimens 5 and 6 during the cyclic tests was very similar to their behavior during monotonic tests. Screws formed a plastic hinge at the interface of the spline and CLT, with bearing occurring in the CLT (associated with NDS failure mode III_s). Photos of this can be seen in Figure 3.40(a) (specimen 5) and Figure 3.40(b) (specimen 6).

<div align="center">
(a)   (b)
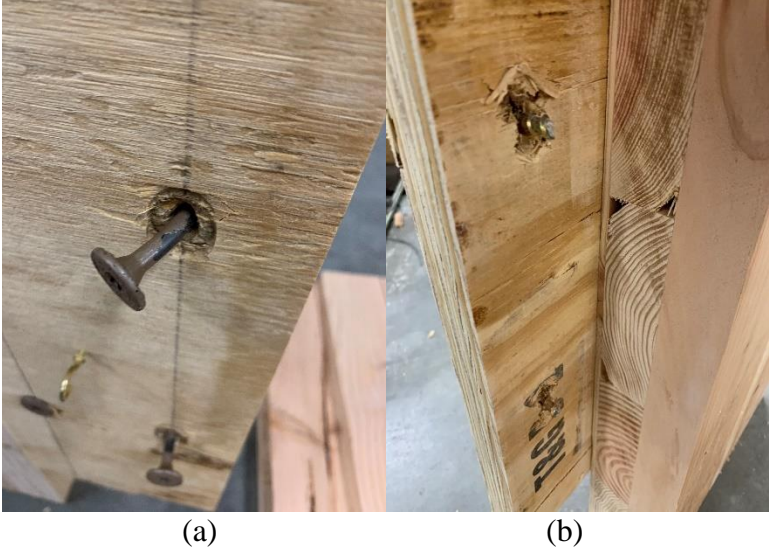
Figure 3.40. Spline Cyclic Test Failure
</div>

Specimen 7 and 8, during cyclic testing, had failures that were defined by NDS failure mode III$_s$. A plastic hinge formed in the screw between the CLT and angle bracket and often ruptured at this location. The behavior was dominated by wood crushing, but also by the plastic deformation of the angle brackets. Photos of this can be seen in Figure 3.41(a) (specimen 7) and Figure 3.41(b)(c) (specimen 8).

| (a) | (b) | (c) |
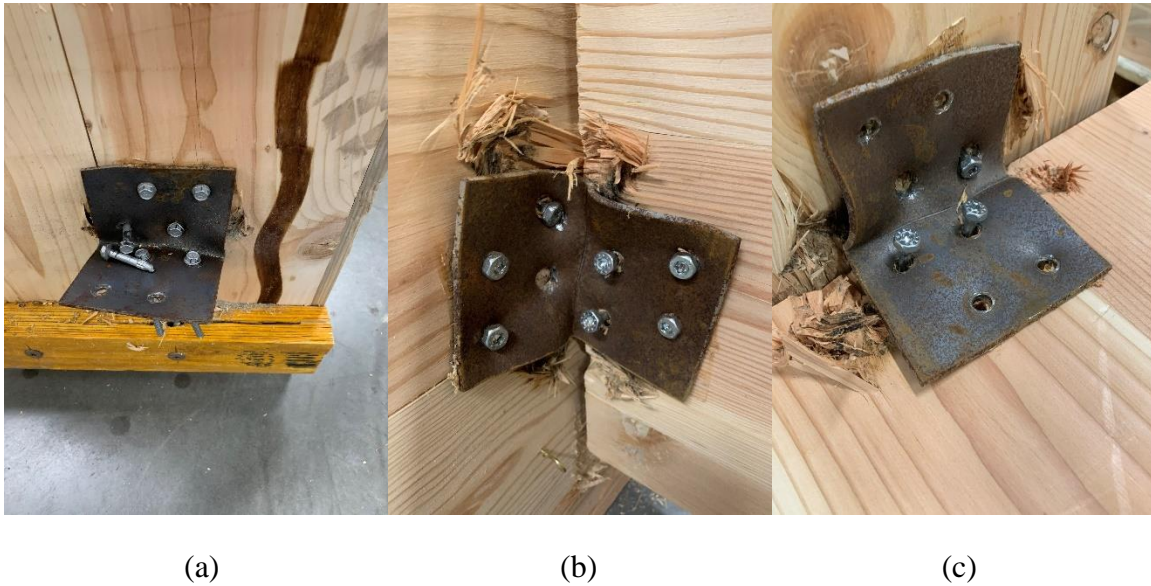
Figure 3.41. Load-Bearing Wall-to-Floor Cyclic Test Failure

The non-load-bearing wall-to-floor specimens' behavior in the cyclic tests was largely dominated by the plastic deformation of the angle brackets. However, a similar failure of the fasteners to the load-bearing specimens did occur. A significant amount of wood crushing was observed from bearing of the screws, and from bearing of the angle bracket as it tried to rotate. Photos of this can be seen in Figure 3.42(a) (specimen 9) and Figure 3.42(b) (specimen 10).

(a)   (b)

Figure 3.42. Non-Load-Bearing Wall-to-Floor Cyclic Test Failure

3.4.3. Results

3.4.3.1. Monotonic Test Results

The results of the monotonic tests are presented in this section including various forms of presentation: (i) tabulated peak load, reference displacement and load per fastener for each specimen as an average of the two tests performed (Table 3.9), (ii) force-displacement curves for all monotonic tests conducted (Figure 3.43), and (iii) force-displacement curves of individual monotonic tests (Figure 3.44 to Figure 3.53).

Table 3.9. Monotonic Test Results

Specimen	Monotonic Peak Load (kip)	Reference Displacement Δ_{ref} (in)	Monotonic Load per fastener (kip)
1	18.39	0.86	1.839
2	19.91	0.85	1.991
3	26.40	0.72	1.650
4	25.18	0.59	1.574
5	9.50	1.98	1.187
6	9.99	2.09	1.249
7	16.42	1.74	1.026
8	19.47	2.15	1.217
9	11.49	1.64	0.718
10	15.30	2.25	0.956

(Results are the average of 2 tests)
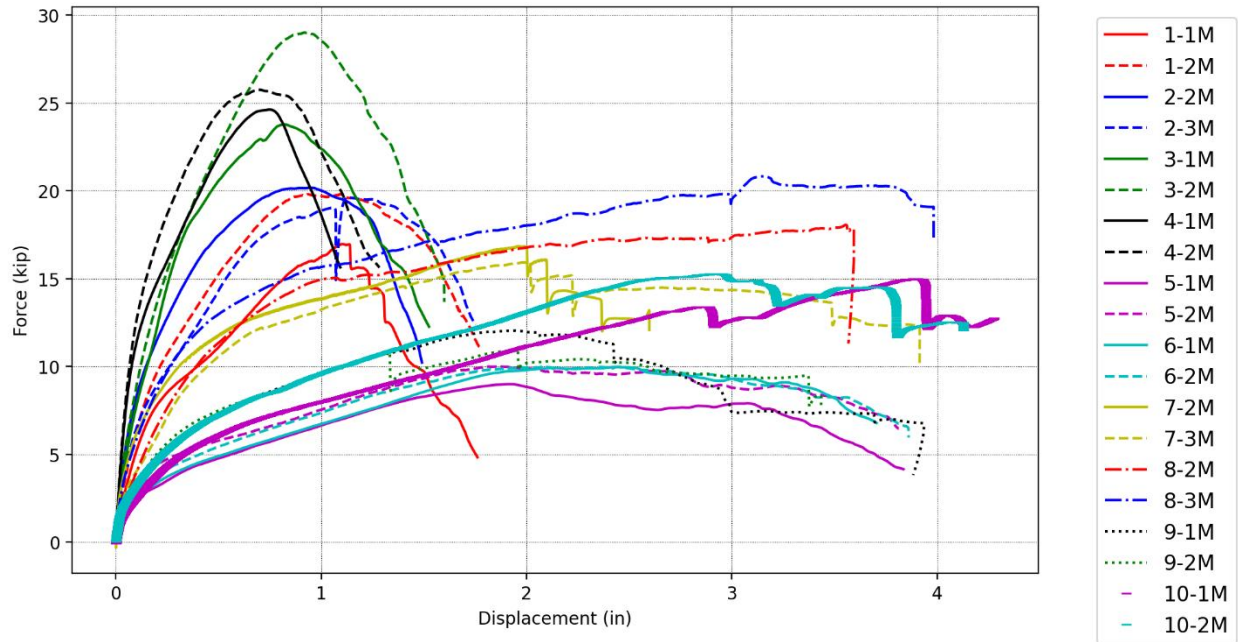
Figure 3.43. All Monotonic Results
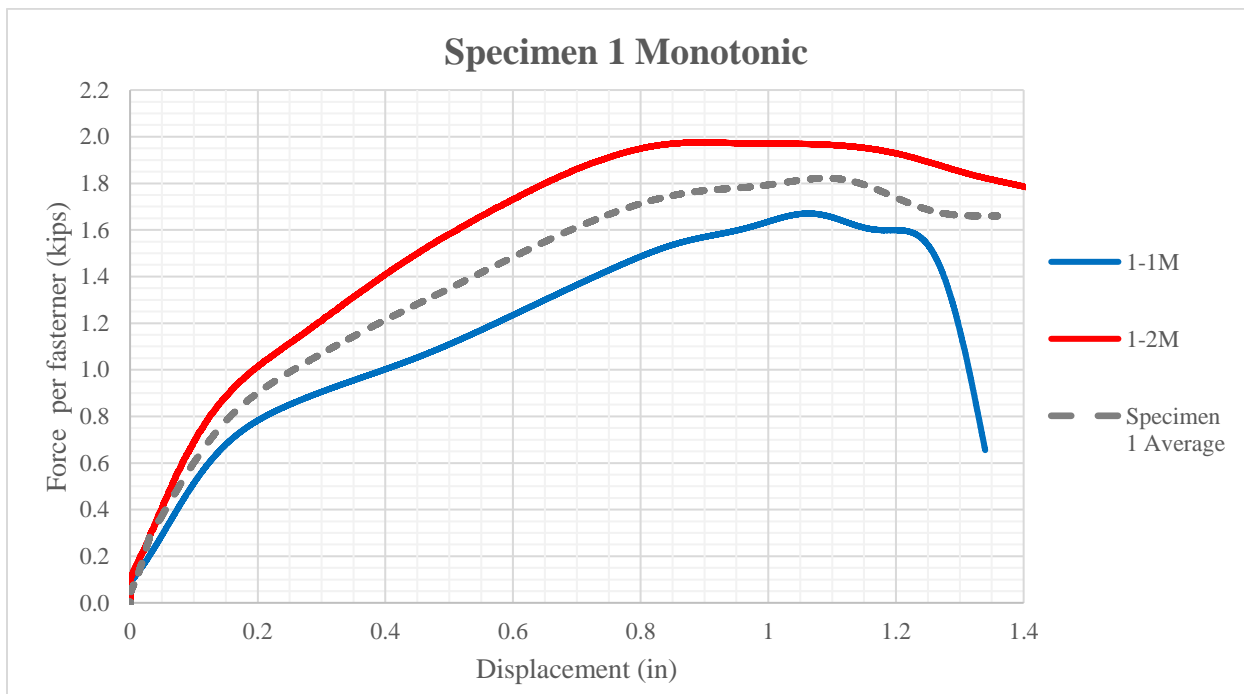
Figure 3.44. Specimen 1 Monotonic Results
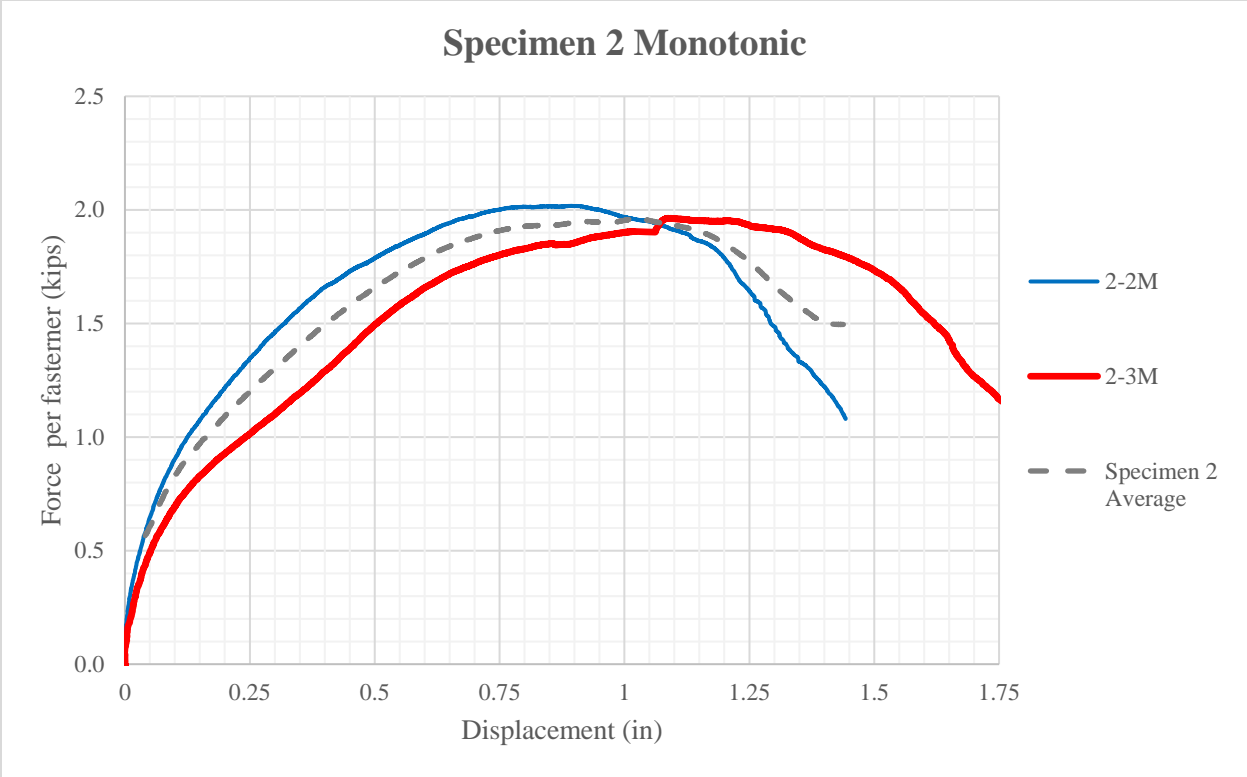
Figure 3.45. Specimen 2 Monotonic Results
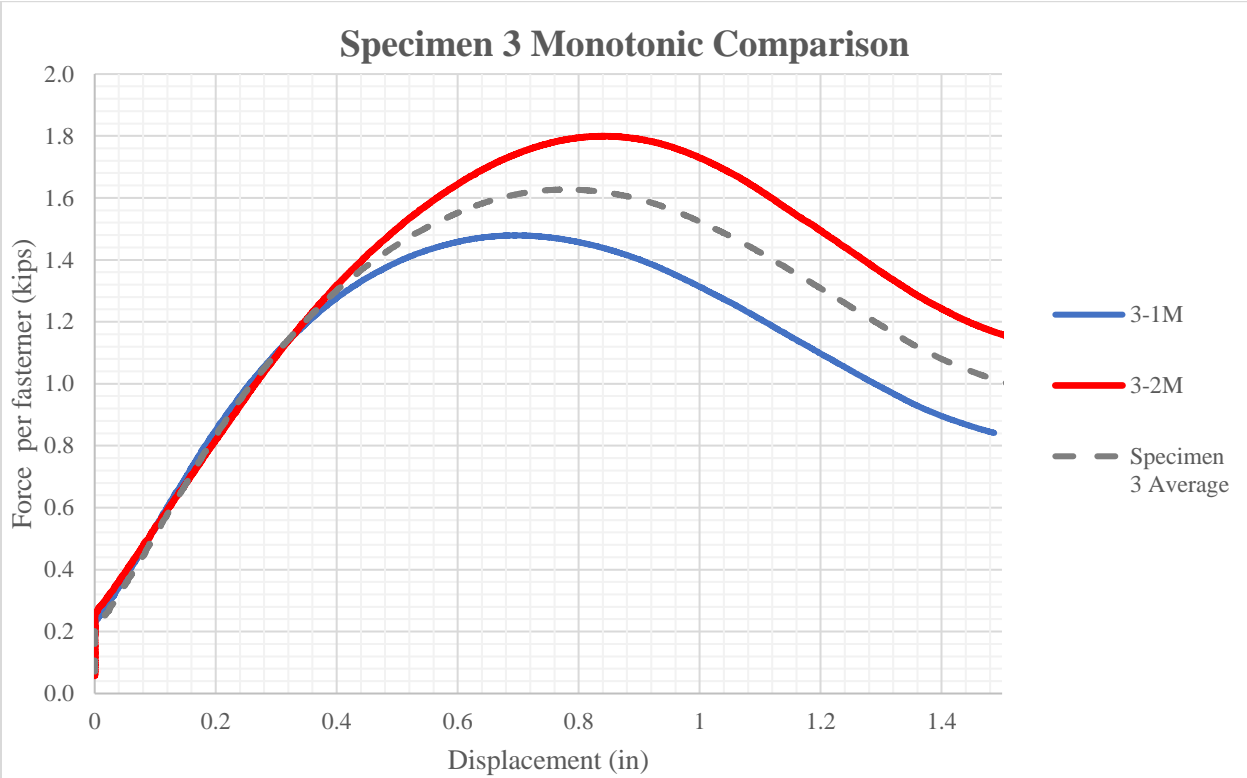
Figure 3.46. Specimen 3 Monotonic Results
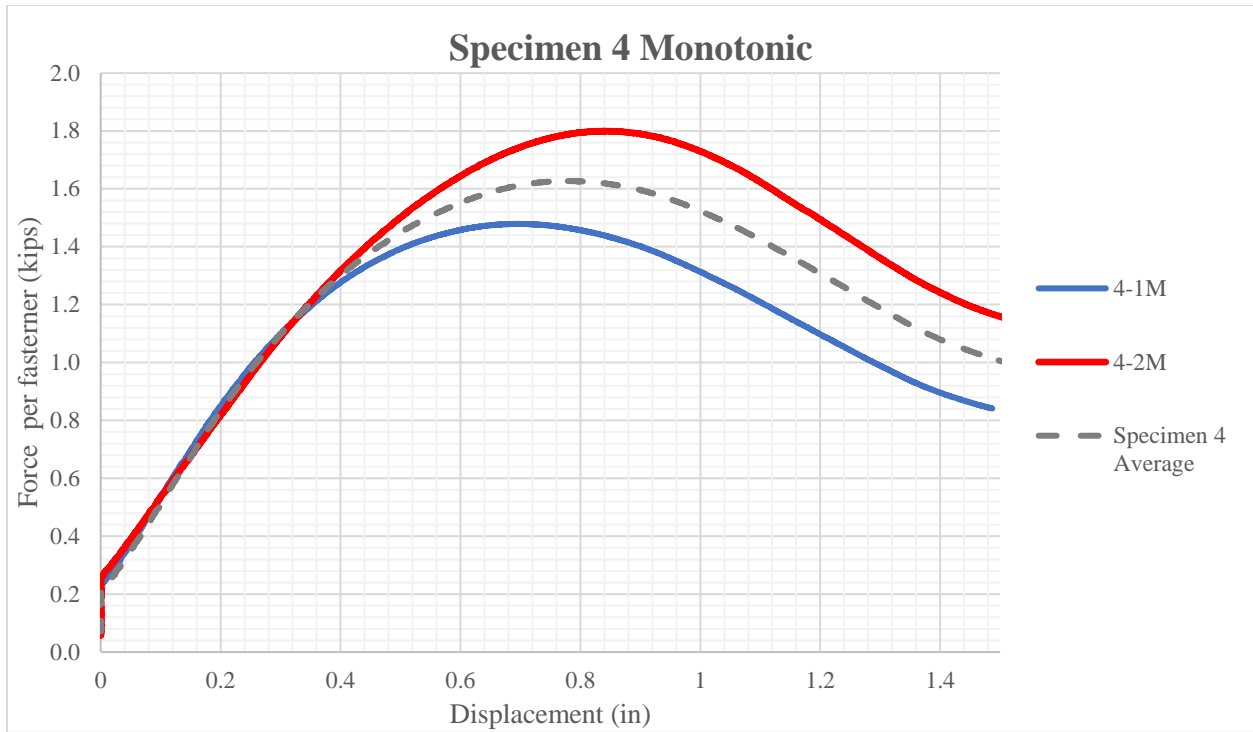
Figure 3.47. Specimen 4 Monotonic Results
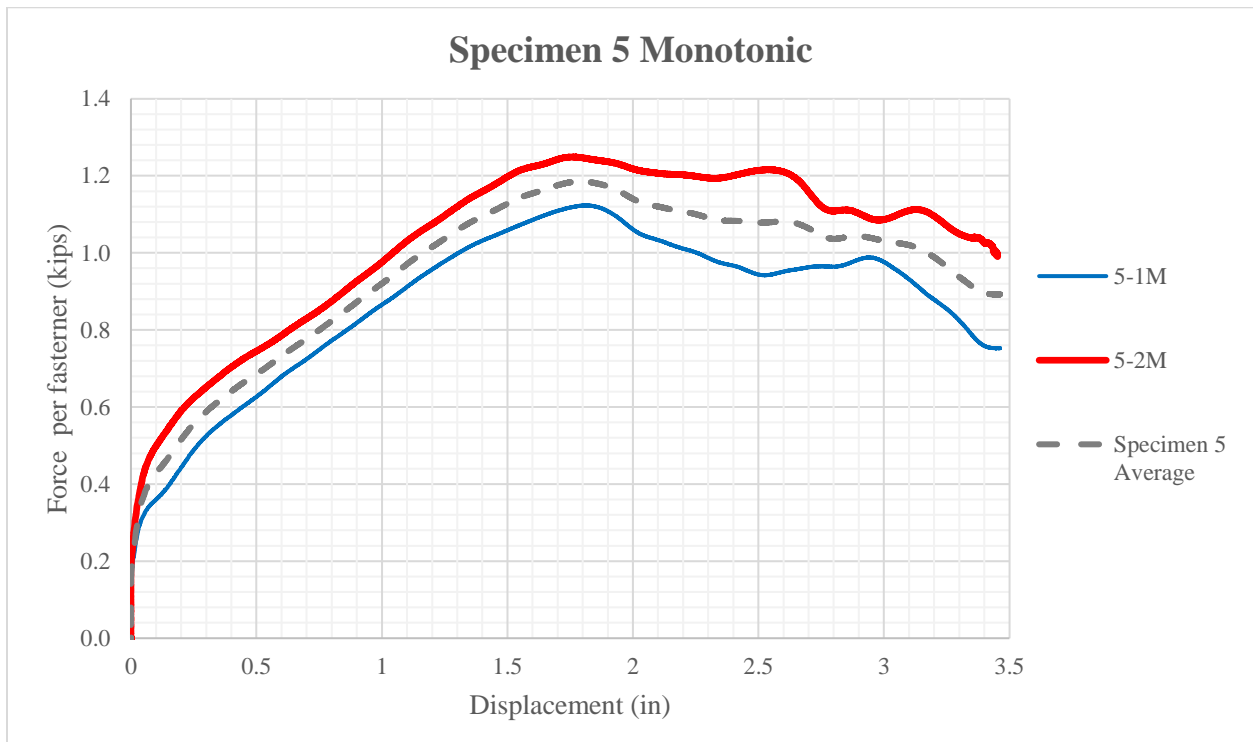
Figure 3.48. Specimen 5 Monotonic Results
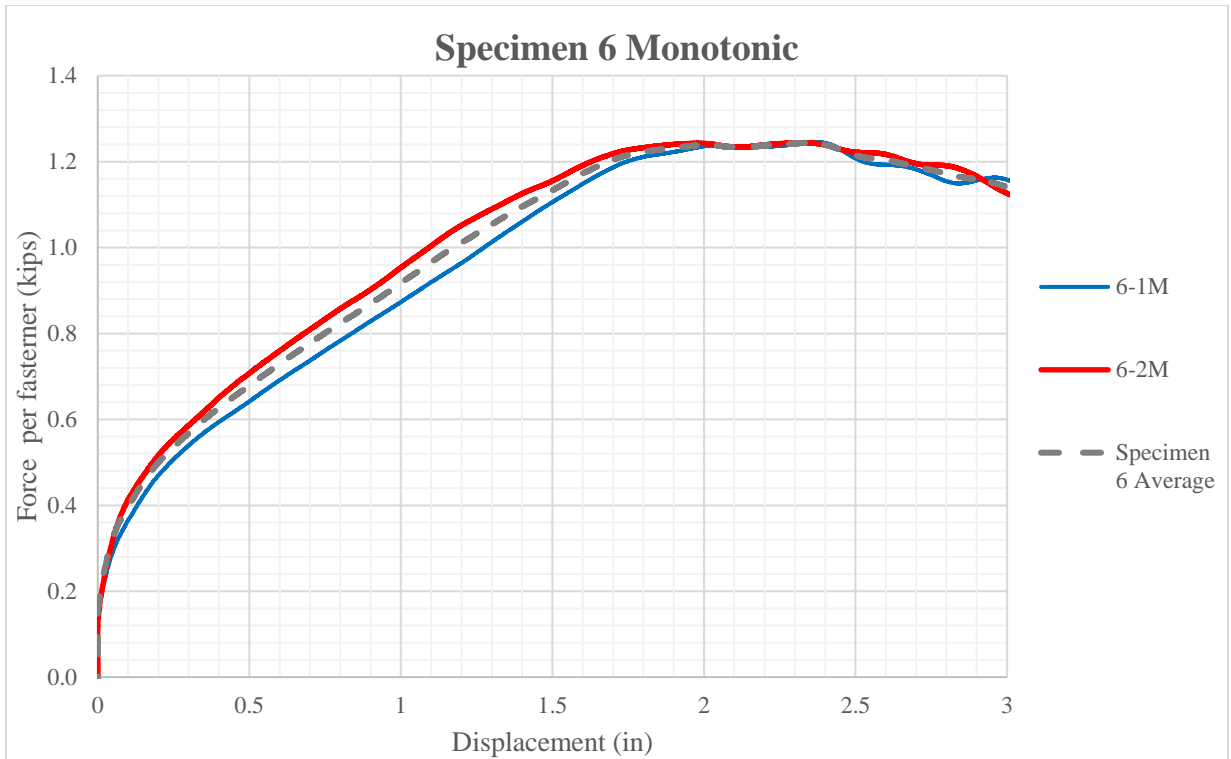
Figure 3.49. Specimen 6 Monotonic Results
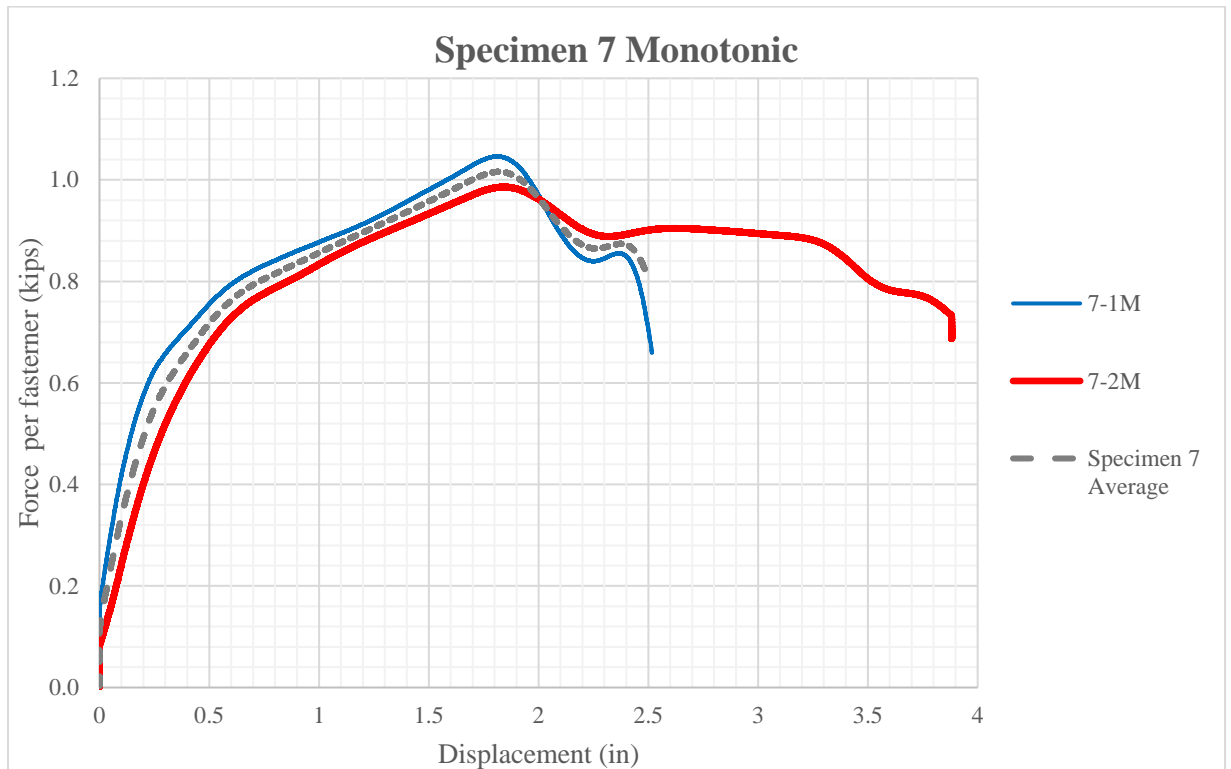
Figure 3.50. Specimen 7 Monotonic Results
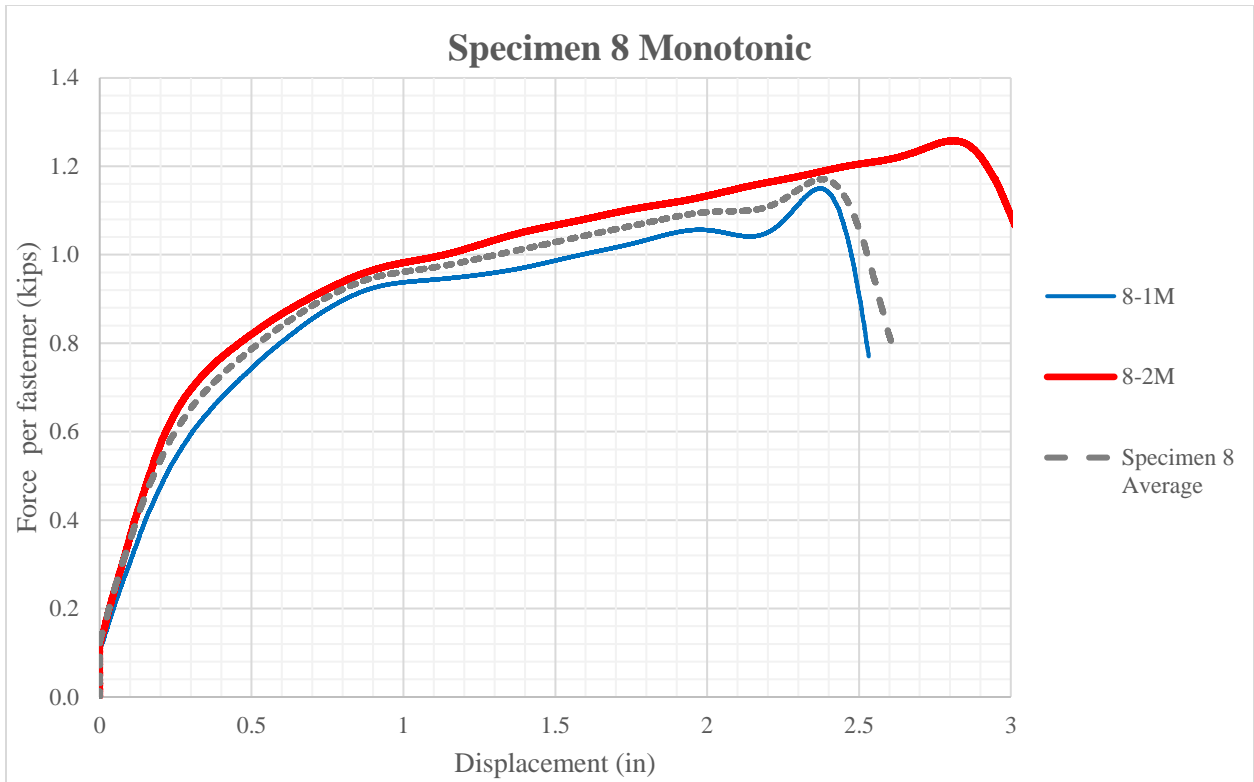
Figure 3.51. Specimen 8 Monotonic Results
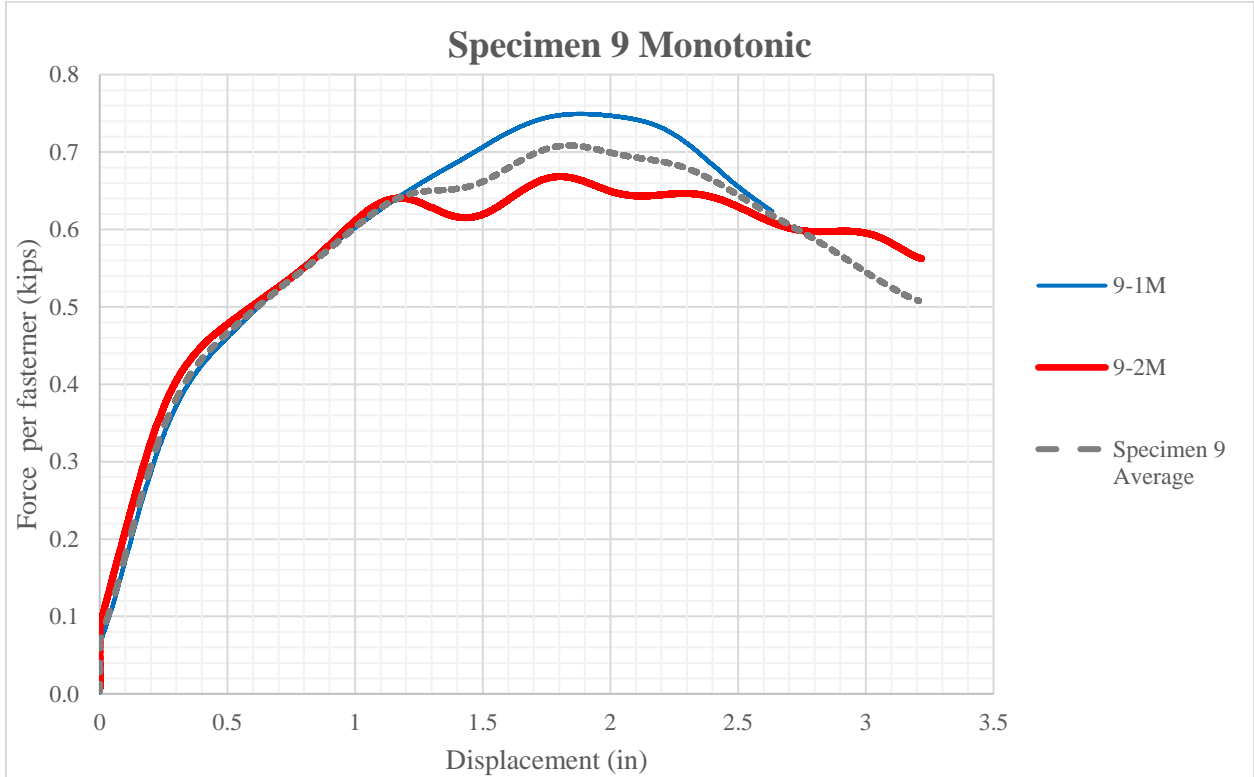
Figure 3.52. Specimen 9 Monotonic Results
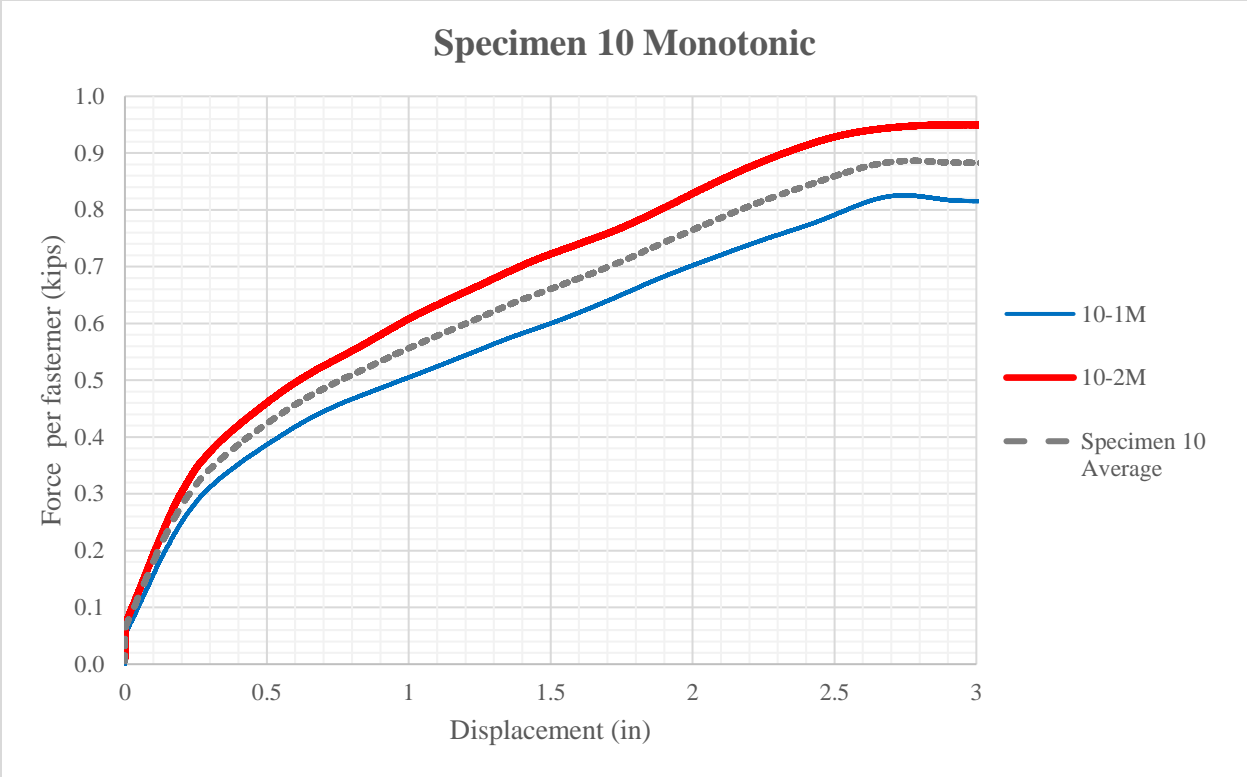
Figure 3.53. Specimen 10 Monotonic Results

3.4.3.2. Cyclic Test Results

The results of the cyclic tests are summarized herein and are presented in the form of force-displacement curves for each specimen configuration (showing all 10 runs per connection configuration) - Figure 3.54 to Figure 3.63.
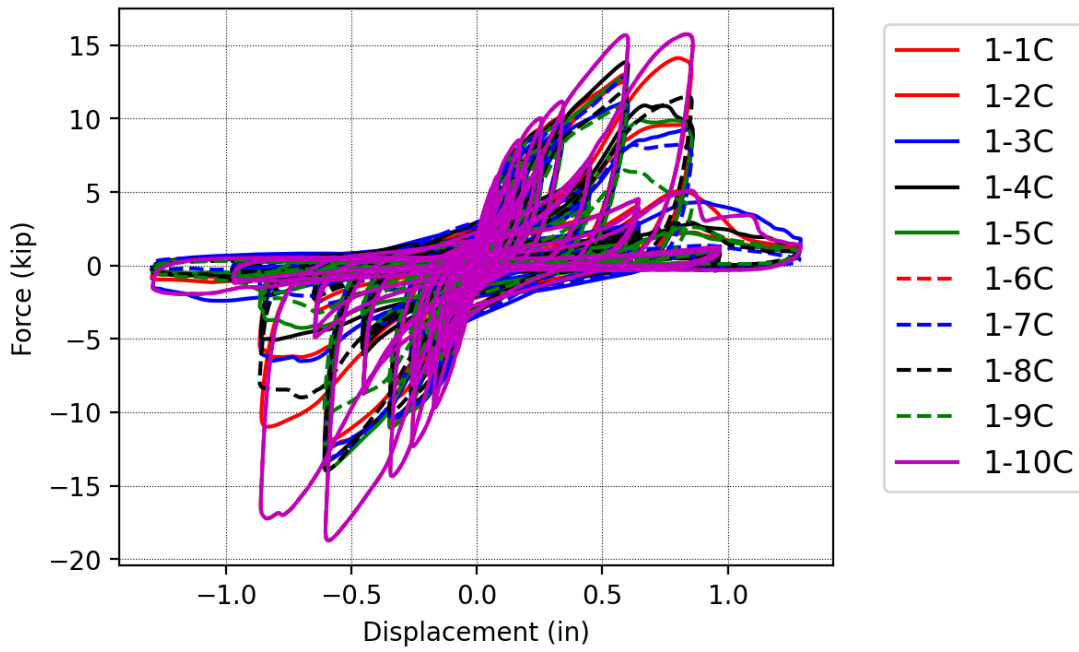
Figure 3.54. Specimen 1 Cyclic Test Results
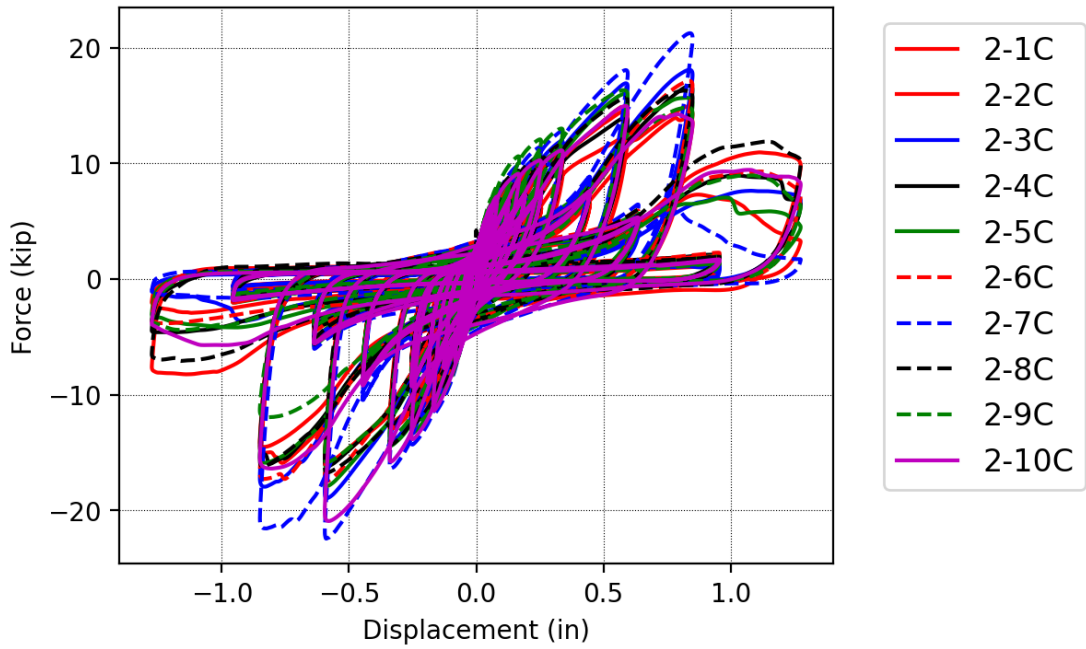
Figure 3.55. Specimen 2 Cyclic Test Results
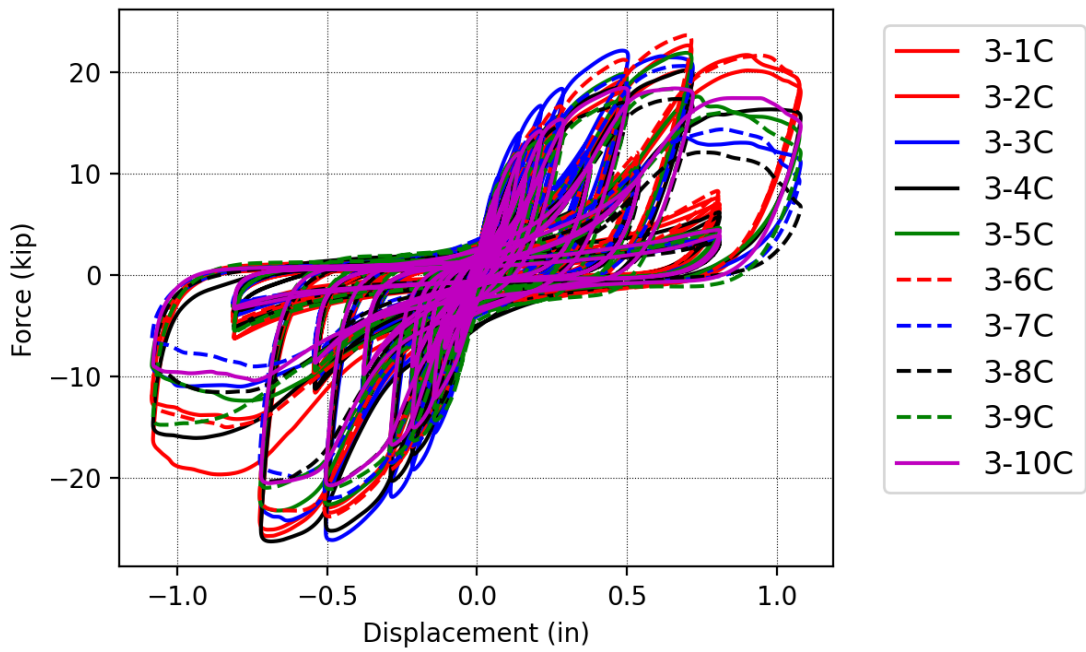
Figure 3.56. Specimen 3 Cyclic Test Results
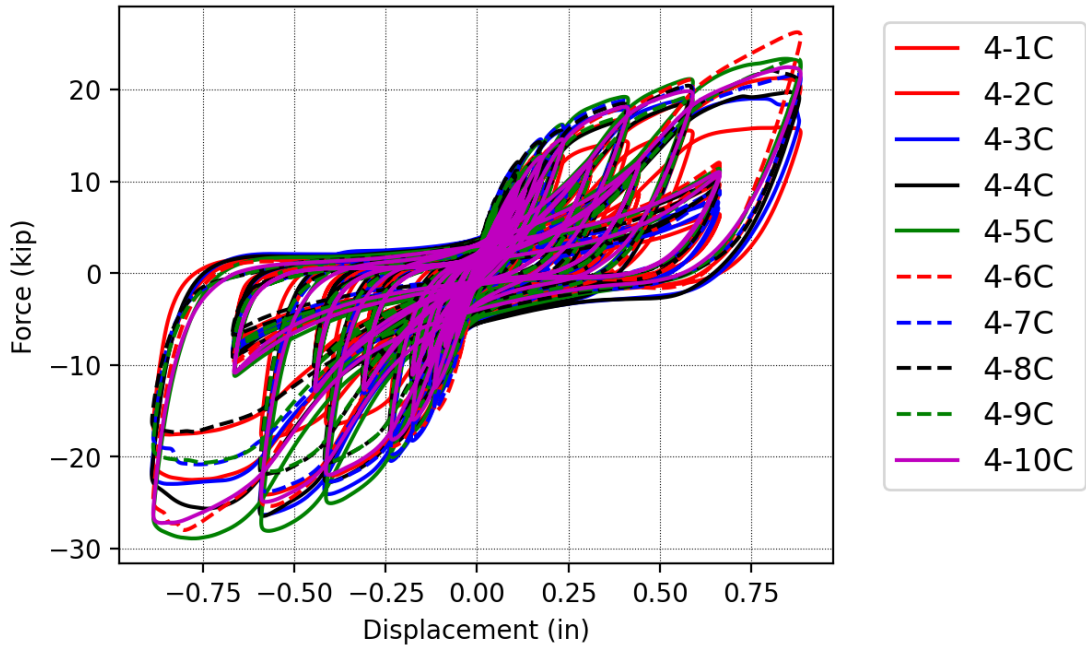
Figure 3.57. Specimen 4 Cyclic Test Results
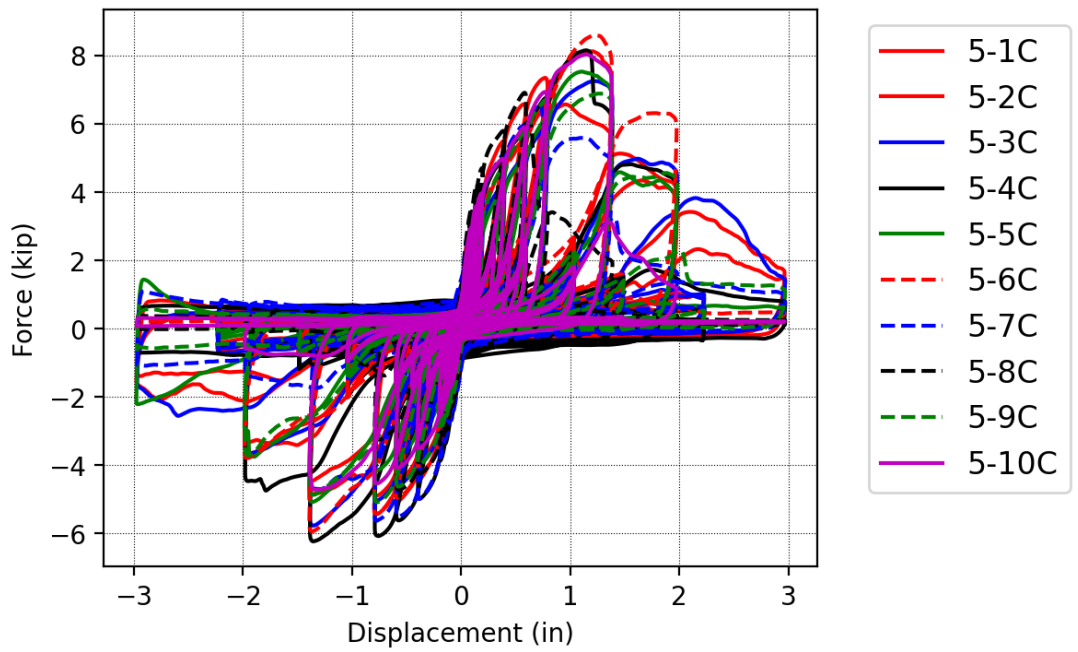
Figure 3.58. Specimen 5 Cyclic Test Results
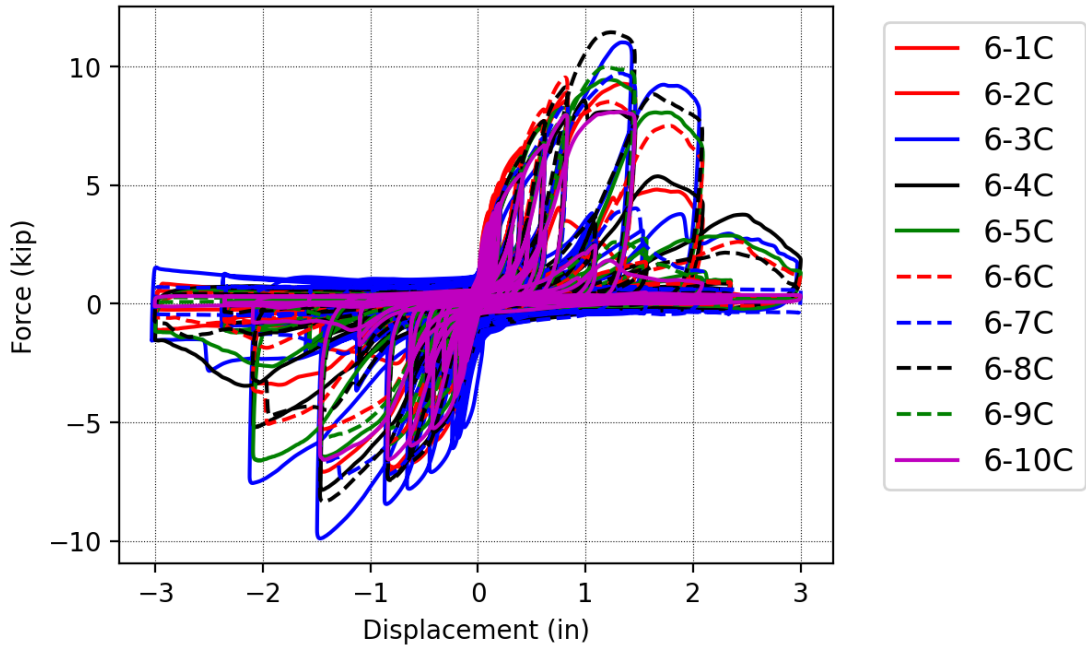
Figure 3.59. Specimen 6 Cyclic Test Results
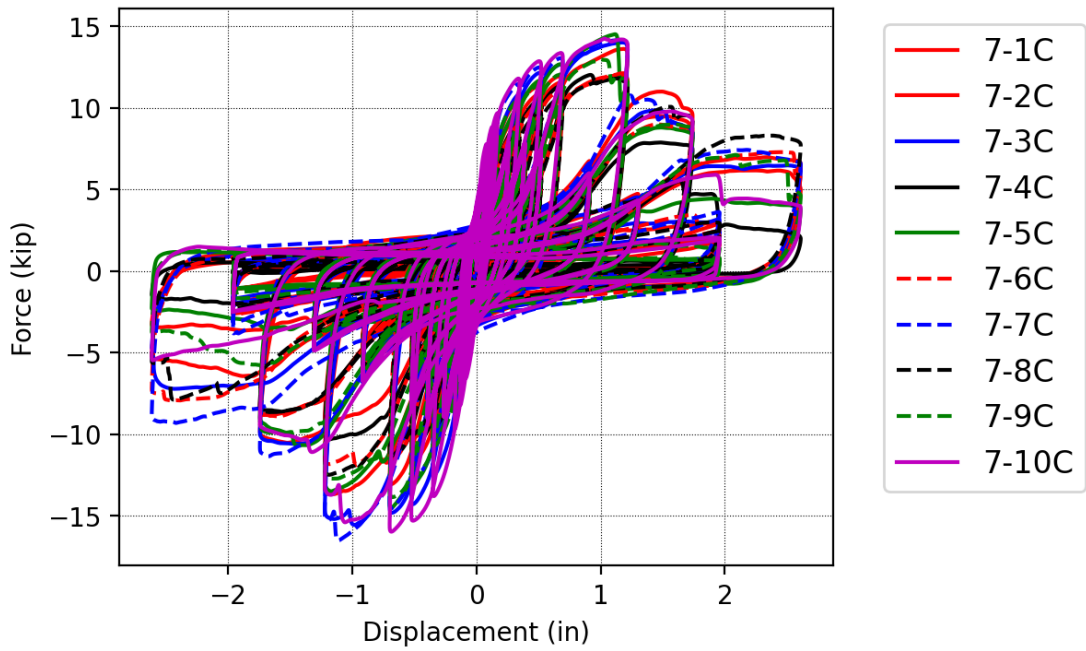
Figure 3.60. Specimen 7 Cyclic Test Results
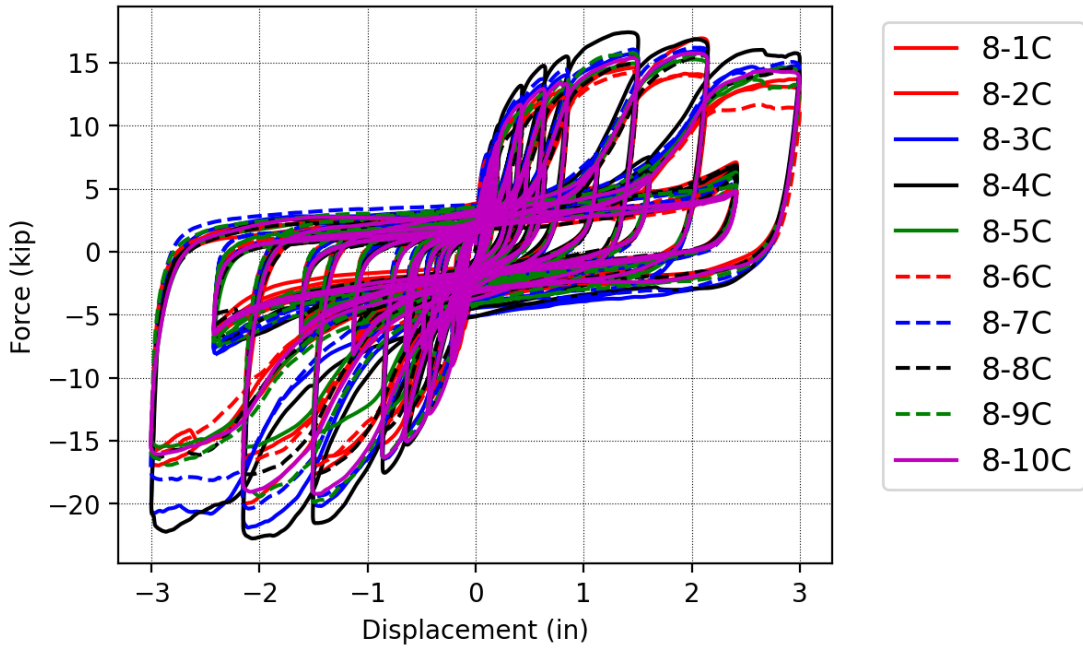
Figure 3.61. Specimen 8 Cyclic Test Results
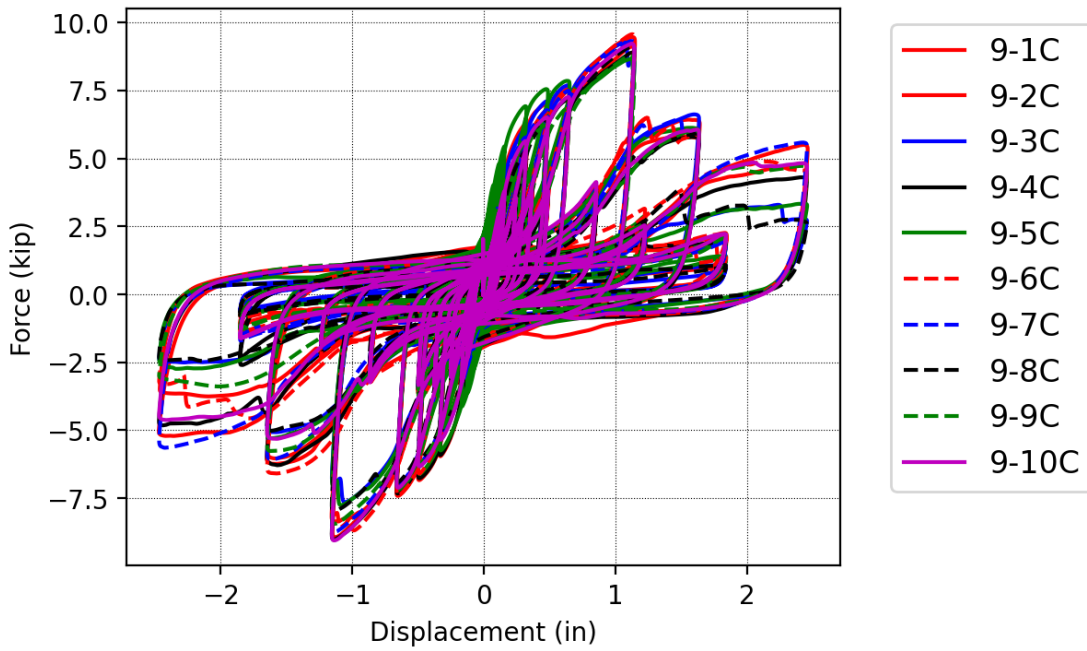
Figure 3.62. Specimen 9 Cyclic Test Results

74
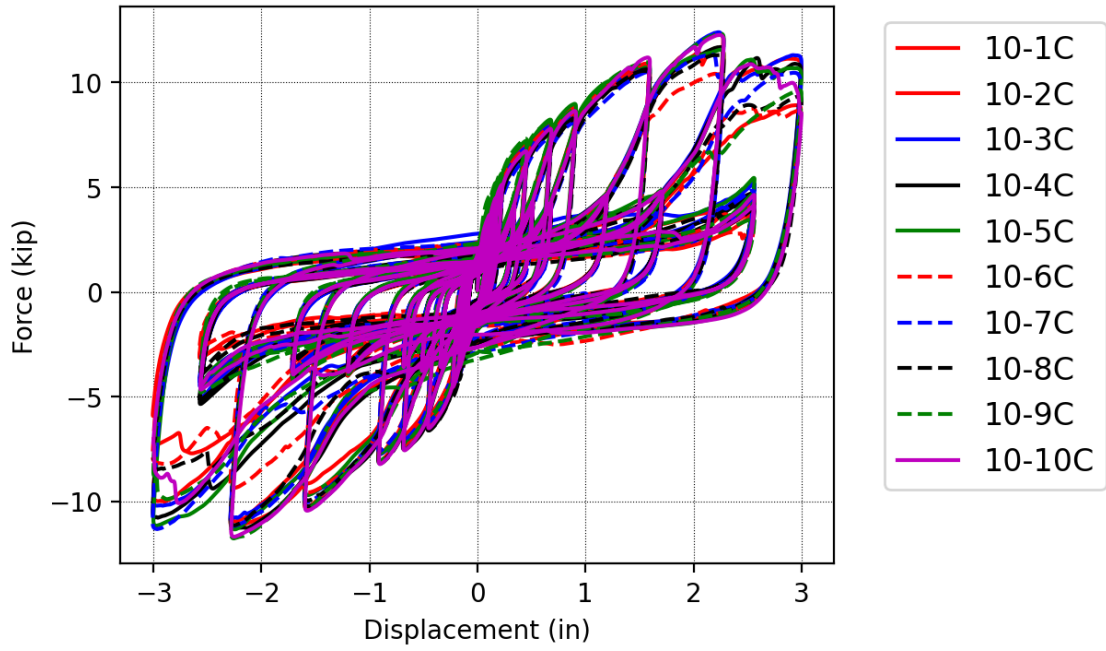
Figure 3.63. Specimen 10 Cyclic Test Results

3.4.4. Discussion

The ideal CLT connection consists of both high stiffness and high ductility. The connection should be both strong and able to undergo significant displacement. Looking at each different configuration, many of the different connections exhibit this type of behavior, and there is little difference between fasteners of the same type made by different manufacturers. The main difference between manufacturers of screws is the strength, but that is specified differently for each screw.

3.4.4.1. Discussion of Panel-to-Panel Tests

The configuration with the highest experimental strength relative to strength predicted by LRFD design were specimens 1 and 2 – the half-lap connections with fasteners installed at 90 degrees. These two configurations had nearly 4 to 5 times more strength in both monotonic and cyclic loading conditions than was predicted. This can be attributed to the factors of safety that are already built into the code and the fact that this is a connection whose behavior is easy to predict given that it has been studied before.

The specimens that had fasteners installed at both 90 degrees and 45 degrees showed similar peak loads in monotonic and cyclic loading conditions. This is promising as it is very beneficial to have a connection that does not seem to show less strength under cyclic loading. Specimens 3 and 4 showed both relatively high stiffness and relatively high ductility.

The spline connection was found to be far more ductile than the half-lap connection as both configurations that were tested led to nearly double the reference deformation when compared to the half-lap configurations. While the spline connection is more ductile, its fasteners exhibit far less strength, and do not outperform code predictions as well.

76

3.4.4.2. Discussion of Wall-to-Floor Tests

The wall to floor tests all showed one thing in common. It became clear that the angle bracket was designed to be slightly too thin. It had too much plastic deformation that it did not allow for the screws to be the main failure mechanism. In every configuration, the angle bracket yielded at the same time as the screws began to form plastic hinges. This led to rather large displacements, but reduced the peak load carried by the specimen. The capacity of each configuration could be increased by increasing the thickness of the angle bracket.

Additionally, the capacity of the non-load-bearing configurations could be increased by eliminating the half-inch gap that is specified as a part of detailing the connection and allowing for installation of the wall panel. While this may not be possible to eliminate in practice, reducing this gap will increase the capacity of the connection as the larger gap allows for more rotation of the angle bracket, reducing the overall stiffness of the connection. This issue could be resolved in a real building as there is stiffness provided to the diaphragm coming from other locations, such as the wall perpendicular to the wall in question.

4.   HYSTERETIC MODELS CAPTURING THE CONNECTION TEST RESPONSE

4.1.   Overview

The purpose of testing specimens in the lab is to obtain valuable information about their behavior. This information can then be used in the future to predict the behavior of connections, or the full system, under a variety of different loading conditions. The specimens were tested under a standard cyclic loading protocol so that the results could be trusted to be accurate when fitted to a numerical model and those results used under different loading conditions. Given the testing data, codes were written in MATLAB and Jupyter Notebook to fit the numerical models to the data. This was accomplished through finding an algorithm that iterates the model parameters until the difference in force between the numerical and experimental curves is at a minimum. The difference in force is minimized because the displacement is the input and is the same in both instances. Following this methodology, the mean parameters are reported.

4.2.   CUREE-SAWS Model

The CUREE-SAWS hysteretic model, as described in Section 2.3. Introduction to Connection Testing, uses sixteen different parameters to describe the cyclic behavior of a connection. The method that was used to optimize the parameters for this hysteretic model using the connection test data was one that centered around iterating the force at each data point until the difference between experiment and model was minimized. This was accomplished through an optimization MATLAB code. The code, first developed by Koliou and Filiatrault (Koliou and Filiatrault 2017), then outputs the parameters that lead to the model that is plotted, and those parameters are taken and used to run the model again as its initial guess. This is done a few times until the output parameters do not change significantly from the input parameters and convergence/minimization of the error is achieved. In this section, the results for fitting the

78

CUREE-SAWS hysteretic model are presented, along with the mean parameters for each cycle

test setup in Figure 4.1 to Figure 4.10. The mean and standard deviation of each parameter for

the CUREE SAWS hysteretic model fitted to the experimental data are also tabulated in Table

4.1.
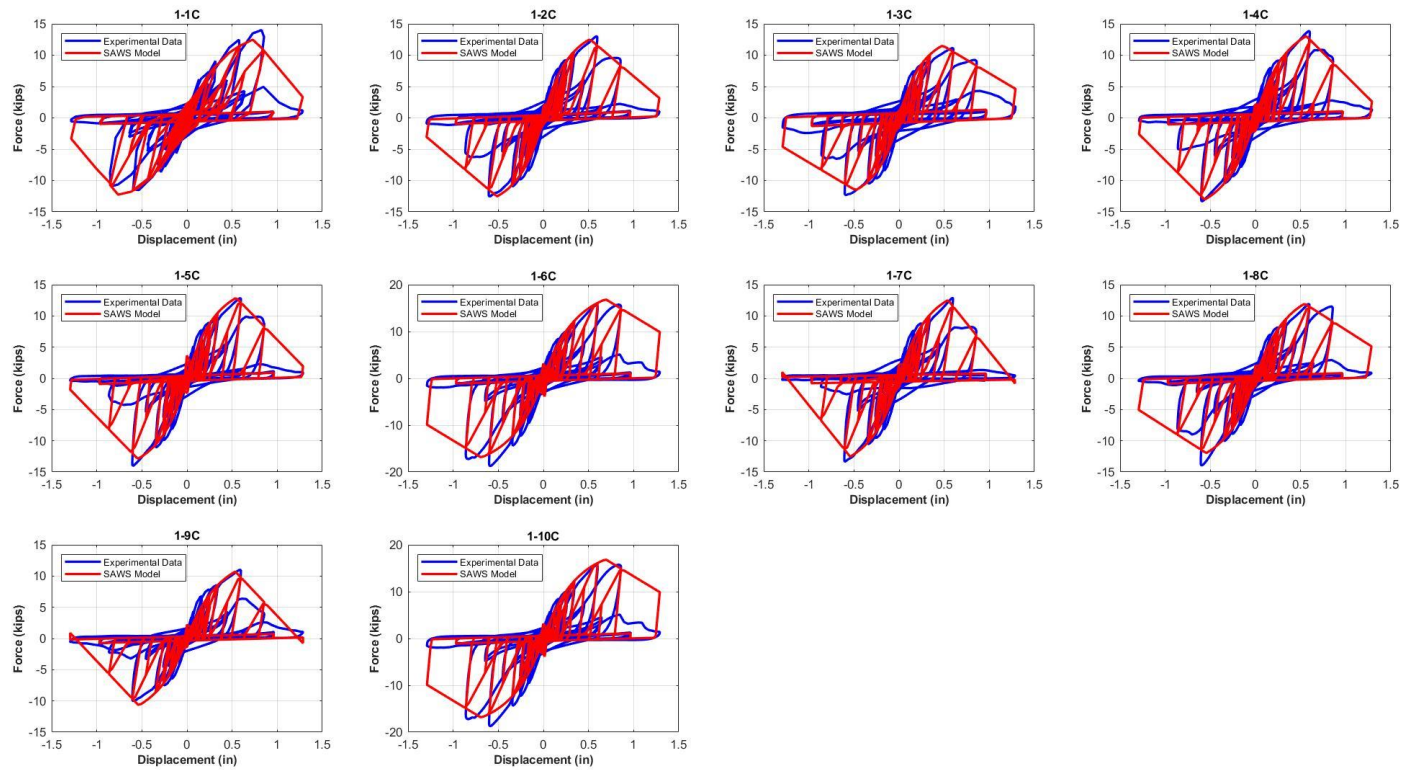
Figure 4.1. Specimen 1 SAWS Model Fits
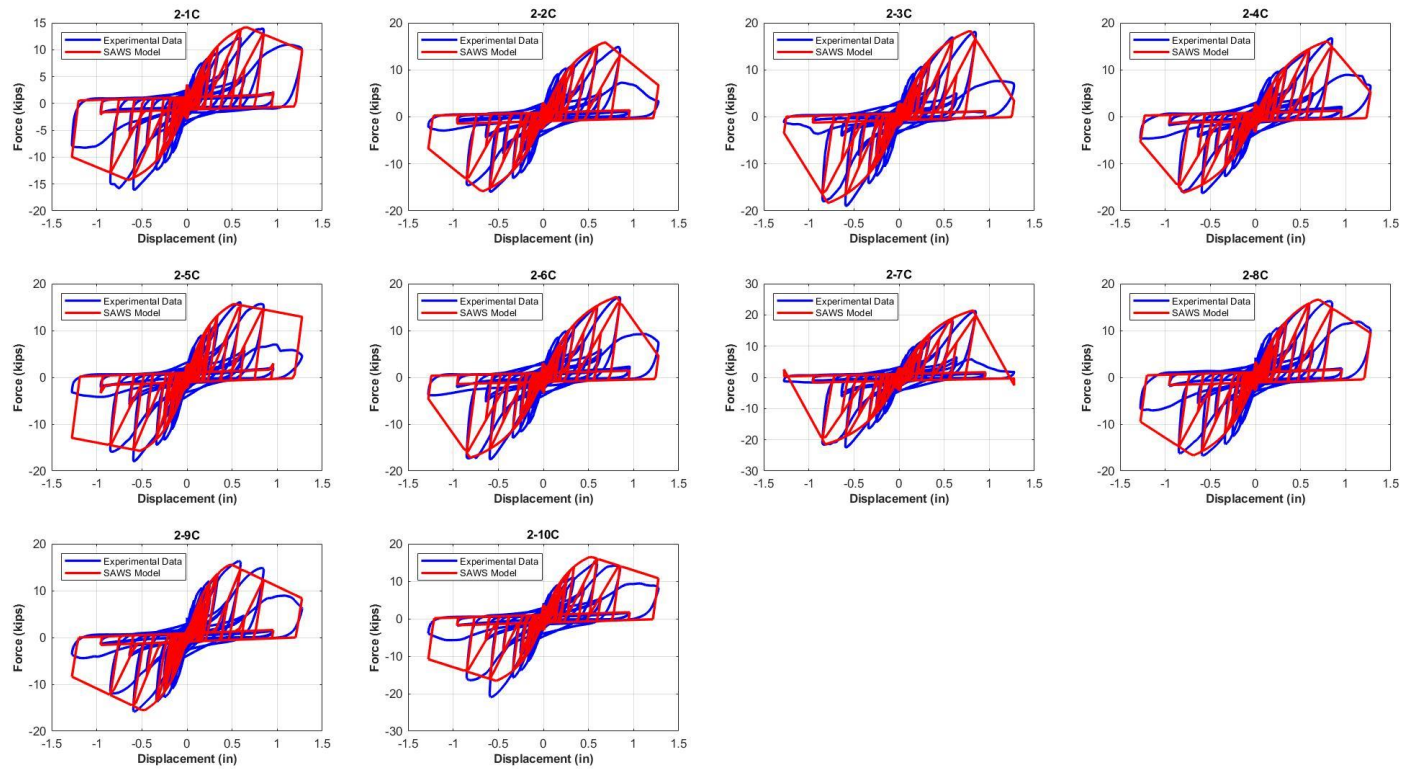
Figure 4.2. Specimen 2 SAWS Model Fits
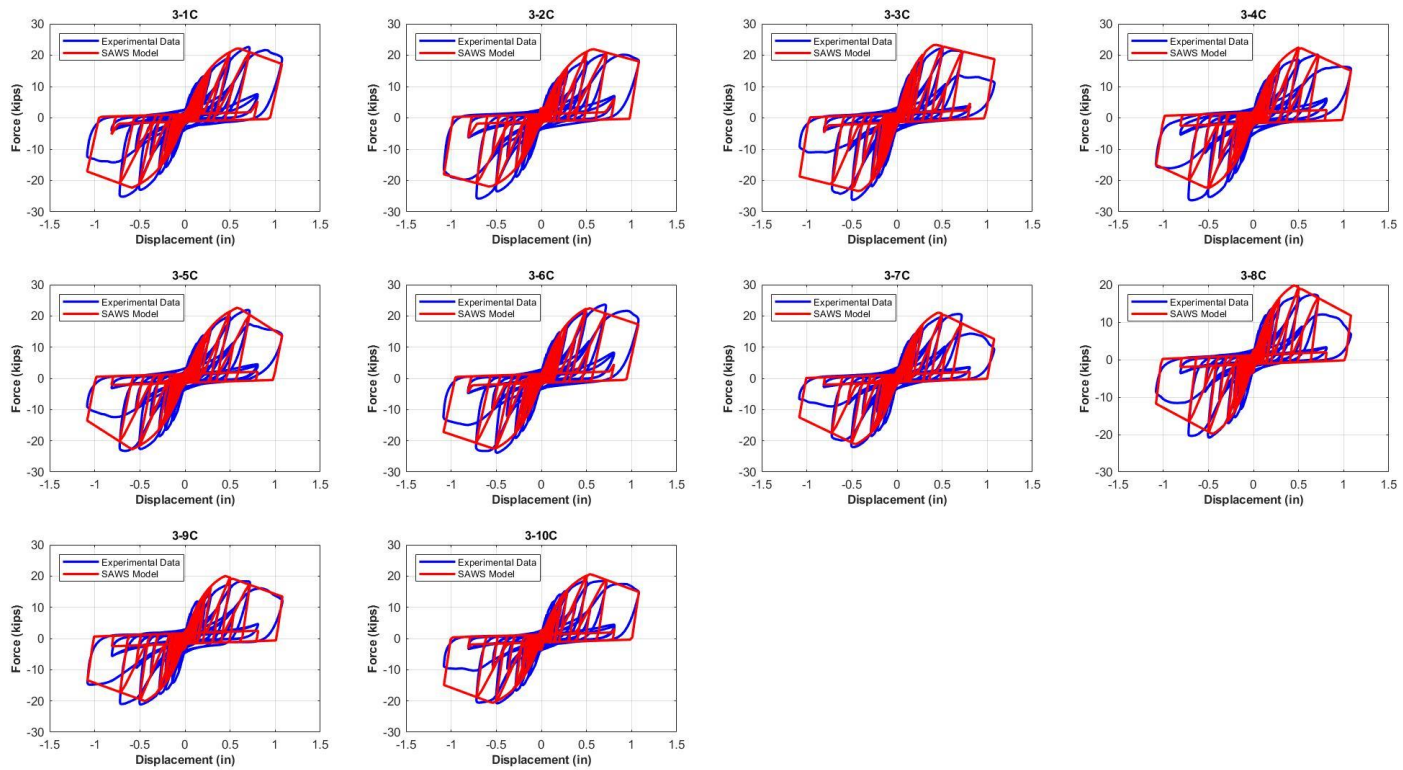
Figure 4.3. Specimen 3 SAWS Model Fits
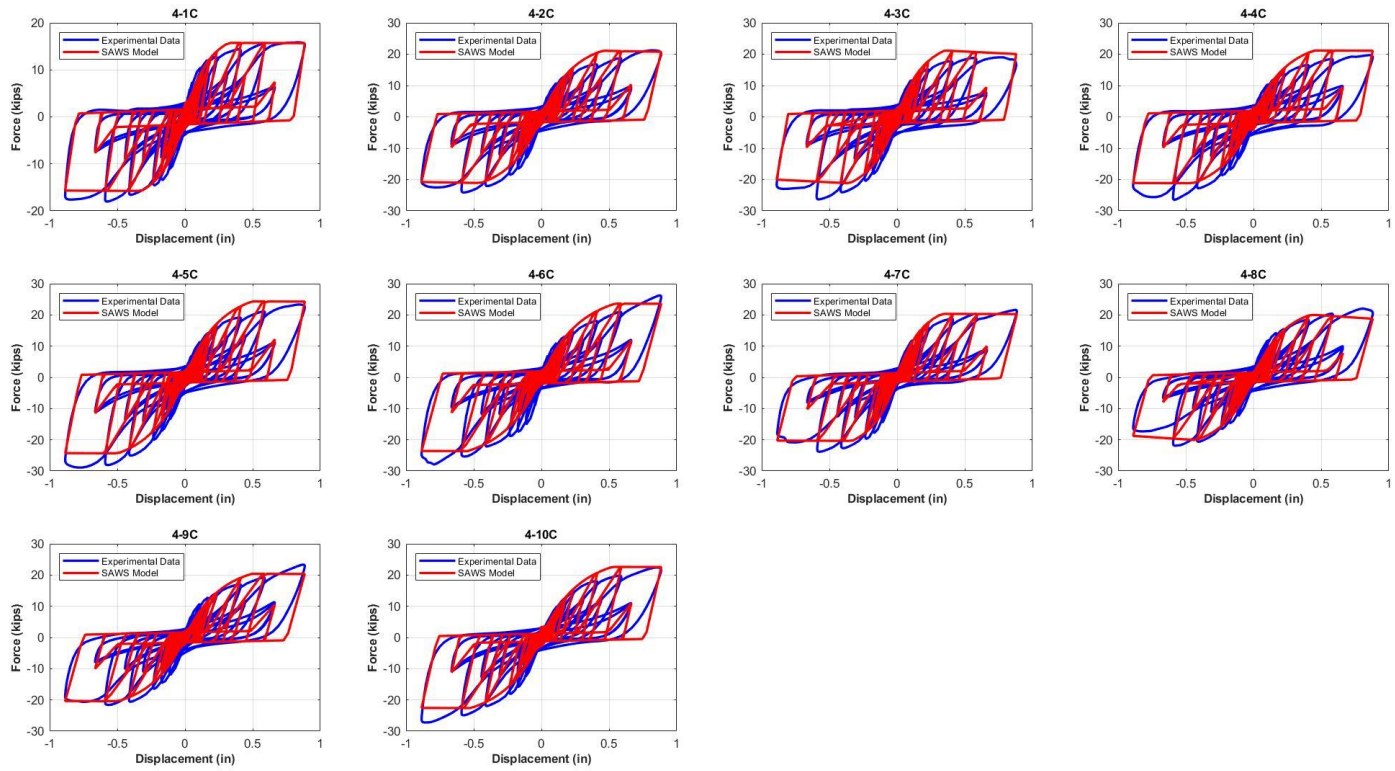
Figure 4.4. Specimen 4 SAWS Model Fits
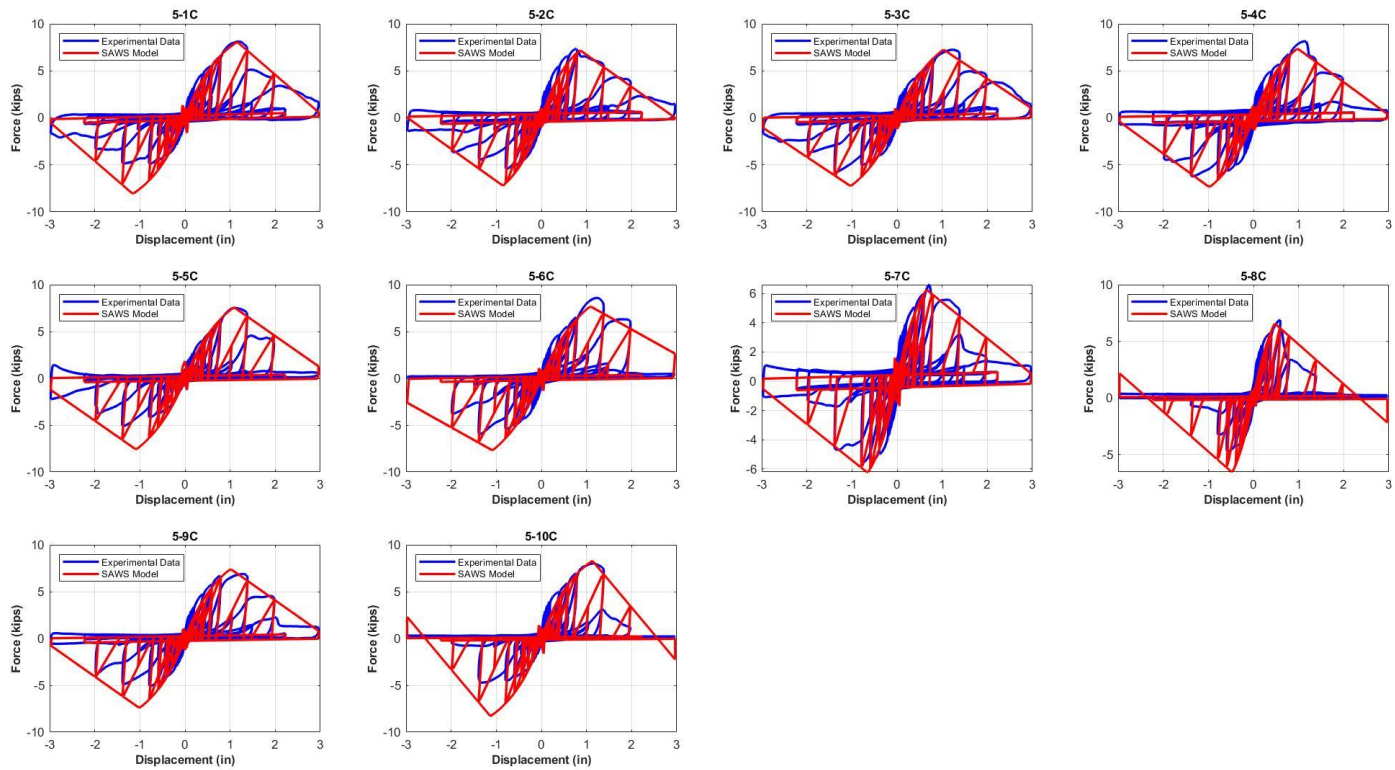
Figure 4.5. Specimen 5 SAWS Model Fits
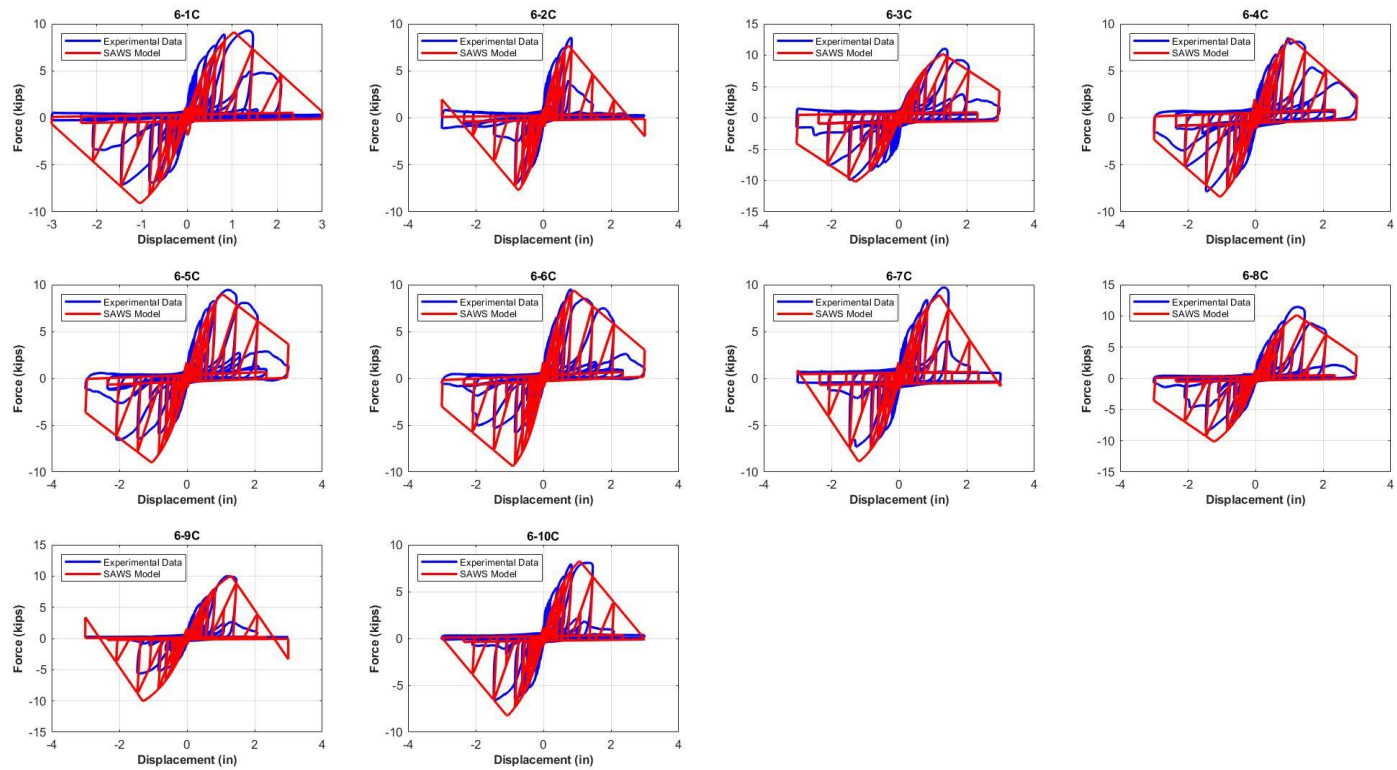
Figure 4.6. Specimen 6 SAWS Model Fits
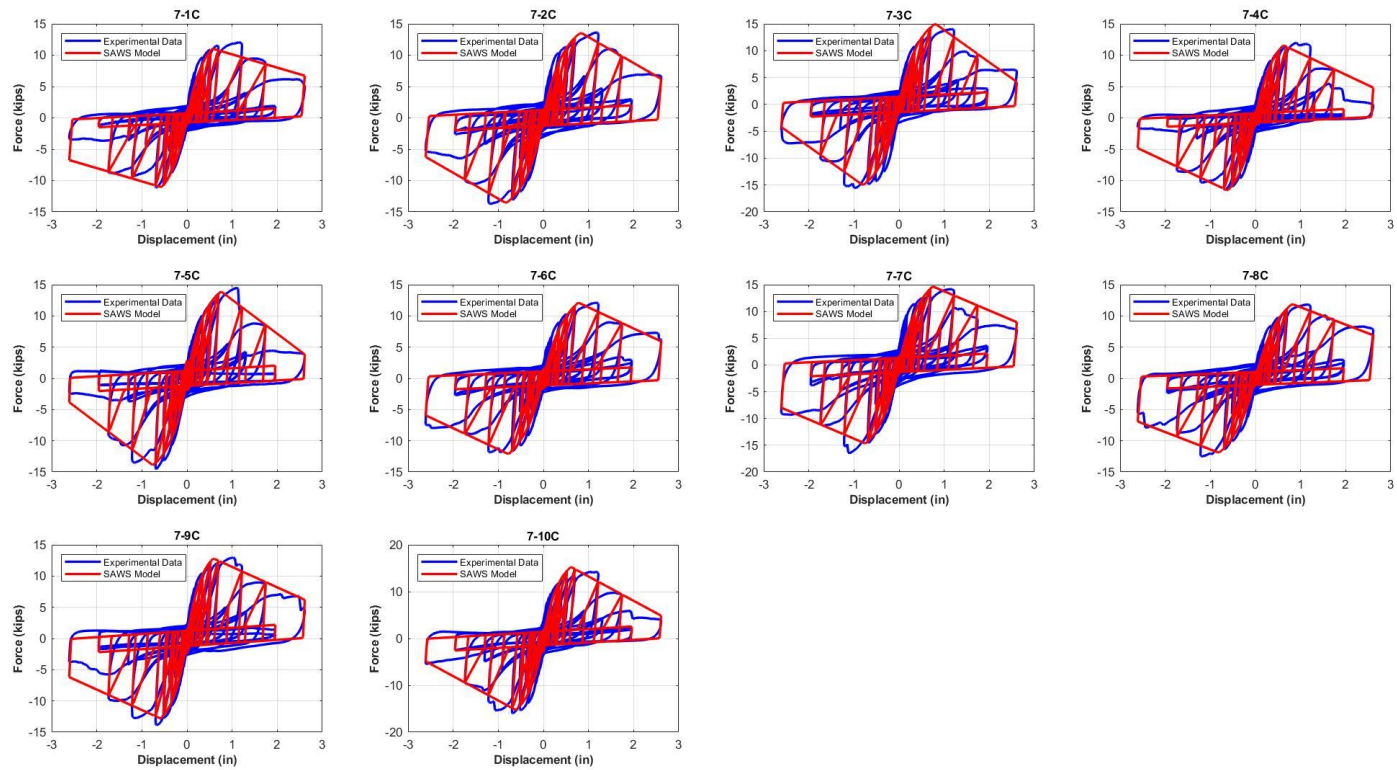
Figure 4.7. Specimen 7 SAWS Model Fits
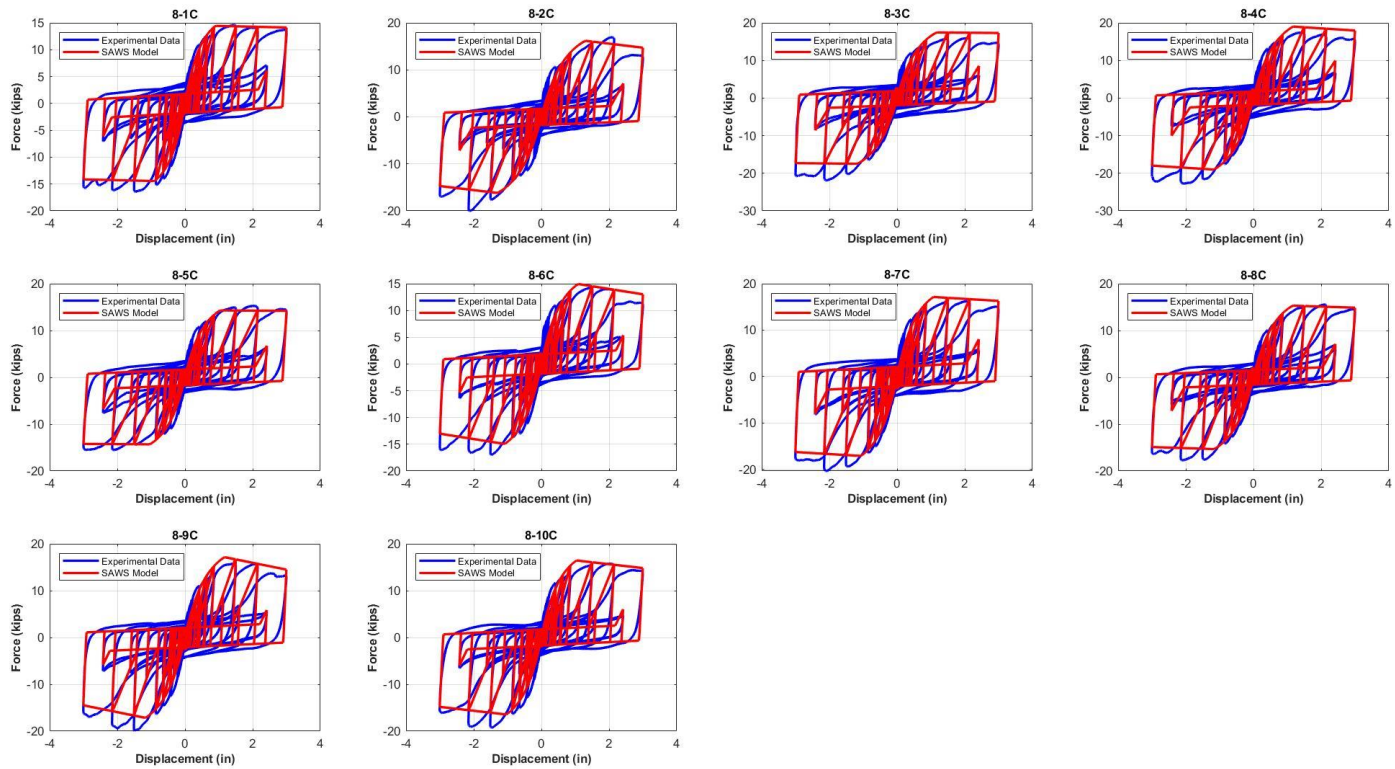
Figure 4.8. Specimen 8 SAWS Model Fits
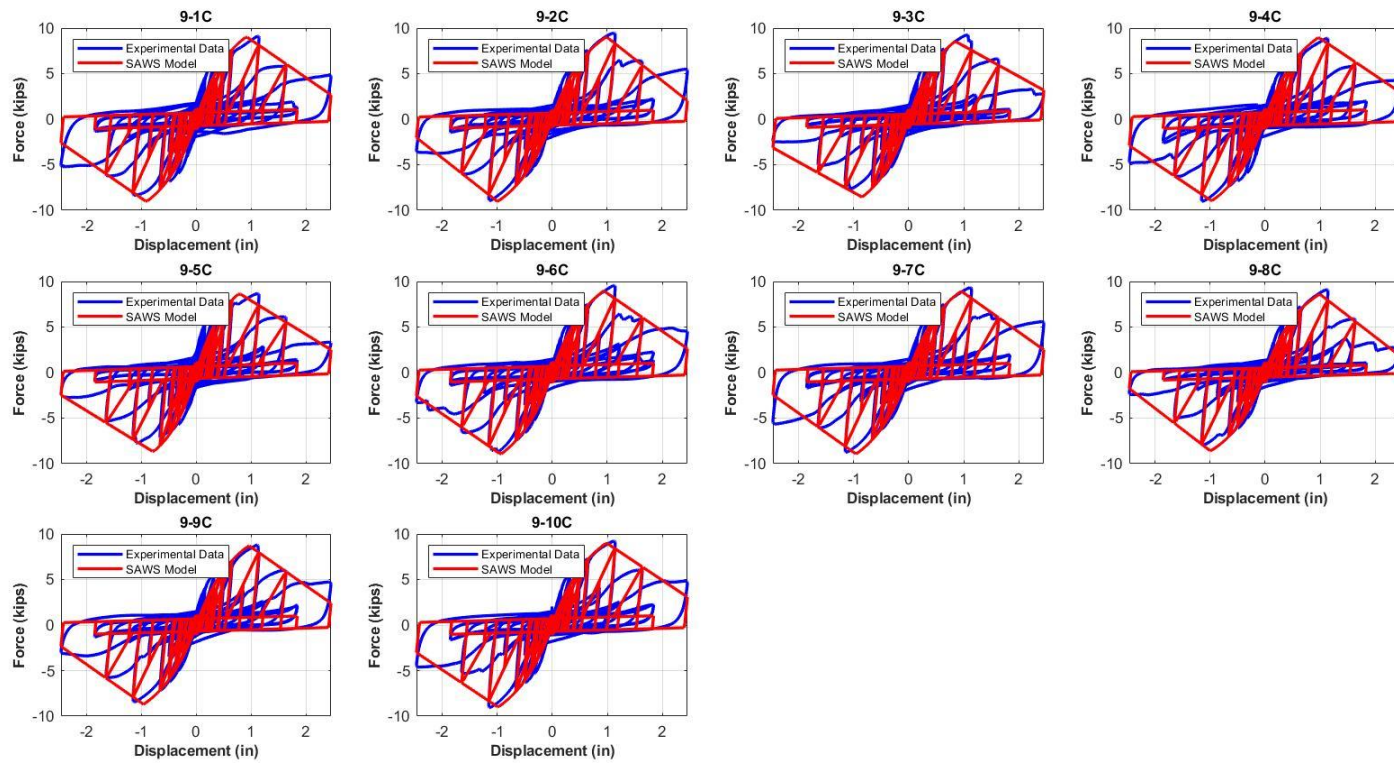
Figure 4.9. Specimen 9 SAWS Model Fits
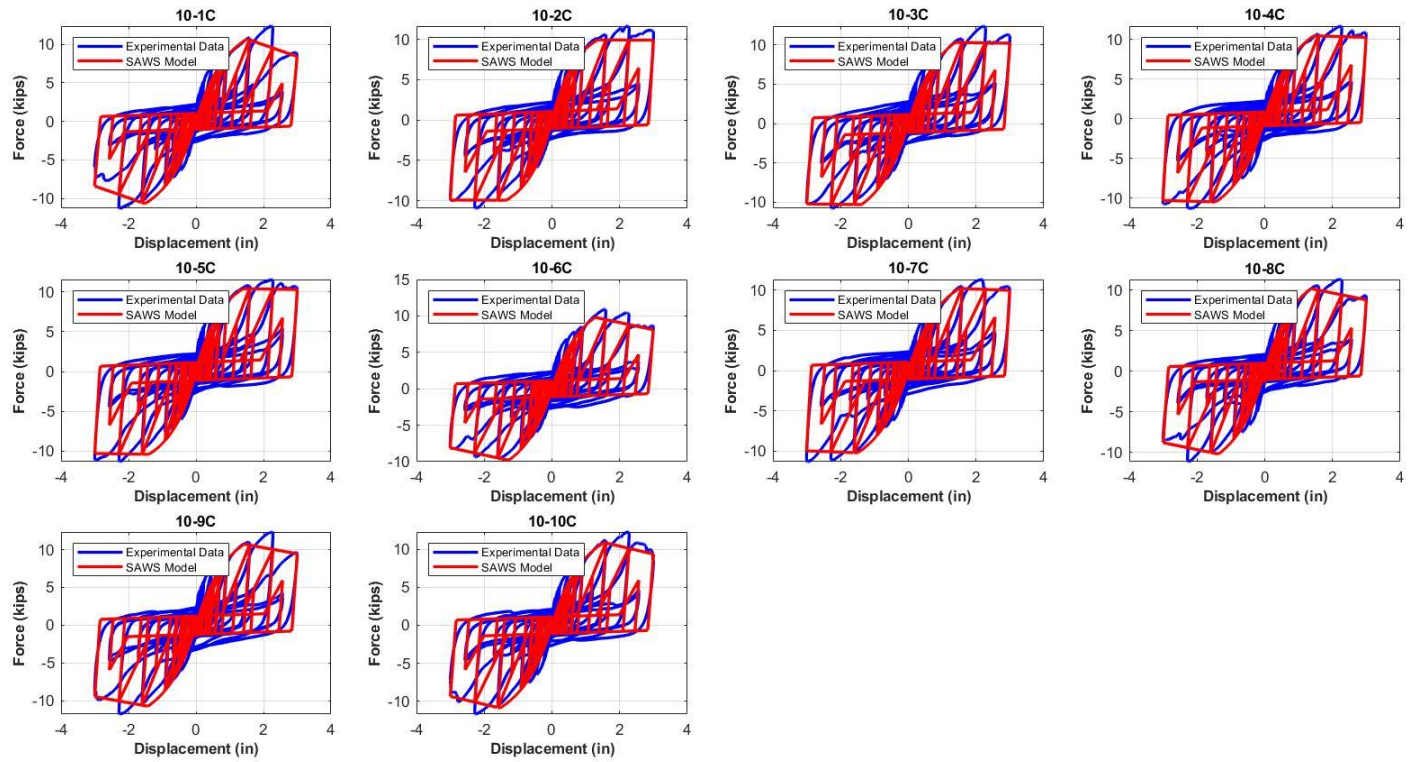
Figure 4.10. Specimen 10 SAWS Model Fits

Table 4.1. CUREE-SAWS Model Parameters for Each Configuration

Test ID	Parameter	F_0 (kips)	k_0 (kips/in)	r_1	r_2	r_3	r_4	F_i (kips)	Δ_{unl} (in)	α	β
					SAWS Model Parameters						
1	Mean	1.552	0.031	0.001	-0.275	2.451	0.009	0.034	1.875	0.500	1.005
	S.D.	0.221	0.004	0.000	0.094	0.712	0.002	0.010	0.151	0.000	0.017
2	Mean	1.943	0.034	0.001	-0.343	2.522	0.010	0.051	1.984	0.500	1.000
	S.D.	0.224	0.006	0.000	0.268	0.389	0.000	0.010	0.023	0.000	0.000
3	Mean	1.572	0.016	0.001	-0.118	1.742	0.010	0.054	1.986	0.502	1.024
	S.D.	0.084	0.002	0.000	0.040	0.311	0.000	0.008	0.024	0.004	0.043
4	Mean	1.519	0.014	0.001	-0.006	1.712	0.010	0.069	1.993	0.562	1.006
	S.D.	0.169	0.002	0.001	0.009	0.247	0.000	0.012	0.012	0.058	0.009
5	Mean	1.267	0.091	0.011	-0.255	5.358	0.006	0.027	1.277	0.507	1.000
	S.D.	0.066	0.016	0.016	0.075	0.642	0.002	0.012	0.139	0.004	0.000
6	Mean	1.459	0.089	0.004	-0.263	5.187	0.005	0.033	1.513	0.505	1.000
	S.D.	0.121	0.013	0.004	0.108	0.477	0.002	0.015	0.094	0.004	0.000
7	Mean	0.984	0.025	0.003	-0.096	2.860	0.010	0.072	1.809	0.637	1.003
	S.D.	0.090	0.004	0.003	0.025	0.496	0.000	0.011	0.188	0.097	0.004
8	Mean	1.171	0.035	0.001	-0.017	4.377	0.010	0.097	1.997	0.521	1.005
	S.D.	0.108	0.003	0.000	0.014	0.546	0.000	0.009	0.004	0.029	0.016
9	Mean	0.720	0.040	0.001	-0.231	3.552	0.010	0.057	1.462	0.569	1.000
	S.D.	0.018	0.003	0.001	0.034	0.174	0.000	0.005	0.036	0.062	0.000
10	Mean	0.796	0.053	0.002	-0.038	4.252	0.010	0.084	1.679	0.504	1.000
	S.D.	0.032	0.004	0.001	0.037	0.530	0.000	0.008	0.132	0.004	0.000

4.3.   Pinching4 Model

The Pinching4 hysteretic model, as described in Section 2.3 Introduction to Connection Testing, is a piecewise defined function that explicitly uses the force and displacement values of the envelope curve (the curve that encloses the entire force-displacement diagram). The method that was used to find the parameters for the model was somewhat different from what was used to find the SAWS model parameters. Because the Pinching4 material model has so many defining parameters that can be manually adjusted, the approach that was taken differed. Out of the ten cyclic tests that were done for each configuration, a representative curve was taken and the Pinching4 parameters were fit to this curve. The representative curve is defined as the average of all ten curves. This was performed to capture the average behavior of the specimens over all ten tests. The fitting of the data to the Pinching4 model was accomplished using a Jupyter Notebook and written in Python in collaboration with Milad Roohi (postdoctoral researcher at Colorado State University). The parameters could easily be adjusted to better fit the model to minimize the difference in force between experimental results and what the numerical model predicts. In this section, the results for fitting the Pinching4 hysteretic model are presented, along with the mean parameters for each test setup in Figure 4.11 to Figure 4.20, while the mean values of all parameters of the Pinching4 model are summarized in Table 4.2 and Table 4.3. Standard deviation values are not presented for this model because a representative curve was chosen. Rather than finding the parameters for each curve and averaging them, values for the representative curve were found and can be considered the mean values.
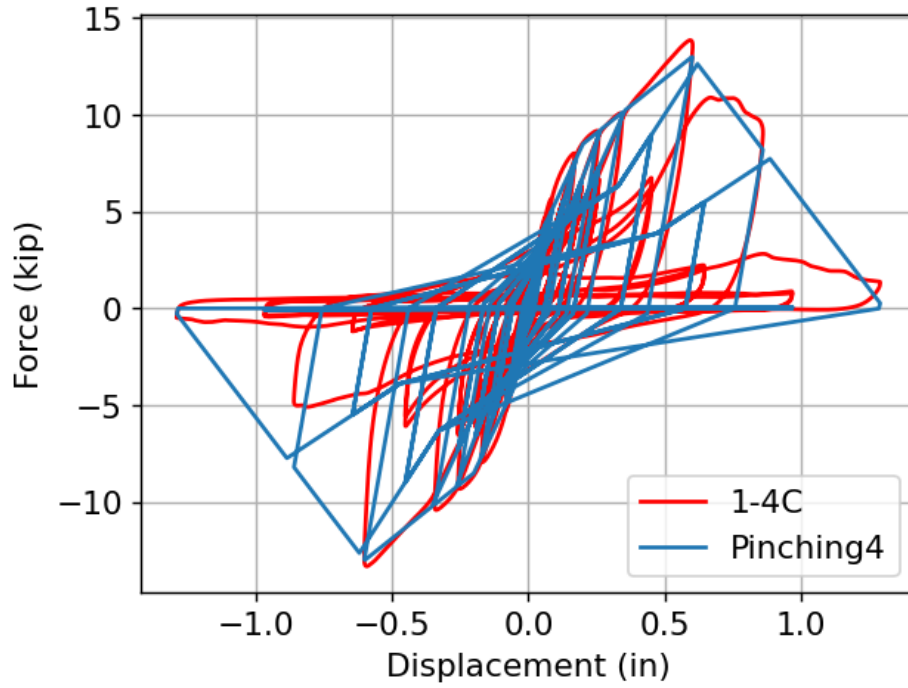
Figure 4.11. Specimen 1 Pinching4 Model Fit
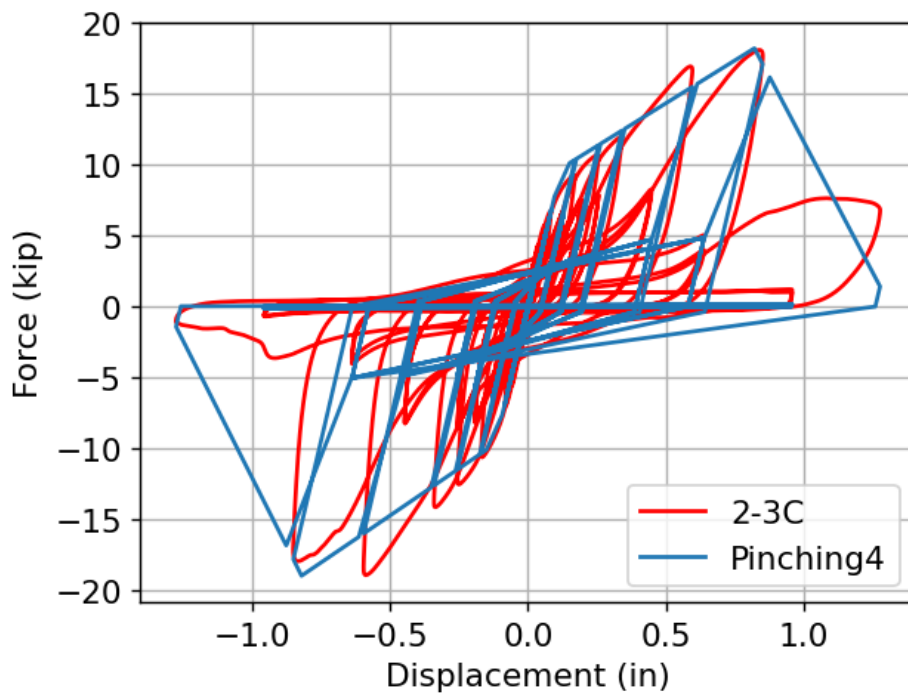
Figure 4.12. Specimen 2 Pinching4 Model Fit
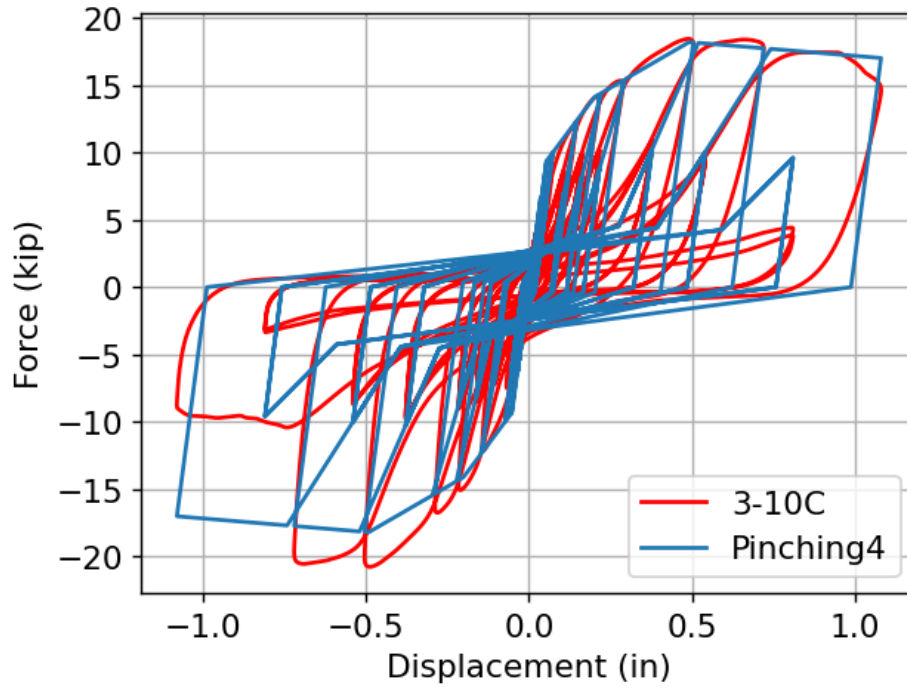
Figure 4.13. Specimen 3 Pinching4 Model Fit
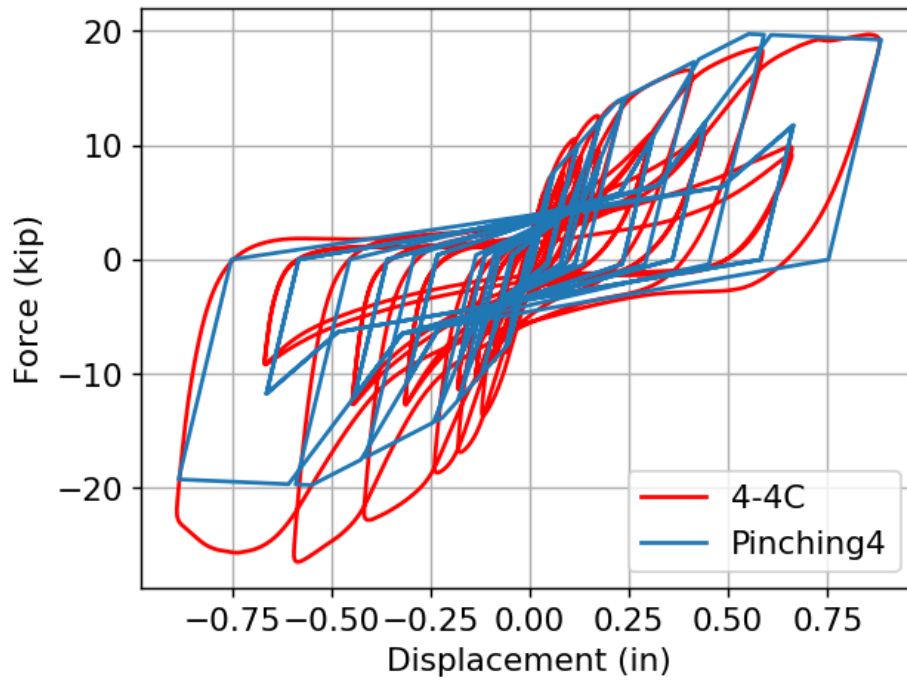
Figure 4.14. Specimen 4 Pinching4 Model Fit
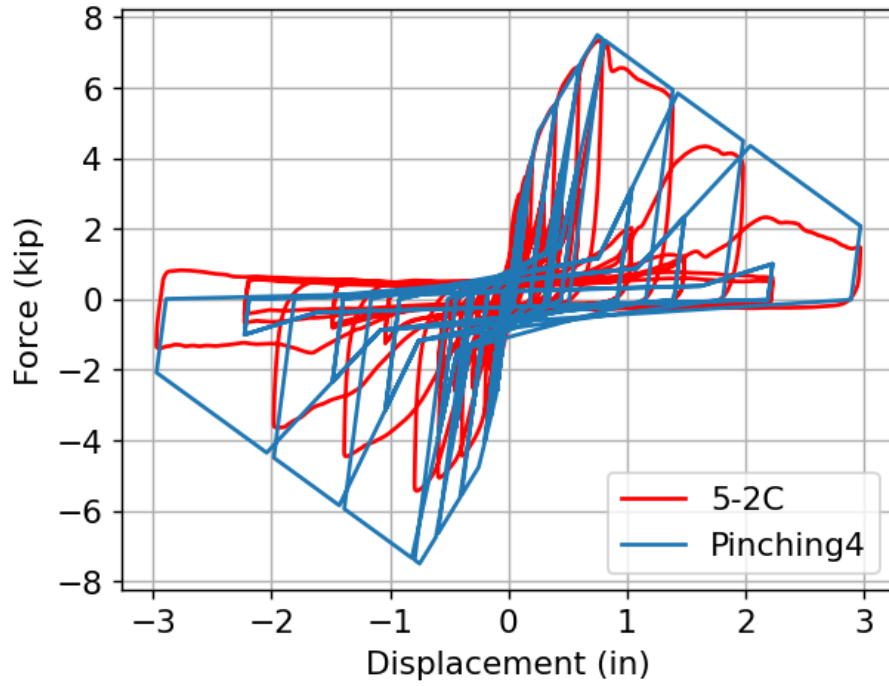
Figure 4.15. Specimen 5 Pinching4 Model Fit
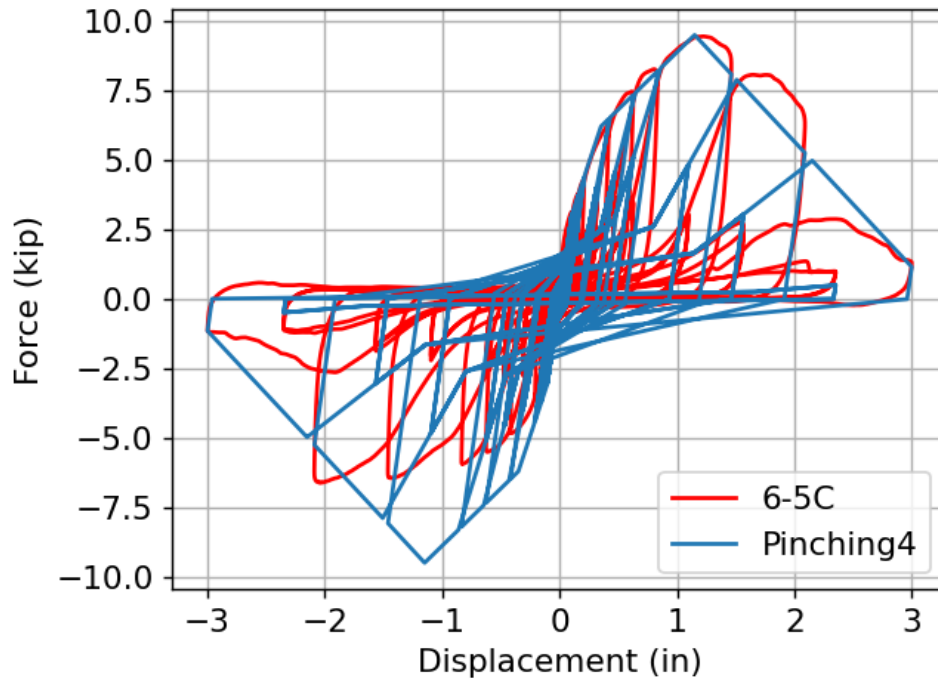
Figure 4.16. Specimen 6 Pinching4 Model Fit
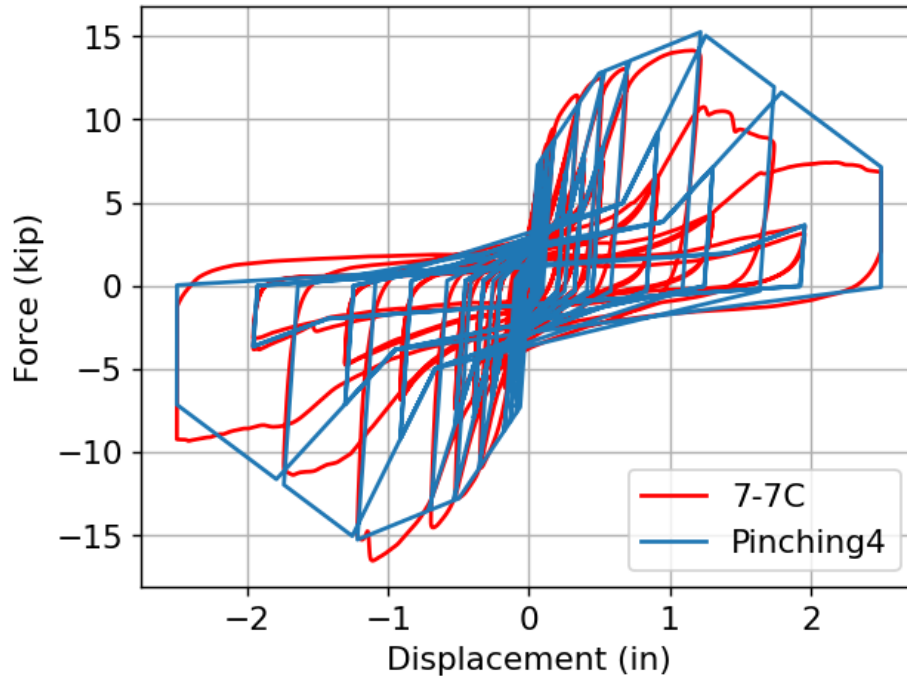
Figure 4.17. Specimen 7 Pinching4 Model Fit
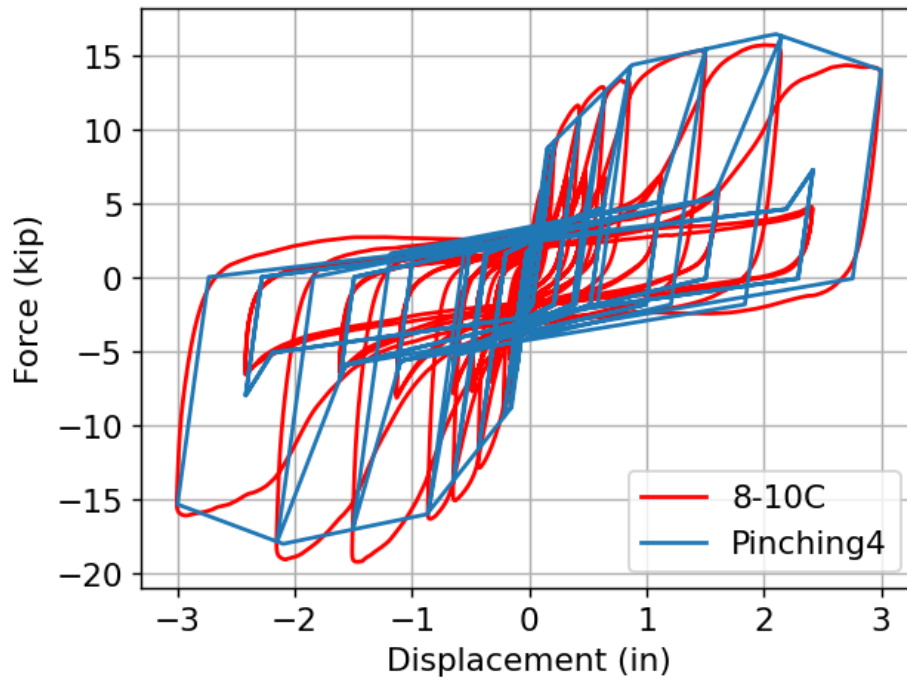
Figure 4.18. Specimen 8 Pinching4 Model Fit
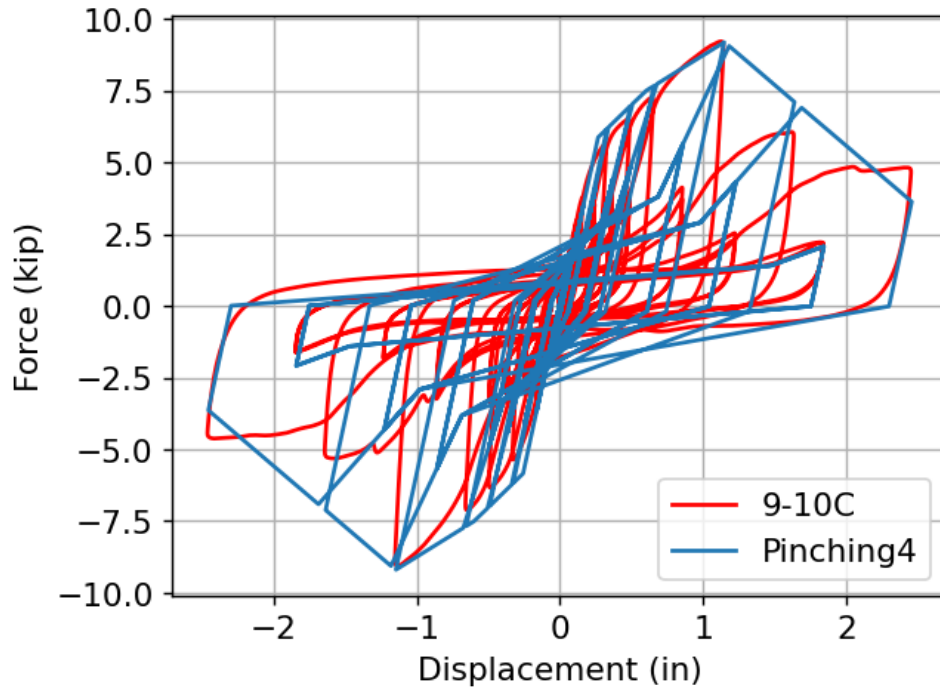
Figure 4.19. Specimen 9 Pinching4 Model Fit
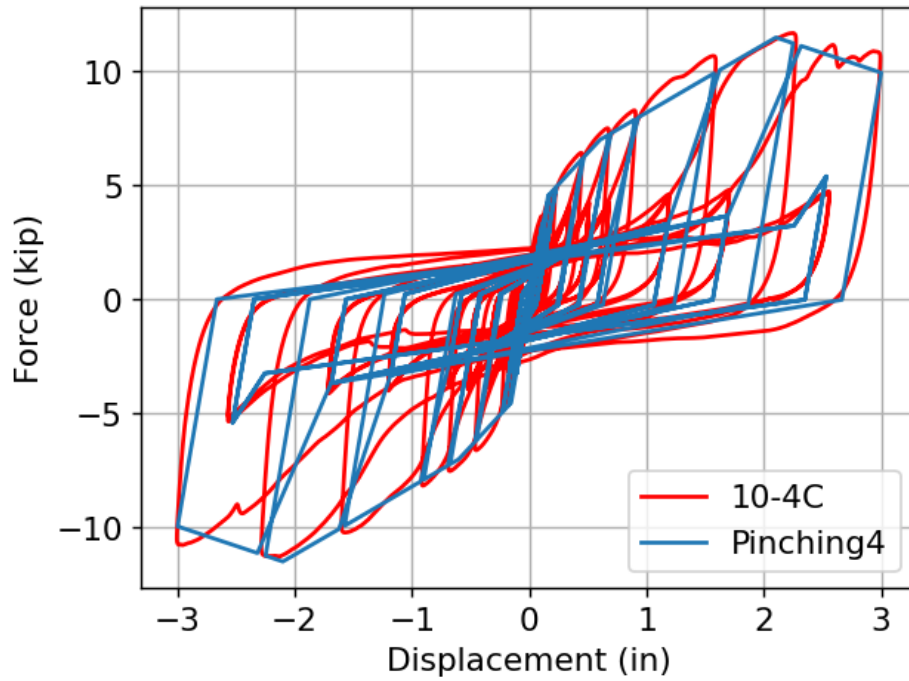
Figure 4.20. Specimen 10 Pinching4 Model Fit

Table 4.2.Pinching4 Envelope Fitted Parameters

Pinching4 Positive Response Envelope Parameters (Negative are opposite)									
Test ID	Parameter	ePf_1 (kip)	ePf_2 (kip)	ePf_3 (kip)	ePf_4 (kip)	ePd_1 (in)	ePd_2 (in)	ePd_3 (in)	ePd_4 (in)
1	Mean	4.00	8.50	13.00	0.10	0.05	0.20	0.60	1.30
2	Mean	7.50	10.10	18.20	0.50	0.09	0.15	0.82	1.30
3	Mean	9.25	14.10	18.20	0.10	0.05	0.20	0.49	9.50
4	Mean	7.25	13.85	19.75	0.10	0.05	0.22	0.55	13.50
5	Mean	2.65	4.75	7.50	0.55	0.10	0.25	0.75	3.60
6	Mean	3.00	6.20	9.50	0.25	0.10	0.35	1.15	3.20
7	Mean	7.25	12.75	15.25	0.68	0.06	0.50	1.22	3.52
8	Mean	8.75	14.40	16.50	0.50	0.15	0.88	2.10	8.00
9	Mean	5.80	7.50	9.20	0.50	0.25	0.60	1.15	3.20
10	Mean	4.50	7.00	11.50	0.50	0.15	0.60	2.10	8.50

Table 4.3. Pinching4 Parameter Ratios

Pinching4 Parameter Ratios										
Test ID	Parameter	rDispP	fForceP	uForceP	rDispN	fForceN	uForceN	GammaK	GammaD	GammaF	GammaE
1	Mean	0.53	0.33	0.02	0.53	0.33	0.02	0,0,0,0	0.97,0,0,0,0.03	0,0,0,0	1.00
2	Mean	0.73	0.30	0.02	0.73	0.30	0.02	0,0,0,0	0.97,0,0,0,0.03	0,0,0,0	1.00
3	Mean	0.53	0.25	0.02	0.53	0.25	0.02	0,0,0,0	0.97,0,0,0,0.03	0,0,0,0	1.00
4	Mean	0.53	0.33	0.02	0.53	0.33	0.02	0,0,0,0	0.97,0,0,0,0.03	0,0,0,0	1.00
5	Mean	0.53	0.20	0.02	0.53	0.20	0.02	0,0,0,0	0.97,0,0,0,0.03	0,0,0,0	1.00
6	Mean	0.53	0.33	0.02	0.53	0.33	0.02	0,0,0,0	0.97,0,0,0,0.03	0,0,0,0	1.00
7	Mean	0.53	0.33	0.02	0.53	0.33	0.02	0,0,0,0	0.97,0,0,0,0.03	0,0,0,0	1.00
8	Mean	0.73	0.33	0.02	0.73	0.33	0.02	0,0,0,0	0.97,0,0,0,0.03	0,0,0,0	1.00
9	Mean	0.58	0.42	0.02	0.58	0.42	0.02	0,0,0,0	0.97,0,0,0,0.03	0,0,0,0	1.00
10	Mean	0.73	0.33	0.02	0.73	0.33	0.02	0,0,0,0	0.97,0,0,0,0.03	0,0,0,0	1.00

4.4. Discussion

After performing a thorough study of the cyclic testing results gained from the experimental testing program, a few different conclusions can be drawn when fit to the two different hysteretic models. Both models do an adequate job at representing the force-displacement relationship that exists for all connection configurations. The main goal of modeling the behavior of the connection is to adequately predict the force on the connection when subjected to large displacements. This is especially useful information when it comes to modeling the behavior of a building on the larger scale. During pushover analysis, it is necessary to have an accurate prediction of the how the connections will behave when they are significantly plastically deformed.

Comparing the two models to each other, the Pinching4 model fits the experimental data more closely overall, and more specifically, it fits the data much more closely when the connection could still be considered elastic. For the first few cycles, the connection behaves in an elastic manner, and because the Pinching4 model allows for more fine-tuning in this range, the model can fit the experimental data more closely. Before any failure of the connection occurs, it could be said that the Pinching4 model can be used to fit the experimental data nearly-perfectly. After failure, the fit becomes less perfect. However, it fits the data better overall compared to the CUREE-SAWS model. Because the Pinching4 model uses the philosophy of fitting the "envelope" curve, it does a better job of completely enclosing the hysteresis than does the CUREE-SAWS model. The CUREE-SAWS model can predict forces that are greater than or less than the actual force that is observed but gets within an acceptable range of uncertainty. The Pinching4 model never predicts less force than is observed, and often gets extremely close to the

actual observed force. In this way, it is a more accurate model to use as the modeler will never be underestimating the strength of the connection.

From the study of the connections in this thesis, the Pinching4 model is a better representation of the force-displacement behavior of both types of CLT connections that were studied. For wall-to-floor connections specifically, it accurately fits the experimental data extremely well. This is important as these are the most critical connections to evaluate in the seismic force resisting system when determining a collapse mechanism. The in-plane stiffness of the CLT shear walls is very high, so the behavior of wall-to-floor connections is critical. It is recommended to use the Pinching4 model for full-scale building models of balloon framed CLT buildings in the future. While the panel-to-panel connections are not quite as critical, they determine the predominate behavior that controls the in-plane behavior of the shear wall (sliding, rocking, sliding-rocking, etc.). Even though these are less critical in determining a collapse mechanism, it is still recommended that the Pinching4 model be used in modelling these connections in balloon-framed buildings in the future. This assessment is corroborated by other research done by Shen, et al, when modelling the cyclic behavior of different angle brackets used in CLT shear wall connections (Shen, Schneider et al. 2013).

5.   FINITE ELEMENT MODELING

Finite Element Modeling (FEM) was utilized to conduct numerical simulations of the connection tests that were completed in the laboratory. Accurately modelling the behavior of the connection tests was useful in validating assumptions that were made about the different materials and helpful in predicting behavior of the connection configurations in ways that were not tested in the lab. For example, an out-of-plane test was not done on the wall-to-floor configurations on the small scale. Behavior of this connection was observed during the full-scale biaxial test and could be further studied by means of FEM after the models had been validated.

5.1.   Modeling Assumptions

The commercial software package, Abaqus, was used for all Finite Element Analysis for this thesis. Abaqus has two options when choosing to run FE simulations: a standard or explicit formulation. Abaqus/Explicit was used for all simulations as it models all loading as dynamic, and always provides a solution, given that the time step is small enough to allow for convergence. Every connection was modeled along its line of symmetry. Only half of the connection was modeled, as it could be reasonably assumed that the behavior would be symmetric. This symmetric behavior was confirmed experimentally as the behavior of one side of the connection was always the same as the other side as the load was applied at an equal distance between the two connection points.

The material properties were the most important variable to consider at the outset of modeling. Elastic and plastic material properties needed to be determined, or assumed with a reasonable degree of certainty, in order to ensure that the model was giving reasonable results. For all CLT, it was taken to be Grade V1 CLT (Douglas Fir), as was eventually used in the experimental tests. The elastic behavior of the CLT was taken as orthotropic, and elements of the

elastic material matrix were directly specified in Abaqus (dependent on modulus of elasticity and Poisson's ratio). As seen in Table 5.1, the CLT material properties that were used were presented by Shahnewaz, Alam, and Tannert, who performed finite element modelling on CLT shear walls (Shahnewaz, Alam et al. 2018). The plywood material properties (Table 5.1) were used came from Gerrand's research on the orthotropic behavior of plywood (Gerrand 1987). The LVL material properties came from Janowiak, et al., and can be seen in Table 5.1 (Janowiak, Hindman et al. 2001).

Table 5.1. Material Properties

	Modulus of Elasticity (ksi)			Shear Modulus (ksi)			Poisson's Ratio					
	E_1	E_2	E_3	G_{12}	G_{23}	G_{13}	v_{12}	v_{23}	v_{13}	v_{21}	v_{32}	v_{31}
CLT	1697	1305	145	82	106	15	0.35	0.07	0.35	0.35	0.07	0.35
Plywood	1262	1262	232	132	21	21	0.04	0.48	0.48	0.04	0.09	0.09
LVL	2400	84.5	84.5	69.1	51.4	9.3	0.41	0.34	0.33	0.41	0.34	0.33

Using the properties in Table 5.1, elements of the orthotropic material constitutive matrix can be specified directly in Abaqus by using the equations below obtained from the Abaqus User Documentation and can be seen in Figure 5.1.

$$
\begin{Bmatrix} \sigma_{11} \\ \sigma_{22} \\ \sigma_{33} \\ \sigma_{12} \\ \sigma_{13} \\ \sigma_{23} \end{Bmatrix} =
\begin{bmatrix}
D_{1111} & D_{1122} & D_{1133} & 0 & 0 & 0 \\
 & D_{2222} & D_{2233} & 0 & 0 & 0 \\
 & & D_{3333} & 0 & 0 & 0 \\
 & & & D_{1212} & 0 & 0 \\
 & sym & & & D_{1313} & 0 \\
 & & & & & D_{2323}
\end{bmatrix}
\begin{Bmatrix} \varepsilon_{11} \\ \varepsilon_{22} \\ \varepsilon_{33} \\ \gamma_{12} \\ \gamma_{13} \\ \gamma_{23} \end{Bmatrix}
= [D^{el}]
\begin{Bmatrix} \varepsilon_{11} \\ \varepsilon_{22} \\ \varepsilon_{33} \\ \gamma_{12} \\ \gamma_{13} \\ \gamma_{23} \end{Bmatrix}
$$

For an orthotropic material the engineering constants define the **D** matrix as

$D_{1111} = E_1(1 - \nu_{23}\nu_{32})\Upsilon,$

$D_{2222} = E_2(1 - \nu_{13}\nu_{31})\Upsilon,$

$D_{3333} = E_3(1 - \nu_{12}\nu_{21})\Upsilon,$

$D_{1122} = E_1(\nu_{21} + \nu_{31}\nu_{23})\Upsilon = E_2(\nu_{12} + \nu_{32}\nu_{13})\Upsilon,$

$D_{1133} = E_1(\nu_{31} + \nu_{21}\nu_{32})\Upsilon = E_3(\nu_{13} + \nu_{12}\nu_{23})\Upsilon,$

$D_{2233} = E_2(\nu_{32} + \nu_{12}\nu_{31})\Upsilon = E_3(\nu_{23} + \nu_{21}\nu_{13})\Upsilon,$

$D_{1212} = G_{12},$

$D_{1313} = G_{13},$

$D_{2323} = G_{23},$

where

$$\Upsilon = \frac{1}{1 - \nu_{12}\nu_{21} - \nu_{23}\nu_{32} - \nu_{31}\nu_{13} - 2\nu_{21}\nu_{32}\nu_{13}}.$$

Figure 5.1. Abaqus User Documentation Orthotropic Material Definition (2020)

Once the elements of the orthotropic material constitutive matrix were defined for the elastic behavior of the CLT, the plastic behavior of the CLT was defined by specifying the yield stress as 6.39 ksi, as presented in research by Jalilifar et al. (2021). Isotropic hardening was specified as the plastic hardening mechanism.

Contact interaction properties in Abaqus were specified using the "hard" contact method in the normal direction and the penalty contact method in the tangential direction. For the penalty method, when the CLT was in contact with other CLT it was assumed to act frictionless, when CLT was in contact with steel or a steel fastener the friction coefficient was assumed to be 0.5, and when steel was in contact with other steel the friction coefficient was assumed to be 0.3. Considering the behavior of the interaction of the steel fasteners with the wood to model wood crushing adequately, a "soft" contact approach was taken. In Abaqus, the user can define a bilinear pressure-overclosure curve that approximates pressure and separation between the master and slave surfaces. What was found to work properly was the approach originally determined by Jalilifar et al. (2021) when studying CLT diaphragm connections. This approach was to use an initial stiffness of 500 ksi and a secondary stiffness of 2,000 ksi, with the yielding overclosure being 0.005 in.

The mesh that was developed for each part utilized 3-dimensional linear hexahedral elements, and when needed, used enhanced hourglass controls to help prevent errors of excessive distortion under large displacements. This problem occurred, in most cases, in areas around the interaction of the screw with the wood. When studying the specimens under large displacements, excessive distortion of the elements often occurred in these locations. Enhanced hourglass control was used to prevent this issue. For specimens 3 and 4, a free meshing approach was taken

as it was difficult to develop a mesh using hex elements around the area where the angled

fasteners were modeled. In those areas, linear tetrahedral elements were used.

For monotonic simulations, the displacement was applied to the model at a constant

displacement rate to mimic what was done during experimental testing. For cyclic simulations,

the applied displacement was done exactly as it was done experimentally – by following CUREE

loading protocol. The reference displacement used for each finite element simulation was the

same as was calculated from the experimental results.

5.2.   Panel-to-Panel Finite Element Models

There were six different panel-to-panel connection finite element models that were

developed to represent the six different panel-to-panel connections that were tested in the lab. Of

the six connections, there are three different types of configurations, with the difference between

the pairs of models being a change in fastener type. For this reason, just the model for specimen

1 will be presented as representative for specimen 1 and 2, just the model for specimen 3 will be

presented as representative for specimen 3 and 4, and just the model for specimen 5 will be

presented as representative for specimen 5 and 6. However, the results for all six configurations

can be found in FEA Validation.

Modelling the panel-to-panel connection tests was important in determining effective

modelling assumptions as there is a greater amount of data to which to compare the numerical

results. Not only can the numerical results be compared to the experimental results presented in

this thesis, but they can be compared to other finite element models produced by others.

Configuration 1 was a half-lap specimen using self-tapping screws to connect the main and side members together. The bottom was modelled as a fixed connection, and the along the side of the main member, a symmetry boundary condition was applied. The displacement control was applied to the main member, as it was in the lab. Figure 5.2 shows the boundary conditions placed on the finite element model. The mesh that was developed, as seen in Figure 5.3, Figure 5.4 and Figure 5.5, was made up of a total of 47,677 elements. Figures of the stress distribution at 1 inch of displacement can be seen in Figure 5.6, Figure 5.7, and Figure 5.8. The total run times of the monotonic and cyclic analysis were 40 minutes and 19 hours, respectively, on a computer with 12 cores with a CPU clock rate of 2.4 GHz and 24 GB of RAM.
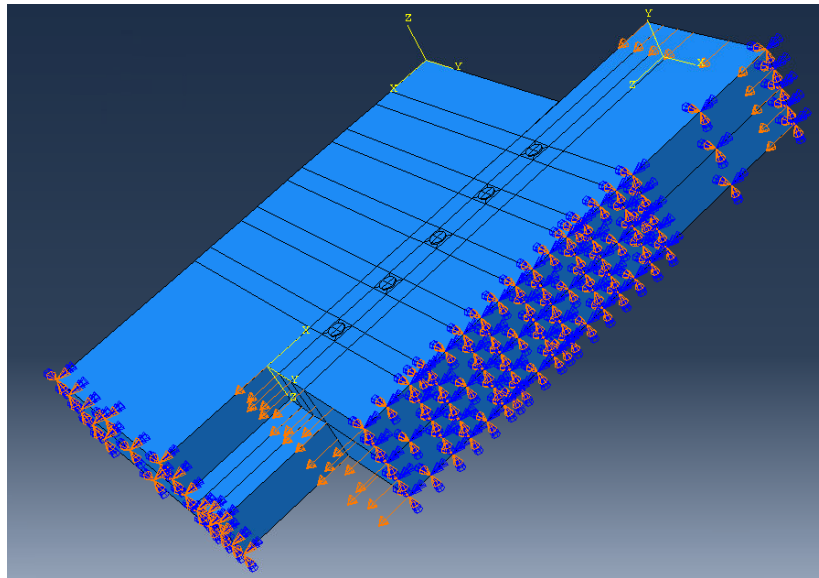
Figure 5.2. Specimen 1 Monotonic Boundary Conditions
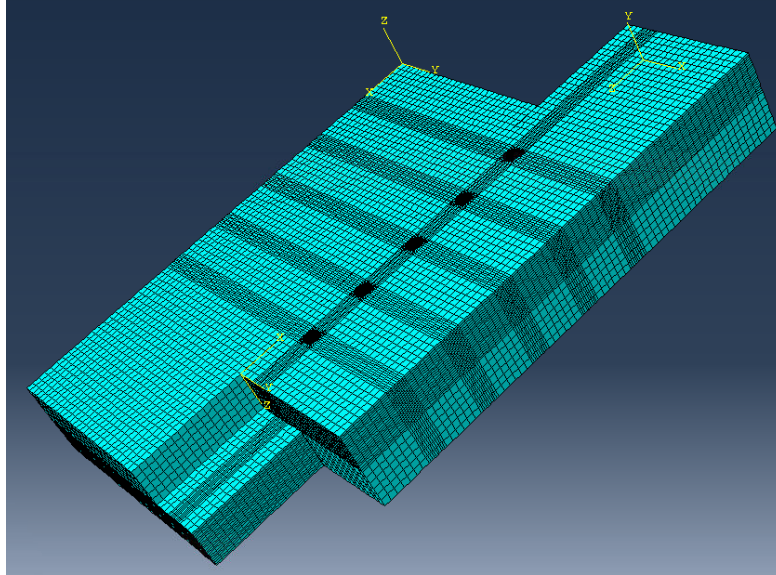
Figure 5.3. Specimen 1 Mesh
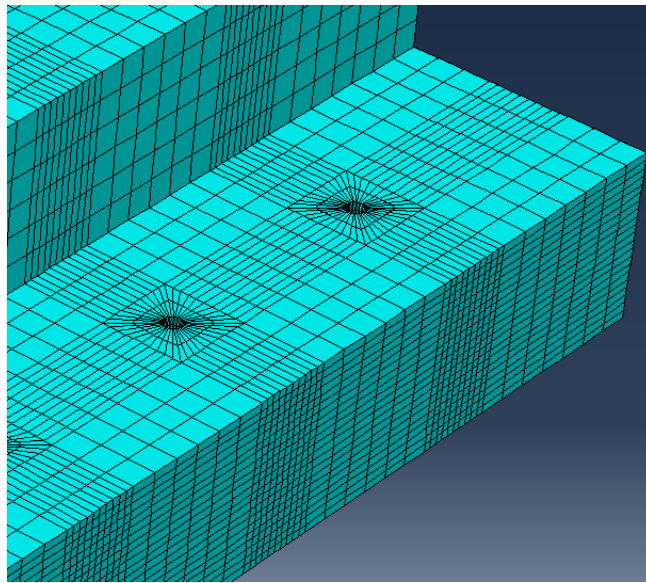
Figure 5.4. Specimen 1 Mesh on CLT
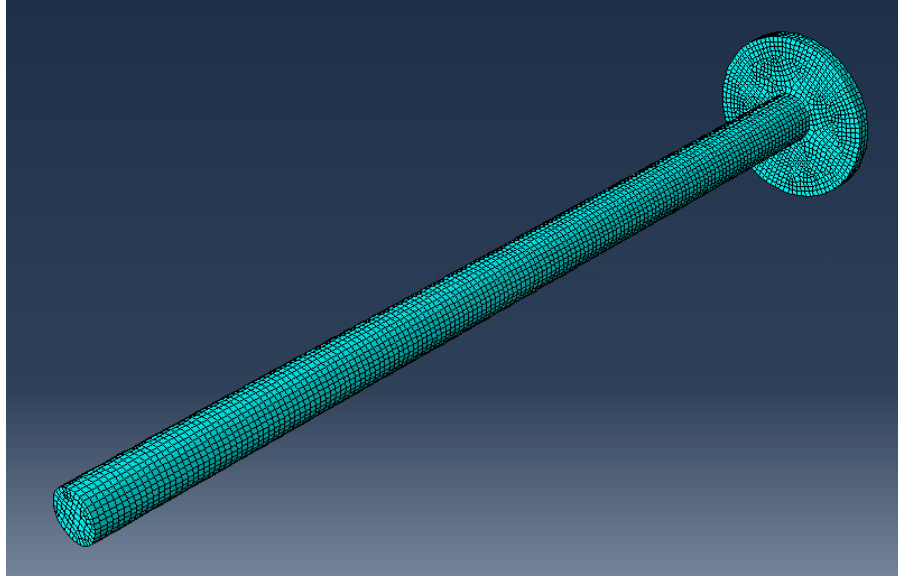
Figure 5.5. Specimen 1 Mesh on Screw
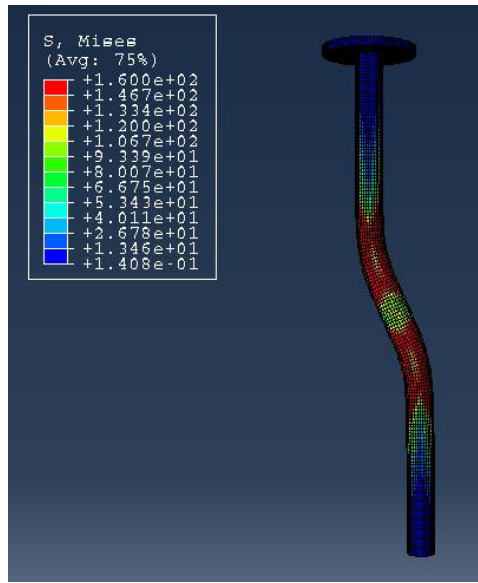
Figure 5.6. Specimen 1 Stress Distribution on Screw
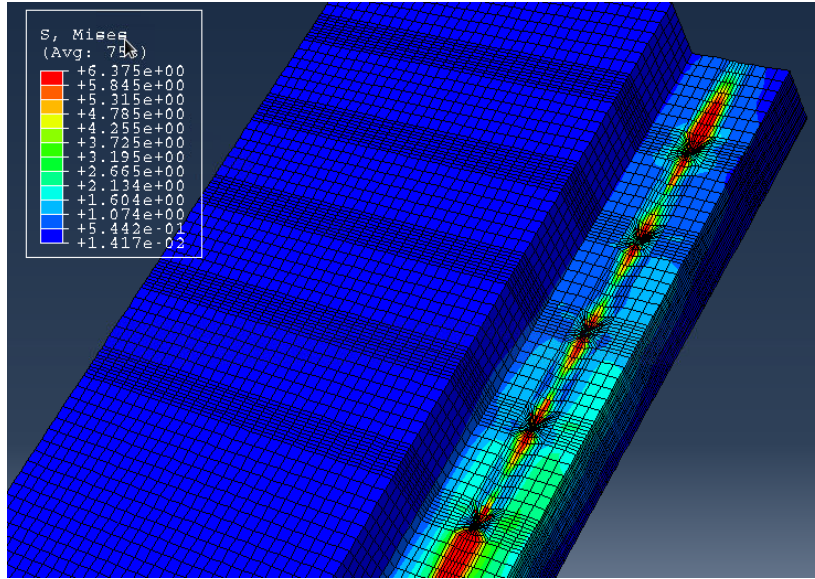
Figure 5.7. Specimen 1 Stress Distribution on Side Member
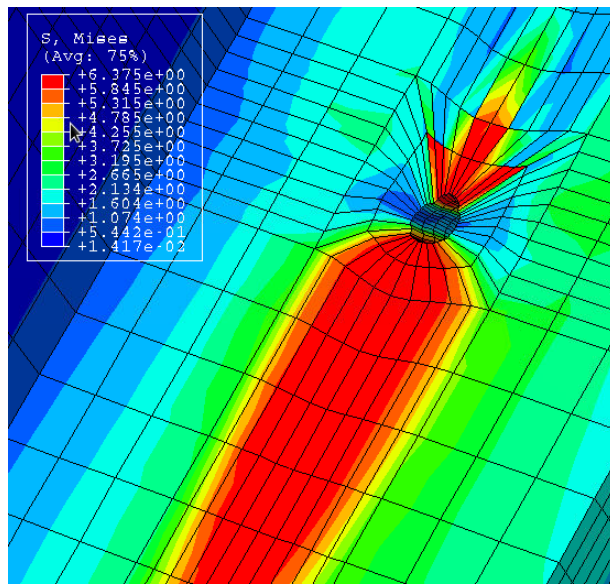
Figure 5.8. Specimen 1 Close-Up of Stress Distribution on CLT

<u>Specimen 3</u>

Configuration 3 was a half-lap specimen using self-tapping screws to connect the main and side members together. Four fasteners were installed at 90-degrees and four were installed at 45-degrees in opposing directions. The bottom was modelled as a fixed connection, and the along the side of the main member, a symmetry boundary condition was applied. The displacement control was applied to the main member, as it was in the lab. Figure 5.9 shows the boundary conditions placed on the finite element model. The mesh that was developed, as seen in Figure 5.10 and Figure 5.11, was made up of a total of 263,337 elements. Figures of the stress distribution at 1 inch of displacement can be seen in Figure 5.12 and Figure 5.13. The total run times of the monotonic and cyclic analysis were 225 minutes and 71 hours, respectively, on a computer with 12 cores with a CPU clock rate of 2.4 GHz and 24 GB of RAM.

Figure 5.9. Specimen 3 Boundary Conditions
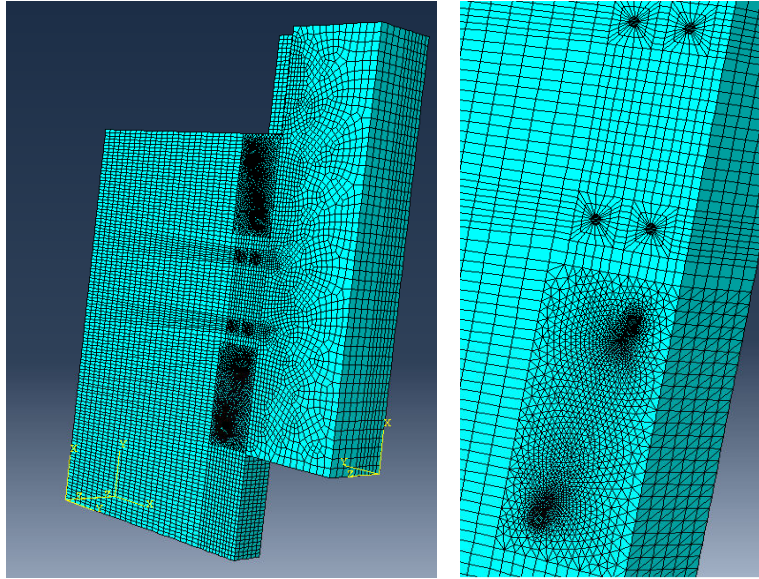
Figure 5.10. Specimen 3 Mesh
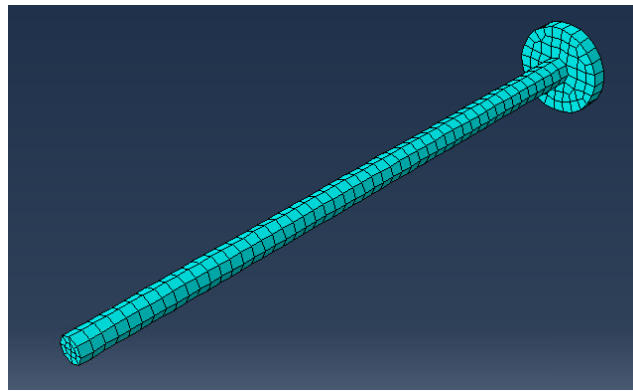
Figure 5.11. Specimen 3 Mesh on Screw
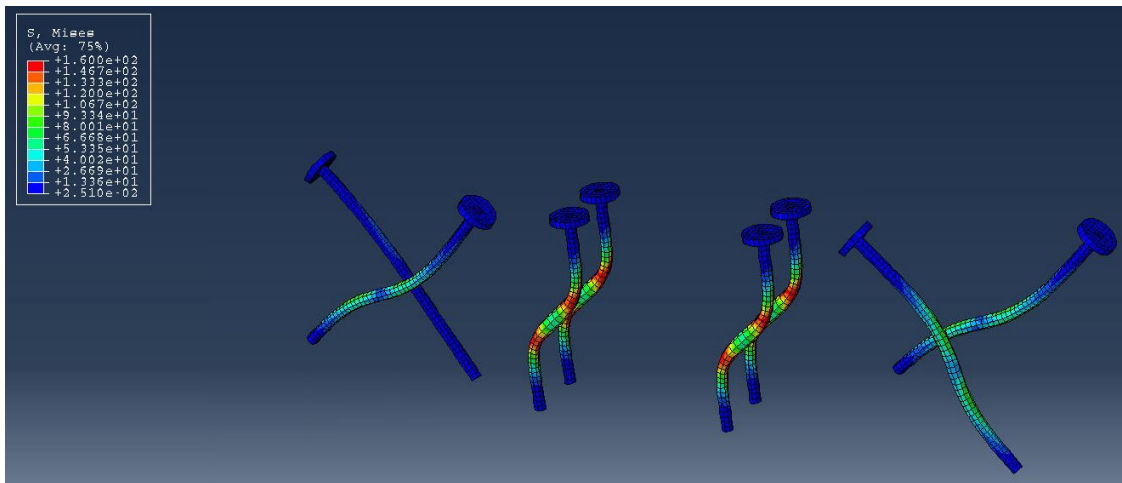
Figure 5.12. Specimen 3 Stress Distribution on Fastener Group
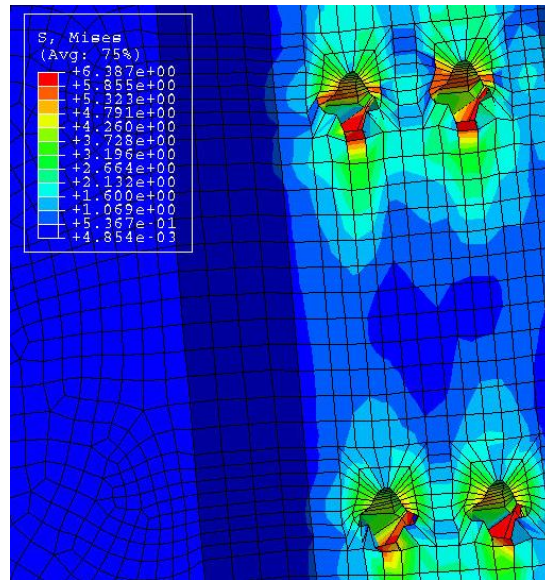
Figure 5.13. Specimen 3 Stress Distribution on CLT

Specimen 5

Configuration 5 was a half-lap specimen using self-tapping screws to connect the main and side members together. The bottom was modelled as a fixed connection, and the along the side of the main member, a symmetry boundary condition was applied. The displacement control was applied to the main member, as it was in the lab. Figure 5.14 shows the boundary conditions placed on the finite element model. The mesh that was developed, as seen in Figure 5.15, Figure 5.16, Figure 5.17, and Figure 5.18, was made up of a total of 84,788 elements. Figures of the stress distribution at 1 inch of displacement can be seen in Figure 5.19, Figure 5.20, and Figure 5.21. The total run times of the monotonic and cyclic analysis were 68 minutes and 48 hours, respectively, on a computer with 12 cores with a CPU clock rate of 2.4 GHz and 24 GB of RAM.
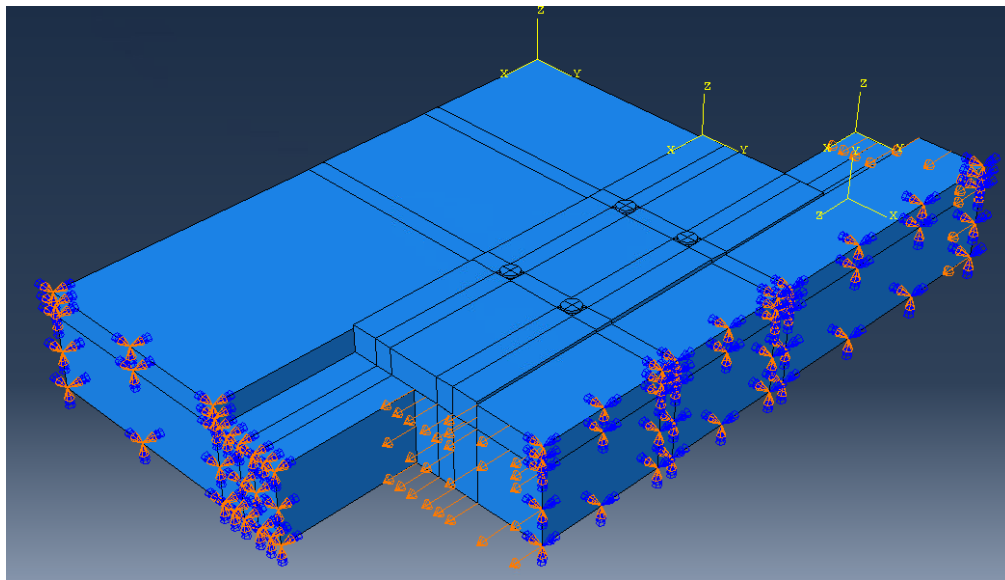
Figure 5.14. Specimen 5 Boundary Conditions
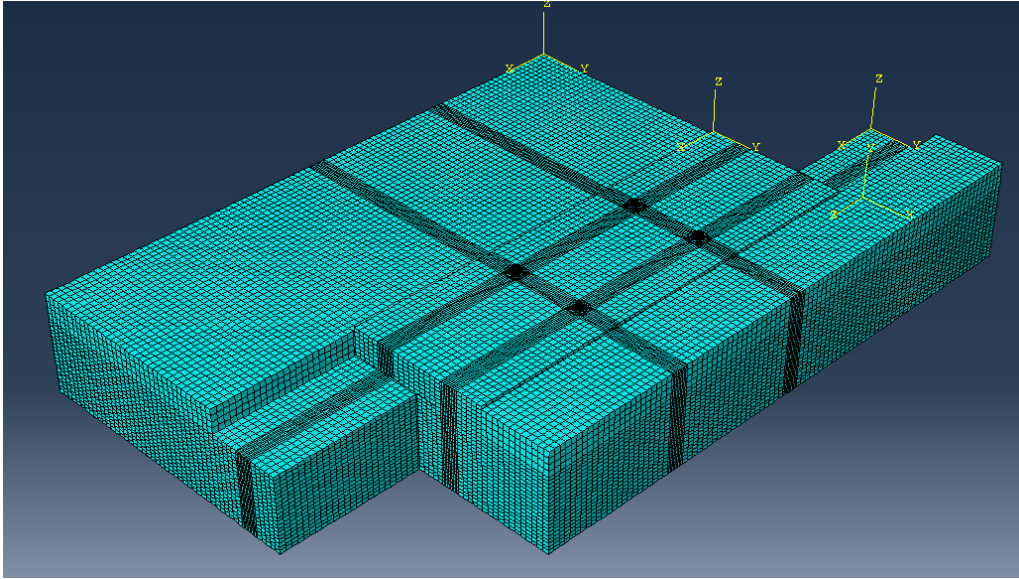
Figure 5.15. Specimen 5 Mesh
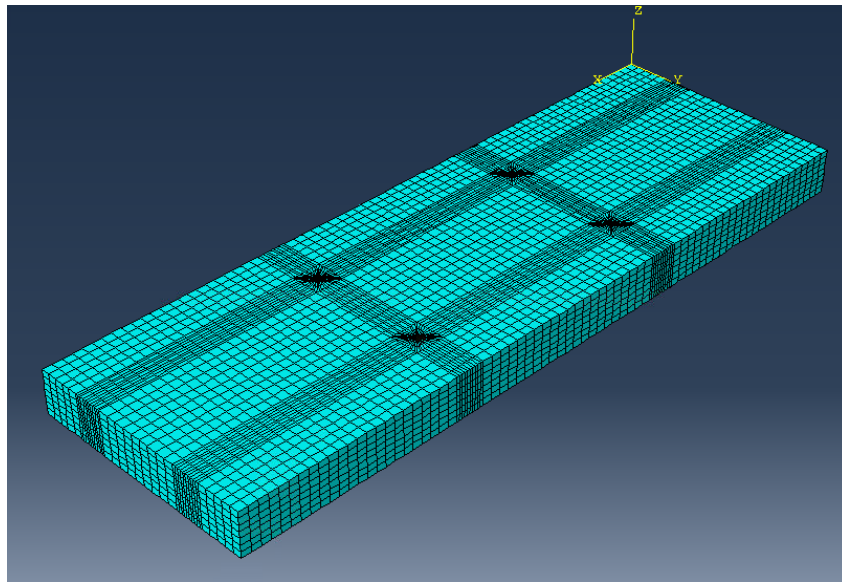
Figure 5.16. Specimen 5 Mesh on Plywood Spline

Figure 5.17. Specimen 5 Mesh on Screw

Figure 5.18. Specimen 5 Mesh on CLT

Figure 5.19. Specimen 5 Stress Distribution on Screws
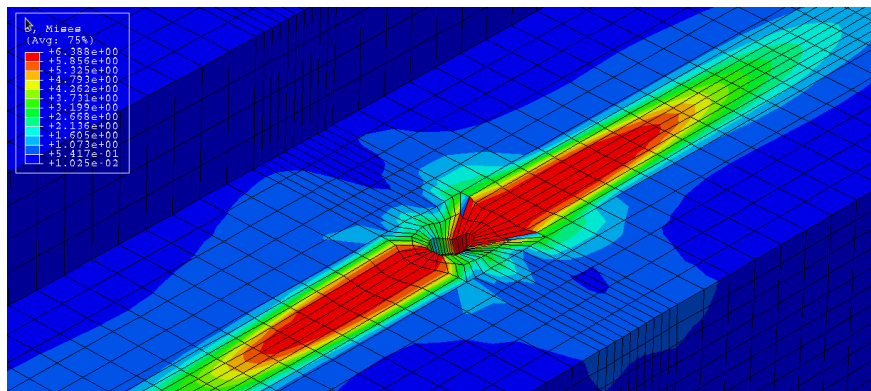
Figure 5.20. Specimen 5 Stress Distribution on CLT

Figure 5.21. Specimen 5 Stress Distribution on Plywood Spline

114

5.3.   Wall-to-Floor Finite Element Models

There were four different wall-to-floor finite element models that were developed to represent the four different wall-to-floor connections that were tested in the lab. In this section, two of the models will be presented, as the formulation of both load-bearing and both non-load-bearing models were very similar. The only difference between specimens 7 and 8 and specimens 9 and 10 were different properties of the fasteners that were used. For this reason, just specimen 7 and specimen 9 will have their models presented in this section, but the results of all four models are discussed in FEA Validation.

<u>Specimen 7</u>

Configuration 7 was a wall-to-floor load-bearing specimen using self-tapping screws, an angle bracket and an LVL bearing support to connect the main and side members together. The bottom was modelled as a fixed connection, and the along the side of the main member, a symmetry boundary condition was applied. The displacement control was applied to the main member (floor), as it was in the lab. Figure 5.22 shows the boundary conditions placed on the finite element model. The mesh that was developed, as seen in Figure 5.23, Figure 5.24, Figure 5.25, Figure 5.26, and Figure 5.27, was made up of a total of 68,888 elements. Figures of the stress distribution at 1 inch of displacement can be seen in Figure 5.28, Figure 5.29, and Figure 5.30. The total run times of the monotonic and cyclic analysis were 135 minutes and 64 hours, respectively, on a computer with 12 cores with a CPU clock rate of 2.4 GHz and 24 GB of RAM.

115
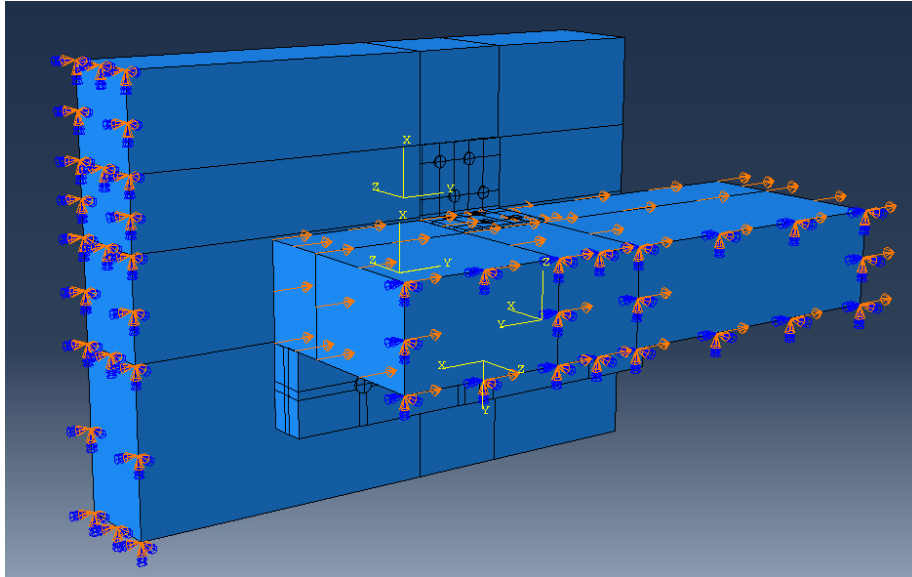
Figure 5.22. Specimen 7 Boundary Conditions
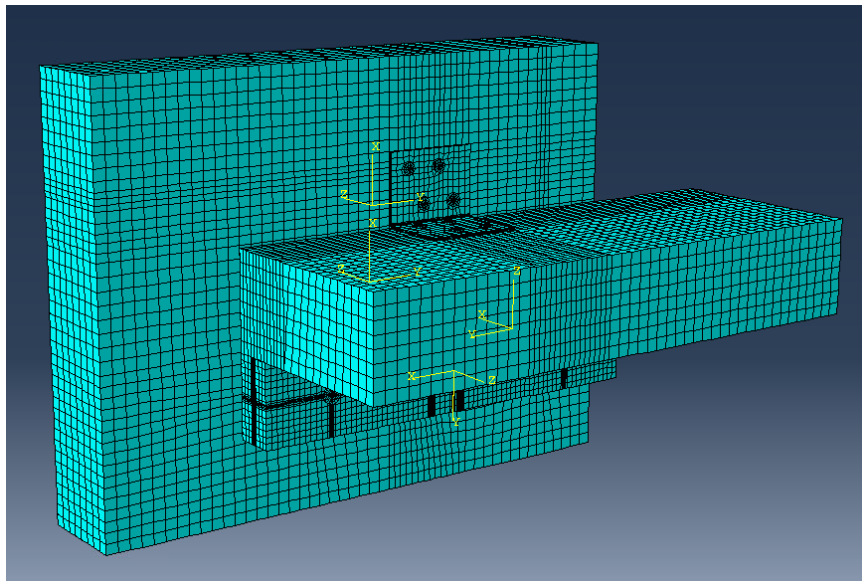
Figure 5.23. Specimen 7 Mesh

116
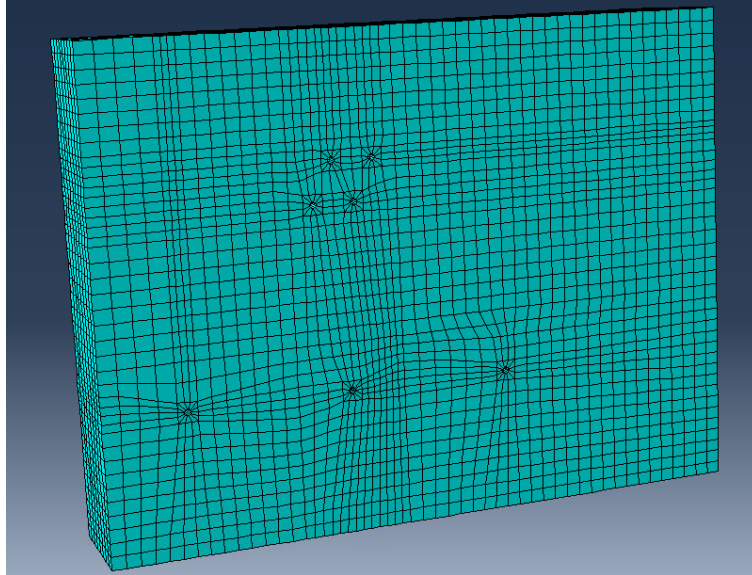
Figure 5.24. Specimen 7 Mesh on CLT
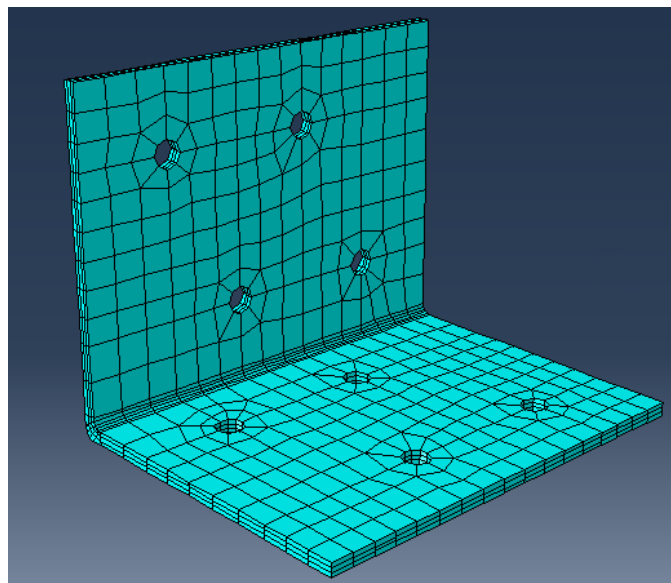
Figure 5.25. Specimen 7 Mesh on Angle Bracket

117
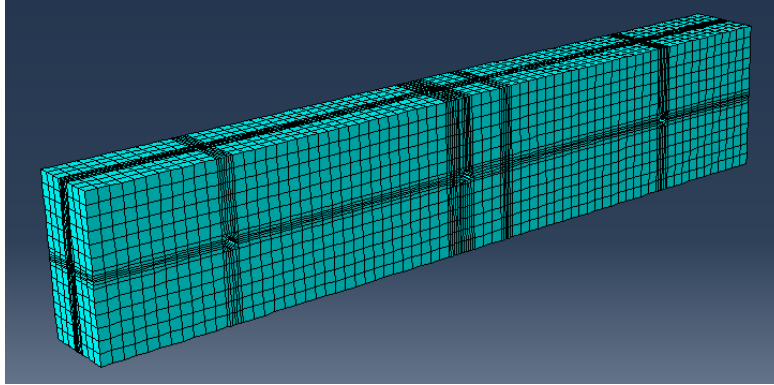
Figure 5.26. Specimen 7 Mesh on LVL
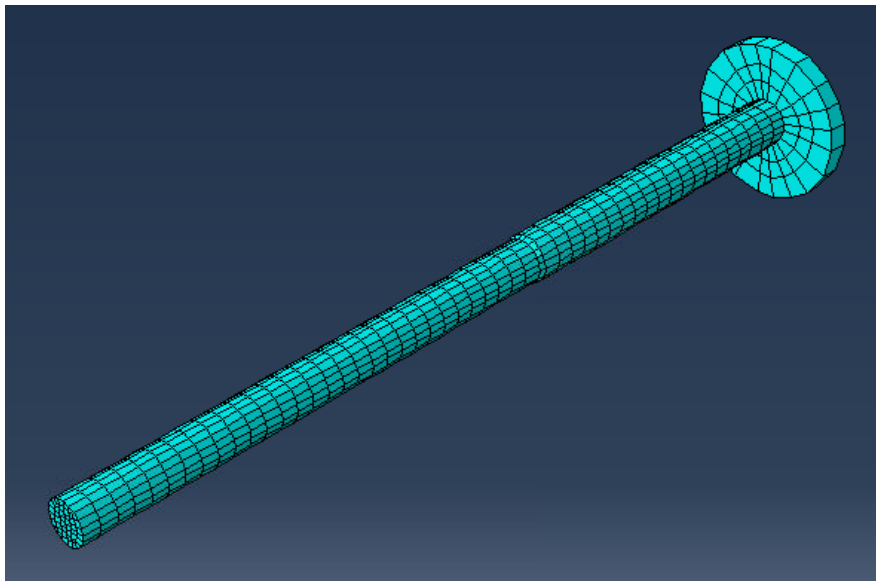
Figure 5.27. Specimen 7 Mesh on Screw
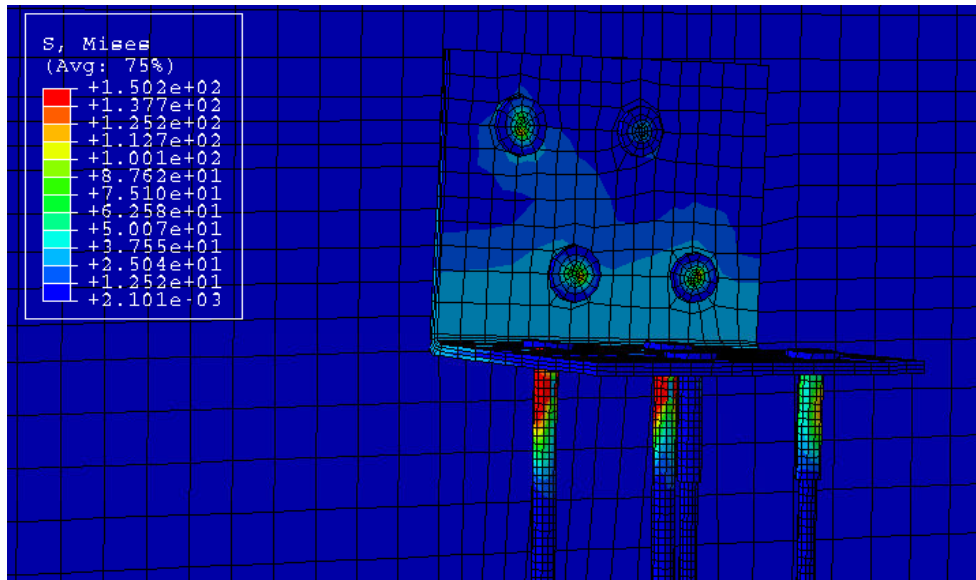
Figure 5.28. Specimen 7 Stress Distribution on Fastener Group
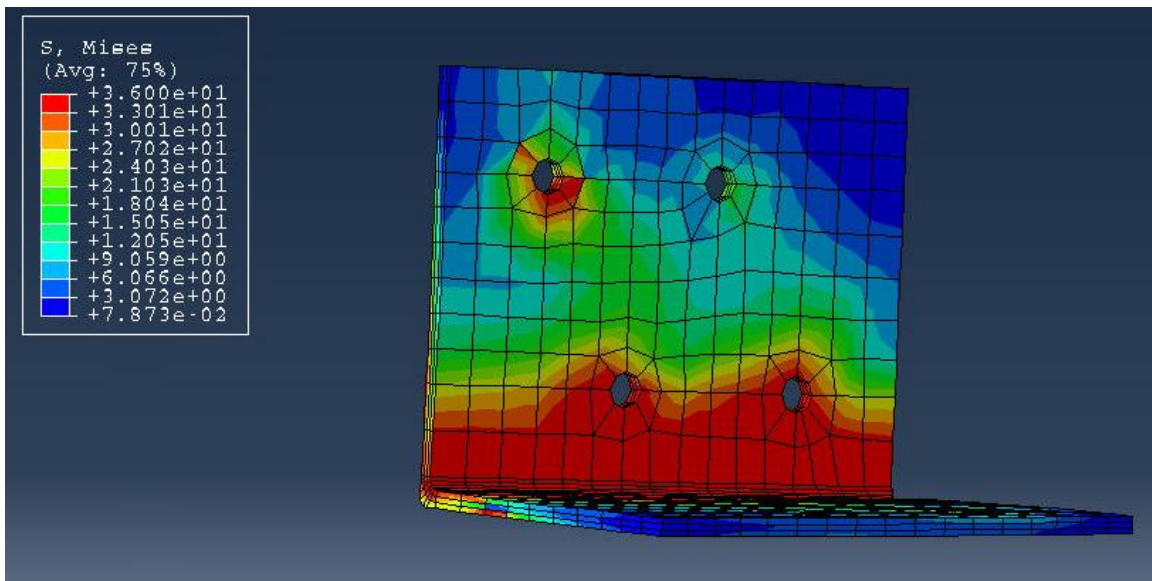
Figure 5.29. Specimen 7 Stress Distribution on Angle Bracket

119
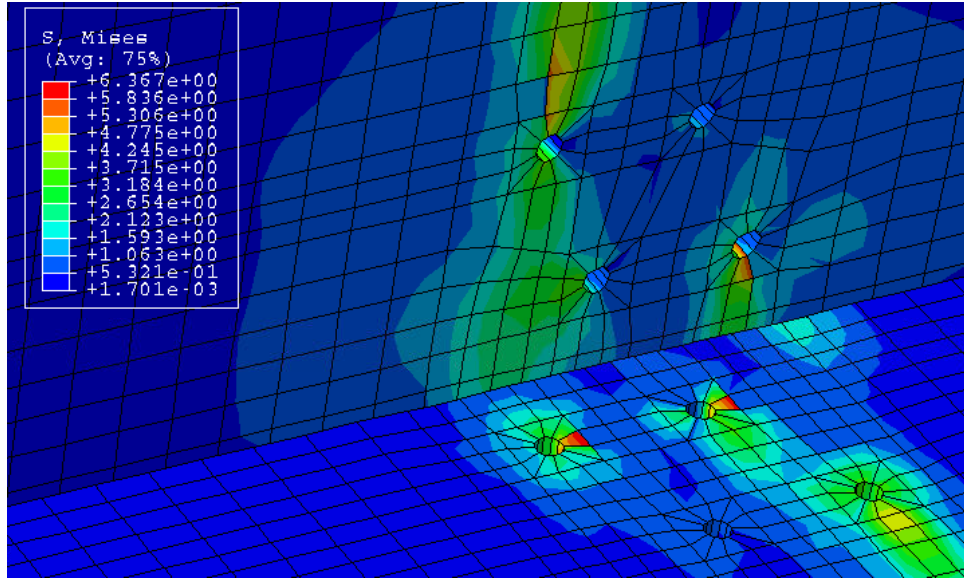
Figure 5.30. Specimen 7 Stress Distribution on CLT

Configuration 9 was a wall-to-floor non-load-bearing specimen using self-tapping screws and angle brackets to connect the main and side members together. The bottom was modelled as a fixed connection, and the along the side of the main member, a symmetry boundary condition was applied. The displacement control was applied to the main member (floor), as it was in the lab. Figure 5.31 shows the boundary conditions placed on the finite element model. The mesh that was developed, as seen in Figure 5.32, Figure 5.33, Figure 5.34, and Figure 5.35, was made up of a total of 69,567 elements. Figures of the stress distribution at 1 inch of displacement can be seen in Figure 5.36, Figure 5.37, Figure 5.38, and Figure 5.39. The total run times of the monotonic and cyclic analysis were 67 minutes and 46 hours, respectively, on a computer with 12 cores with a CPU clock rate of 2.4 GHz and 24 GB of RAM.
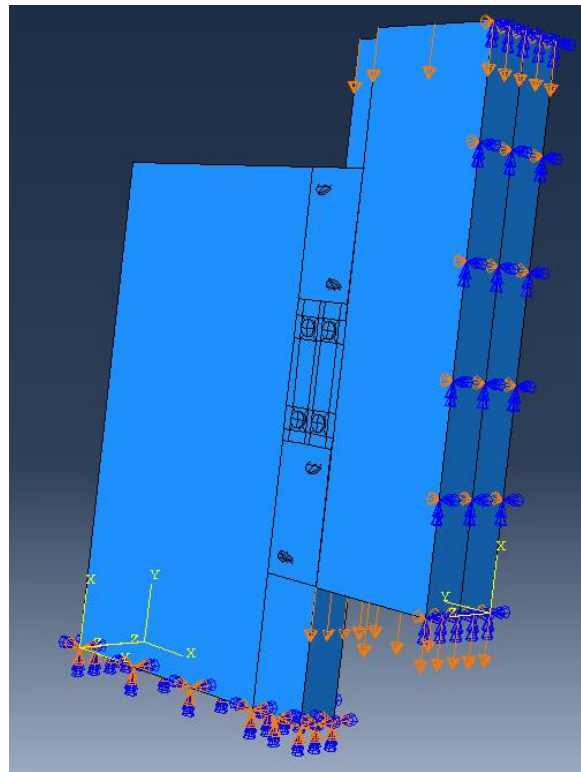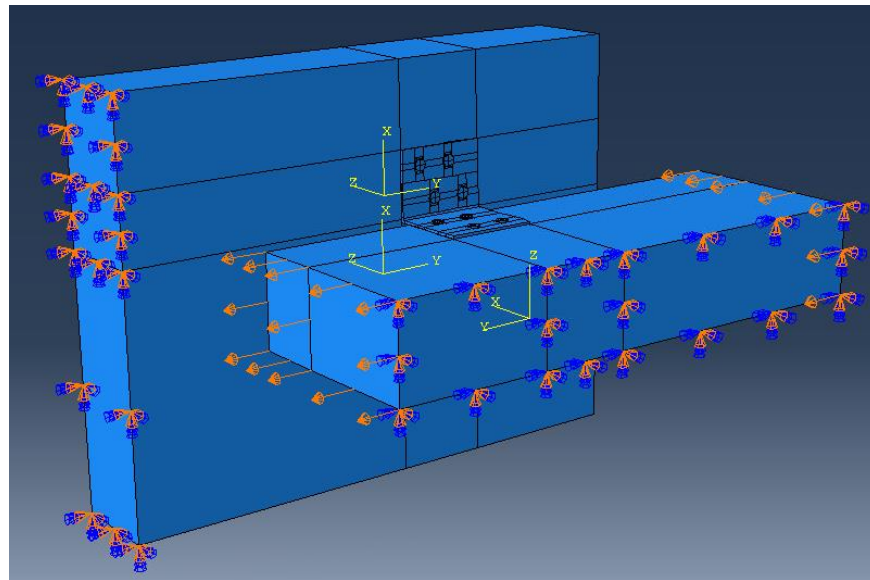

Figure 5.31. Specimen 9 Boundary Conditions
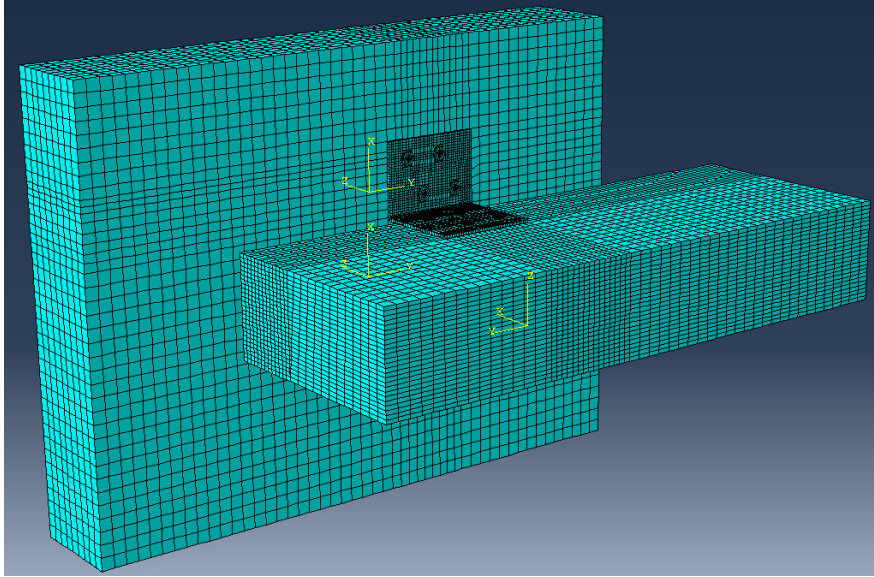
Figure 5.32. Specimen 9 Mesh
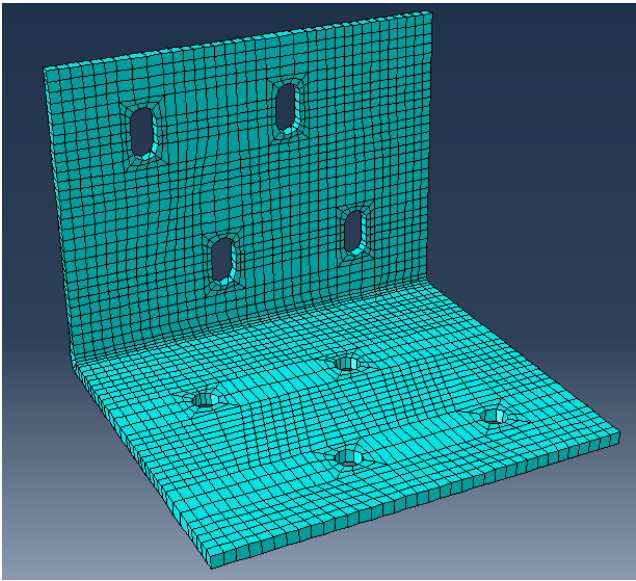
Figure 5.33. Specimen 9 Mesh on Angle Bracket
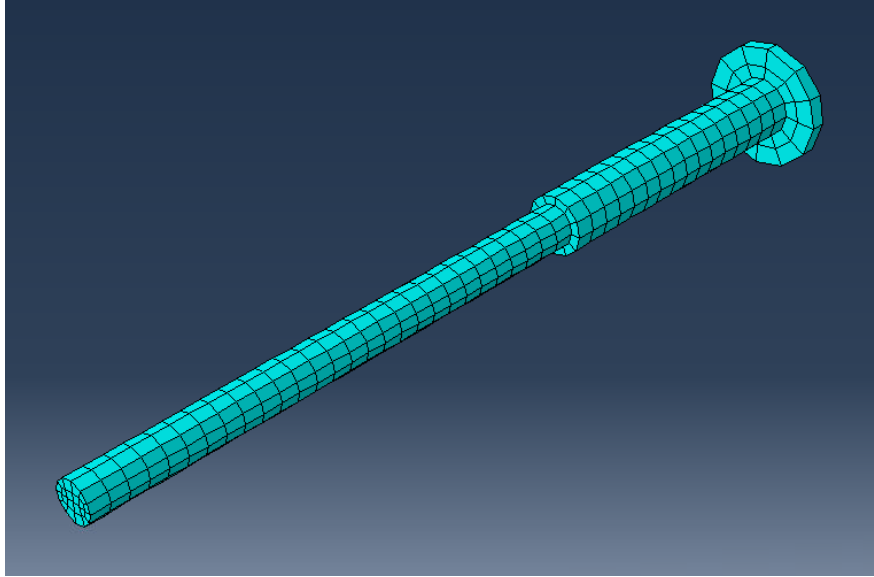
Figure 5.34. Specimen 9 Mesh on Screw
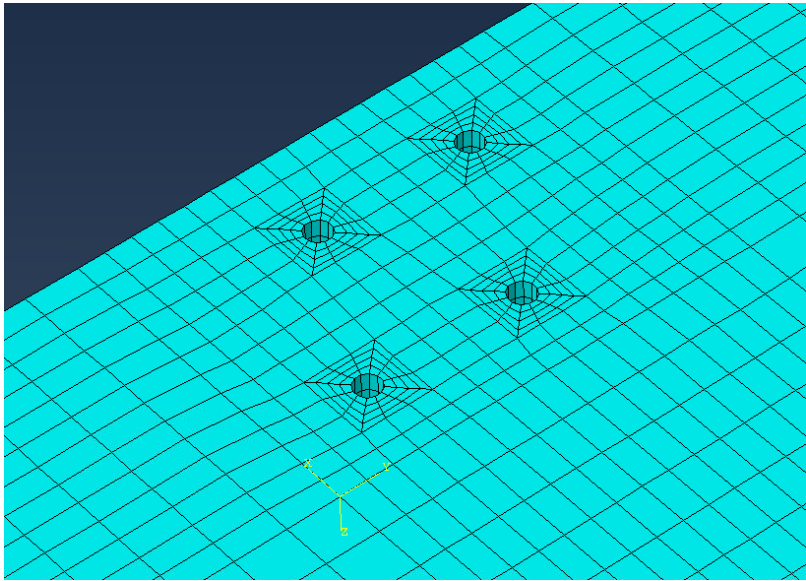

Figure 5.35. Specimen 9 Mesh on CLT
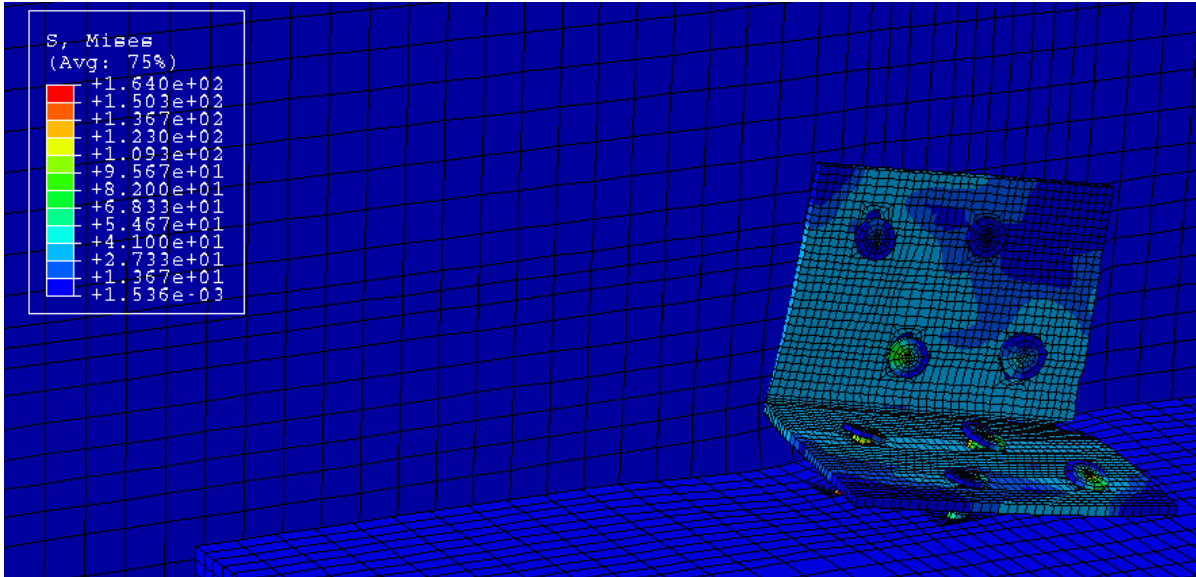
Figure 5.36. Specimen 9 Stress Distribution

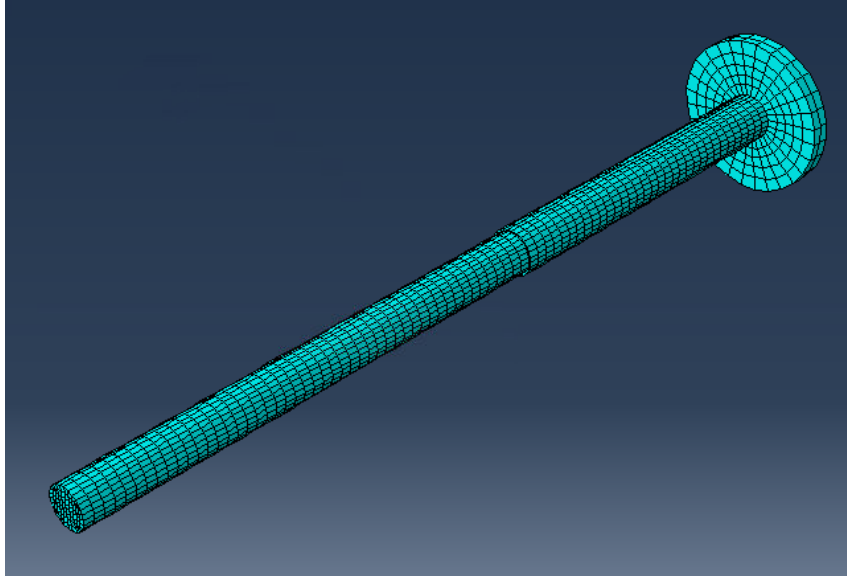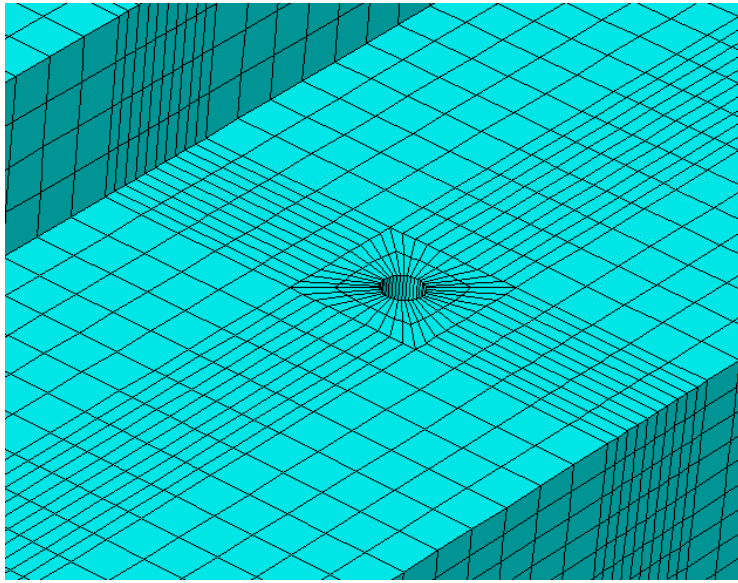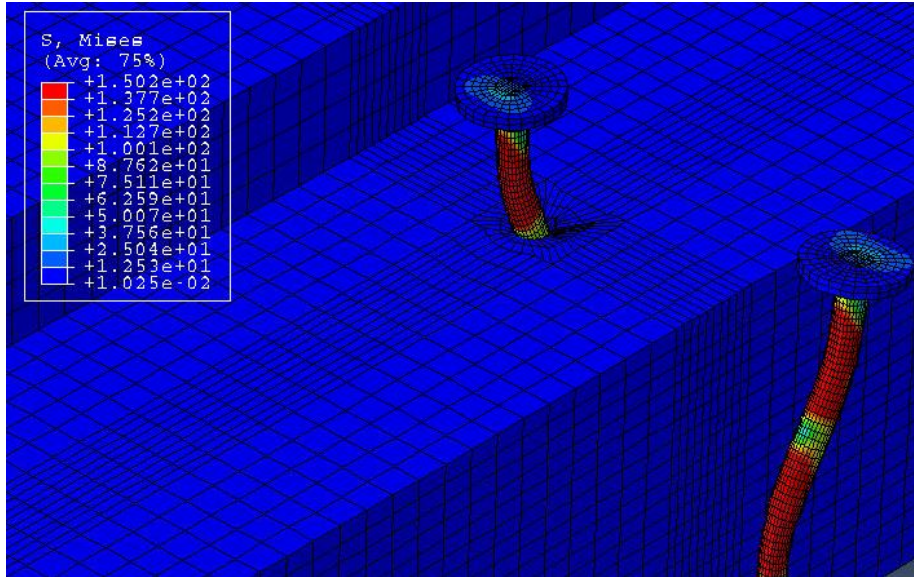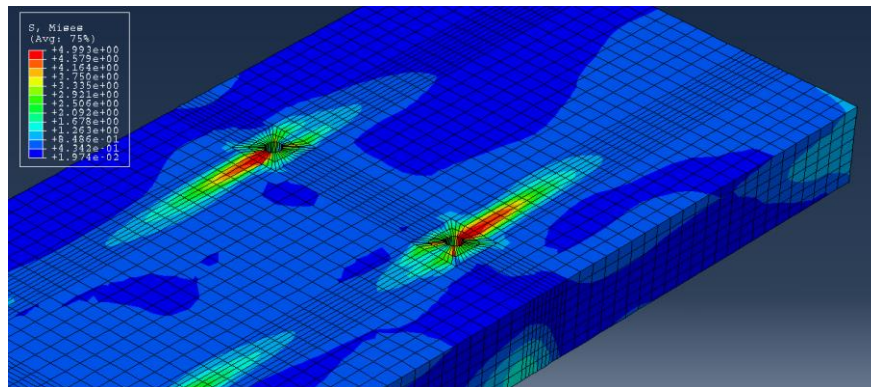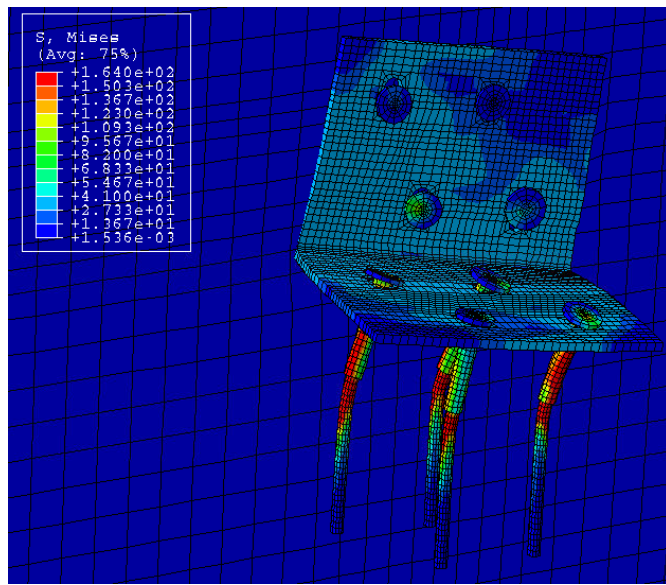Figure 5.37. Specimen 9 Stress Distribution on Fastener Group
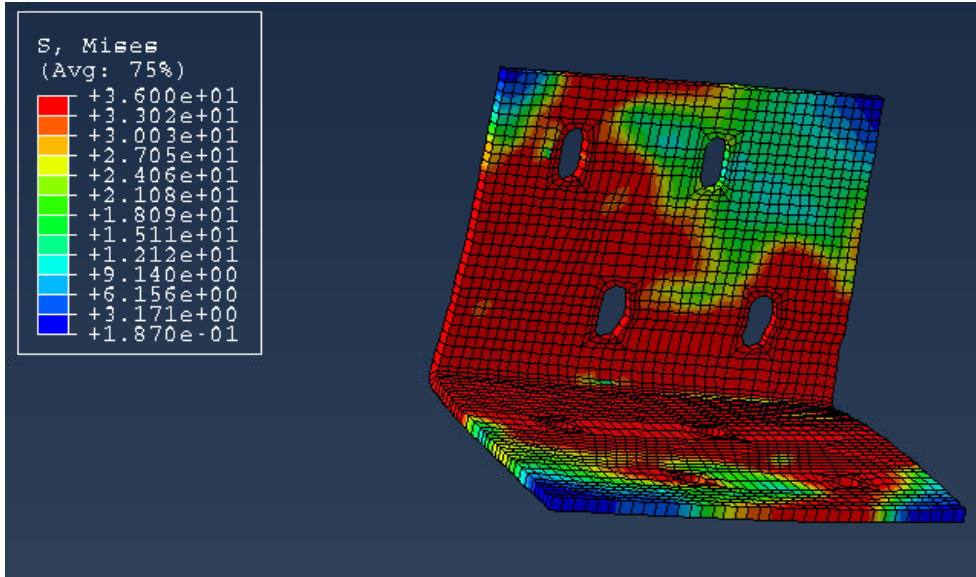
Figure 5.38. Specimen 9 Stress Distribution on Angle Bracket
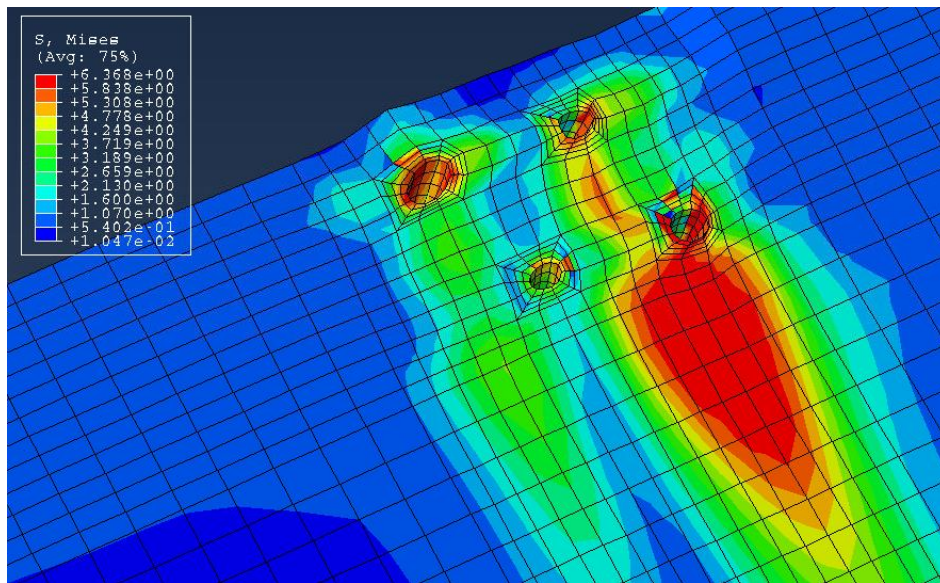
Figure 5.39. Specimen 9 Stress Distribution on CLT

5.4. FEA Results

This section presents the results of the finite element analysis as compared to the experimental results that were obtained in the lab. All comparisons were made to the average test results – an average of two tests for monotonic tests and an average of ten tests for cyclic tests. Table 5.2 compares the initial stiffness and peak load of the monotonic tests done in the lab with the pushover analysis completed using Abaqus finite element software. Table 5.3 compares the initial stiffness, load at first cycle, and peak load of the cyclic tests that were completed to the dynamic finite element analysis that was completed using Abaqus finite element software. Figure 5.40 through Figure 5.59 compare the monotonic and cyclic force-displacement curves that were obtained in the lab and that were obtained through Abaqus finite element analysis.

Table 5.2. Monotonic Finite Element Comparison

| Configuration | Monotonic Results | | | | | |
| | Initial Stiffness (kip/in) | | | Peak Load (kip/screw) | | |
	Test	Abaqus	% difference	Test	Abaqus	% difference
1	5.1	4.52	12.8%	1.84	1.95	5.6%
2	3.8	3.1	22.6%	1.99	2.11	5.7%
3	3.46	4.88	29.1%	1.65	1.54	7.1%
4	3.56	4.56	21.9%	1.57	1.62	3.1%
5	2.03	1.83	10.9%	1.18	1.29	8.5%
6	1.54	1.6	3.8%	1.25	1.28	2.3%
7	1.87	1.58	18.4%	1.03	1.06	2.8%
8	2.4	1.97	21.8%	1.22	1.21	0.8%
9	1.2	0.91	31.9%	0.72	0.75	4.0%
10	1.2	1.01	18.8%	0.88	0.81	8.6%

(Results are normalized per screw)

Table 5.3. Cyclic Finite Element Comparison

| Configuration | Cyclic Results | | | | | | | | |
| | Initial Stiffness (kip/in) - tension | | | Load at First Cycle (kip/screw) - tension | | | Peak Load (kip/screw) - tension | | |
	Test	Abaqus	% difference	Test	Abaqus	% difference	Test	Abaqus	% difference
1	7.0	7.83	10.6%	0.42	0.47	10.6%	1.41	1.49	5.4%
2	8.33	6.33	31.6%	0.56	0.38	47.4%	1.61	1.69	4.7%
3	10.25	8.75	17.1%	0.41	0.35	17.1%	0.94	1.14	17.5%
4	8.5	8.25	3.0%	0.34	0.33	3.0%	0.89	1.11	19.8%
5	3.8	4	5.0%	0.38	0.4	5.0%	0.59	0.65	9.2%
6	3.8	3.4	11.8%	0.38	0.34	11.8%	0.77	0.76	1.3%
7	2.0	1.88	6.4%	0.16	0.15	6.7%	0.23	0.28	17.9%
8	4.44	2.31	92.2%	0.48	0.25	92.0%	0.76	0.80	5.0%
9	1.5	0.75	100.0%	0.12	0.06	100.0%	0.405	0.41	1.2%
10	3.25	1.75	85.7%	0.26	0.14	85.7%	0.5	0.53	5.7%

(peak load is at last cycle of model convergence, results normalized per screw)

126
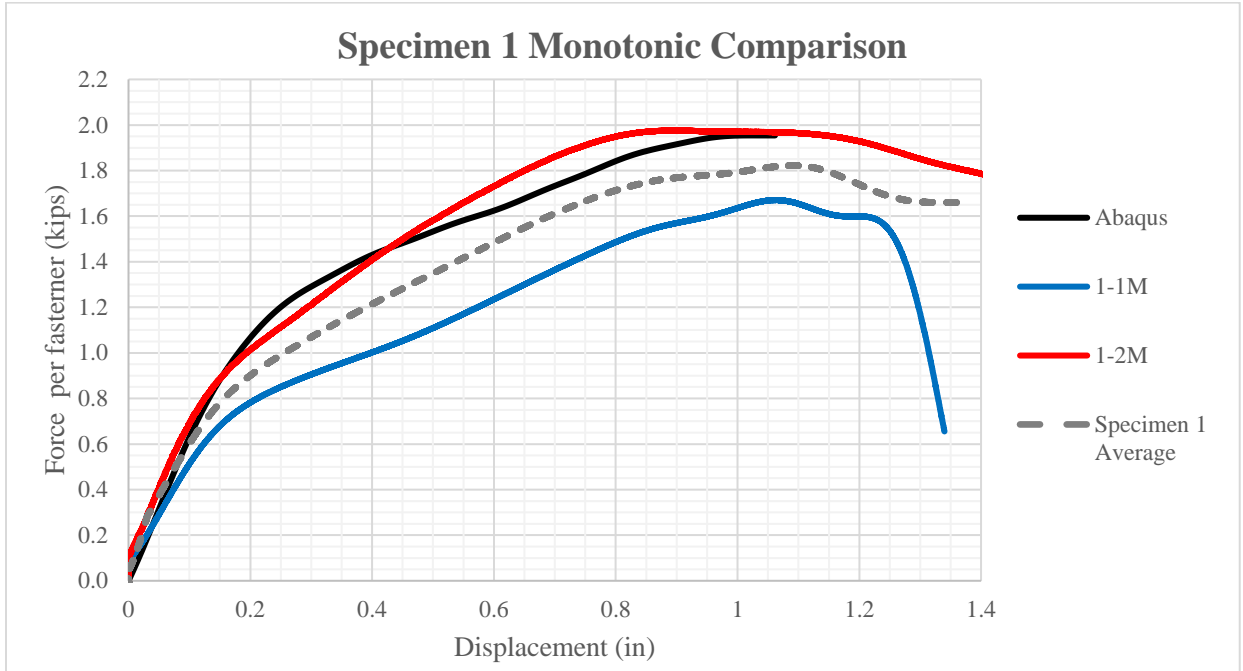
Specimen 1

Figure 5.40. Specimen 1 Monotonic Comparison
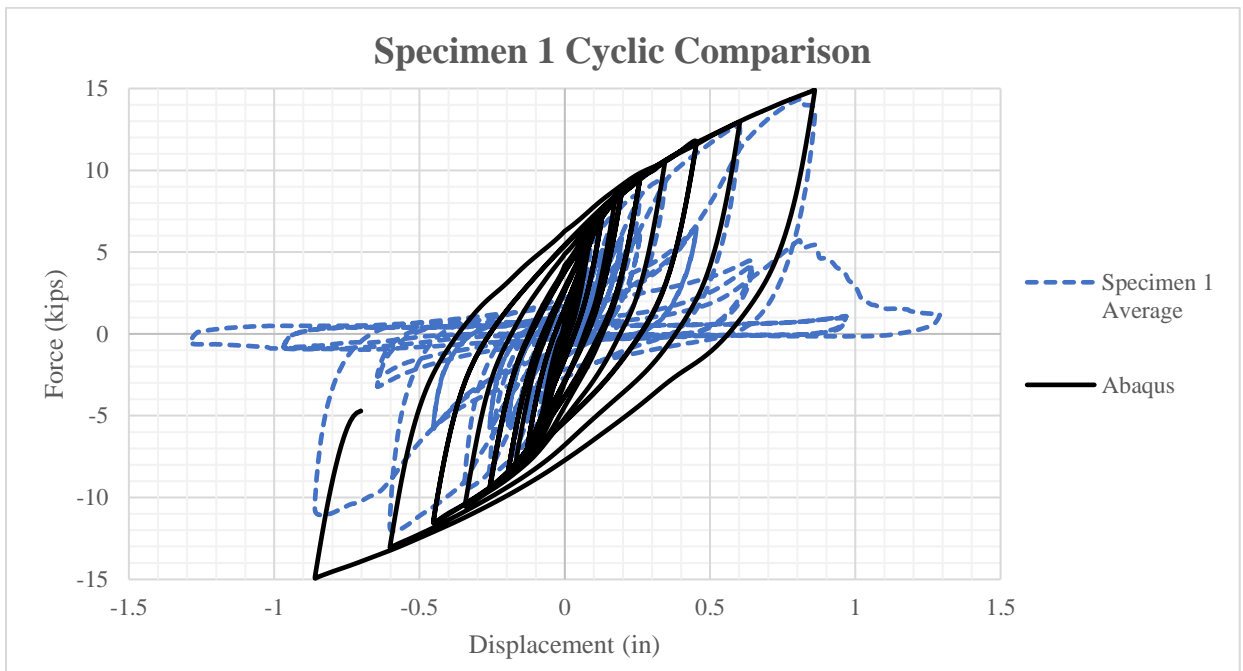
Figure 5.41. Specimen 1 Cyclic Comparison

Specimen 2
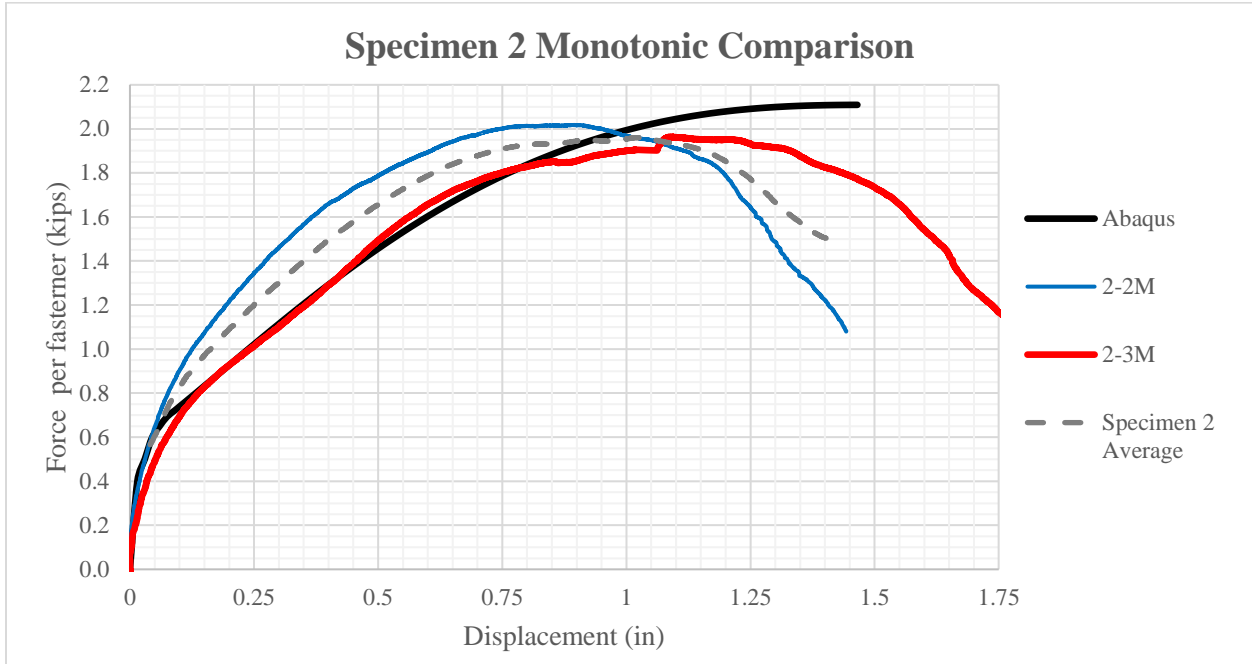
Figure 5.42. Specimen 2 Monotonic Comparison
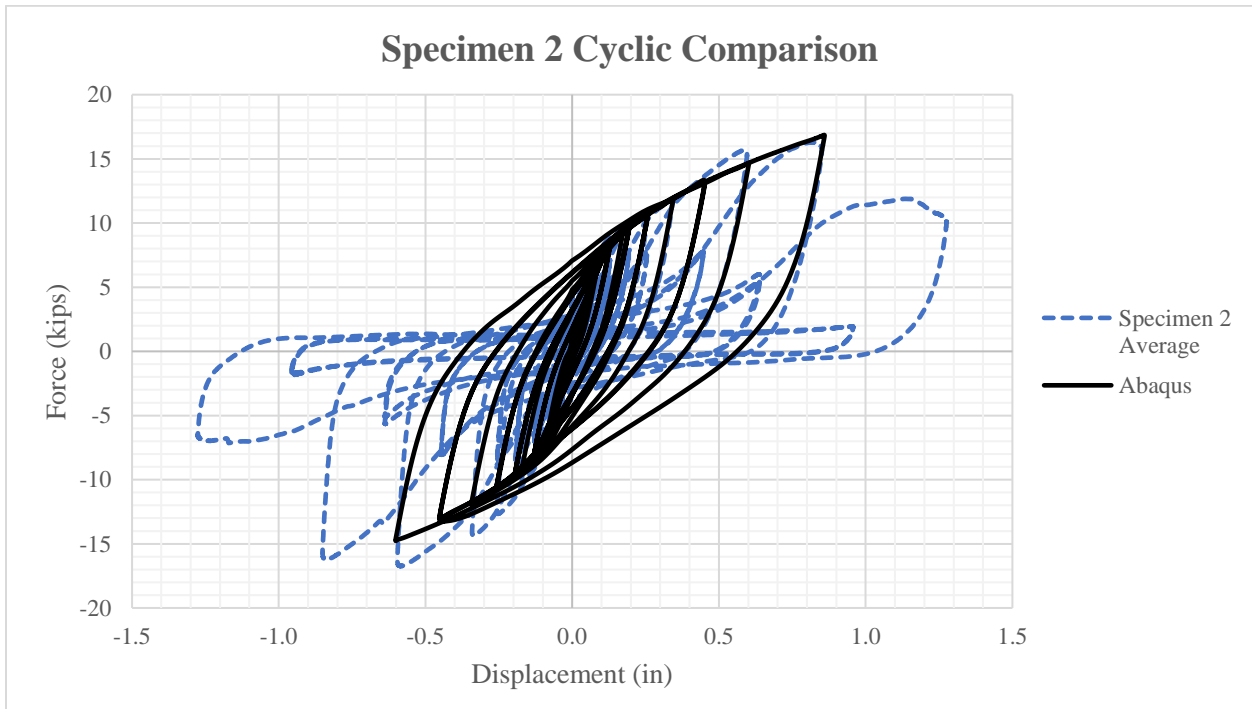
Figure 5.43. Specimen 2 Cyclic Comparison

Specimen 3
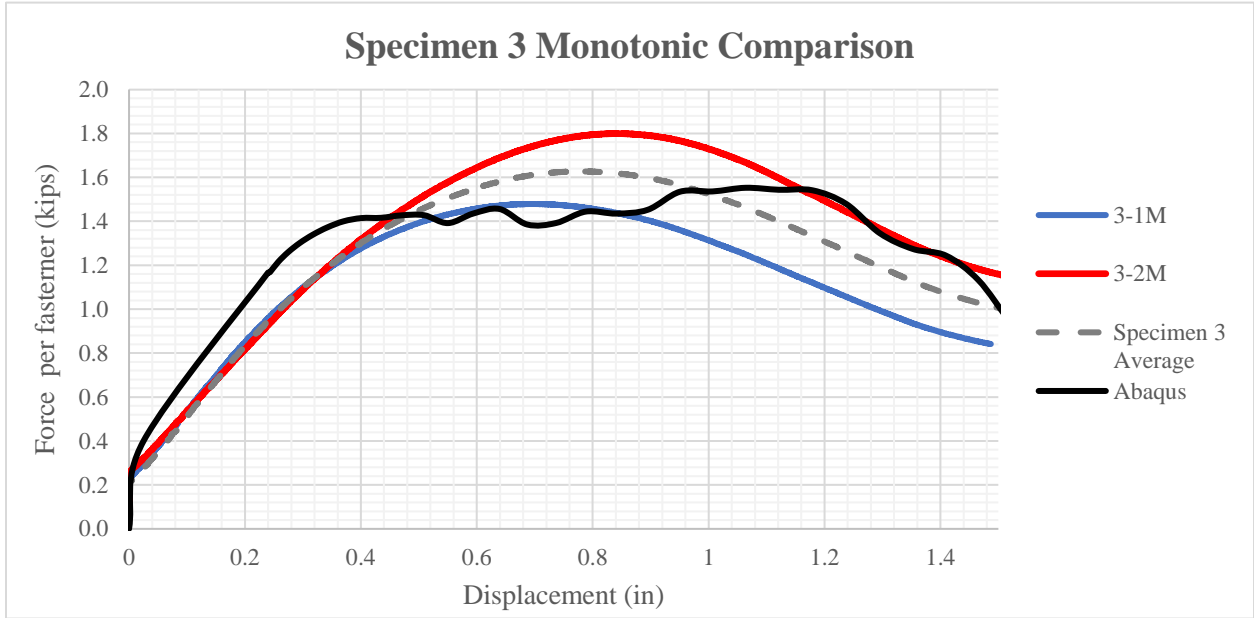
Figure 5.44. Specimen 3 Monotonic Comparison
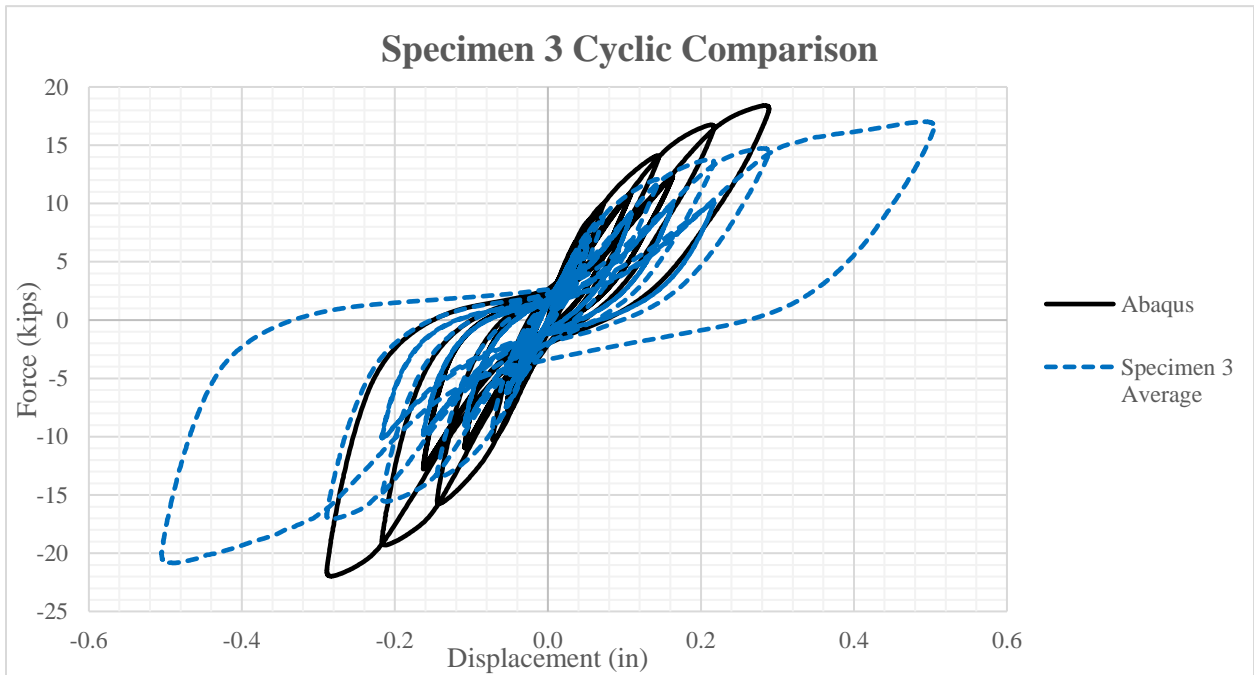
Figure 5.45. Specimen 3 Cyclic Comparison

Specimen 4
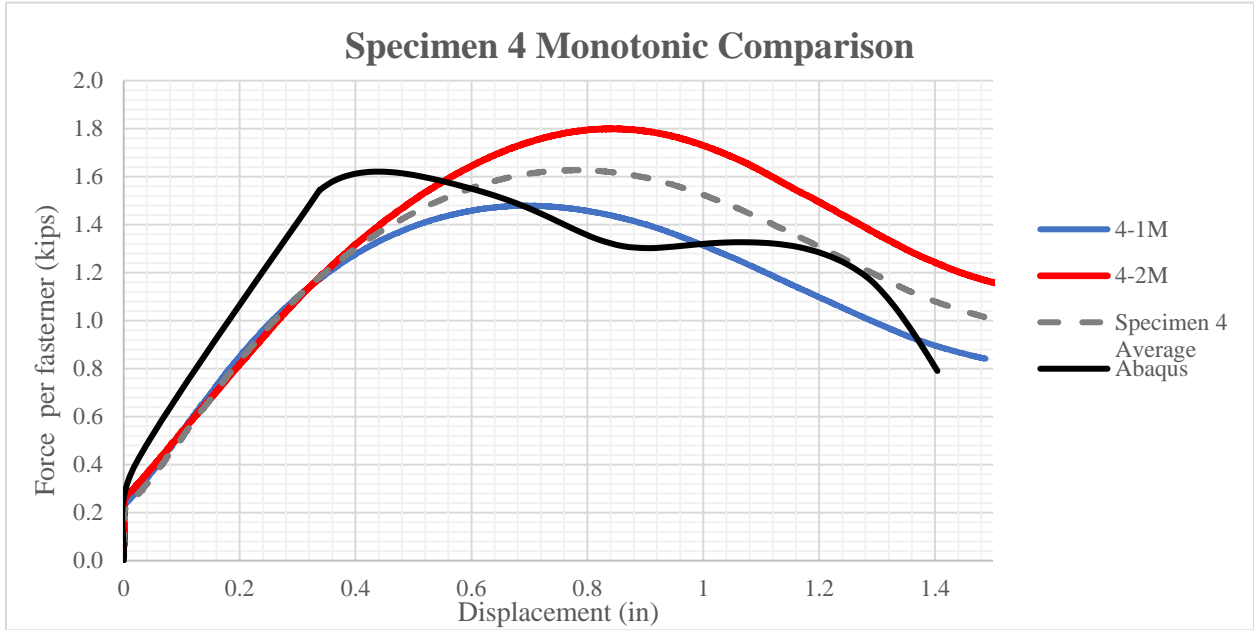
Figure 5.46. Specimen 4 Monotonic Comparison
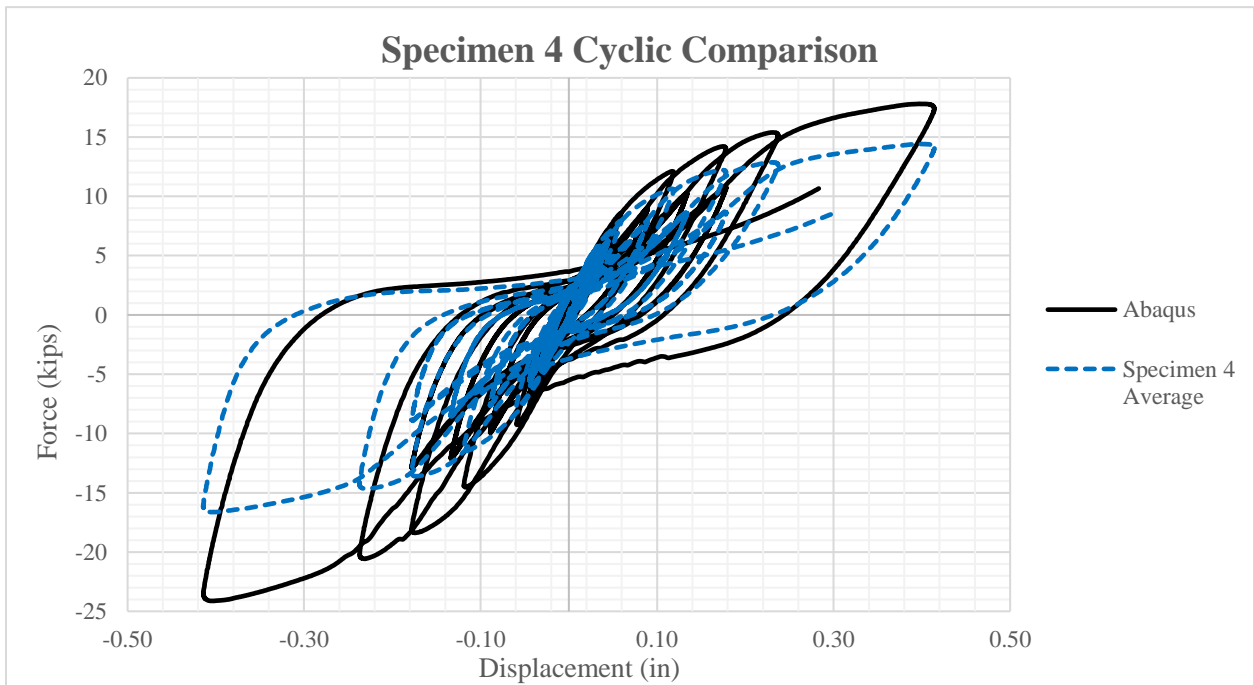
Figure 5.47. Specimen 4 Cyclic Comparison

Specimen 5
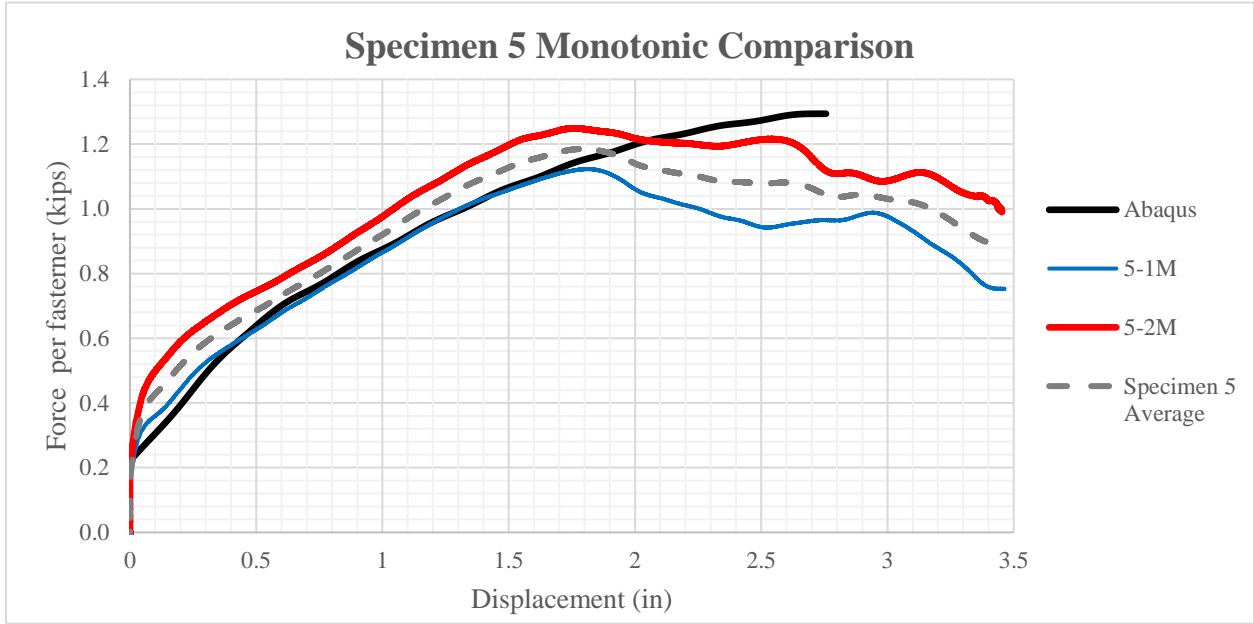
Figure 5.48. Specimen 5 Monotonic Comparison
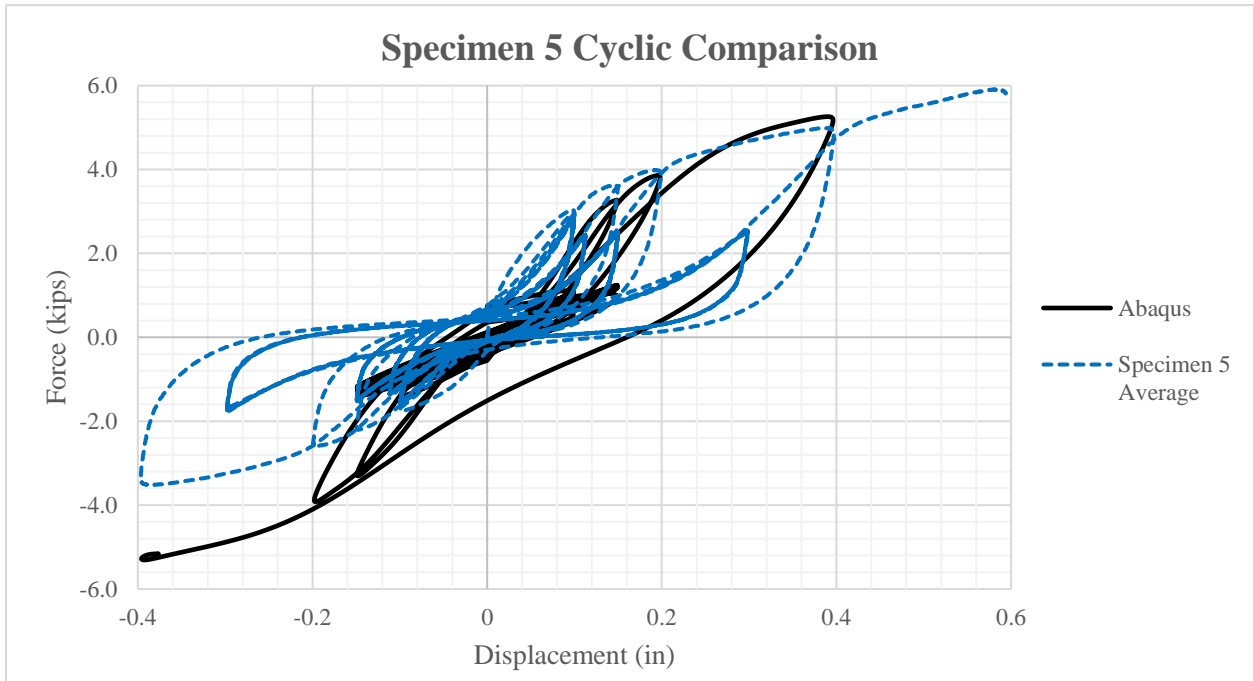
Figure 5.49. Specimen 5 Cyclic Comparison

Specimen 6
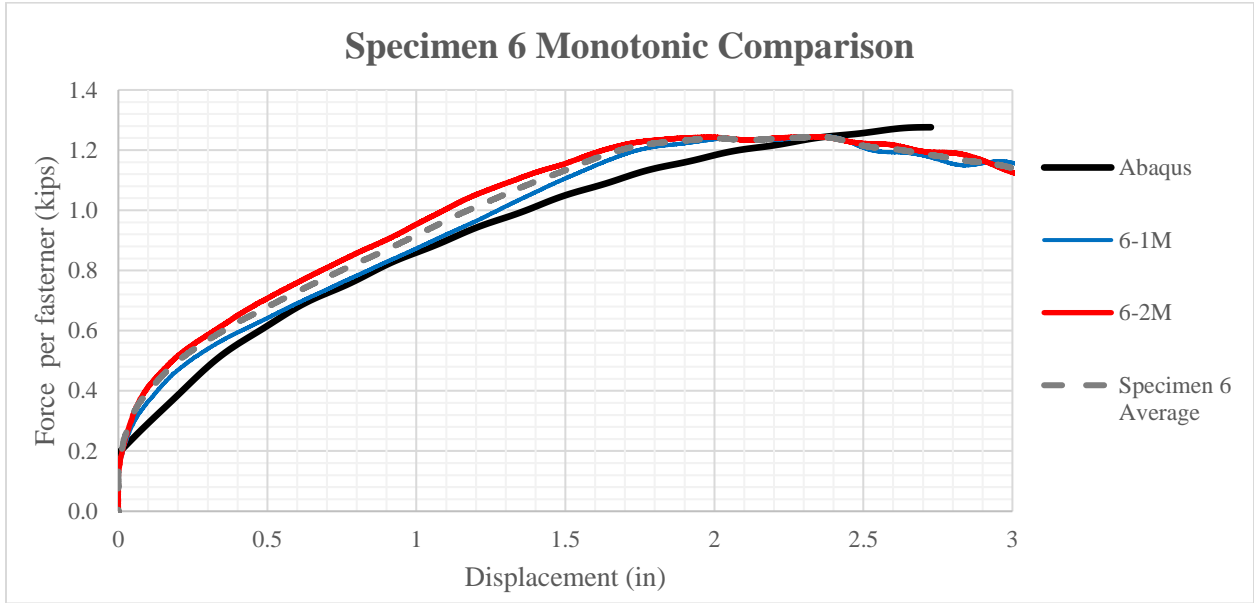
Figure 5.50. Specimen 6 Monotonic Comparison
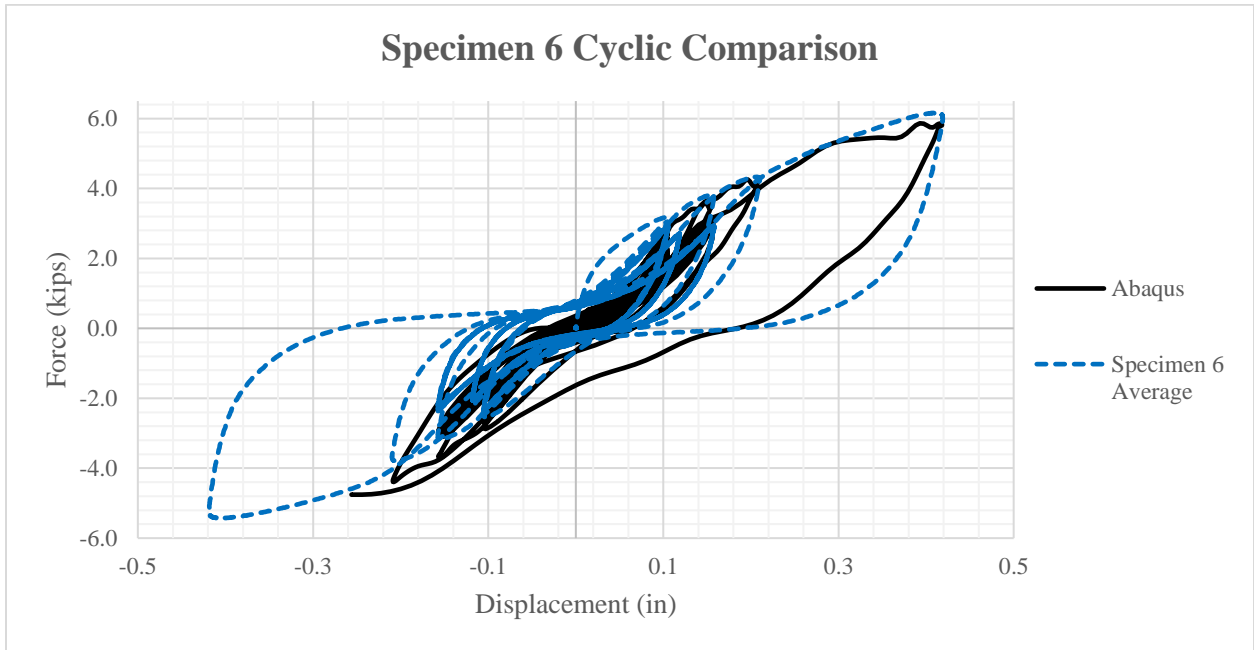
Figure 5.51. Specimen 6 Cyclic Comparison

Specimen 7
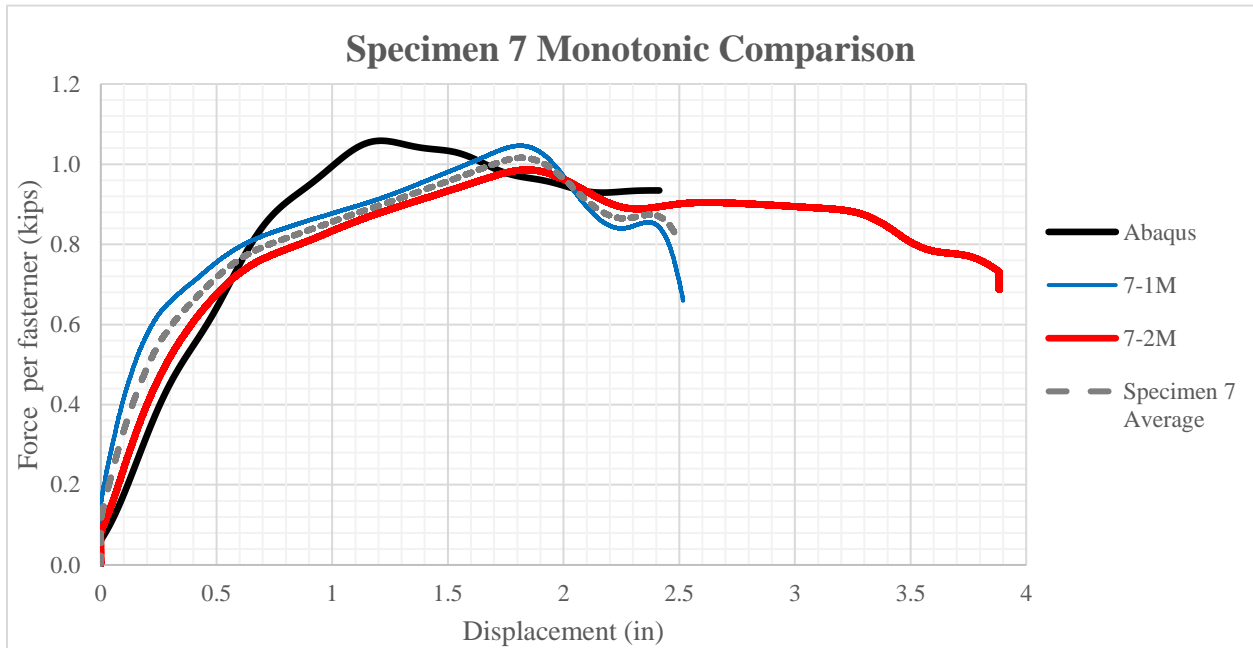
Figure 5.52. Specimen 7 Monotonic Comparison
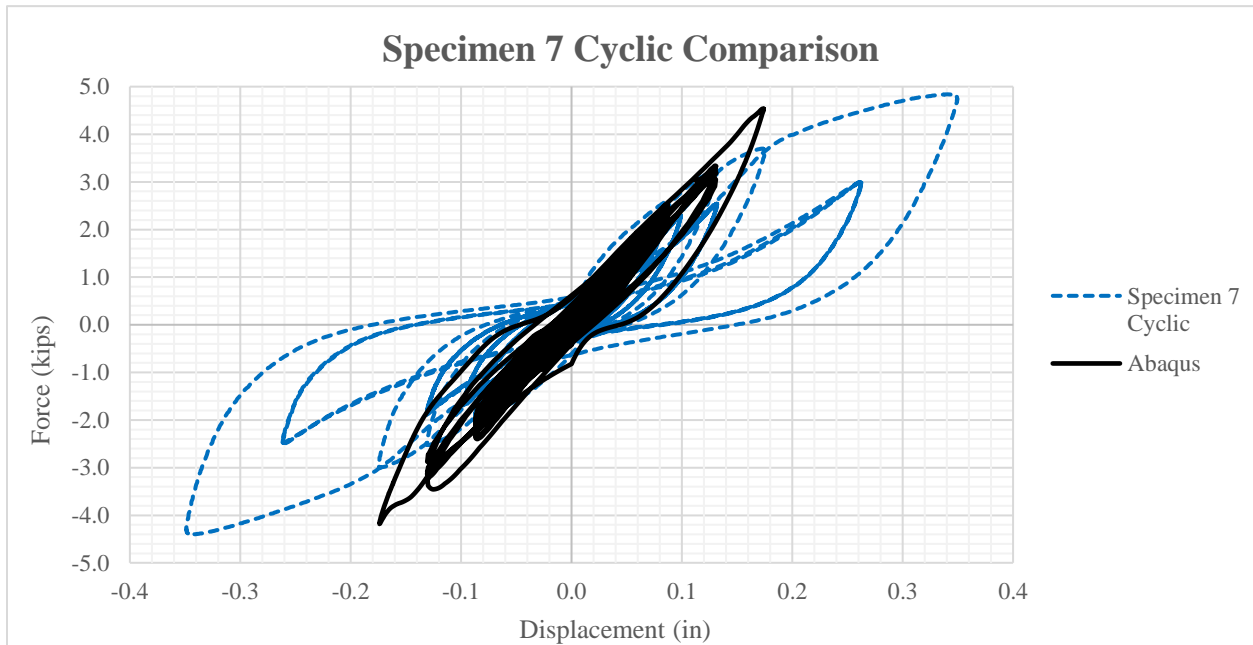
Figure 5.53. Specimen 7 Cyclic Comparison

Specimen 8
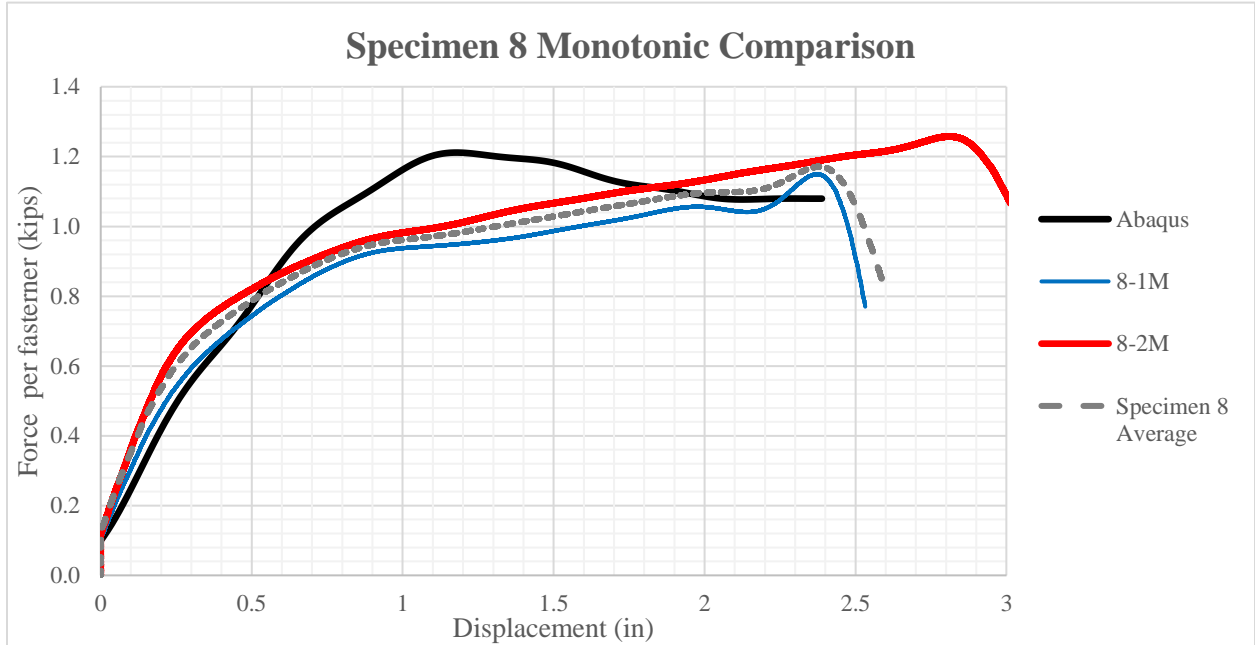
Figure 5.54. Specimen 8 Monotonic Comparison
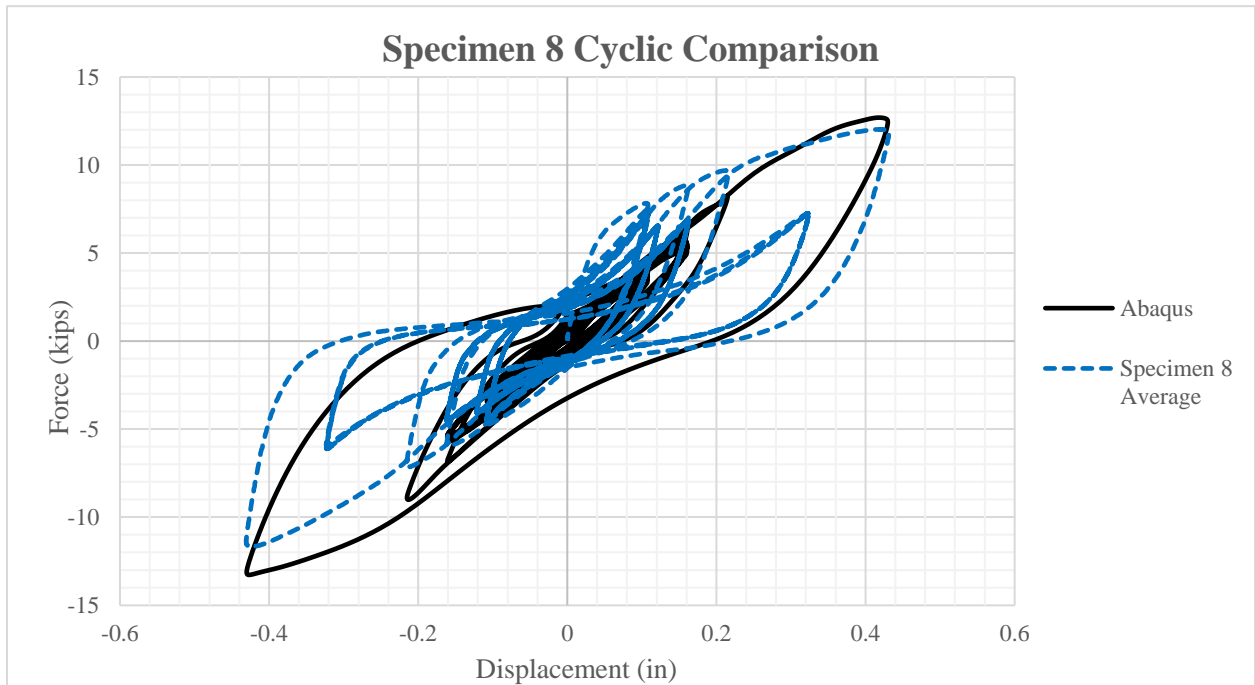
Figure 5.55. Specimen 8 Cyclic Comparison

Specimen 9
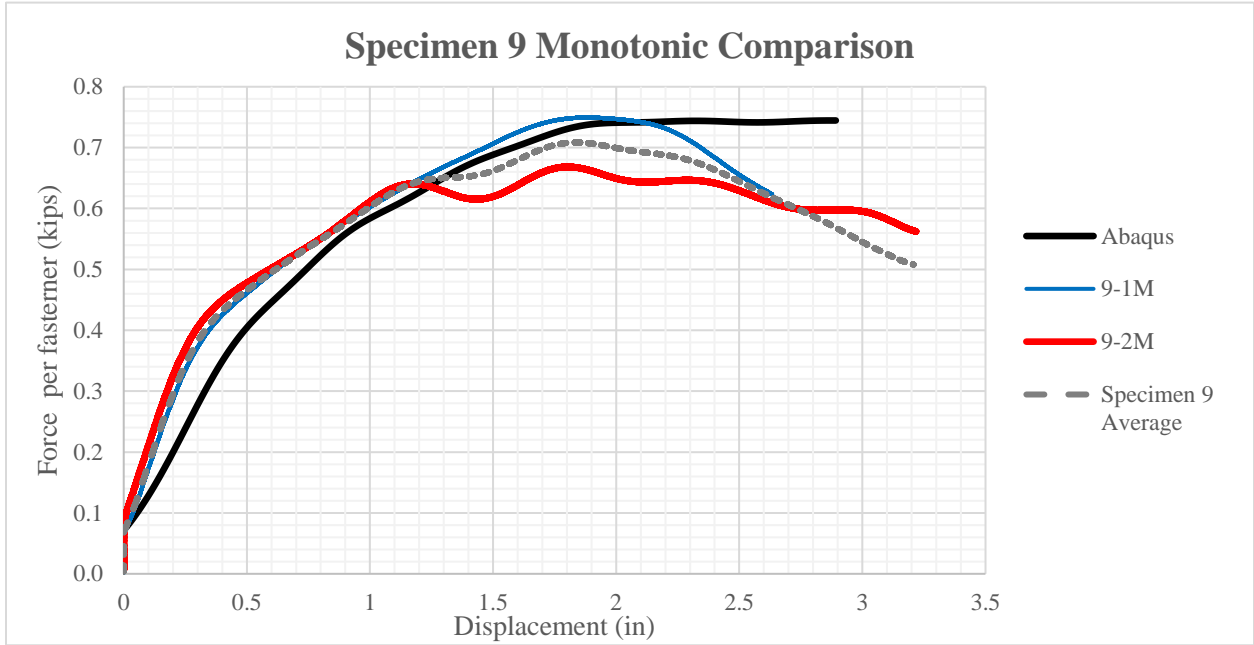
Figure 5.56. Specimen 9 Monotonic Comparison
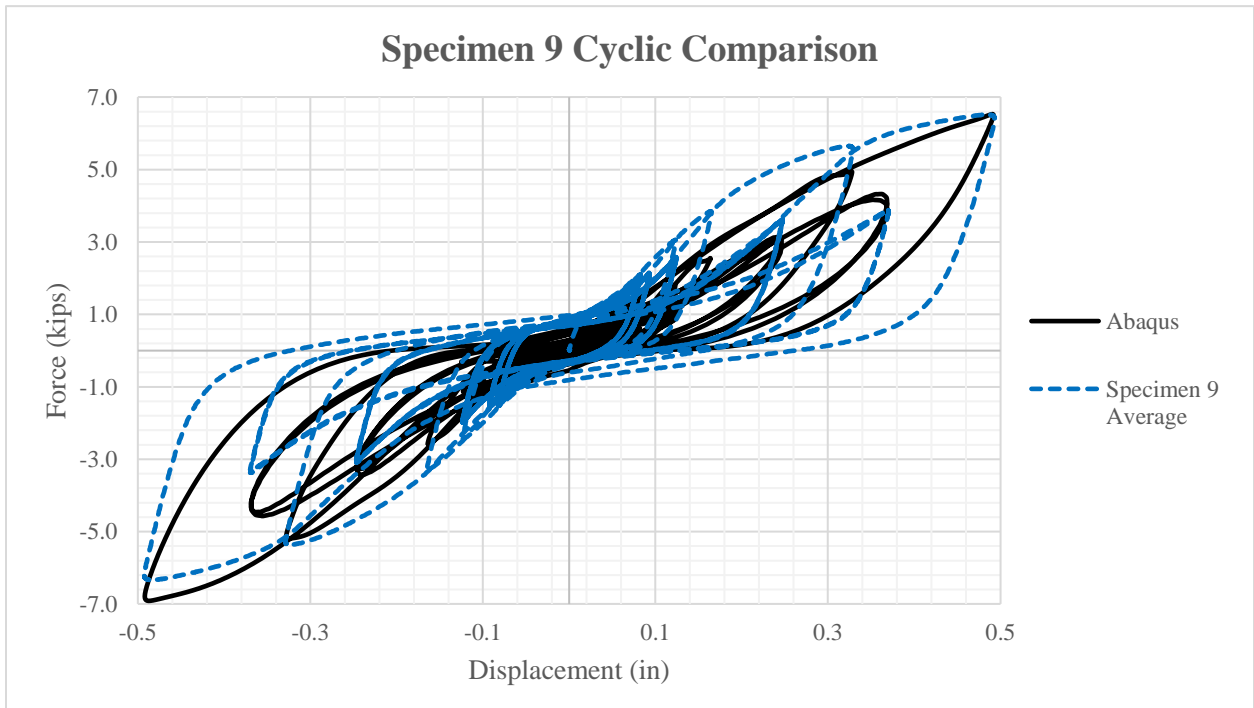
Figure 5.57. Specimen 9 Cyclic Comparison

Specimen 10
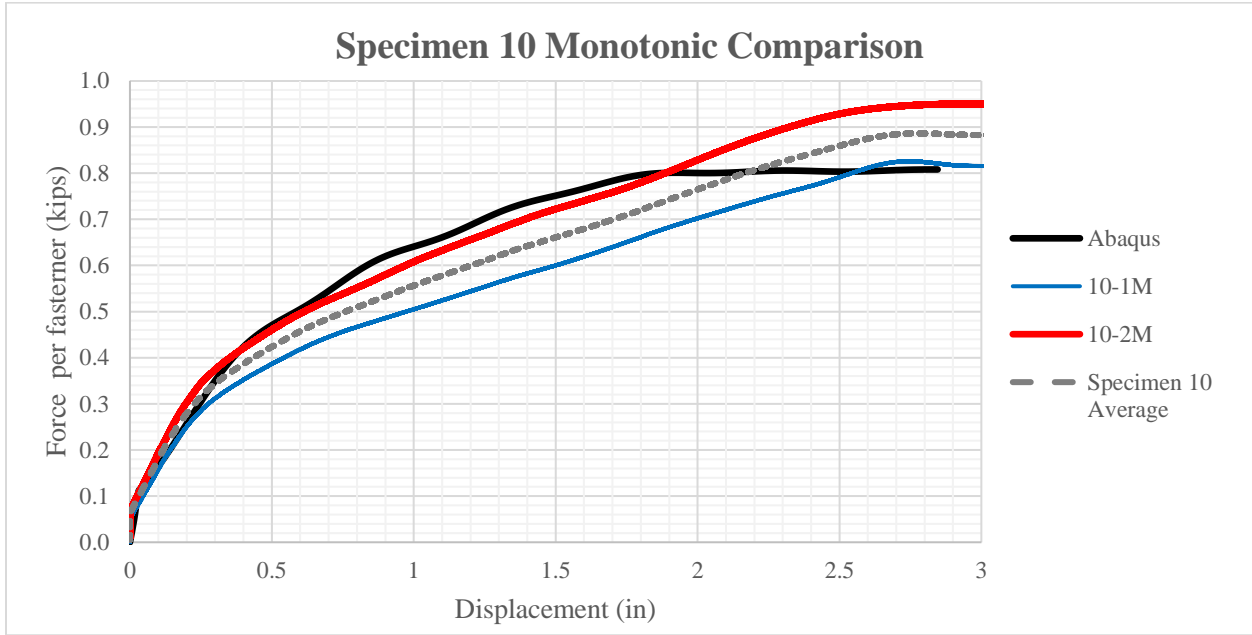
Figure 5.58. Specimen 10 Monotonic Comparison
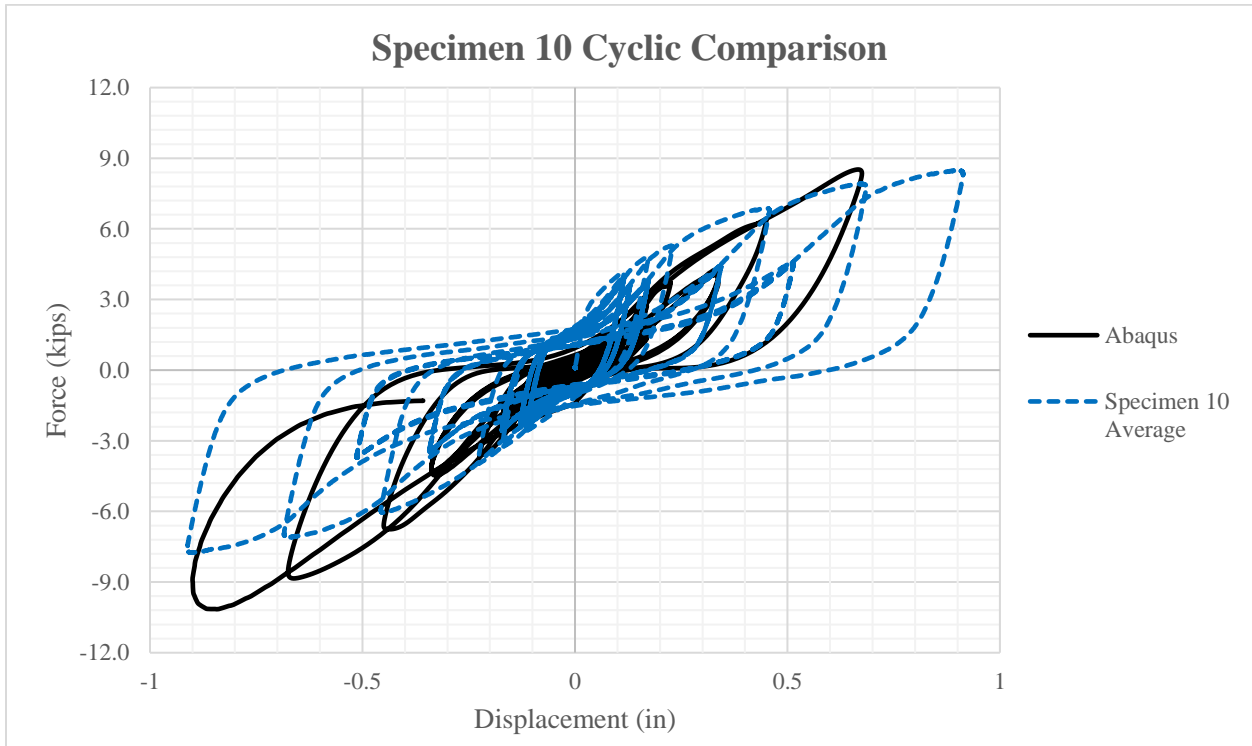
Figure 5.59. Specimen 10 Cyclic Comparison

5.5.   FEA Validation and Discussion

To validate the results obtained from Abaqus finite element modelling, both monotonic and cyclic analysis results were compared to the experimental results presented in 3.4.3. Results. For monotonic pushover analysis, the results were compared with both tests done in the lab on each specimen, respectively, along with the average calculated for each specimen. For cyclic analysis, the results were compared with the average of the ten specimens tested in the lab.

Validating the results obtained from finite element analysis was critical in understanding the behavior of the specimens that were tested, along with providing further insight into the validity of modeling assumptions that were made. For example, the way that the contact between the fasteners and the CLT was modeled has no predefined process. Calibrating the models to fit the experimental data was necessary to provide contact controls that were realistic and could continue to be used into the future. To begin, this connection was modelled as a 'hard contact' connection – one where there was no overclosure allowed between elements. This means that the screw could crush the wood, but the two surfaces always stayed in contact. By modelling the connection with 'soft contact' controls, this allowed a predefined amount of overclosure between elements to occur based on the pressure each element experienced. Calibrating this contact control proved to be challenging but using experimental data by which to compare results made the process much smoother and more accurate altogether.

Certain models were calibrated more closely to the experimental data than others and, therefore, ought to be given more credence. Some of the models were better at predicting maximum force during the monotonic simulation, while others accurately represented stiffness throughout the simulation. Taking this into account, further finite element modeling could prove helpful in determining the controlling factors leading to these differences. Even with this in

mind, the modeling assumptions provided in Section 5.1 can be used as a reference for further finite element modeling of CLT connections – specifically when using V1 Douglas Fir.

Beginning by evaluating the ability of the finite element models to estimate peak load, it was apparent that this was the strength of the models that were developed. All models were able to predict the peak load during monotonic simulation within 10% of the average value obtained in the lab. Specimen 8 was even able to predict the peak load to within 0.8% accuracy. Predicting initial stiffness and load at the first cycle during cyclic simulation was less accurate. Predictions for initial stiffness ranged from within 3% to within 100% difference for cyclic simulations and from within 3.8% to within 31.9% difference for monotonic simulations. While some models were able to accurately predict initial stiffness (specimen 5 and 6, namely), others did not seem to converge until larger displacements were achieved. To combat this issue, the step time was increased in dynamic simulations to allow for better convergence. While this did help with convergence, it often greatly increases run time.

Looking more closely at specimens 8, 9, and 10, they seemed to have more difficulty approximating initial stiffness and load at first cycle than many of the other models. It seems that the main reason for this was the difficulty in creating a consistent mesh in the areas where the initial small displacements caused stress in the material. Areas like the angle bracket with slots on one side and around the interface of the long screws into the LVL bearing support below caused issues with creating a consistent mesh. Because the mesh was less uniform in these areas, it was unable to approximate initial stiffness well. When the displacements became large enough, this issue went away because the problem areas were only a small part of the whole mesh that was involved. This can be demonstrated by comparing the load at first cycle to the peak load. For specimen 8 this difference decreased from 92% to just 5%. For specimen 9 this difference

138

decreased from 100% to just 1.2%. For specimen 10 this difference decreased from 85.7% to just

5.7%. This data demonstrates that the non-uniform mesh only caused problems under small

displacements but was minimal when the displacements increased. These results are presented in

Table 5.3.

5.6.   Future Investigations

Given that the models have been developed and verified to a certain degree of accuracy when compared to experimental data, further investigation can be done to ascertain behavior and strength of the connection types that were tested. By using the finite element models to explore further, one would gain insight into connection behavior that was unable to be tested directly in the lab because of monetary or other limitations. Specifically, the out-of-plane behavior of the wall-to-floor connections were unable to be tested experimentally as it would have required another test setup and loading protocol. Loading the wall-to-floor connection out-of-plane was done during the biaxial wall test but could not be isolated and measured all on its own, therefore, modelling it was of particular interest. Finite element simulations of this connection are an area of further interest, specifically when it comes to balloon-style construction.

A simulation of the biaxial test could prove useful in helping to further calibrate connection hysteretic models and to predict system behavior. While using Abaqus may be too computationally expensive for a large-scale model as in the biaxial wall test, other programs could be used to investigate this area. The data provided in Chapter 6 of this thesis could be used in validating the results provided by such an investigation.

Lastly, using the modeling assumptions provided in this thesis, finite element analysis could be used to evaluate the capability of new balloon-style wall-to-floor connection methods that are developed. Finite element analysis could be used to predict their behavior before experimental testing and the models could be adjusted to fit experimental data after. This approach could prove itself useful in testing new connection methods and evaluating their ability to be used.

6. BIAXIAL WALL TEST

6.1. Test Program Overview

The experimental testing presented in this chapter was performed at the Texas A&M University RELLIS Campus in the Structural and Materials Testing Laboratory (SMTL).

6.1.1. Overview

The design of the biaxial wall test came, in part, from previous research on CLT shear walls used in platform-style construction. When presenting results in front of the code provision updating committees (which is one of the overall objectives for balloon-style CLT construction project funded by HUD), it is useful to weed out any potential sources of uncertainty. No biaxial wall test was conducted on platform-style CLT shear walls, so their behavior had to be reasoned-through rather than presented. Having the data to back up claims of a specific R-value for a shear wall system further removes any uncertainty in the design process and allows designers to be more confident in their ability to design with CLT balloon-frame shear walls. A test setup and test matrix were developed with the help of the same expert panel that was consulted for the connection tests (Chapter 4). The team determined that the most cost-efficient and effective setup was to design a test that would be to scale for one story of a balloon-framed shear wall. This includes testing with a floor connected and without a floor. The concept included inducing a displacement in the x-direction (in-plane) and y-direction (out-of-plane) of the wall concurrently, meaning that the two displacements were always equal. This concept, called cloverleaf loading protocol, was used on concrete columns by Akguzel et al. (Akguzel and Pampanin 2010).

Three different test setups were determined to be essential in developing a piecewise study of the behavior of CLT balloon-frame shear walls. First, a test was designed to investigate the out-of-plane behavior of CLT shear walls, an inherent research gap in many CLT shear wall

studies. Second, a test was designed to investigate the biaxial behavior of CLT shear walls without any floor diaphragms attached. Lastly, a test was designed to investigate the behavior of balloon-frame CLT shear walls with a floor diaphragm attached.

6.1.2. Test Design

The biaxial wall test was designed according to the limitations of the Structural and Materials Testing Laboratory at Texas A&M's Center for Infrastructure Renewal. The basic limitations that drove the test design included the capacity of the actuators to be used in each direction of loading, the baseplate that was available for testing, the reaction frame that could be used to accomplish the test setup, and the layout of holes on the strong-wall and strong-floor that determined the location of the test referencing the reaction frame and wall. A general test setup was decided upon before the intimate details were designed. The general test design included the testing of a 1.5:1 aspect ratio wall made up of two panels, with the height being 12-feet and the width being 8-feet. The location of the floor was determined to be located at the line of action of the actuator in the 'in-plane' direction. This put the center of the floor at a height of 10-feet and 6-inches. The floor was a single panel with dimensions of 3-feet by 8-feet.

The two actuators that were chosen to be used for the test had a total stroke of 30-inches, or 15-inches in tension and 15-inches in compression. Given the desire to use the full displacement capacity of the actuators, the test setup was designed to begin testing with the actuators connected to the specimen while at mid-stroke. A SolidWorks model was used to coordinate the biaxial test design and ensure all fixtures fit up correctly and the correct clearance holes were chosen on the wall and floor. The original design model that was used as a baseline for fixture design can be seen in Figure 6.1.
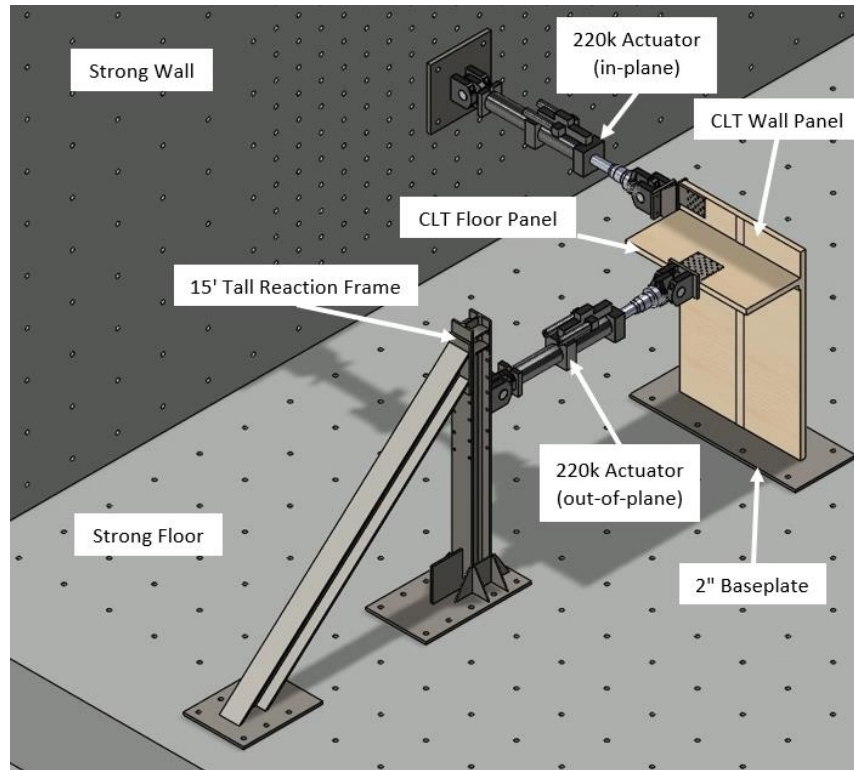
Figure 6.1. Biaxial Test Design Constraints

With the initial design constraints determined, fixtures needed to be designed to connect

the actuators to the wall and floor panels. Three different fixtures were required as there were

three different connection configurations: in-plane connection to wall panel, out-of-plane

connection to floor panel, and out-of-plane connection to wall panel. Steel was chosen as the

material out of which to make the fixtures as it provided ease of design, high strength (low

deflections), and easy connection to the actuators. For the in-plane connection to the wall panel,

the approach was to apply the force from the actuator in a way that mimics the position of the

lateral diaphragm force mostly closely. The elevation of the application of the load could be

provided at 9-ft, 10-ft and 6-in, or 12-ft, determined by the location of the holes on the wall.

Elevation of 10-ft and 6-in was the most ideal as it allowed room for the floor connection

components while also allowing for ample connection room above the floor. A design load of

200-kips was used for all fixtures as they were designed for the full capacity of the actuators. A

143

bolted connection through the wall panel was designed as it allowed for easy assembly and

disassembly, while providing significantly less fasteners than a screwed connection. To

accomplish the goal of having the in-plane force at the location of the diaphragm, the fixture was

designed to connect above and below the diaphragm. To cut the total weight of the fixture, a

tapered-web box section was designed according to AISC Steel Design Specifications (AISC

2016). A drawing of the in-plane fixture can be seen in Figure 6.2.
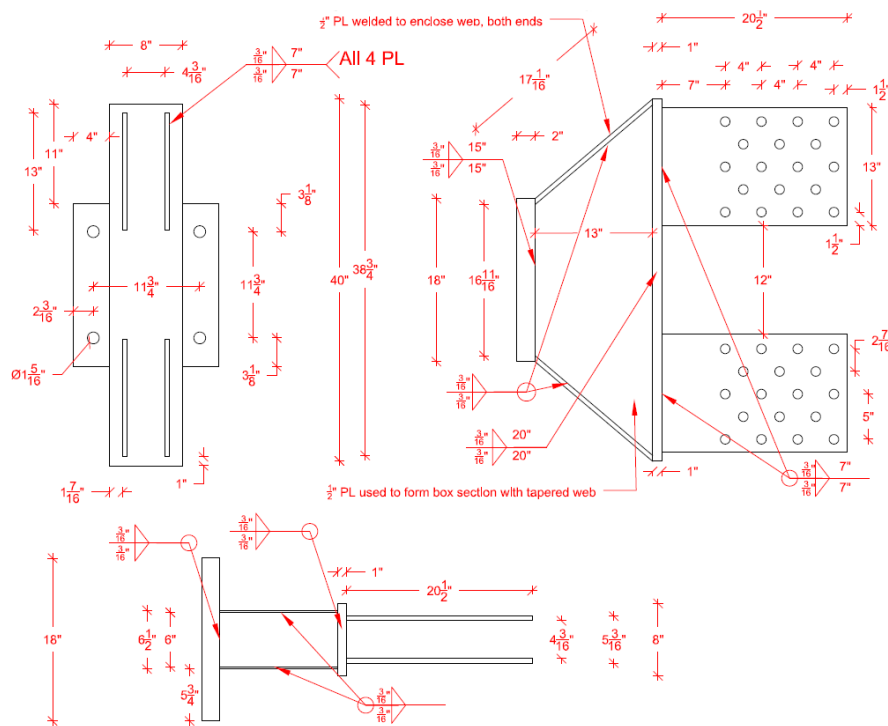
Figure 6.2. In-Plane Fixture Drawing

The out-of-plane fixture to connect the floor to actuator to the floor was also designed to

the capacity of the actuator. A bolted connection was chosen for this application as well and a

box section was used to apply the load in the center of the floor. The fixture is bolted to the foot

of the actuator using 1-1/4" threaded rods and then bolted to the floor using 1" A325 bolts. All

calculations were performed according to AISC Steel Design Specifications. A drawing of the

out-of-plane fixture can be seen in Figure 6.3. A figure including both fixtures in the model can

be seen in Figure 6.4, while a photo showing the two fixtures constructed can be seen in Figure

6.5.
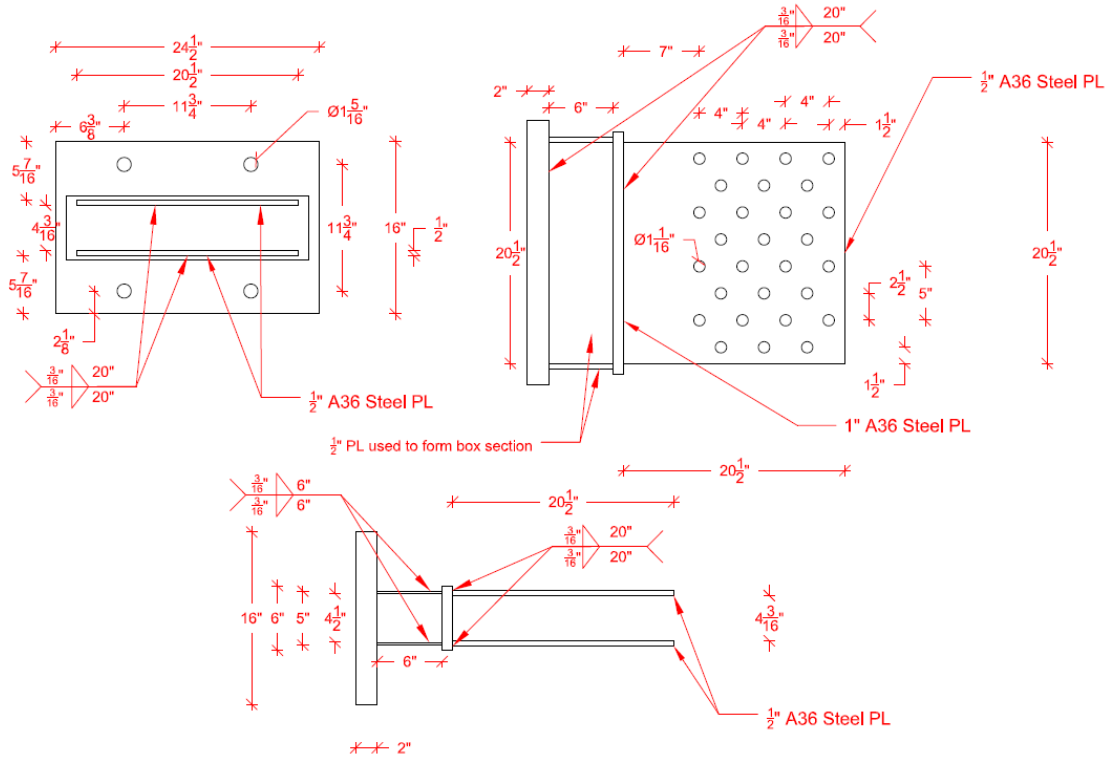
Figure 6.3. Out-of-Plane Fixture Drawing
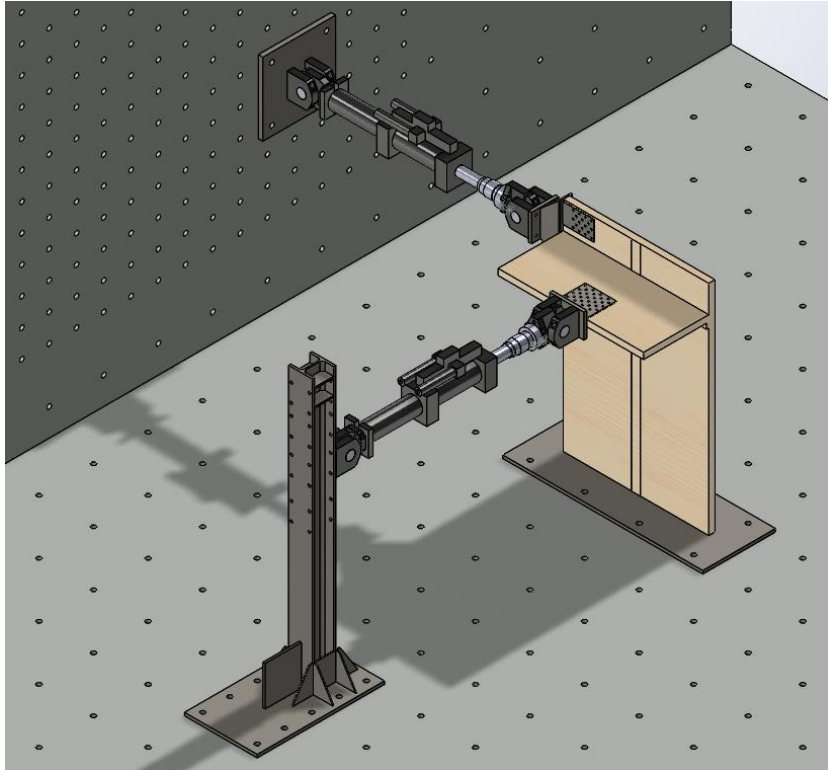
Figure 6.4. Test Setup with Floor diaphragm
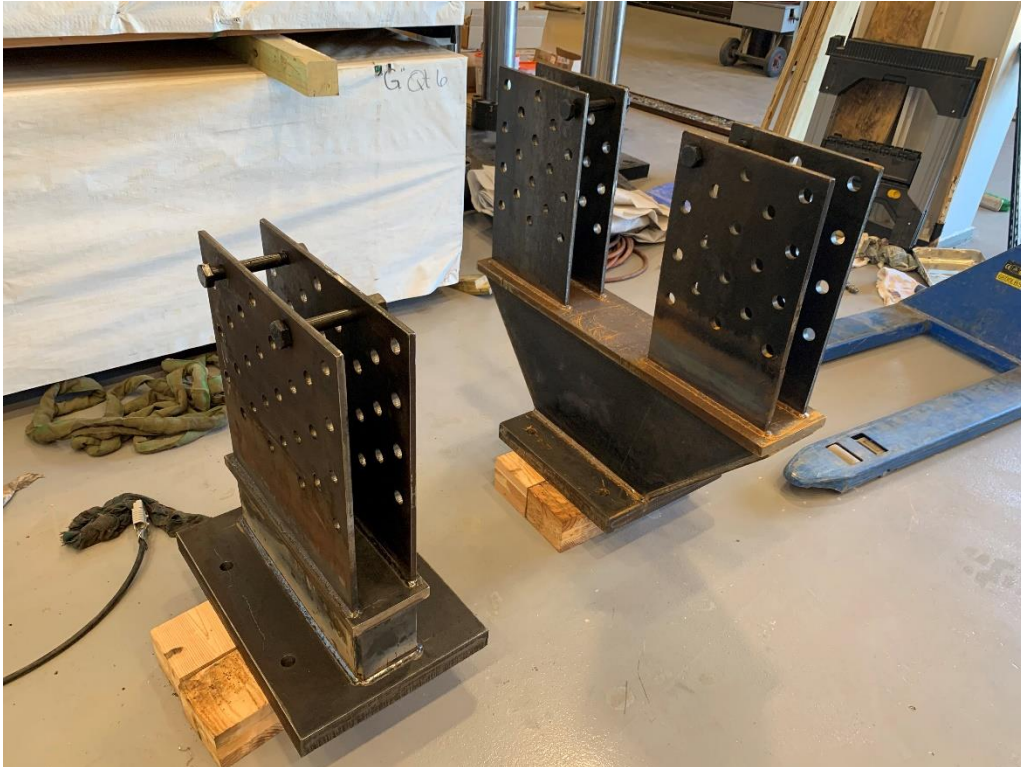
Figure 6.5. Biaxial Test Fixtures

Connecting the out-of-plane actuator to the CLT wall panel when the floor was not a part

of the test proved to require more creativity. During the tests when the floor is included, the CLT

floor panel acts as a "spreader beam" to distribute the load across the wall panel in a uniform

way. Without the floor, the load needed to be applied to the wall in a way that could be similar to

this. Applying the load as point loads at the 1/3 points of the wall was the method that was

chosen. This was accomplished by using a 6-ft header as a "spreader beam" and designing stub

columns that could through-bolt onto the CLT wall panel. The stub columns were designed out

of W12x193 that used as a diaphragm to construct the header. In order to attach these stub

columns to the wall panel, the flanges needed to be coped and a plate was welded to the web to

allow for bearing on the wall while clearing the fixtures already attached to the panel. A drawing

of the stub columns can be seen in Figure 6.6, and a figure showing the header and stub column

assembly can be seen in Figure 6.7.
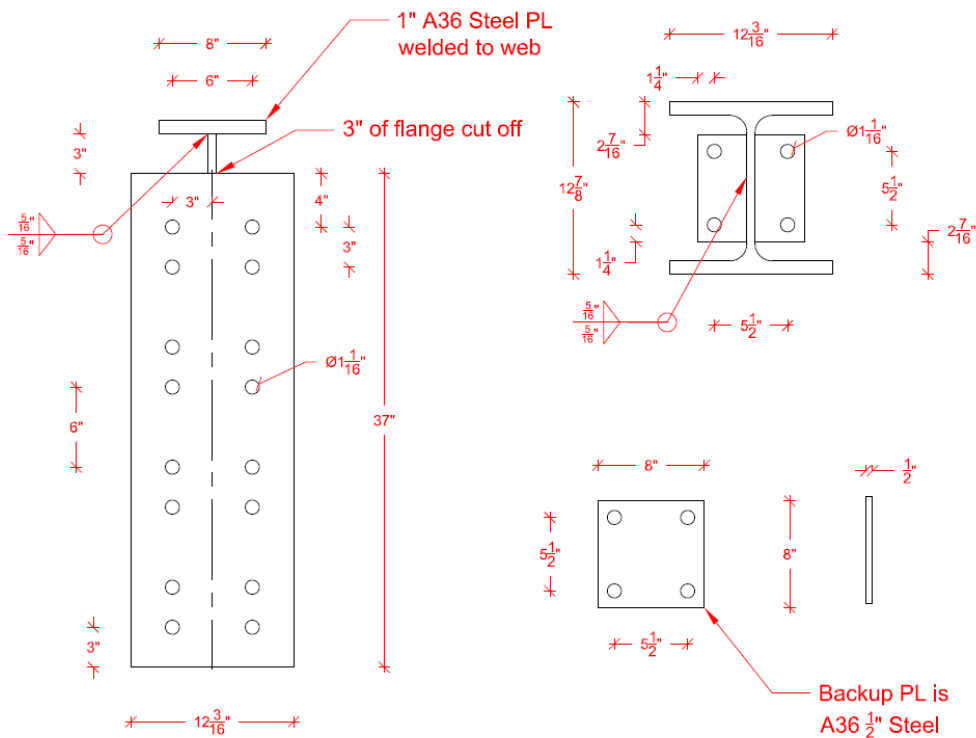
Figure 6.6. Stub Column Drawing

147
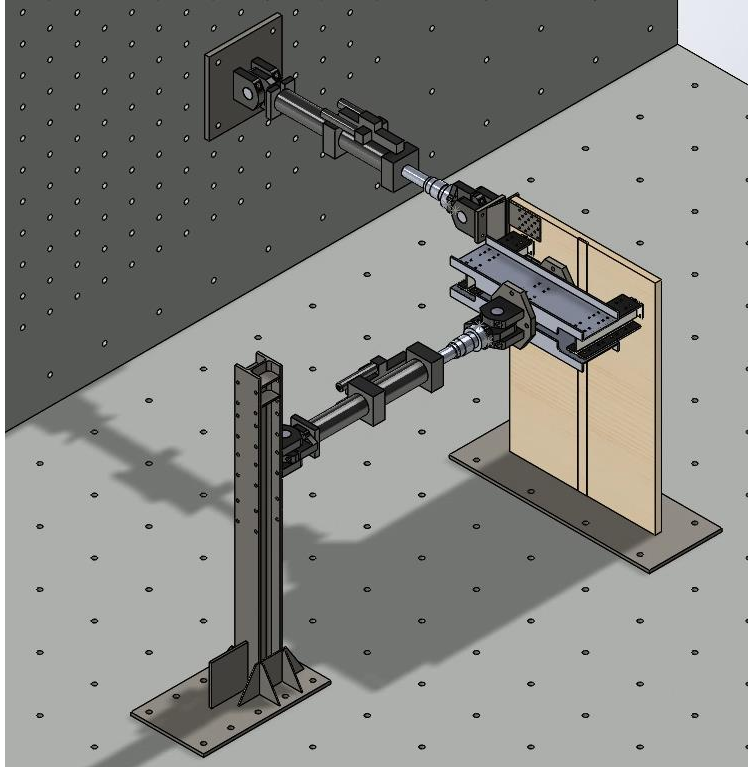
Figure 6.7. Test Setup without Floor diaphragm

6.1.3. Test Matrix

The purpose of the biaxial test matrix was to expand upon the connection testing research

performed before the full-scale tests. Following a piecewise study approach, three different types

of tests were decided upon. The purpose of doing a test with out-of-plane only loading was to

demonstrate the performance of the connections in that direction, as the in-plane direction is

generally well-studied. After this performance was qualified, it was easier to separate the cause

of different types of behavior in the biaxial tests. Following this same approach, a test was

conducted (one of each type of connection) to study the biaxial behavior of the CLT shear wall

without adding in the floor connection. This was conducted to help separate the any observations

during this test from when the floor was included. Lastly, a test was designed to study the biaxial

behavior of a balloon framed CLT shear wall that at full-scale. The test matrix is summarized in

Table 6.1. Drawings of each configuration can be seen in Figure 6.8 through Figure 6.11.

148

Table 6.1. Biaxial Wall Test Matrix

Biaxial Wall Tests			
Configuration	Test Type	Panel-to-Panel Connection	Loading
B1		Half-lap	Cloverleaf
B2	With Floor Diaphragm	Half-lap	Cloverleaf
B3		Surface Spline	Cloverleaf
B4		Half-lap	Cloverleaf
B5	Wall Only	Surface Spline	Cloverleaf
B6		Surface Spline	CUREE
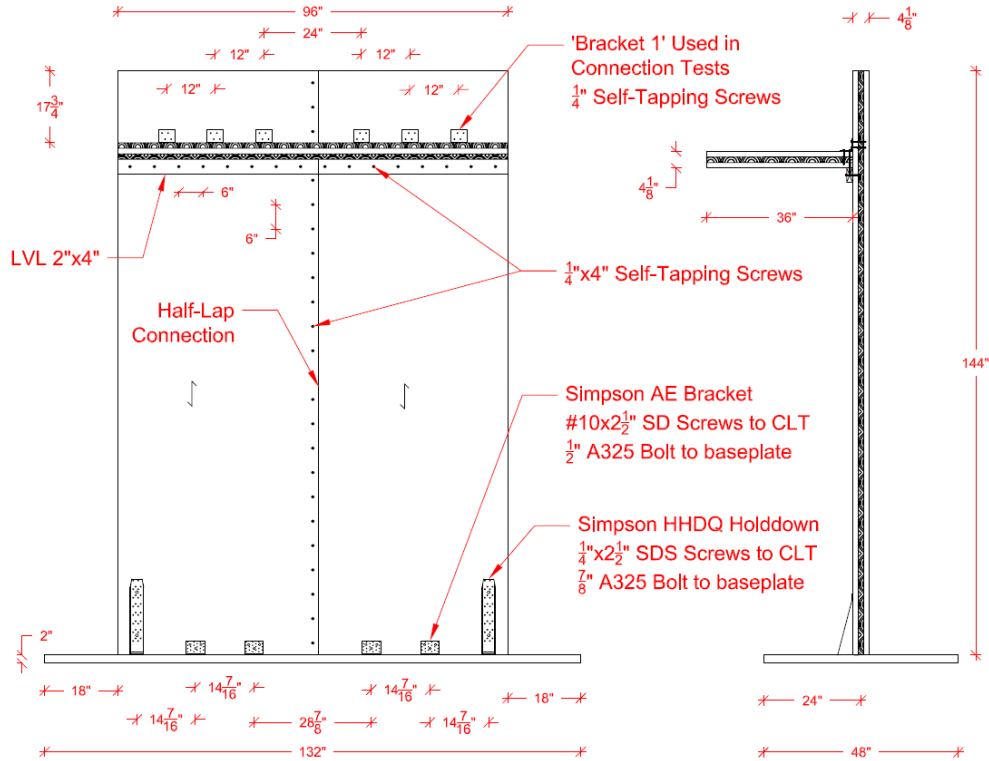
Figure 6.8. Test Configuration B1 and B2

149
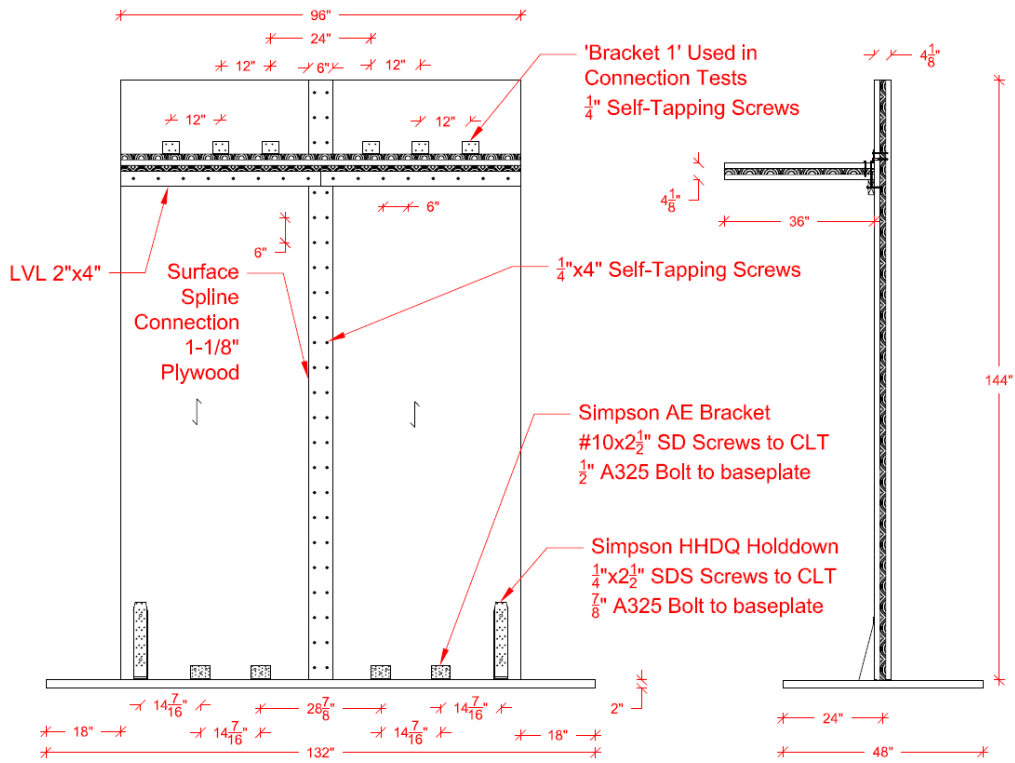
Figure 6.9. Test Configuration B3
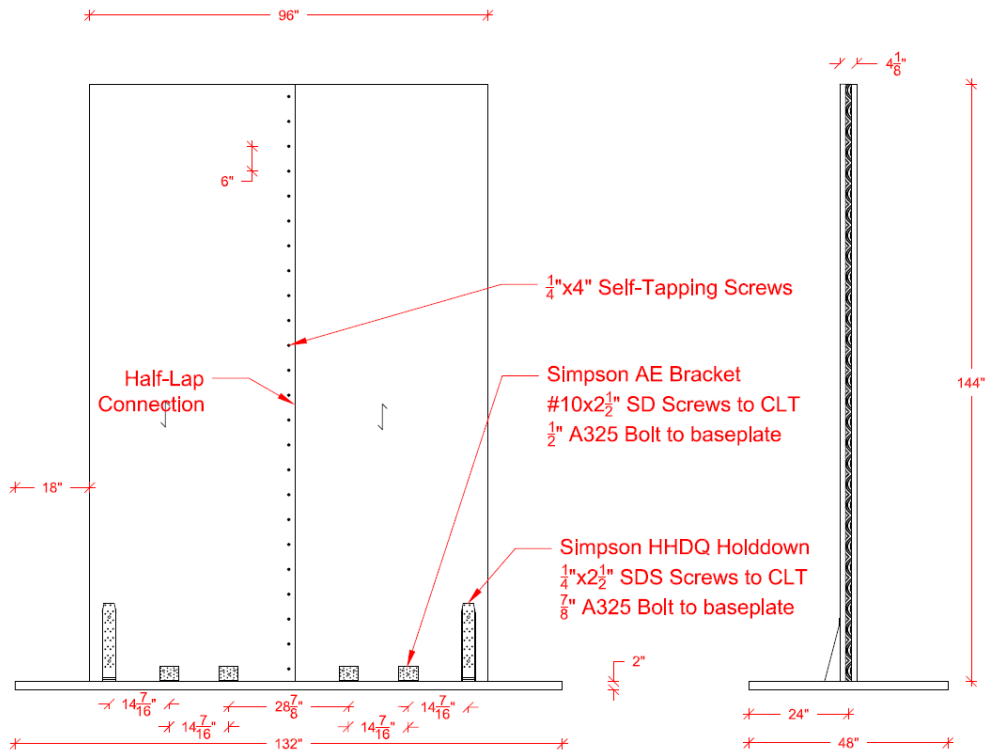
Figure 6.10. Test Configuration B4

150
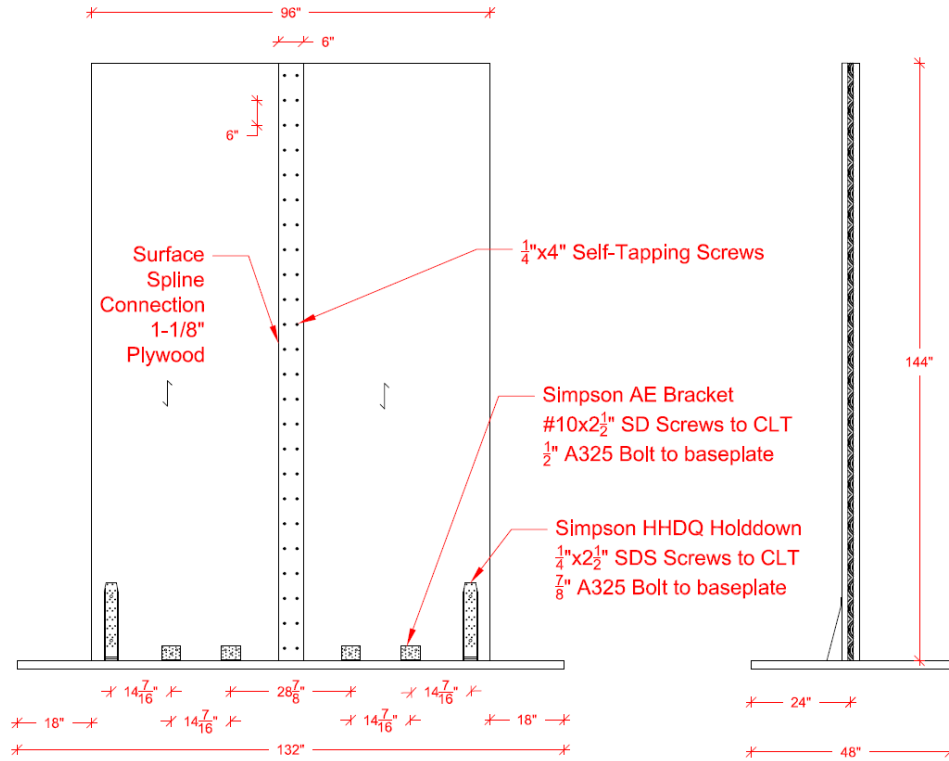
Figure 6.11. Test Configuration B5 and B6

A variety of different connection components were used to construct the specimens listed in the test matrix, with most of the components being provided by Simpson StrongTie. All self-tapping screws, hold downs, and foundation clips were provided by Simpson StrongTie, the wall-to-floor diaphragm angle brackets were a generic design also used in the connection test program (Chapter 4), and the bolts were typical A325 structural bolts ordered from Bolt Depot. Figure 6.12 shows every connection component used to complete the biaxial test matrix.
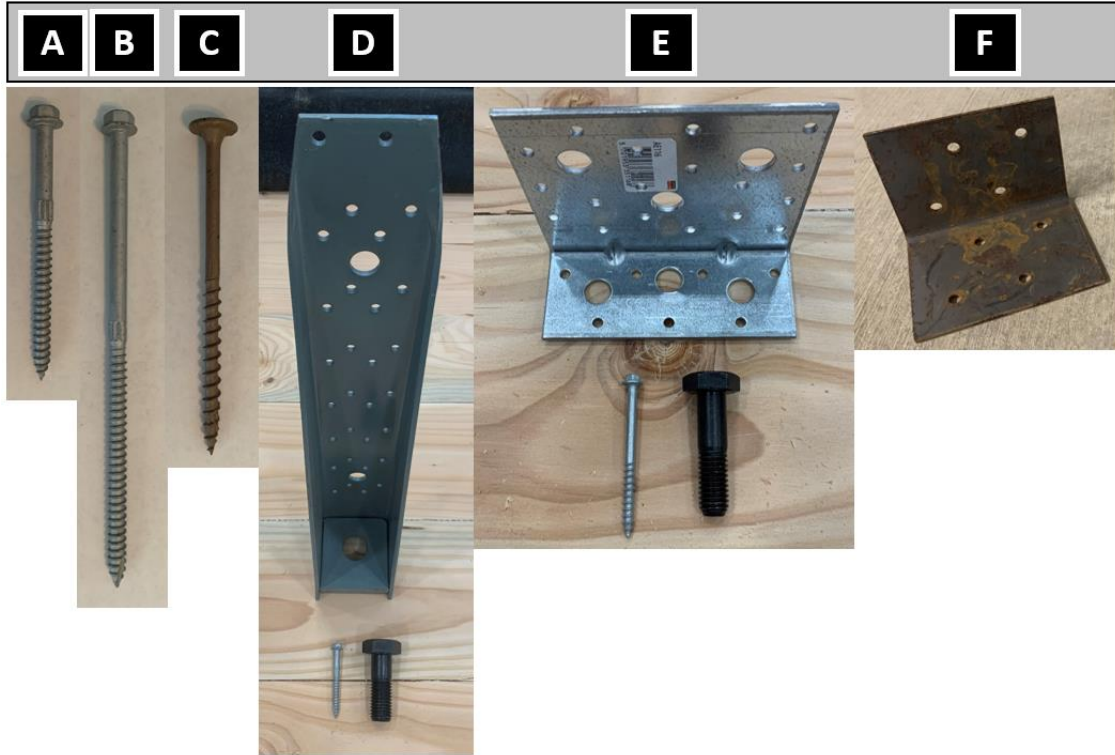
Figure 6.12. Biaxial Test Connection Components

Referring to Figure 6.12(a), the floor diaphragm was connected to the wall using Simpson StrongTie SDS wood screws that were ¼-in diameter and 3.5-inches in length. The floor diaphragm was tied to the LVL ledger below using the same Simpson StrongTie SDS wood screws but in 6-inch length, as seen in Figure 6.12(b). Simpson StrongTie SDWS self-tapping timber screws, 0.22-inch diameter and 4-inch length, were used to attach the LVL ledger, make the half-lap connection and make the surface spline connection. A photo of this screw is shown in Figure 6.12(c). The hold down that was used was the Simpson StrongTie HHDQ14 utilizing SDS2.5 screws and a A325 7/8-inch bolt as seen in Figure 6.12(d). The foundation clip used in all tests was Simpson StrongTie's AE116 bracket that uses SD10212MB screws and three A325 ½-inch bolts to attach to the baseplate, as seen in Figure 6.12(e). The angle bracket used to attach the floor diaphragm to the wall was a custom designed bracket using A36 steel, with dimensions of 3-inches tall by 4-inches wide and 1/8-inch thick, as seen in Figure 6.12(f).

6.2.   Construction of Test Setup

The construction of the test setup focused on precision in manufacturing each part, with the goal of reducing eccentricity in the test as much as possible. The biaxial wall tests have inherent torsion that is intended as a part of the test but limiting any additional torsion that could be added to the test by means of manufacturing error was the primary concern. The primary way this was accomplished was through the precision manufacturing the baseplate. By using a steel baseplate that is bolted to the floor and has holes that are used to bolt the angle brackets down, this allowed for consistency in locating the wall for each test. The holes for the angle brackets and hold down connectors were laid out, drilled, and tapped with a high degree of accuracy. A drawing of the baseplate layout can be seen in Figure 6.13, and a photo showing the angle bracket hole pattern cut and tapped into the baseplate can be seen in Figure 6.14.
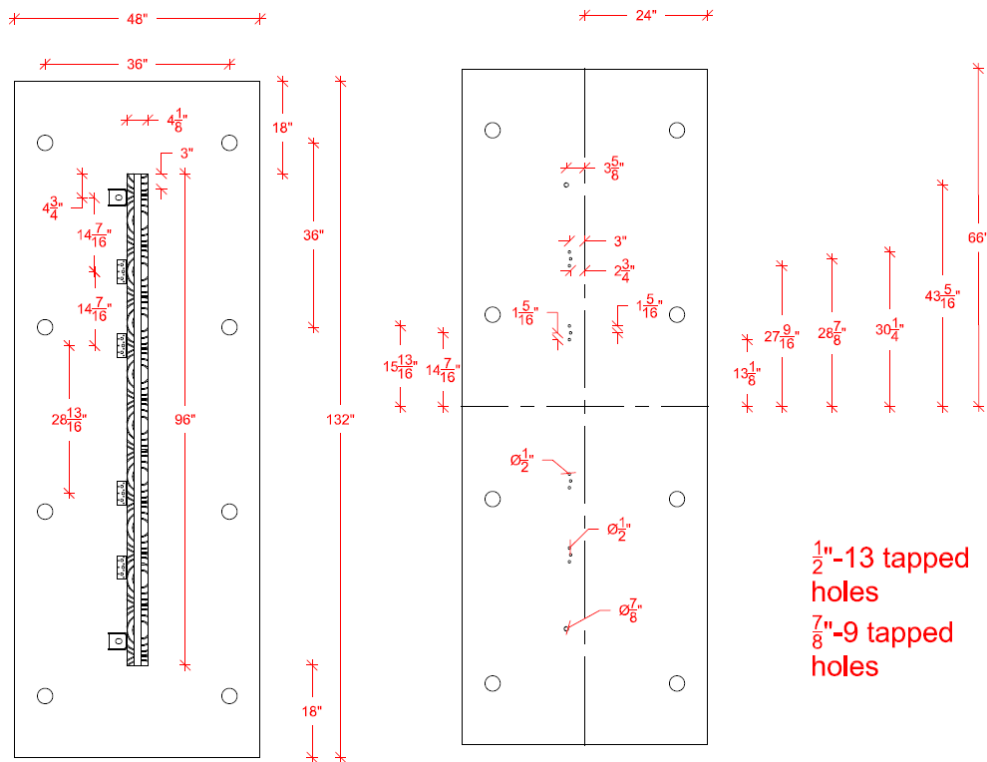
Figure 6.13. Baseplate Layout Drawing

Figure 6.14. Angle Bracket Hole Pattern

The second way that precision manufacturing was accomplished in the construction of the test was through the design and fabrication of steel fixtures to use to attach the actuators to the wall and floor panels. After the fixtures were designed, they were fabricated by Brazos Industries, a steel plate fabricator in Bryan, Texas. Rather than trying to fabricate these fixtures in-house, it was left to professionals to ensure each fixture was built within the correct construction tolerances. A photo of the fixtures can be seen in Figure 6.5.

The last way that manufacturing played a key role in the test setup was in the locating of the bolt holes that needed to be drilled in the wall and floor panels for each test. If a hole were misaligned, it would cause problems for the fit up and installation of the bolts prior to testing. If the pattern was misaligned, then it would cause eccentricity in the test that is unwanted. To remove any error in the alignment of the bolt holes, the fixtures themselves were used as the template for drilling on the CLT specimens. The panels were raised by crane and placed into the

fixtures, and the bolt holes were drilled using a wood auger bit. A photo of the floor diaphragm construction can be seen in Figure 6.15, and the wall panel construction can be seen in Figure 6.16.

Figure 6.15. Floor Diaphragm Construction
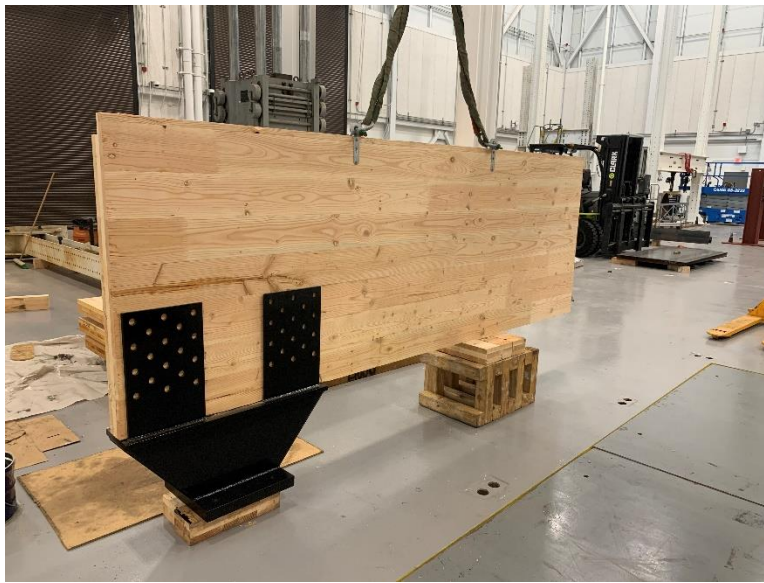
Figure 6.16. Wall Panel Construction

Constructing the test setup involved laying out the pattern of holes on the strong floor and strong wall that were to be used during testing and filling with post-tensioned DYWIDAG threadbars. First, the 220-kip actuator that was to be used to apply the in-plane load was moved into position on the strong wall, held in place by DYWIDAG threadbars tensioned to 60 kips per threadbar. With that actuator in place on the wall, the reaction frame used to resist the out-of-

plane 220-kip actuator was assembled in its spot on the floor. After assembly, DYWIDAG threadbars were used to secure it to the floor, again tensioned to 60 kips per threadbar. A photo of the reaction frame can be seen in Figure 6.17. Before the actuator could be secured to the reaction frame, thick-walled tubing was machined to fit between the flanges of the reaction frame to allow for both flanges to act together. This can be seen in Figure 6.18.

Figure 6.17. Reaction Frame

Figure 6.18. Actuator Connection to Reaction Frame

Additionally, shoring frames and single post shores were used to support the weight of the actuators. This was done using a single shoring frame with a CLT panel on top and two additional post shores under the point where the actuator rests on the frame. A photo of the shoring can be seen in Figure 6.19. With the actuators in place, the final task to complete before construction and placement of any test specimens was to set the baseplate at the correct location on the strong floor and tension its threadbars. A decision was made to increase the force on each DYWIDAG threadbar used to tie the baseplate down to prevent any possible movement of the baseplate during testing. Eight threadbars tensioned to 100 kips each were used to secure the baseplate. A photo of the post-tensioning process can be seen in Figure 6.20. The process of post-tensioning involves using a hydraulic jack to pull on the threadbar until a specified pressure (which correlates to a force in the bar) and then turning the nut to keep the load in the threadbar after the jack is released.

Figure 6.19. Shoring Used to Support Actuator

Figure 6.20. DYWIDAG Post-tensioning

The process of building each test specimen before attaching the actuators involved using the crane to hoist each wall panel into place and install all the screws attaching the hold down brackets and angle brackets to the baseplate. The wall panels were then attached to each other, using self-tapping wood screws (and a plywood spline for those that called for it). When the test specimen included a floor, the LVL ledger was screwed to the wall at the proper height and the CLT floor was hoisted into place. Angle brackets were used to attach the floor to the wall and LVL ledger. Before testing, the actuators were both extended to their starting position and 1-inch bolts were pounded through the CLT wall and floor making the attachment to each actuator secure and allowing for no movement at the attachment point. Post-shores were used to give additional support to the floor before testing but were removed prior to beginning any test. For the test specimens that did not include a floor, the actuators were attached shortly after the wall had been constructed – again using 1-inch bolts to make the connection. A photo of the test setup before test B1 was completed can be seen in Figure 6.21. A photo of the test setup before test B4 was completed can be seen in Figure 6.22.

Figure 6.21. Test Setup Including Floor Diaphragm

Figure 6.22. Wall-Only Test Setup

6.3. Instrumentation

Instrumenting the full-scale biaxial wall test involved attempting to capture the motion of both wall panels and the floor diaphragm, along with attempting to separate these behaviors and look at them independently. To do this, a number of string potentiometers (string pots) and LVDTs (linear variable differential transformer) were used at various locations on each specimen. A full list of the instrumentation used to accomplish the measurements in this thesis is found in Table 6.2. There are five different types of motion that characterize the deflection of a shear wall, both in-plane and out-of-plane. All five types (described well by Chen and Popovski (Chen and Popovski 2020)) – bending, shear, sliding, rotation, and slip – contribute to the deflection caused by lateral forces placed on a CLT shear wall. Each component that contributes to lateral deflection can be separated by instrumenting different parts of the specimen.

The shear force that placed on the specimen by inducing a lateral load at the given height is resisted primarily by the area of each panel but slip between panels can occur as the fasteners begin to yield and crush the wood. Slip between panels can be obtained by placing LVDTs at different points along the height of the wall panel connection point and placing string pots at the base of two different wall panels (on each side of the connection). These are used to determine how much displacement is happening between the two panels at the connection point as there is little shear deflection occurring within the panels themselves. Referring to Figure 6.23, these are referred to as channels 8 and 9 (string pots), and channels 20 and 23 (LVDTs). Photos of these instruments can be seen in Figure 6.25 and Figure 6.27.

The global rotation of the wall panel acting as one is typically referred to as uplift. This is countered by placing string hold-downs at each end of the wall panel. Rotation displacement is instrumented by placing string pots measuring vertical displacement at each end of the wall

161

panel. Referring to Figure 6.23, these are referred to as channels 6 and 11. Photos of these instruments can be seen in Figure 6.24 and Figure 6.25.

Sliding of the wall panel is counteracted primarily by the four shear brackets that have been installed along the length of the foundation and secondarily by the two hold-down brackets as well. This is instrumented, in-plane and out-of-plane, by use of string pots placed along the base of the wall. Referring to Figure 6.23, in-plane sliding is measured with channels 5 and 12 and out-of-plane sliding is measured with channels 7 and 10. Photos of these instruments can be seen in Figure 6.24 and Figure 6.25.

Lastly, both shear and bending deformations are very difficult to measure with instrumentation (especially on wood). The typical approach that is used is to group these two contributors to deflection as one and find them during post-processing of the data. That was the approach of this experimental study as well. Additionally, LVDTs were placed at the foundation baseplate to capture any sliding in either direction that would attempt to throw off an accurate measurement of total displacement. Referring to Figure 6.23, these LVDTs are given as channels 24 and 25 and the total displacement and load in each direction are given as channels 1-4. Photos of these instruments can be seen in Figure 6.24.

After accounting for the displacement of the wall panel, it was important to instrument the movement of the floor diaphragm with respect to the wall panel. It was assumed that its motion stays relatively along the path of the applied displacement of the actuator to which it is connected. Therefore, what is needed is to find how it separates from the wall panel, i.e. its 3D displacement profile. The vertical and horizontal displacement of the floor diaphragm with respect to the wall panel were captured with string pots, as seen in Figure 6.23. The out-of-plane displacement of the floor diaphragm with respect to the wall panel was captured with LVDTs as

it was assumed this would be of less magnitude than the other directions, as seen in Figure 6.23.

Photos of these instruments can be seen in Figure 6.26, Figure 6.27 and Figure 6.28.

Table 6.2. Biaxial Wall Test Instrumentation Plan

Channel	Device	Measurement	With Floor	Without Floor
1	220A Load	In-Plane Load	x	x
2	220A Displacement	In-Plane Displacement	x	x
3	220B Load	Out-of-Plane Load	x	x
4	220B Displacement	Out-of-Plane Displacement	x	x
5	SP-1 (12 in)	Sliding on west side of wall	x	x
6	SP-2 (12 in)	Uplift on west side of wall	x	x
7	SP-3 (12 in)	Out of plane sliding on west side of wall	x	x
8	SP-4 (12 in)	Uplift on west side of panel connection	x	x
9	SP-5 (12 in)	Uplift on east side of panel connection	x	x
10	SP-6 (12 in)	Out of plane sliding on east side of wall	x	x
11	SP-7 (12 in)	Uplift on east side of wall	x	x
12	SP-8 (12 in)	Sliding on east side of wall	x	x
13	SP-9 (12 in)	Vertical floor-wall displacement on west	x	
14	SP-10 (12 in)	Lateral displacement of diaphragm on west	x	
15	SP-11 (12 in)	Vertical floor-wall displacement west of connection	x	
16	SP-12 (12 in)	Vertical floor-wall displacement east of connection	x	
17	SP-13 (12 in)	Lateral displacement of diaphragm on east	x	
18	SP-14 (12 in)	Vertical floor-wall displacement on east	x	
19	LVDT-1	Out of plane floor-wall displacement on west	x	
20	LVDT-2	Lateral displacement between panels above diaphragm	x	x
21	LVDT-3	Out of plane floor-wall displacement at connection	x	
22	LVDT-4	Out of plane floor-wall displacement at east	x	
23	LVDT-5	Lateral displacement between panels at mid-height	x	
24	LVDT-6	E-W sliding of baseplate	x	x
25	LVDT-7	N-S sliding of baseplate	x	x

(a)   (b)
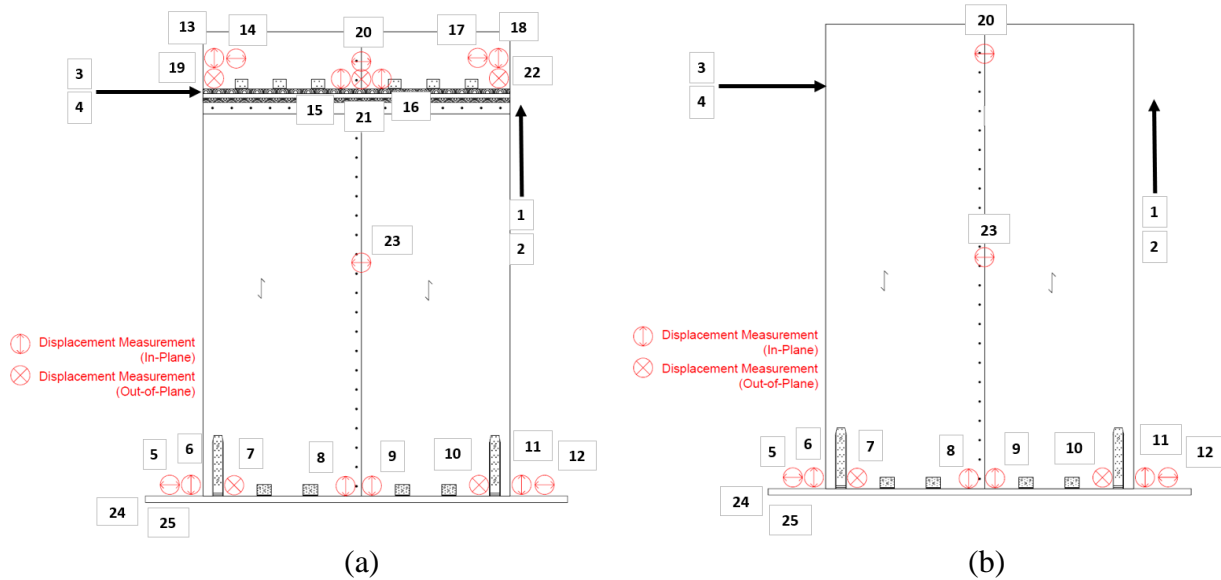
Figure 6.23. Biaxial Wall Test Instrumentation Schematic
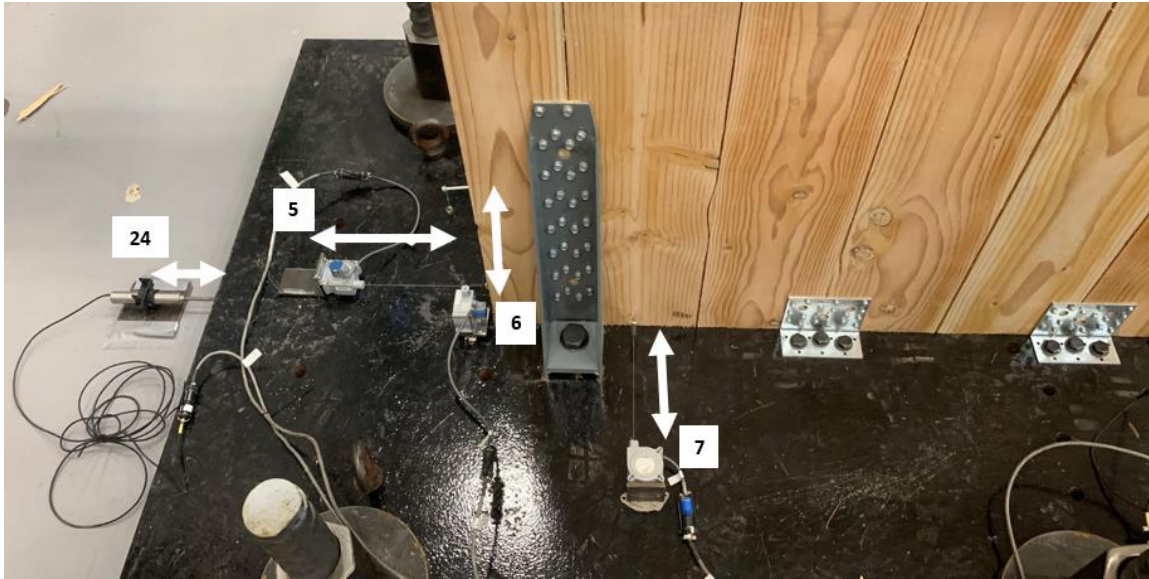
Figure 6.24. West Foundation Instrumentation
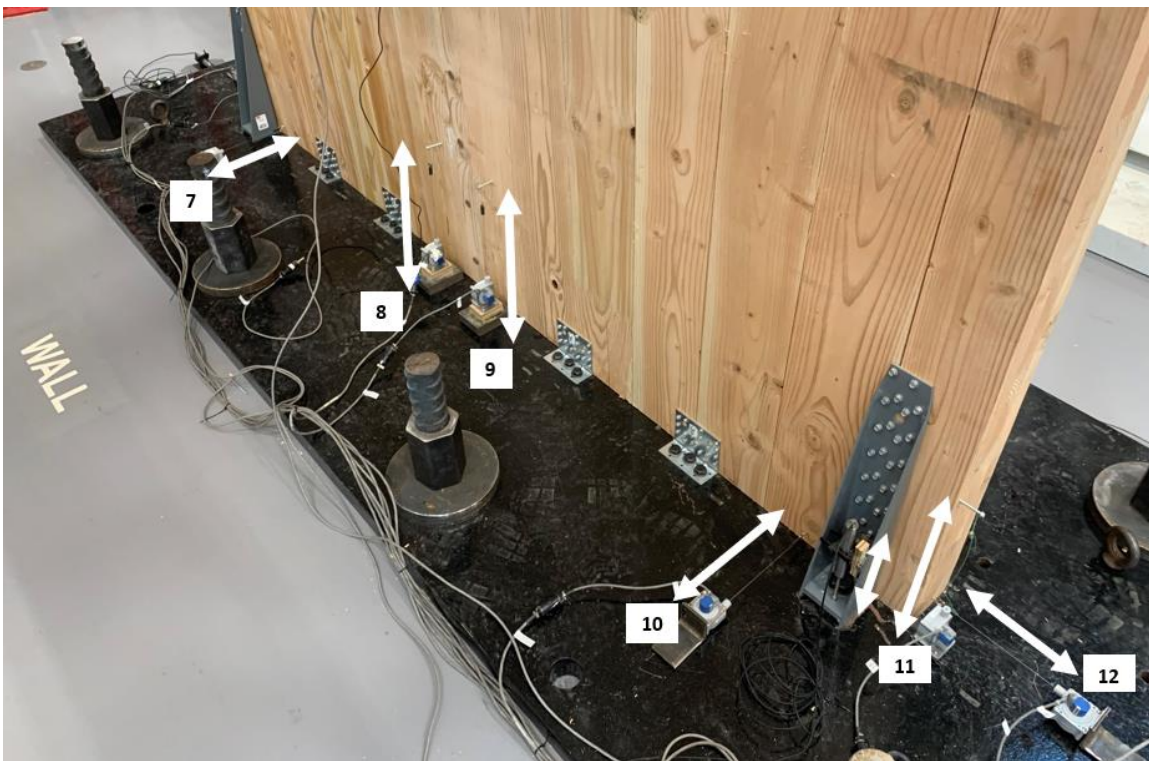
Figure 6.25. East Foundation Instrumentation
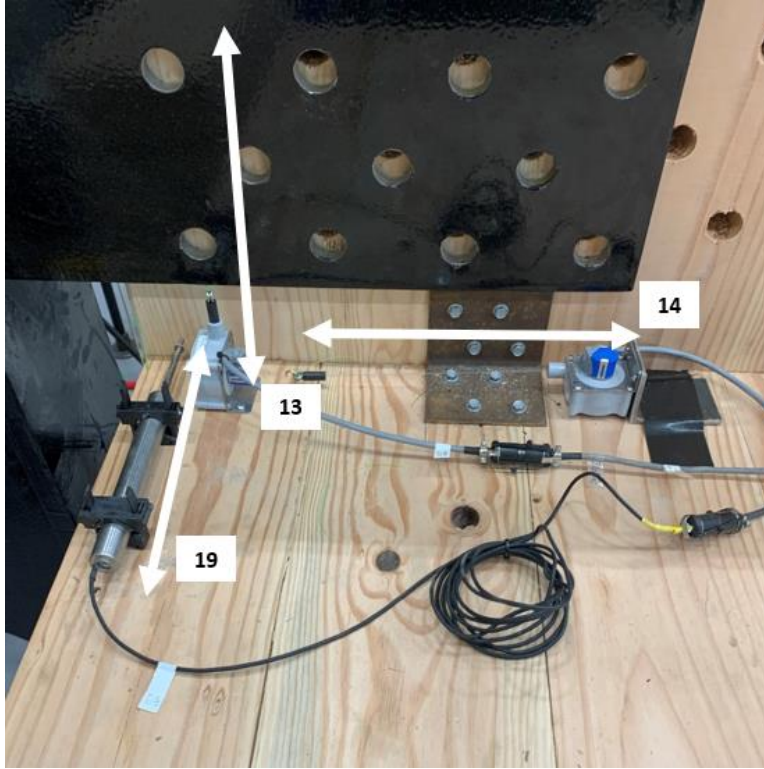
Figure 6.26. West Floor Diaphragm Instrumentation
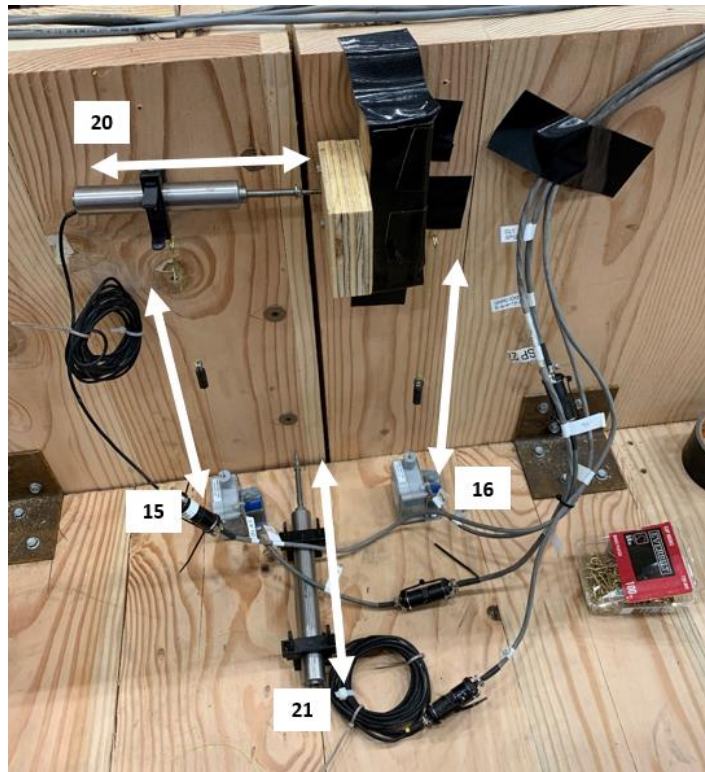
Figure 6.27. Panel-to-Panel Connection Instrumentation on Floor Diaphragm
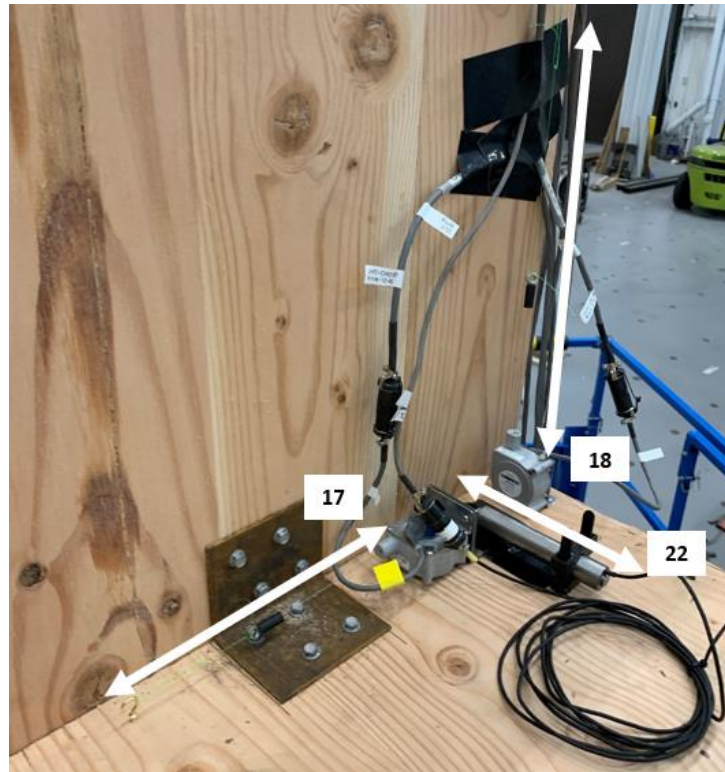
Figure 6.28. East Floor Diaphragm Instrumentation

Additionally, there were a few changes made to the instrumentation plan during completion of the test matrix. Before test B4, an LVDT was added to the east hold-down bracket to measure the amount of bending occurring in the bracket's baseplate. This can be seen in Figure 6.29. Before test B5, the way panel-to-panel sliding and separation was instrumented was changed. Instead of using LVDTs, it was accomplished using two different string pots at 90-degrees to each other. This can be seen in Figure 6.30.

Figure 6.29. LVDT Used to Capture Hold-down Plate Deflection

Figure 6.30. String Pots Used to Measure Panel Separation

6.4. Testing

6.4.1. Loading Protocol

The purpose of doing the full-scale biaxial test was to observe both the global behavior of balloon-style construction and the behavior of the connections when loaded constantly in both directions. Because there are always two components to ground motion produced by an earthquake, it is essential to understand how the system behaves when loaded equally in both directions as is this is the worst case. The loading procedure that was chosen for five of the six tests is called "cloverleaf loading protocol"(Akguzel and Pampanin 2010). As done in other studies using the cloverleaf protocol, a target radius was chosen and then each cloverleaf that radiates outward was calculated using polar coordinates by way of a sinusoidal curve in both the 'x' and 'y' directions. For purposes of this study, a final radius of approximately 7.75 inches was chosen as it leads to nearly 6 inches of maximum displacement in each direction. Additionally, eight cloverleaf patterns were chosen at a uniform distance apart. The displacement rate was chosen to be 10 inches/minute as it provided a quasistatic loading condition while also limiting the total time of each test to under half an hour. The test was paused after two consecutive 'cloverleafs' had been completed, the damage was documented, and then the test proceeded forward. The displacement profile can be seen in Figure 6.31, along with each component in Figure 6.32 and Figure 6.33.
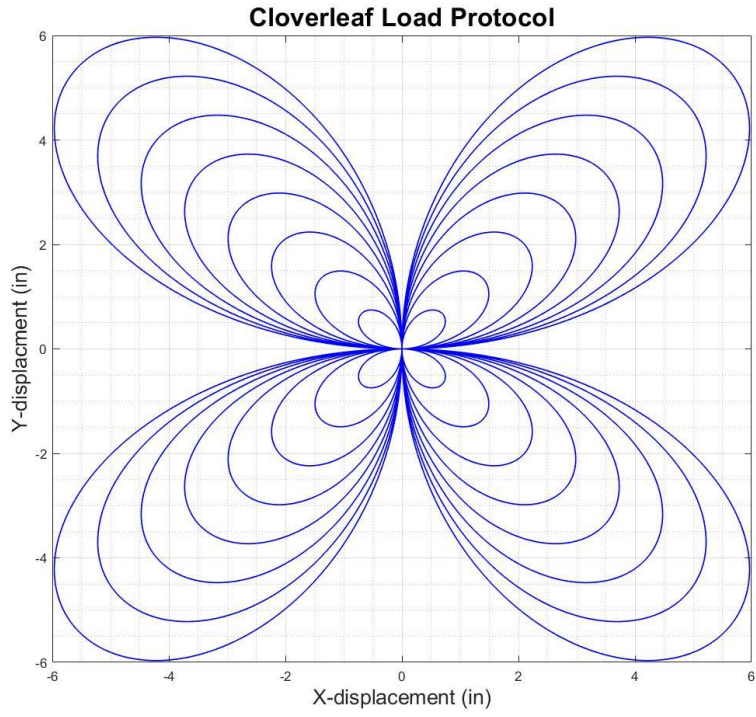
Figure 6.31. Cloverleaf Displacement Profile
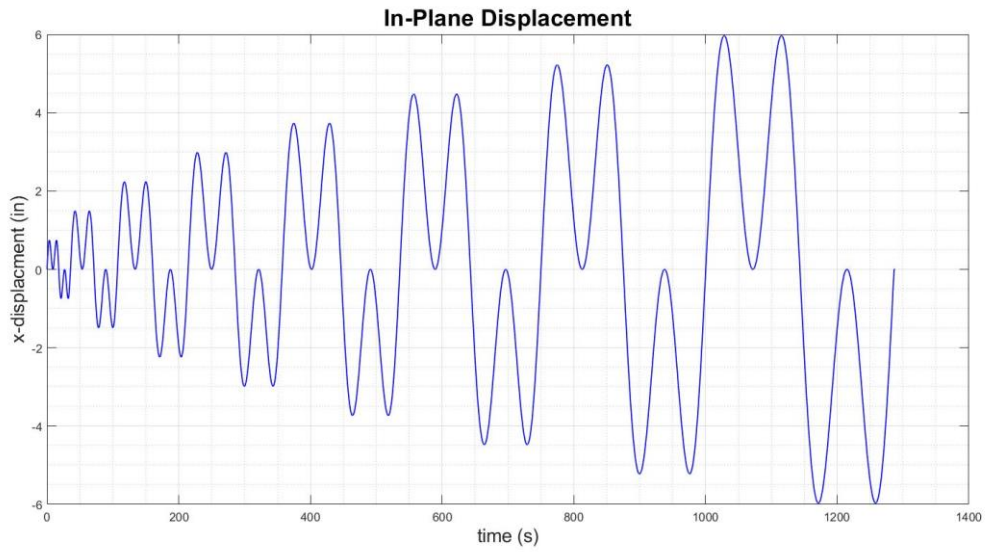
Figure 6.32. In-Plane Displacement Profile

170
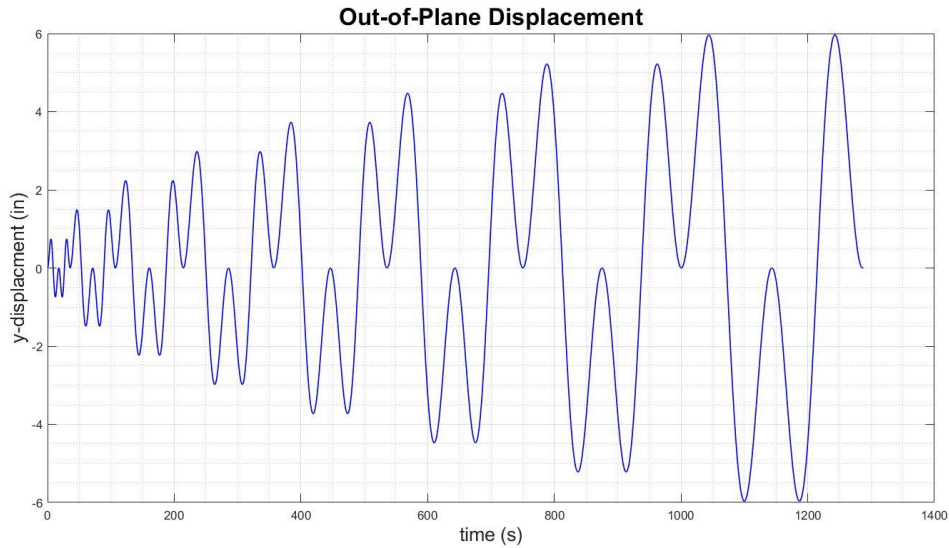
Figure 6.33. Out-of-Plane Displacement Profile

Test configuration B6 was not conducted with the same loading protocol as the other

tests. Keeping with the goal of trying to separate where each displacement is coming from, an

out-of-plane-only test was done. To observe the behavior of CLT balloon-framed shear walls

out-of-plane was something that had never been done prior to this research. It was decided that

the CUREE loading protocol should be adopted as was done with the experimental testing

program that tested only connections in one direction (Chapter 4). In the same manner as

configurations B1 through B5, a maximum displacement was chosen to 10 inches and a

reference displacement calculated from this to develop a loading profile. The loading rate was

increased slightly, to 12 inches/minute, just to keep the total time of the test under half an hour.

More information on the CUREE loading protocol is provided in section 3.4.1.2 Cyclic Load

Protocol. The loading profile that was used for test configuration B6 is plotted in Figure 6.34.

171
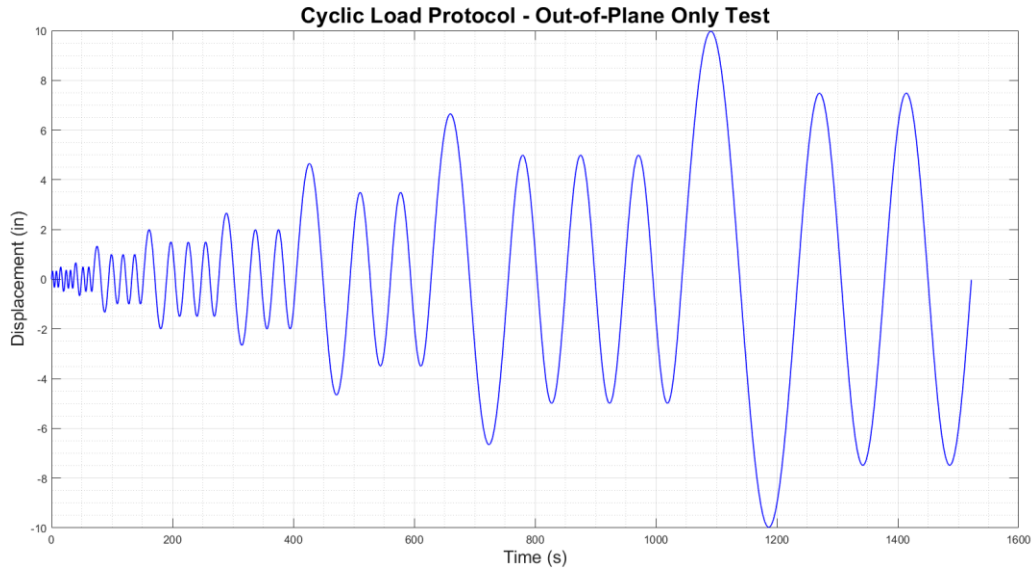
Figure 6.34. Configuration B5 Displacement Profile

6.4.2. Observed Failure Modes

Since no biaxial CLT test had ever been completed prior to this project, it was difficult to try and predict the behavior of the wall specimen when subject to bidirectional loading. Comparing the test to similar in-plane shear wall tests, the hold-downs, foundation shear connectors, and panel-to-panel connections were designed to allow for a hybrid sliding-rocking approach to govern the in-plane behavior of the wall. The out-of-plane behavior of the wall was predicted to be different in compression and in tension as there were only foundation connections on one side of the foundation. The stiffness of the wall in the out-of-plane direction was greater when subjected to compressive loads and less when subjected to tensile loads. Additionally, the stiffness of the wall in the out-of-plane direction is significantly lower than the in-plane stiffness. This led to the prediction of largely mismatched loads in the two directions. The final prediction was that there would be a problem of torsion inherent in the test, especially with the use of only one actuator in the out-of-plane direction. Typically, when CLT shear walls are tested for their in-plane strength, they are restricted for rotating about the base (torsionally) to keep the behavior

172

of the wall strictly in one plane. The nature of the biaxial test is one that leads to torsion that is resisted elsewhere when it comes to a full building system. This problem was expected, and one that could not be fully overcome – although further testing could pursue overcoming this problem.

Initial observations of the behavior of the balloon-framed CLT wall system when subjected to biaxial loading include the system's inherent susceptibility to torsion, the great benefit of a combined sliding-rocking behavior, the system's dependence the strength of its hold-down connectors, and the system's ability to withstand extreme out-of-plane inter-story drift while sustaining very little damage. First, it became very apparent that the wall (especially when tested with the floor diaphragm included) has an inherent susceptibility to torsion and resists the torsional load mainly by overloading its hold-down brackets. The system's problem with resisting torsion was most evident when both the in-plane and out-of-plane actuators were both applying a compressive load to the wall. The in-plane compression pushes the system to buckle out-of-plane, and the out-of-plane compression helps to achieve this. The amount of torsion induced on the system was move evident right before achieving the maximum load in and out-of-plane. The problem can be seen best from above, as in Figure 6.35.
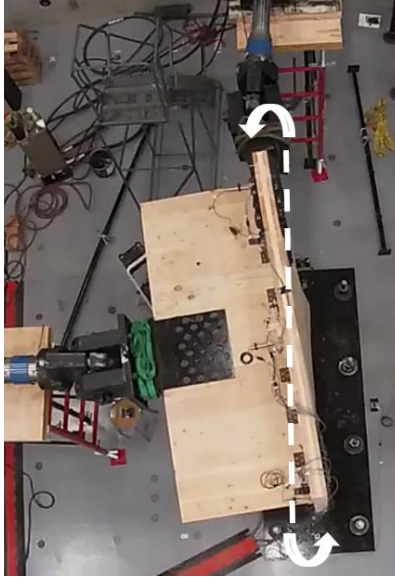
Figure 6.35. Test B2 from Above Showing Torsion

The second major observation gleaned during the biaxial wall tests was that designing a

wall system that exhibits combined sliding-rocking behavior is to be preferred over a system

where the panels exhibit little rocking between them. When energy can be dissipated through the

panel-to-panel connections, higher displacements are required in order to resist the same loads.

The test that exhibited the greatest combined sliding-rocking behavior was configuration B4

(half-lap with no floor diaphragm). Test B4 was the only configuration where a significant

number of fasteners used for panel-to-panel connections sheared off. In all other tests, the

greatest number of fasteners to fail at the panel-to-panel connection location was two (on test

B2). During test B4, every fastener ended up shearing off. This behavior is preferred over as it

leads to significantly lower forces in the hold-down connections. When the panels are free to

rock between one another, less force can be transferred to the hold-downs. This observation was

made because the hold-downs failed in markedly different ways when comparing the test B4 to

test B2.

Figure 6.36. Test B2 Hold-down Failure

Figure 6.37. Test B4 Hold-down Failure

175

It is clear that the hold-down bracket in test B2 experienced higher tension loads on the bolt securing it to the foundation, as seen in Figure 6.36. The failure mode of the hold-down observed in test B2, and other test configurations where sliding-rocking was not the primary behavior of the wall, are to be avoided and the behavior of test B4 to be preferred. As seen in Figure 6.37, test B4's hold downs failed at their attachment point to the ends of the CLT wall panel by way of screws pulling out of the wood and the wood itself shearing out in a block-shear manner. When the wall is able to fully develop the forces needed for this to occur, larger drift ratios are able to be achieved and a better system as a whole is the result.

The third major observation when looking at the behavior of the CLT walls subjected to bidirectional loading was that the overall behavior of the specimen was highly dependable on the behavior of the hold-down brackets. During tests B2 and B3, where rupture of the hold-down bracket baseplate was observed at or slightly after the maximum force occurred, the test was unable to continue as there was too much damage at the foundation to safely continue. During tests B1, B4, and B5, the tests were able to be pushed further into the post-peak force-displacement territory as the foundation connections were not damaged in such a fashion that the wall was detached from the foundation.

Looking at each test individually, test B1 was a half-lap specimen with the floor diaphragm included in the test. This test had to eventually be aborted before reaching the goal displacement of 6 inches because the hold-down connection and two shear-resisting angle brackets on the east side of the foundation had both detached completely. The hold-down bracket failed in a block-shear manner where an entire block of wood separated from the panel while still attached to the hold-down. This can be seen in Figure 6.38(a). This caused additionally uplifting forces to be redistributed to the two angle brackets. These two brackets eventually failed in a

176

manner where their bolts pulled through the holes in the short leg of the angle bracket and the

remaining material exhibited a tensile failure. This can be seen in Figure 6.38(b). The hold-down

bracket failed this way partly due to the shear force in the wood as it resists the uplift and partly

due to the tensile force in the wood as it resists the torsion when the wall pulls away. The angle

brackets exhibited the tensile pull-through failure because of the additional uplifting forces they

had to resist and the additional torsion (though the middle angle bracket did not see as a great of

a torsional force). As for the angle brackets used to attach the floor diaphragm to the wall, little

damage was observed. Looking at the panel-to-panel connection, there was one fastener that

failed in shear, and the others began to exhibit the formation of two plastic hinges (typical of

NDS failure mode IV), but very little deformation was observable. Some panel-to-panel rocking

was observed, but was less than expected likely because of the added stiffness of the floor

diaphragm.
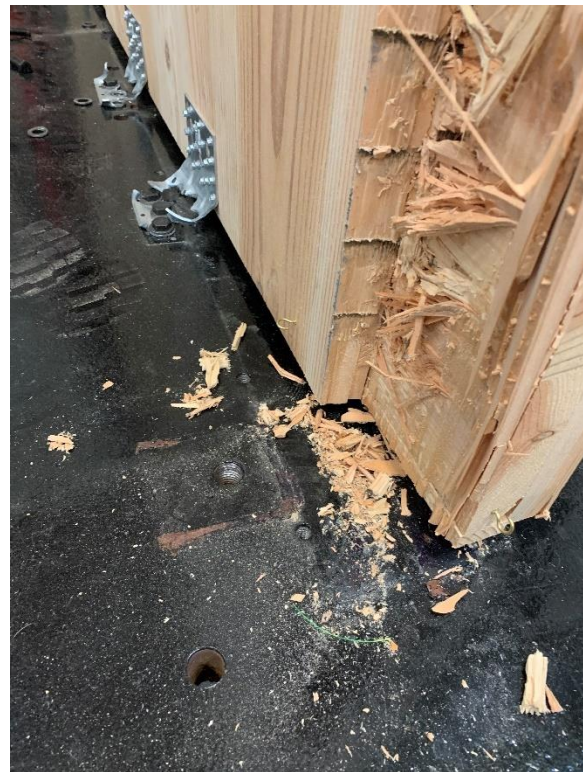
(a)   (b)

Figure 6.38. Failure of Foundation Connections During Test B1

Test B2 was the same configuration as test B1 – a half-lap specimen with the floor diaphragm included in the test. The type of failure that occurred during this test was again dominated by the behavior of the hold-down brackets. The hold-down on the east side of the foundation failed when its baseplate ruptured while exhibiting no other signs of reduced strength (no fasteners pulling out, etc.). The rupture of the hold-down bracket, as discussed previously, can be seen in Figure 6.36. When this hold-down failed, the same behavior as test B1 was observed. The angle brackets began to carry more tensile load as it was redistributed and eventually exhibited a tensile pullout failure. This can also be seen in Figure 6.39(b). The hold-down on the west side nearly reached failure by buckling the first ply of the CLT panel out-of-plane. When the wall had a compressive load in-plane and a tensile load out-of-plane, it put too much torsion on the hold-down for it to handle and the first ply began to separate from the panel and a crack shot back through to the intersection of the second and third ply, as shown in Figure 6.39(a). While there was still capacity for resisting load on the west side of the foundation, the test was discontinued after the east panel was no longer connected to the foundation as all of its brackets had failed. One screw in the half-lap connection sheared off and the others began to exhibit NDS failure mode IV, which can be seen in Figure 6.40. The wall-to-floor connections exhibited no damage as the loads they experienced during the test were very low.

(a)	(b)
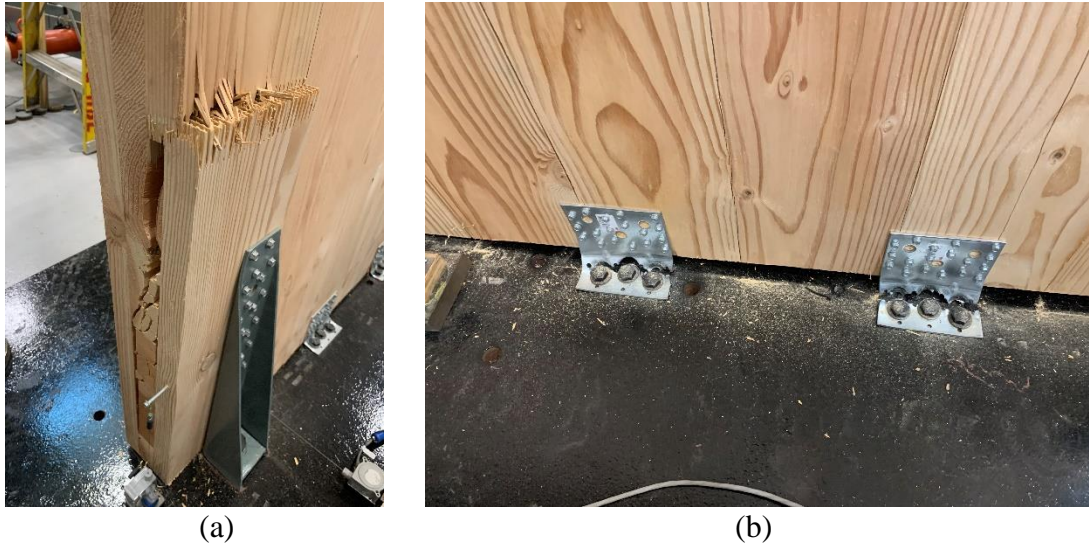
Figure 6.39. Failure of Foundation Connections During Test B2

Figure 6.40. Test B2 Panel-to-Panel Connection Failure

Test B3 was another wall specimen that was tested with the floor diaphragm attached, but this time with a single surface spline connection being used as the panel-to-panel connection method. Overall, test B3 ended up performing in a less ductile manner than the previous two tests. The amount of rocking between panels that was observed was significantly less – and the behavior could be described as more of a combined rocking-sliding behavior where the panels acted more in a singular manner than in a coupled manner, meaning that the panels rock together

as one rather than rocking between each other. This was confirmed by the absence of any damage to the screws used in making the splined connection. Further evidence of this behavior can be seen in the hold-down on the east side of the wall that exhibited a rupture of its baseplate, as in test B2. Because of experience with the uncertainty of previous tests, the test was discontinued before further damage was observed other than just the east hold-down bracket. Additionally, the decision to stop the test was made because a peak load has been reached and one additional cycle post-peak had been achieved (at least in compression). A photo showing the east side of the wall-to-foundation connections can be seen in Figure 6.41. The panel-to-panel connecting screws were undamaged and the wall-to-floor connections were undamaged as well. To show the undamaged wall-to-floor connections in this test, as in tests B1 and B2 as well, see Figure 6.42.

Figure 6.41. Test B3 Damage

Figure 6.42. Test B3 Wall-to-Floor Connections After Testing

Test B4 was a wall-only test utilizing a half-lap to connect the two panels together. The

behavior that was observed was the most rocking-dominate of any test that was performed.

Rather than seeing sliding and uplift dominate the behavior of the test, rocking was characterized

the behavior of the test, and this was shown in the damage at connection points. At the

foundation, the hold-down brackets on each side showed fasteners pulling out of the wood and

wood beginning to exhibit the block-shear behavior, as in test B1, although total separation from

the panel never occurred on either side, as can be seen in Figure 6.43(a). The four angle brackets

on the foundation didn't fail in tension, but rather exhibited a tension and shear failure

concurrently. The fasteners pulled through the wood as they resisted uplift and sliding

simultaneously, but the bracket did begin to yield as it resisted uplifting forces, as seen in Figure

6.43(a). The panel-to-panel connection was where much of the energy was dissipated. Every

fastener eventually sheared off after exhibiting NDS failure mode IV (formation of two plastic

hinges). This also led to the separation of the panels in and out-of-plane, as shown in Figure

6.43(b).

<div align="center">(a)   (b)</div>
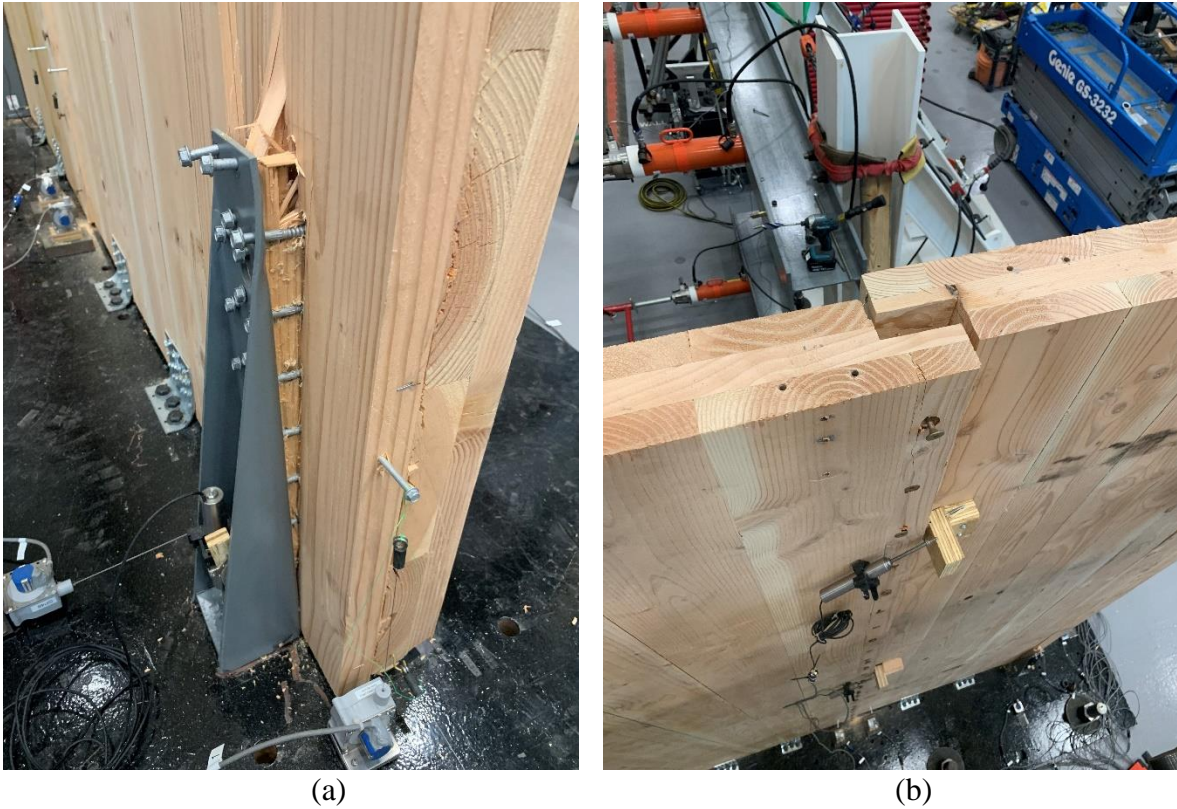
<div align="center">Figure 6.43. Test B4 Damage</div>

Test B5 was another wall-only test, using a single surface spline connection for the panel-to-panel connection method. This test behaved in a manner where the panels rocked together, but not as much as with the half-lap connection method. The panel-to-panel behavior could more be classified as single-coupled as the two panels rock between each other, but also rock as one at times. Because the surface spline connection tends to be more ductile, fasteners did not shear off at the panel-to-panel connection as easily and the damage tends to be focused on the foundation. The hold-down brackets both exhibited pulling out of fasteners and tearing through wood parallel to the grain, as shown in Figure 6.44(b) and Figure 6.45(a). The angle bracket on the east side of the foundation had fasteners pull out of the wood and part of the wall panel began to exhibit a combined tension and shear failure, as seen in Figure 6.44(a). The angle bracket on the

west side of the foundation failed in tension due to the uplifting forces it resisted, as seen in Figure 6.45(b).

<div align="center">(a)   (b)</div>
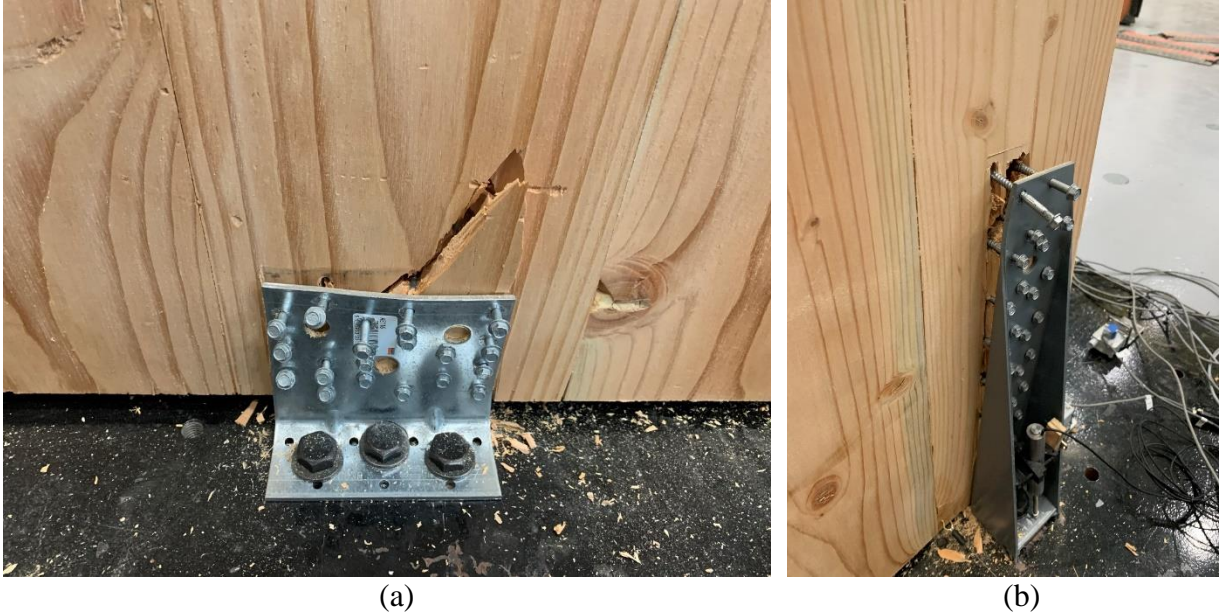
Figure 6.44. Test B5 Foundation Connection Damage (East Side)

<div align="center">(a)   (b)</div>
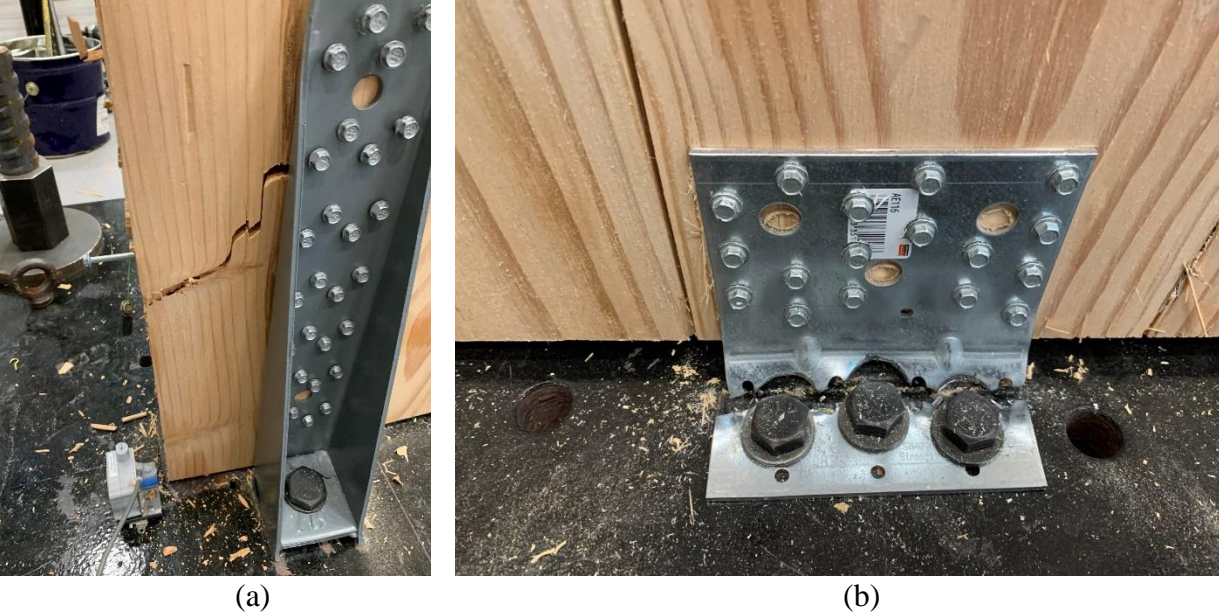
Figure 6.45. Test B5 Foundation Connection Damage (West Side)

Test B6 was a half-lap connected wall-only test, differing from the rest of the test matrix in loading protocol. This test was an out-of-plane-only test. The test reached a maximum drift ratio of nearly 8% (10 inches of displacement at 126 inches of height) while sustaining very little

damage at the foundation or to the panel-to-panel connection. The only observable damage to the specimen after testing was to the hold-down connectors' baseplates. On each side, the baseplates had yielded and shown about 1/8 of an inch of deformation, much like what happened before seeing eventual rupture of the baseplates in tests B2 and B3. This damage can be seen in Figure 6.46.

Figure 6.46. Test B6 Damage to Hold-down Connector

6.4.3. Results

The results of the biaxial wall tests are presented in this section. The maximum force achieved in each test, in each direction, and in both tension and compression are presented in Table 6.3, along with their corresponding displacements. An analysis of deflection contribution to the total deflection observed was performed, along with a characterization of the overall behavior of the wall during each biaxial test, and results were documented in Table 6.4. The mechanical properties of each specimen configuration are presented in Table 6.6 and Table 6.7 for tests B1-B5 and B6, respectively. This includes the maximum force after the first cycle (F_1), the force achieved at the first cycle post-peak (F_{post}), the ultimate force that was obtained during the last cycle (F_u), the displacement where the ultimate force was obtained (d_u), the elastic stiffness (k_e), the plastic stiffness (k_p), and the energy dissipated by the specimen during the test – defined as the area under the force-displacement curve (E_d). The force-displacement curves for each configuration, and in each direction, are presented in Figure 6.47 through Figure 6.57.

The experimental data was filtered using a non-casual low-pass filter in MATLAB. A Butterworth filter was selected to calculate the filtering coefficients and then MATLAB's non-casual filter was used to filter the data.

Table 6.3. Maximum Force and Displacement Summary

Configuration		In-Plane Direction				Out-of-Plane Direction			
		Tension		Compression		Tension		Compression	
		F_{max} (kips)	d_{max} (in)	F_{max} (kips)	d_{max} (in)	F_{max} (kips)	d_{max} (in)	F_{max} (kips)	d_{max} (in)
Including Floor	B1	37.26	2.21	33.18	2.21	0.53	3.76	2.14	1.51
	B2	41.92	2.97	37.22	2.86	0.54	3.70	2.32	2.99
	B3	40.32	2.96	30.75	1.29	1.63	2.41	2.24	2.23
Wall-Only	B4	41.83	2.96	35.54	3.70	1.10	3.72	2.83	2.22
	B5	28.62	2.93	30.94	1.37	1.45	1.12	2.00	2.99

Table 6.4. Analysis of Deflection Contribution

Configuration		In-Plane Direction				Out-of-Plane Direction			Behavior	
		Rocking	Sliding	Uplift	Shear, Bending, and Torsion	Sliding	Uplift	Shear, Bending, and Torsion	Primary Behavior	Panel-to-Panel Behavior
		(%)	(%)	(%)	(%)	(%)	(%)	(%)		(as observed)
Including Floor	B1	10.3	10.5	24.9	54.4	3.9	5.5	90.5	Rocking	Single-Coupled
	B2	13.5	12.8	31.8	41.9	3.6	11.0	85.4	Rocking	Coupled
	B3	11.2	11.9	16.7	60.2	6.7	18.5	74.8	Rocking-Sliding	Single
Wall Only	B4	12.7	8.5	30.3	48.4	4.7	19.7	75.6	Rocking	Coupled
	B5	11.0	8.0	29.0	52.0	15.6	22.8	61.6	Rocking	Single-Coupled

Table 6.5. Out-of-Plane-Only Test Deflection Analysis

Configuration		Sliding	Uplift	Shear and Bending	Primary Behavior	Panel-to-Panel Behavior
		(%)	(%)	(%)		
Wall Only	B6	0.3	1.6	98.2	Shear/Bending	Single

Table 6.6. Mechanical Properties of Test Walls (In-Plane)

Mechanical Properties (In-Plane)											
		Tension				Compression						
Configuration		F_1 (kips)	F_{post} (kips)	F_u (kips)	d_u (in)	F_1 (kips)	F_{post} (kips)	F_u (kips)	d_u (in)	k_e (kips/in)	k_p (kips/in)	E_d (kJ)
With Floor	B1	20.23	34.13	19.07	3.29	23.58	28.26	23.81	3.59	27.25	3.11	36.3
With Floor	B2	22.04	40.41	29.69	3.67	22.41	25.78	23.21	3.70	29.68	4.88	42.7
With Floor	B3	21.72	32.5	29.64	2.98	21.72	28.18	26.48	2.81	29.25	4.00	30.3
Wall Only	B4	18.35	15.51	9.37	5.23	19.54	27.84	20.14	5.22	24.71	9.80	55.3
Wall Only	B5	17.28	27.31	9.59	3.79	21.13	25.11	13.87	3.82	23.27	5.26	41.5

Table 6.7. Mechanical Properties of Test Walls (Out-of-Plane)

Mechanical Properties (Out-of-Plane)												
		Tension				Compression				Tension	Compression	
Configuration		F_1 (kips)	F_{post} (kips)	F_u (kips)	d_u (in)	F_1 (kips)	F_{post} (kips)	F_u (kips)	d_u (in)	k_e (kips/in)	k_e (kips/in)	E_d (kJ)
With Floor	B1	0.37	0.15	0.24	1.91	0.45	2.01	1.63	3.66	0.21	0.60	1.1
With Floor	B2	0.03	0.53	0.48	3.70	0.53	1.67	1.53	3.70	0.03	0.72	1.3
With Floor	B3	0.12	0.43	0.40	2.96	0.48	1.63	1.52	2.26	0.16	0.64	1.1
Wall Only	B4	0.35	1.06	0.46	5.19	0.63	2.19	1.31	5.21	0.47	0.85	2.1
Wall Only	B5	0.06	0.54	0.41	3.97	0.4	1.74	0.97	3.33	0.08	0.54	1.1

Table 6.8. Mechanical Properties of Out-of-Plane-Only Wall Test

Mechanical Properties (Out-of-Plane-Only Test)							
Configuration		Tension		Compression		Tension	Compression	
Configuration		F_{max} (kips)	d_{max} (in)	F_{max} (kips)	d_{max} (in)	k_e (kips/in)	k_e (kips/in)	E_d (kJ)
Wall Only	B6	2.03	8.34	4.52	9.91	0.37	0.88	6.9

Figure 6.47. Test B1 In-Plane Load vs. Displacement

Figure 6.48. Test B1 Out-of-Plane Load vs. Displacement

188

In-Plane Load vs. Displacement

Figure 6.49. Test B2 In-Plane Load vs. Displacement

Out-of-Plane Load vs. Displacement
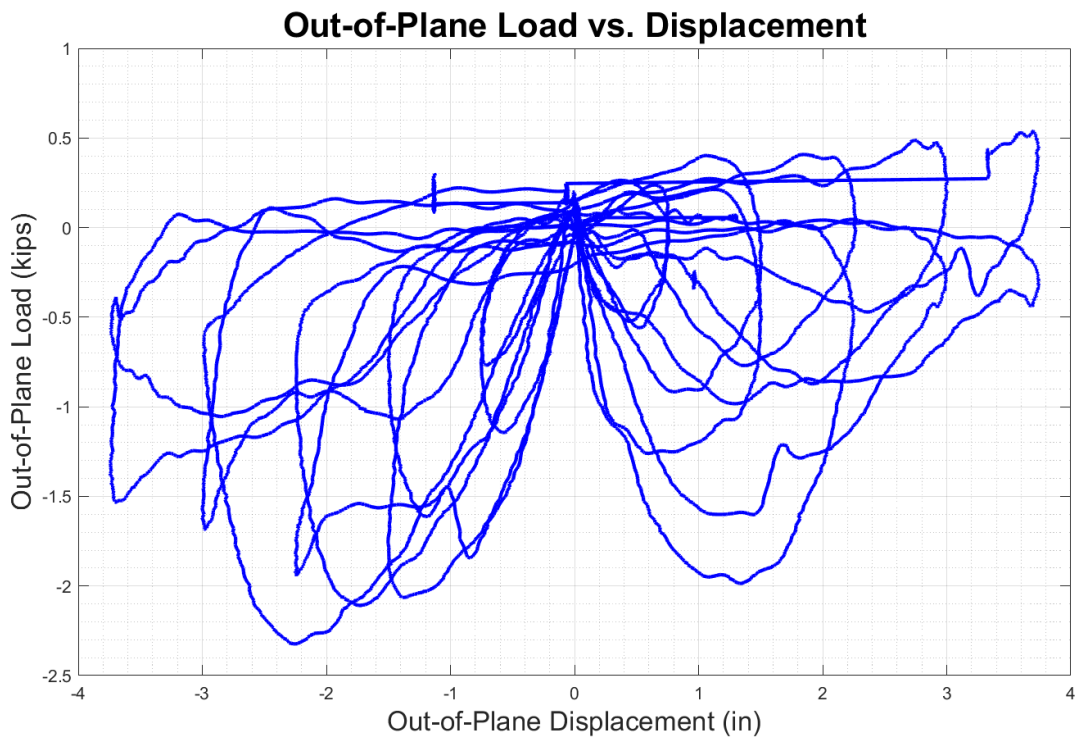
Figure 6.50. Test B2 Out-of-Plane Load vs. Displacement

189

In-Plane Load vs. Displacement
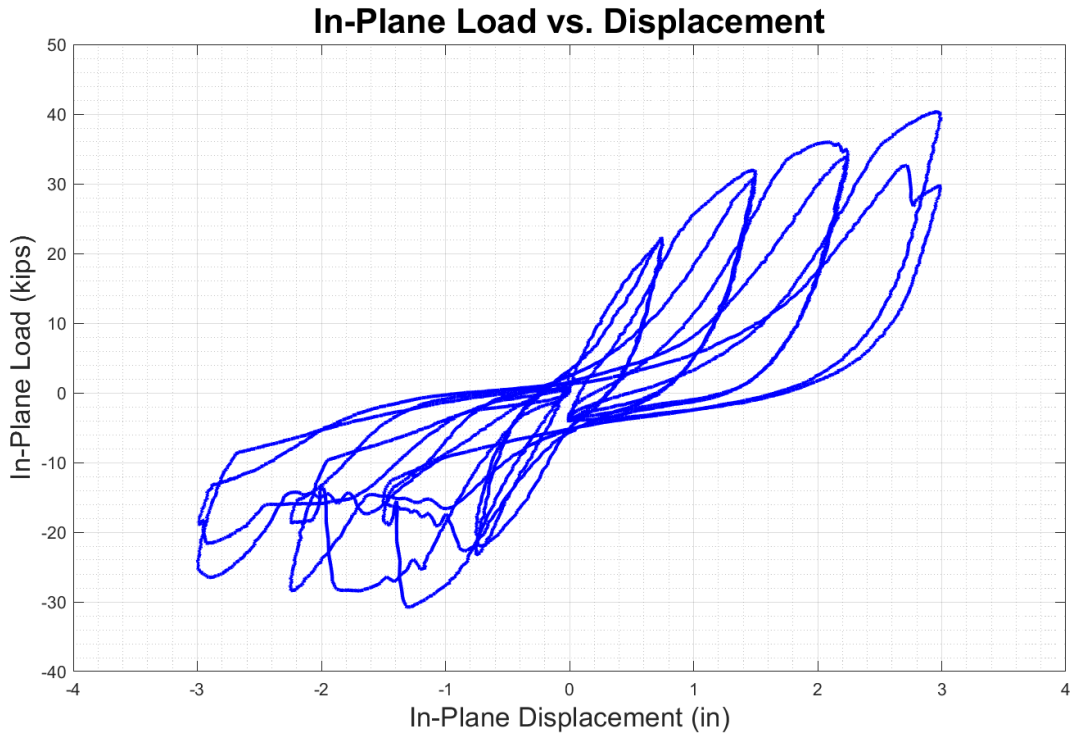
Figure 6.51. Test B3 In-Plane Load vs. Displacement

Out-of-Plane Load vs. Displacement
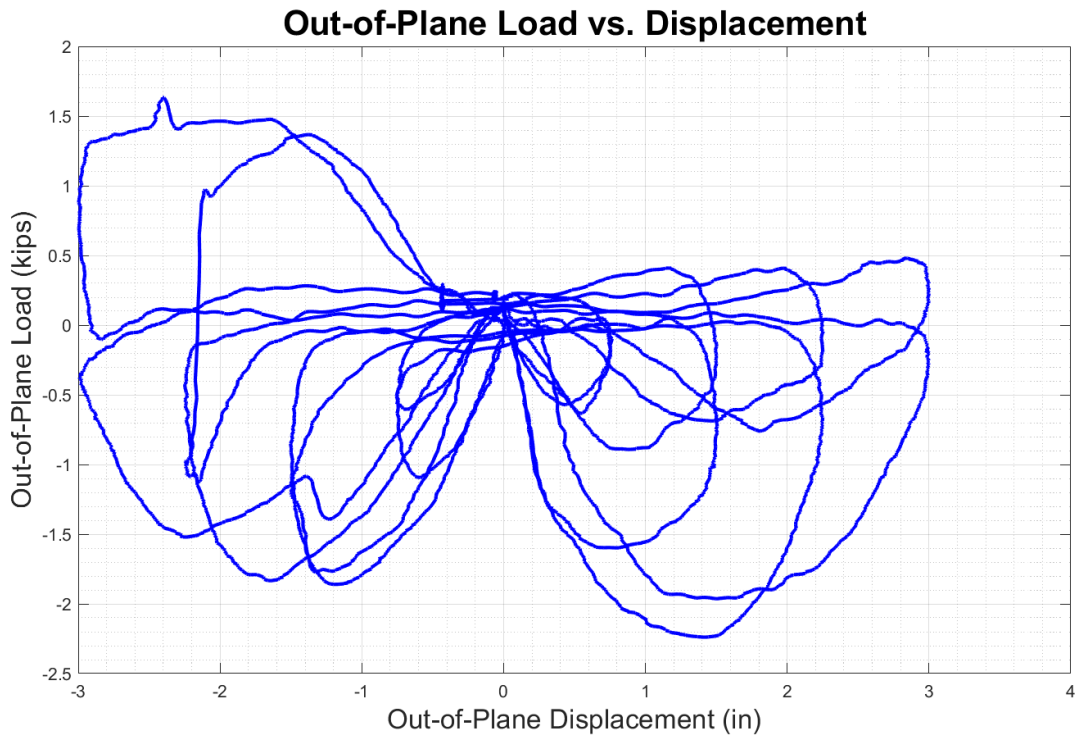
Figure 6.52. Test B3 Out-of-Plane Load vs. Displacement

In-Plane Load vs. Displacement
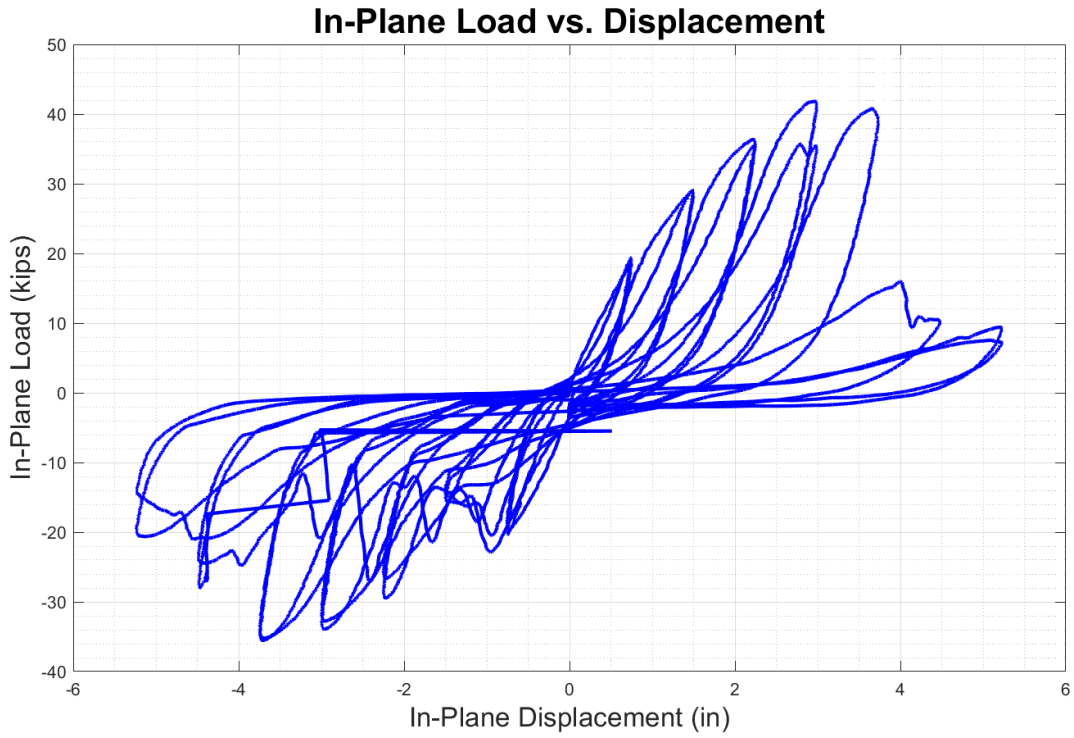
Figure 6.53. Test B4 In-Plane Load vs. Displacement

Out-of-Plane Load vs. Displacement

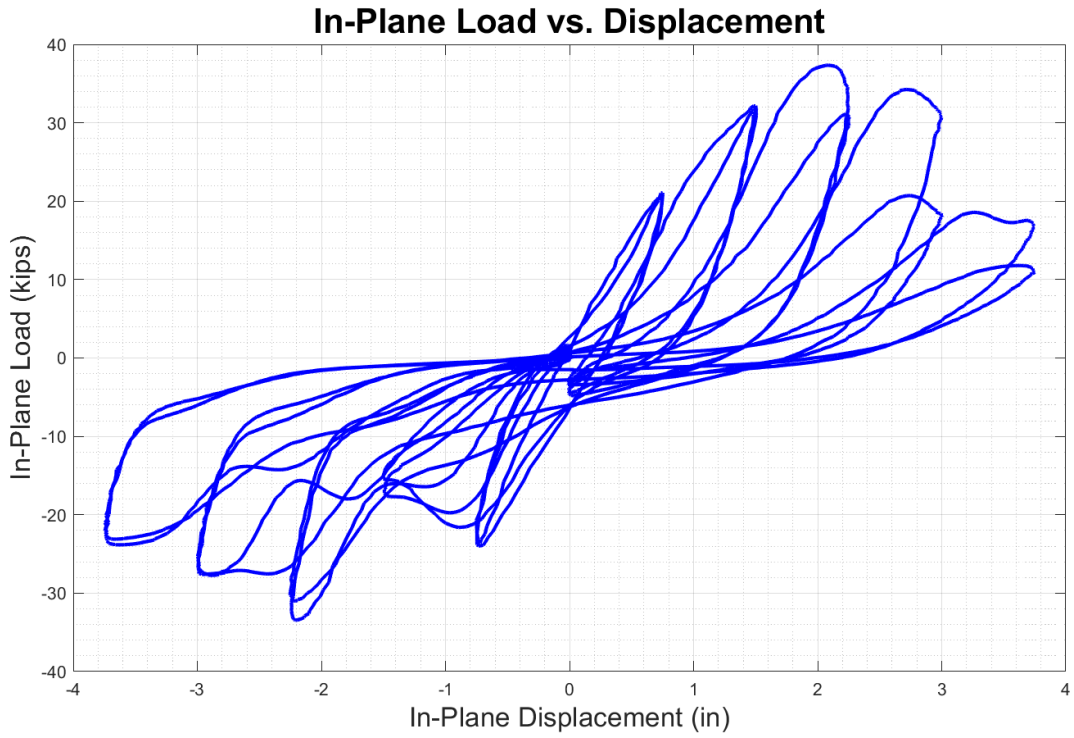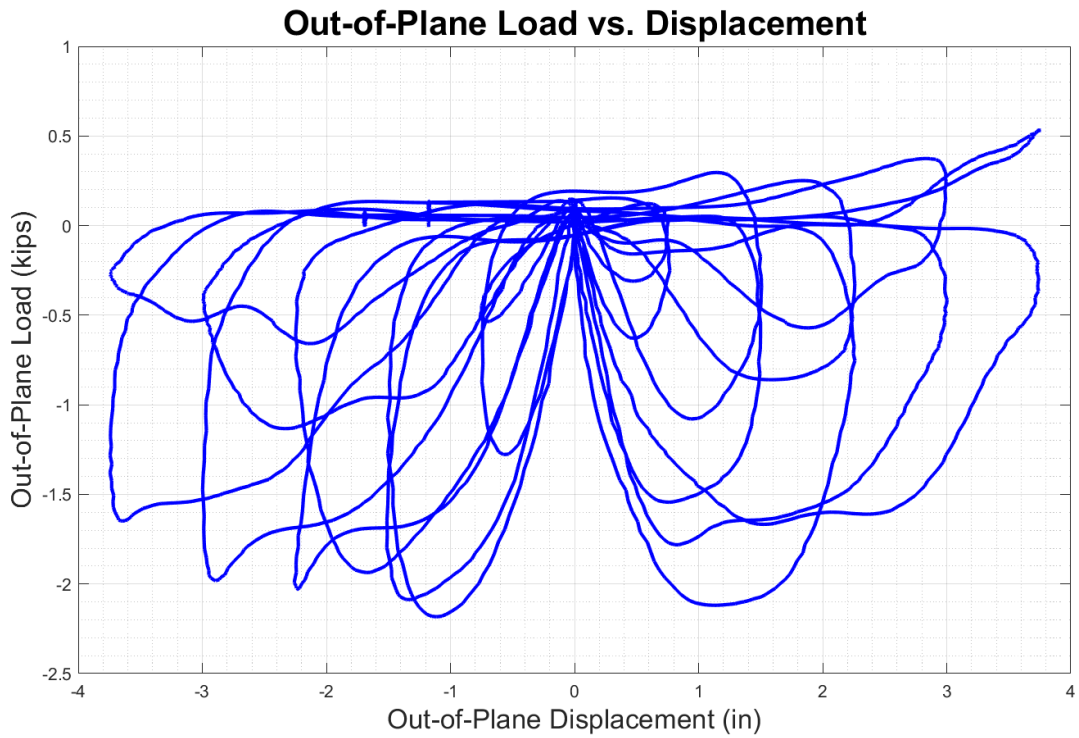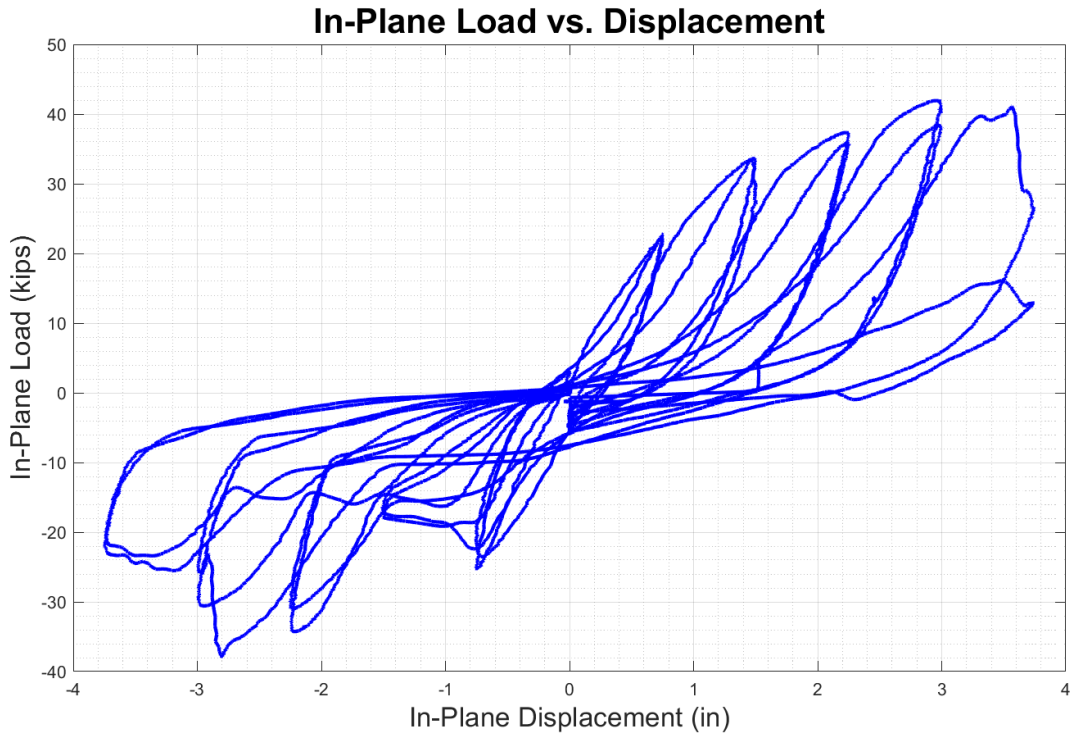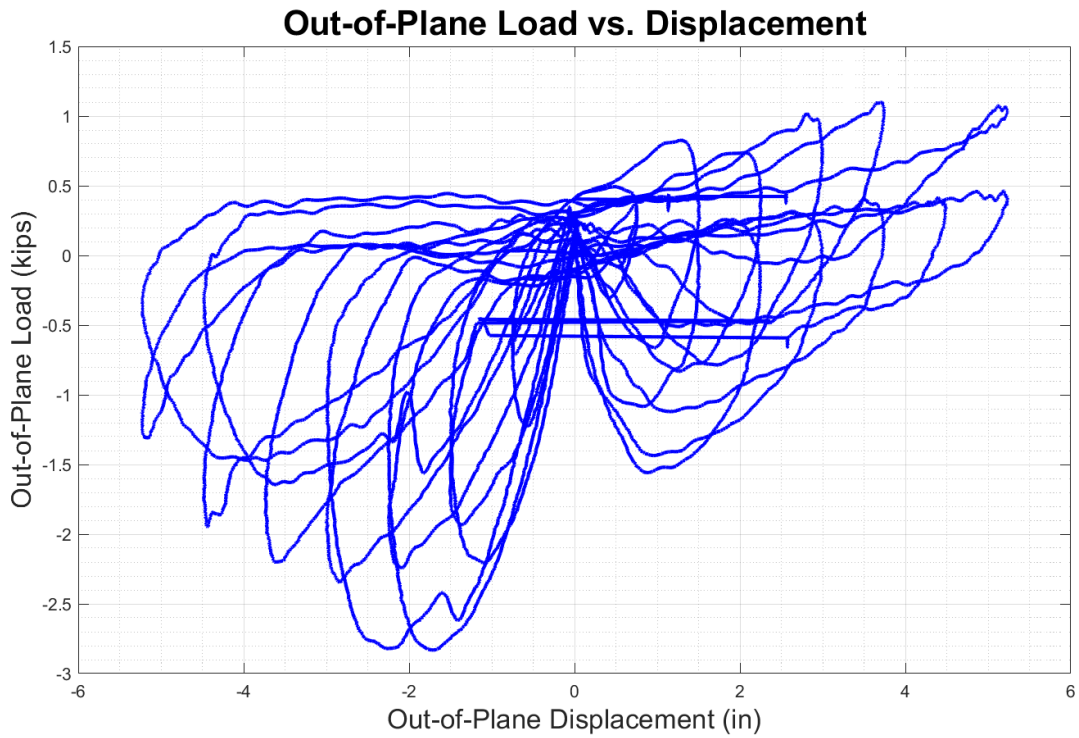Figure 6.54. Test B4 Out-of-Plane Load vs. Displacement

191
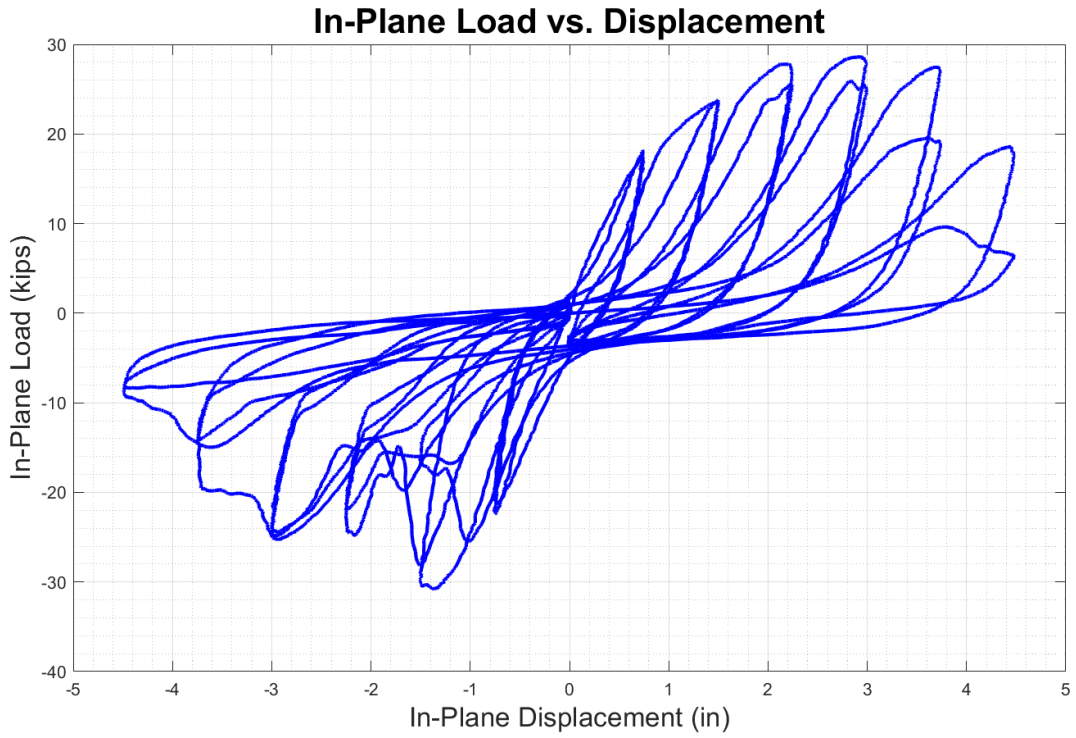
Figure 6.55. Test B5 In-Plane Load vs. Displacement
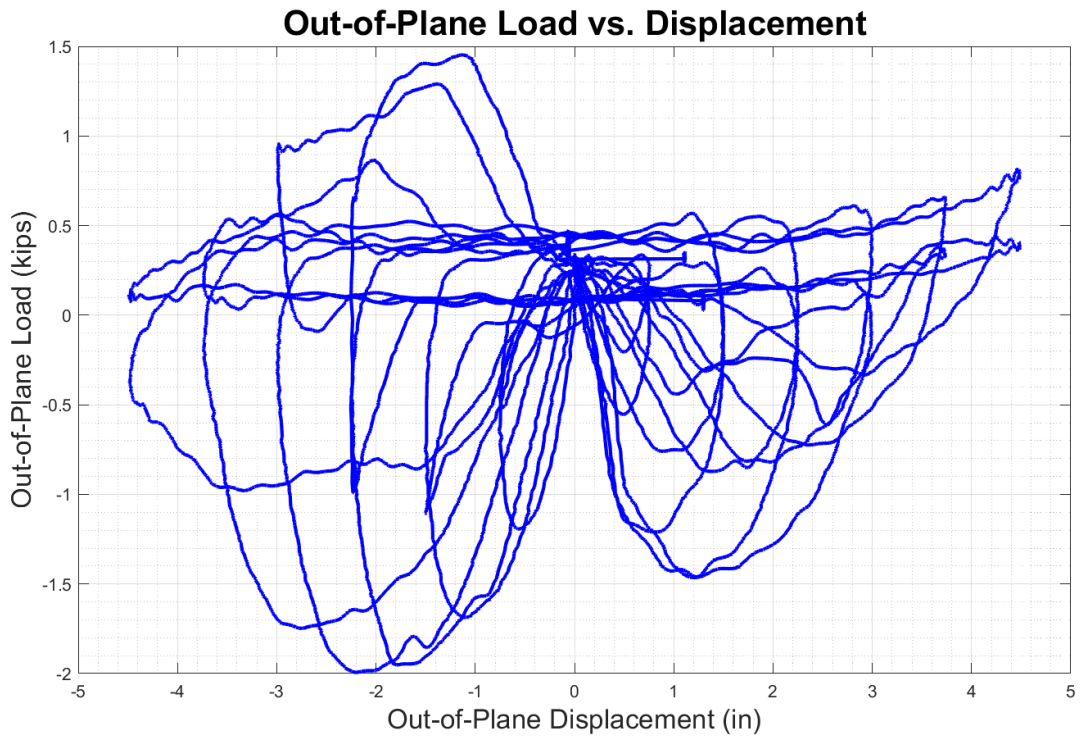
Figure 6.56. Test B5 Out-of-Plane Load vs. Displacement

192
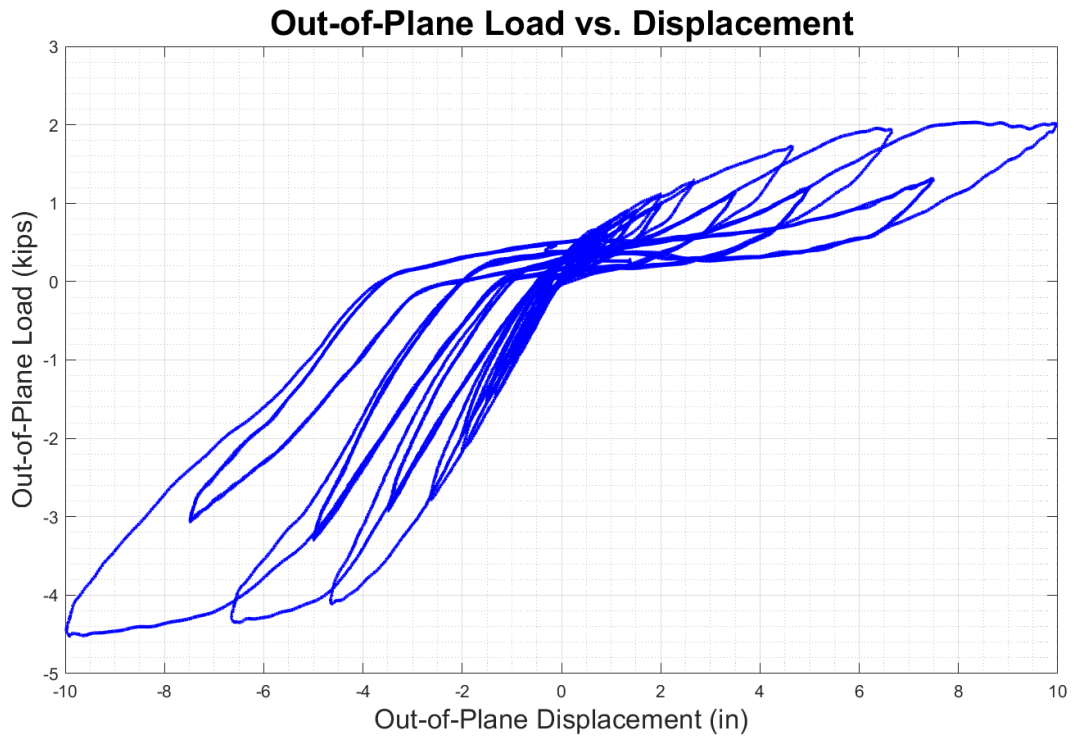
Figure 6.57. Test B6 Load vs. Displacement

6.4.4. Discussion

After analyzing the force-displacement curves, different deflection contributions, and other mechanical properties that were calculated during post-processing of the data, there were many observations that prove useful for future balloon-style construction designs. First, the difference in performance between half-lap and surface spline specimens was characterized by a difference in failure mode. Second, analyzing the contribution of deflection from different parts to the whole was beneficial in understanding how the torsion during the test contributed to the overall response. Third, the out-of-plane load-displacement curves are somewhat misleading given the understanding of how the torsion present in the test led the actuators to fight each other, which may be deemed as a limitation of this study. Fourth, rocking behavior of coupled panels is not prohibited or in any way lessened when a CLT shear wall is loaded in two directions. Fifth, the in-plane stiffness is significantly increased when a floor diaphragm is attached, as would be expected. Sixth, the out-of-plane-only test removes any uncertainty regarding what would happen to a CLT shear wall when loaded out-of-plane and should give designers confidence that it can withstand immense drift ratios while sustaining little damage. Lastly, there are many areas of future research that could improve upon this work and explore the nature of balloon framed CLT shear walls even further summarized in Chapter 7.

The difference in performance between half-lap and surface spline specimens was characterized by a difference in failure mode. The half-lap specimens were characterized mostly by a rocking behavior with coupled panels, meaning the panels rock between each other more than they do as a single panel. The surface spline specimens behaved more in a rocking-sliding manner and were either observed to be working as a single panel or more of a single-couple combined behavior, as it can be observed in Table 6.4. Just looking at the contribution of uplift

194

to the total deflection in tests B2 (half-lap) and B3 (surface spline), test B2 had uplift contribute 31.8% to the overall deflection and test B3 had uplift contribute just 16.7% to the overall deflection. Given that uplift is contributing more to the overall deflection, this leads to the conclusion that more rocking is happening in the system. Plots showing the uplift vs. in-plane load can be seen in Figure 6.58 and Figure 6.59. The difference in failure modes between the two different systems can be seen by where the damage is concentrated. With the half-lap specimens, much more damage occurred to the screws at the panel-to-panel connection point, indicating that more rocking occurred between the panels. With the surface spline specimens, not much damage was observed at the panel-to-panel connection location, indicating that damage occurred mostly at the foundation as rocking was not the dominating behavior.
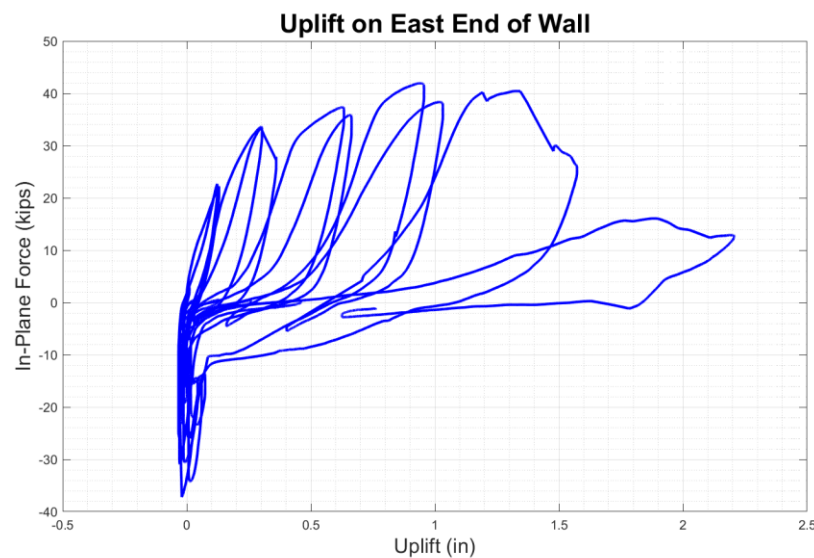
Figure 6.58. Test B2 Uplift on East End of Wall
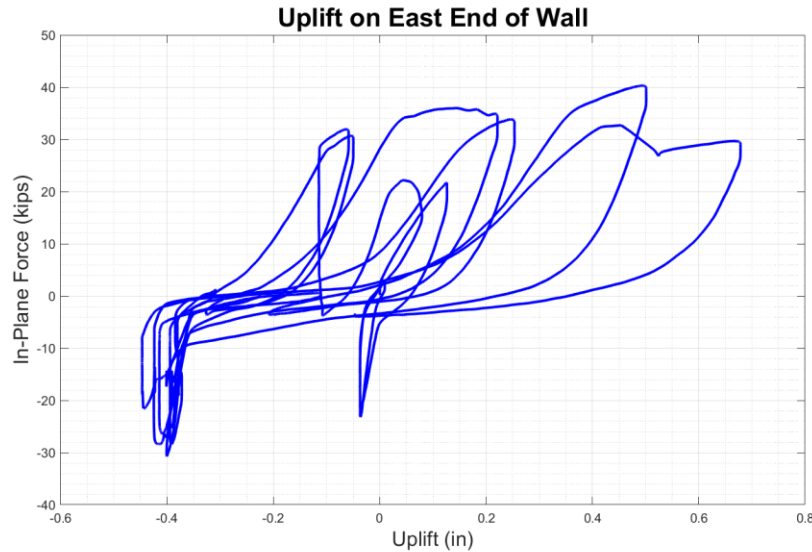
Figure 6.59. Test B3 Uplift of East End of Wall

Analyzing the deflection contribution of different parts of the wall system as it contributes to the total deflection was extremely beneficial as it revealed just how torsion during the test influenced the overall response. Referring to Table 6.4, there are four different types of deflection that contribute to the total in-plane deflection (rocking, sliding, uplift, and shear, bending, and torsion). Out-of-plane deflection differs only in that rocking is not a primary contributor to deflection in that direction. By breaking down how these contribute to the whole, it allowed for classification of overall behavior and panel-to-panel behavior as well. In the out-of-plane direction, it was expected that shear, bending, and torsion constituted the majority of the deflection as the stiffness in that direction was comparatively small. In the in-plane direction, however, it was expected that shear, bending, and torsion play an equal role in deflection contribution. The data revealed that torsion (more so than shear and bending) had a much larger role in the test than was previously expected. Uplift and rocking provided another significant contribution to the overall deflection, with sliding playing the smallest role. Future tests should

aim to reduce the problem of torsion as much as possible to prevent it from playing such a significant role in the test.

Given the test's inherent limitation with torsion, further inspection of the out-of-plane load-displacement curves lead to the conclusion that the in-plane and out-of-plane actuators were loading and unloading one another at different points during the test.This was most evident whenever the out-of-plane actuator attempted to put the specimen into tension. The extremely low stiffness in that direction coupled with the specimen's low torsional resistance led to the in-plane actuator putting the out-of-plane actuator into compression when it should have been in tension. There were times when the actuator was able to put the specimen into tension in this direction, but when the displacements increased this problem always persisted.

After observing the overall behavior of the walls when subjected to bidirectional loading, it became evident that the preferred method of design (rocking behavior with coupled panels) was in no way prohibited by bidirectional loading. The rocking between panels worked as well as it does during a simple in-plane shear wall test. The biaxial wall tests removed an uncertainty of the design's performance in two directions.

By looking at Table 6.6, it is evident that the in-plane stiffness of CLT shear wall is greater when a floor diaphragm is included than when only the wall was tested. The floor diaphragm provides additional resistance to rocking between panels, leading to a greater elastic stiffness than when the floor diaphragm is not present. Comparing test B3 with test B5 (both surface spline specimens), test B3 had an elastic stiffness of 29.25 kip/in and test B5 had an elastic stiffness of 23.27 kip/in. Because the stiffness is lower during the wall only tests, it was able to be taken to greater displacements, dissipating more energy. Test B3 dissipated 30.3 kJ of energy while test B5 dissipated 41.5 kJ of energy in-plane. To further demonstrate how the floor

197

diaphragm affects the system's ability to rock between panels, Figure 6.60 and Figure 6.61 demonstrate how more rocking occurs without the floor diaphragm (test B4) than when it is included (test B2).
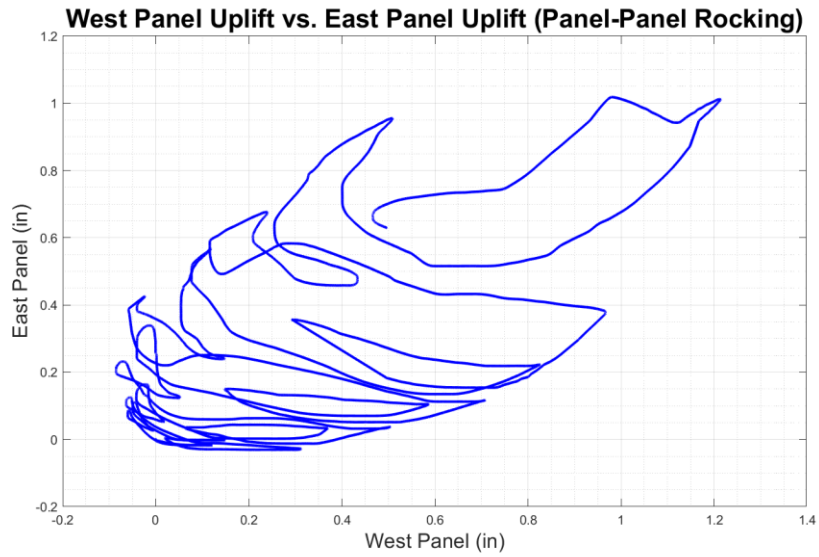
Figure 6.60. Test B2 Panel-to-Panel Rocking
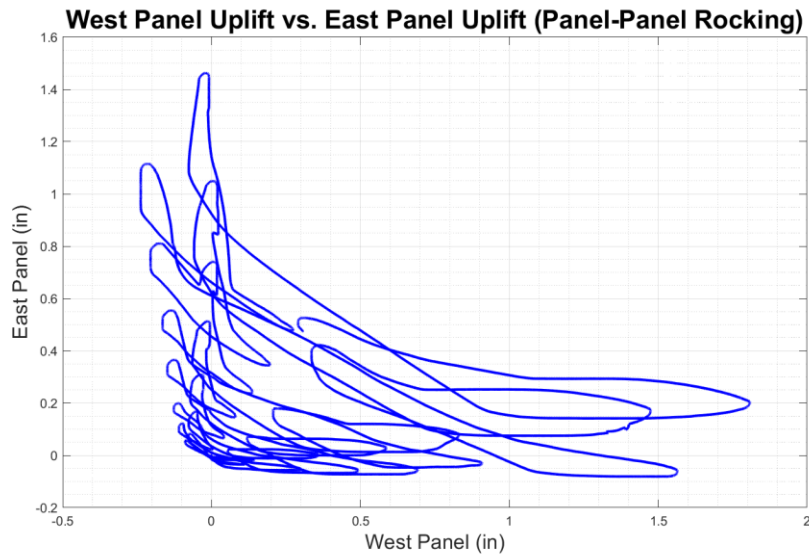
Figure 6.61. Test B4 Panel-to-Panel Rocking

Finally, the out-of-plane-only wall test provided a set of data to remove an uncertainty that remained about the behavior of balloon-framed systems when loaded in that direction. It became clear that damage to the foundation connections and the panel-to-panel connections is primarily caused by the loads placed on the system in the in-plane direction. There is simply not enough stiffness to create any significant damage in this direction. The initial thought of how far to test the wall in this direction centered around the typical limit from ASCE 7-16 of 2% drift. This drift was taken and multiplied by 1.5 for maximum considered earthquake. Testing often has taken MCE and tested to 50% further than this limit, giving a drift ratio of 4.5% as a rule of thumb. This gave the test 6 inches as an initial guess/target. However, the test was run to 10 inches, or 8% drift, as it seemed feasible given the results from the biaxial tests. Given how well the specimen performed at 8% drift, there is little reason to worry about out-of-plane performance of CLT shear walls, especially given that there is stiffness in that direction elsewhere in typical building systems. A plot of test B6 referencing drift ratio is presented in Figure 6.62.
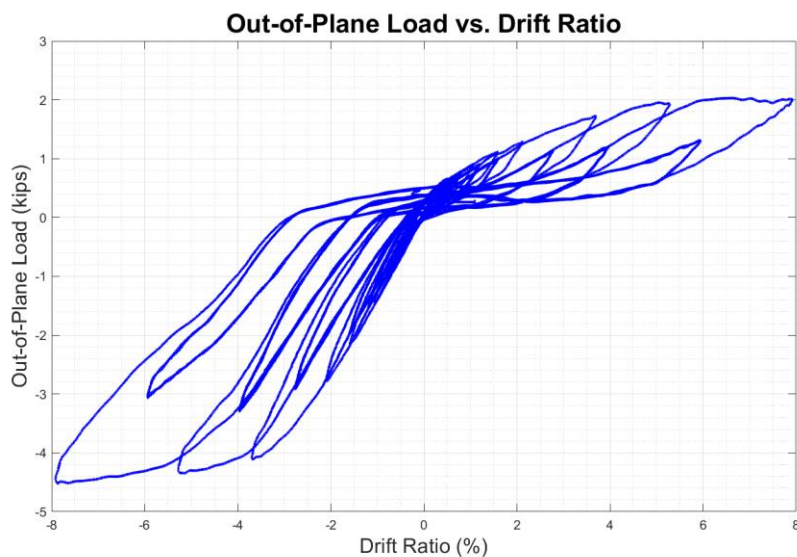
Figure 6.62. Test B6 Load vs. Drift Ratio

7.   SUMMARY, CONCLUSIONS, AND RECOMMENDATIONS

7.1.   Summary

While Cross-Laminated Timber (CLT) is still an emerging building technology, its use can be beneficial structurally and architecturally in many different building scenarios. Research on CLT's use in high seismic areas focuses on connections as this is the way for the building to dissipate energy most efficiently. An in-depth literature review was performed to figure out the knowledge gaps relating to CLT balloon-style construction connections. It was determined that balloon-style wall-to-floor connections had never been tested before, so the objective was to test a load-bearing and non-load-bearing configuration using two different screw manufacturers. As for the panel-to-panel connections, it was determined that two standard connections methods would be tested, along with a configuration utilizing fasteners installed at both 90 and 45-degrees.

This thesis examined the performance of these CLT connections for use in balloon-style construction, specifically for use in high seismic areas. Different wall-to-floor and panel-to-panel connection were identified in the test matrix, tested under monotonic and cyclic loads, and their performance was evaluated. The results were then used to calibrate two different hysteretic models for use in full-scale building models. Finite element analysis (FEA) was performed on these different connection configurations to determine the best way to model these connections – while using the experimental results to which to compare the analysis. Using many of these same connection methods, a full-scale biaxial wall test program was performed to gain further understanding of the behavior of the connections when subjected to bidirectional loading.

7.2.   Conclusions

This section presents the conclusions that were drawn from the different research areas that were investigated within this thesis. The conclusions are presented in the same order as the information was presented in this thesis. The areas include the connection experimental test program, numerical modeling to calibrate the connection cyclic data to hysteretic models, finite element modeling of the connection tests, and the full-scale biaxial wall tests.

7.2.1. Experimental Test Program Conclusions

The following conclusions were drawn from the experimental test program and its goal of evaluating both panel-to-panel and wall-to-floor balloon-style CLT connections:

1. All connection methods that were tested are viable methods of construction for use in balloon-style CLT construction.

2. Half-lap connections provide a much stiffer connection than spline connections, while spline connections provide a much more ductile connection.

3. After testing panel-to-panel connections with fasteners installed at both 45 and 90-degrees, the observation was made that one can design for both stiffness and ductility by using this method. Loading fasteners in shear provides ductility, while loading fasteners in withdrawal adds additional stiffness. The only drawback of this connection method is installation time.

4. To increase the stiffness of the wall-to-floor connections, the thickness of the angle bracket could be increased. The behavior of the wall-to-floor connections was relatively ductile because the angle bracket yielded early in the test and experienced significant post-peak displacement. The significant deformation of the angle bracket became one of

the dominating factors in the overall behavior of the connection. If this is to be mitigated, the thickness of the angle bracket should be increased.

5. Both fastener manufacturers that were tested, Simpson StrongTie and MTC, make adequate fasteners whose performance varies little between the two. The difference is mainly in the yield stress of the two fasteners, which leads to a difference in peak force and stiffness. However, the overall behavior is essentially the same between the two.

6. All configurations outperformed their code predictions, as would be expected. The code provides a significant factor of safety for designers, and a factor of safety of greater than two was observed for nearly all configurations, with some configurations exhibiting a factor of safety of nearly six.

7.2.2. Hysteretic Model Comparison Conclusions

The following conclusions were drawn from the numerical modeling that was done to fit the cyclic experimental data to hysteretic models:

1. The most conservative and accurate way to fit the cyclic data to both the CUREE-SAWS and Pinching4 hysteretic models is to take an 'envelope' approach, fitting the curve to the maximums and keeping positive and negative values equal. This is because the force-displacement curve is highly dependent on the direction loading begins. For example, if loading begins in one direction, the peak load in the opposite direction may be less than the initial direction due to wood crushing and separation of the fastener from the wood.

2. The Pinching4 hysteretic model better captured the hysteretic response that was observed during experimental testing because it has more parameters to better fit the envelope curve than the CUREE-SAWS model does. While the CUREE-SAWS model provided an

adequate model of the experimental data, the Pinching4 is the preferred hysteretic model for these types of connections.

7.2.3. Finite Element Model Conclusions

The following conclusions were drawn from the finite element modelling that was completed in this thesis:

1. Soft contact controls are the best way to model CLT-fastener interaction as they can more accurately represent wood crushing and splitting than hard contact controls.

2. The modelling assumptions presented in this thesis can reasonably be assumed to be accurate after comparing the results to the experimental data, and therefore, the properties presented can be used by others to reproduce these results or for other finite element modelling projects.

3. The models that were built can predict peak load and displacement relatively well (both monotonic and cyclic) but tend to struggle to have the same accuracy representing initial stiffness.

7.2.4. Biaxial Wall Test Conclusions

The following conclusions were drawn from the biaxial wall tests that were completed:

1. Torsion played a significant role in the behavior of the biaxial wall tests. It was expected that torsion would lead to some additional force in the system, but it became evident that there was more torsion in the test than would be present in a real balloon-framed shear wall system.

2. Damage due to out-of-plane drift is not a concern when designing balloon-framed CLT shear walls. While the out-of-plane stiffness is low, stiffness is typically provided in that direction from other areas of the lateral force resisting system.

3. The preferred in-plane deflection behavior of balloon-framed CLT shear wall systems is single-coupled. This means that the panels can rock between each other, but also rock together as one panel at the same time. In this manner, the system can dissipate the most energy. The different behaviors of the panels specifically affect the failure mode of the hold-downs and having a hold down that avoids cracking of the baseplate is the most optimal system.

4. Of the panel-to-panel connection methods that were tested, the half-lap connection is preferred for wall-to-wall connections. It allows for quicker construction and allows for the preferred panel-to-panel behavior as was observed. The half-lap specimens had a stiffer in-plane connection and dissipated more energy than the surface spline connections. While this could change with varying the fastener spacing, the construction time benefit leads to the half-lap connection being preferred.

5. As should be expected, in-plane stiffness is greater when a floor diaphragm is included in the system rather than when just the shear wall is considered by itself. While this should not be considered in the design process, designers should be aware of this extra factor of safety that will be built into their shear wall designs if a floor diaphragm is included.

6. The out-of-plane stiffness was greatly affected by the load being applied in both directions. When the wall was tested in the out-of-plane-only direction, the stiffness was observed to be nearly ten times as great. During bidirectional loading, it can be reasonably assumed that the stiffness in the in-plane direction is also reduced to some extent.

7.3.   Recommendations

Based on the research that was presented throughout this thesis, the recommendations that follow ought to be used for design of balloon-style CLT shear wall systems and for the testing of CLT connections and CLT shear walls.

1. For connection tests, ensure that there is no eccentricity involved in the direct shear tests as were performed in this study.

2. For future biaxial shear wall tests, it is recommended that torsion be minimized to whatever extent that it can. Using two actuators at the extreme ends of the out-of-plane direction could be one way to reduce the torsional problem inherent in this type of testing.

3. The Pinching4 hysteretic model should be used to represent CLT connection cyclic behavior as it does a better job of fitting the envelope curve and is able to be fine-tuned more easily.

4. Soft contact controls should be used when modelling CLT and fastener interaction in finite element software. While it is difficult to determine what is the most accurate representation of experimental data, soft contact can numerically represent wood crushing and splitting in a way that hard contact controls are not.

7.3. Areas of Future Work

The purpose of this thesis was to investigate the narrow scope of work that filled the specific research gap that was identified. Through the process of testing, modelling, and analyzing the data, it became apparent that there are other areas that could benefit from further exploration. Many different connections were tested in this research, and many have been tested by others. The biaxial wall test presented in this thesis is the first of its kind and much more

research is needed to fully understand the behavior of CLT shear walls when subjected to bidirectional loading. The following areas of future work can add to the body of research moving forward:

1. Determine different wall-to-floor connection methods that may be used in balloon-style CLT construction and test them in the lab using the same methodology presented in this thesis.

2. Further finite element modelling is necessary to fully understand the best way to model fastener-wood interaction. Soft contact is the best method, but a proper way to calibrate the connection controls is needed.

3. Further CLT shear wall tests using bidirectional loading are necessary to understand the behavior of different configurations, to investigate better foundation connection methods, to research other panel-to-panel connection methods, and to further characterize system behavior.

REFERENCES

(2018). National Design Specifications for Wood Construction. Virginia, American Wood Council.

(2020). "Abaqus user manual." Abacus.

Aghayere, A. and J. Vigil (2017). Structural Wood Design–ASD/LRFD, CRC Press.

AISC (2016). "Manual of Steel Construction, Load and Resistance Factor Design."

Akguzel, U. and S. Pampanin (2010). "Effects of variation of axial load and bidirectional loading on seismic performance of GFRP retrofitted reinforced concrete exterior beam-column joints." Journal of Composites for Construction **14**(1): 94-104.

Brandner, R., G. Flatscher, A. Ringhofer, G. Schickhofer and A. Thiel (2016). "Cross laminated timber (CLT): overview and development." European Journal of Wood and Wood Products **74**(3): 331-351.

Cavanagh, T. (1997). "Balloon houses: The original aspects of conventional wood-frame construction re-examined." Journal of Architectural Education **51**(1): 5-15.

Ceccotti, A., C. Sandhaas, M. Okabe, M. Yasumura, C. Minowa and N. Kawai (2013). "SOFIE project–3D shaking table test on a seven-storey full-scale cross-laminated timber building." Earthquake Engineering & Structural Dynamics **42**(13): 2003-2021.

Chen, Z. and M. Popovski (2020). "Mechanics-based analytical models for balloon-type cross-laminated timber (CLT) shear walls under lateral loads." Engineering Structures **208**: 109916.

Daneshvar, H., J. Niederwestberg, C. Dickof, J.-P. Letarte and Y. H. Chui (2019). "Cross-Laminated Timber Shear Walls in Balloon Construction: Seismic Performance of Steel Connections." Modular and Offsite Construction (MOC) Summit Proceedings: 405-412.

Dujic, B., S. Aicher and R. Zarnic (2006). Testing of wooden wall panels applying realistic boundary conditions. Proceedings of the 9th World Conference on Timber Engineering, Portland, Oregon, USA.

Flatscher, G. and G. Schickhofer (2015). "Shaking-table test of a cross-laminated timber structure." Proceedings of the Institution of Civil Engineers - Structures and Buildings **168**(11): 878-888.

Gavric, I., M. Fragiacomo and A. Ceccotti (2012). "Strength and deformation characteristics of typical X-lam connections." Proceedings of WCTE.

Gavric, I., M. Fragiacomo and A. Ceccotti (2015). "Cyclic behavior of typical screwed connections for cross-laminated (CLT) structures." European Journal of wood and wood products **73**(2): 179-191.

Gerrand, C. (1987). "The equivalent orthotropic elastic properties of plywood." Wood Science and Technology **21**(4): 335-348.

Gosain, N. K., R. H. Brown and J. O. Jirsa (1977). "Shear requirements for load reversals on RC members." ASCE J Struct Div **103**(7): 1461-1476.

Hossain, A., I. Danzig and T. Tannert (2016). "Cross-laminated timber shear connections with double-angled self-tapping screw assemblies." Journal of Structural Engineering **142**(11): 04016099.

Hossain, A., M. Popovski and T. Tannert (2018). "Cross-laminated timber connections assembled with a combination of screws in withdrawal and screws in shear." Engineering Structures **168**: 1-11.

Izzi, M., A. Polastri and M. Fragiacomo (2018). "Modelling the mechanical behaviour of typical wall-to-floor connection systems for cross-laminated timber structures." Engineering Structures **162**: 270-282.

Jalilifar, E., Koliou, M., and Pang, W. (2021). "Experimental and Numerical Characterization of Monotonic and Cyclic Performance of Cross Laminated Timber Dowel Connections." Journal of Structural Engineering **147**(7): 04021102.

Janowiak, J. J., D. P. Hindman and H. B. Manbeck (2001). "Orthotropic behavior of lumber composite materials." Wood and fiber science **33**(4): 580-594.

Joyce, T., M. Ballerini and I. Smith (2011). Mechanical behaviour of in-plane shear connections between CLT wall panels. Proceedings of the CIB Working Commission W18–Timber Structures. 44th meeting, Alghero.

Karacabeyli, E. and B. Douglas (2013). CLT: handbook cross-laminated timber, FPInnovations.

Koliou, M. and A. Filiatrault (2017). "Development of wood and steel diaphragm hysteretic connector database for performance-based earthquake engineering." Bulletin of Earthquake Engineering **15**(10): 4319-4347.

Krawinkler, H., F. Parisi, L. Ibarra, A. Ayoub and R. Medina (2001). Development of a testing protocol for woodframe structures, CUREe Richmond, CA.

Pei, S., J. W. v. d. Lindt, M. Popovski, J. W. Berman, J. D. Dolan, J. Ricles, R. Sause, H. Blomgren and D. R. Rammer (2016). "Cross-Laminated Timber for Seismic Regions: Progress and Challenges for Research and Implementation." Journal of Structural Engineering **142**(4): E2514001.

Polastri, A., I. Giongo and M. Piazza (2017). "An innovative connection system for cross-laminated timber structures." Structural Engineering International **27**(4): 502-511.

Popovski, M., I. Gavric and J. Schneider (2014). "Performance of two-storey CLT house subjected to lateral loads." FP Innovations Research Rep., FPIPRODUCT-1-6896, Vancouver, BC, Canada.

Popovski, M. and E. Karacabeyli (2012). Seismic behaviour of cross-laminated timber structures. Proceedings of the World Conference on Timber Engineering.

Rinaldin, G., C. Amadio and M. Fragiacomo (2013). "A component approach for the hysteretic behaviour of connections in cross-laminated wooden structures." Earthquake Engineering & Structural Dynamics **42**(13): 2023-2042.

Robertson, A. B., F. C. Lam and R. J. Cole (2012). "A comparative cradle-to-gate life cycle assessment of mid-rise office building construction alternatives: Laminated timber or reinforced concrete." Buildings **2**(3): 245-270.

Schneider, J., E. Karacabeyli, M. Popovski, S. F. Stiemer and S. Tesfamariam (2014). "Damage Assessment of Connections Used in Cross-Laminated Timber Subject to Cyclic Loads." Journal of Performance of Constructed Facilities **28**(6): A4014008.

Shahnewaz, M., S. Alam and T. Tannert (2018). "In-plane strength and stiffness of cross-laminated timber shear walls." Buildings **8**(8): 100.

Shen, Y.-L., J. Schneider, S. Tesfamariam, S. F. Stiemer and Z.-G. Mu (2013). "Hysteresis behavior of bracket connection in cross-laminated-timber shear walls." Construction and Building Materials **48**: 980-991.
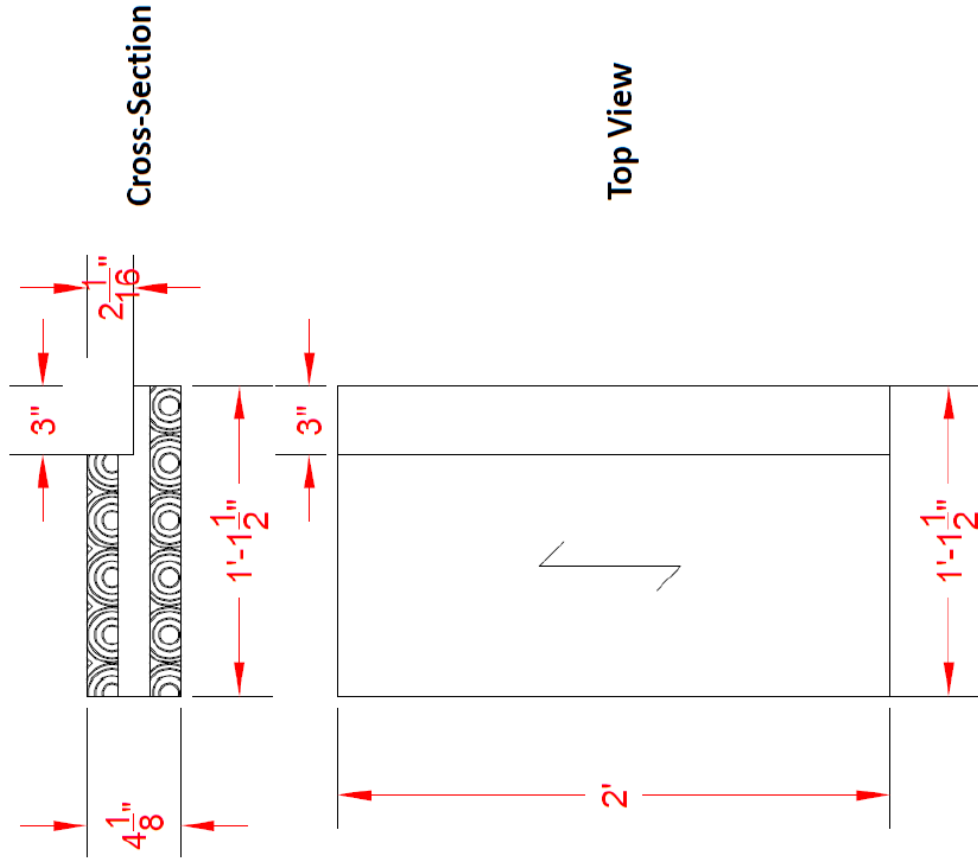
CLT Connection Tests: Texas A&M University

Dr. Maria Koliou and Benjamin Hayes

Drawing	Application	Quantity
A	Half-Lapped, Side Member	120
B	Half-Lapped, Main Member	60
C	Spline, Side Member	60
D	Spline, Main Member	30
E	Wall-to-Floor Panel 1	150
F	Wall-to-Floor Panel 2	30
G	Biaxial Test, Spline	6
H	Biaxial Test, Half-Lapped	6
I	Biaxial Test, Floor Panel	6

Cross-Section

$2\frac{1}{16}$"

3"

$1'-1\frac{1}{2}$"

$4\frac{1}{8}$"

Top View

3"

$1'-1\frac{1}{2}$"

2'

Drawing: A

Application: Half-lapped, side member

Quantity: 120

212

Cross-Section

Top View

$4\frac{1}{8}$"

$2\frac{1}{16}$"

1'-3"

3"

3"

2'

3"

1'-3"

Drawing: **B**

Application: Half-lapped, main member

Quantity: **60**

Cross-Section

Top View

3"

1"

$4\frac{1}{8}$"

3"

1"

2'
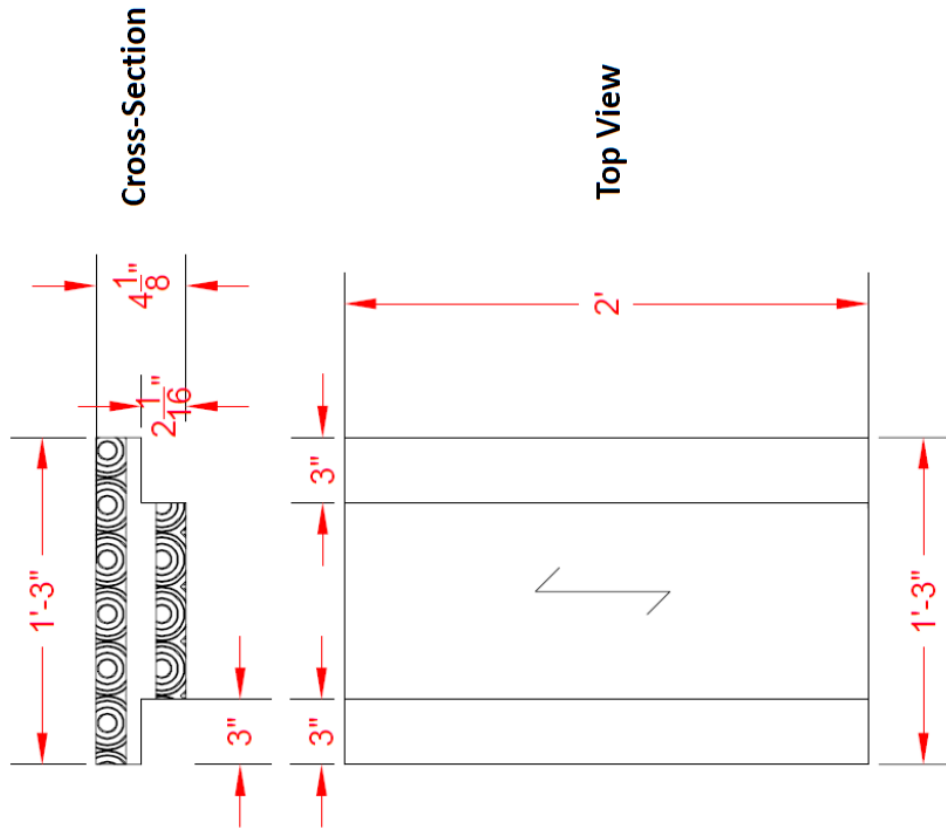
Drawing: C

Application: Spline, side member

Quantity: 60

214

Cross-Section

Top View

$4\frac{1}{8}"$

3"

1'

1"

2'

3"

1'

Drawing: D

Application: Spline, main member

Quantity: 30

215
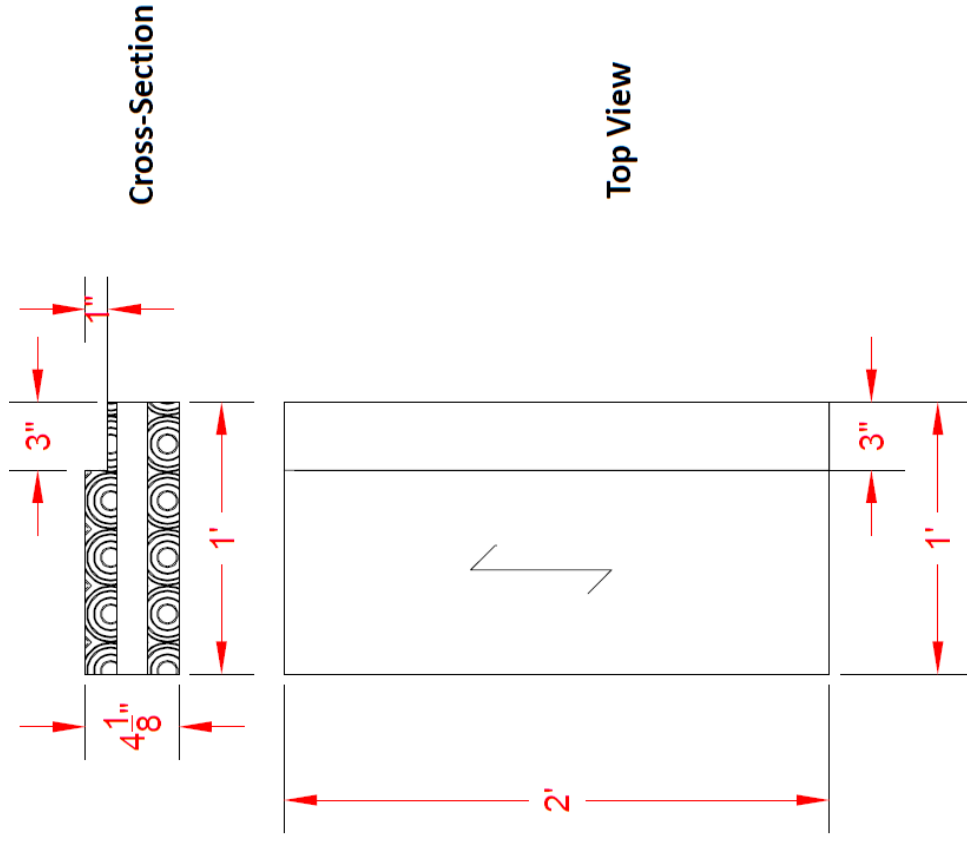
Drawing: **E**

Application: Wall-to-floor panel 1

Cross-Section

Top View

$4\frac{1}{8}"$

1'-6"

1'-6"

2'

Quantity: **150**

Cross-Section

Top View

1'-6"

1'-6"

$4\frac{1}{8}$"

2'
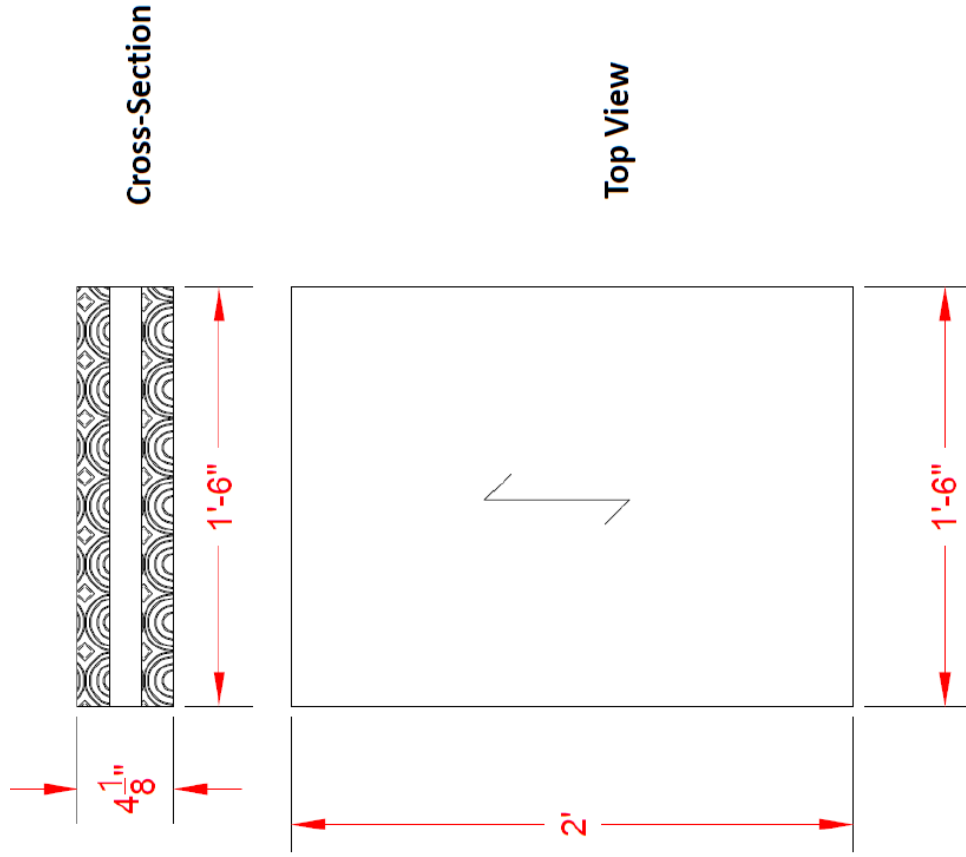
Drawing: **F**

Application: Wall-to-floor panel 2
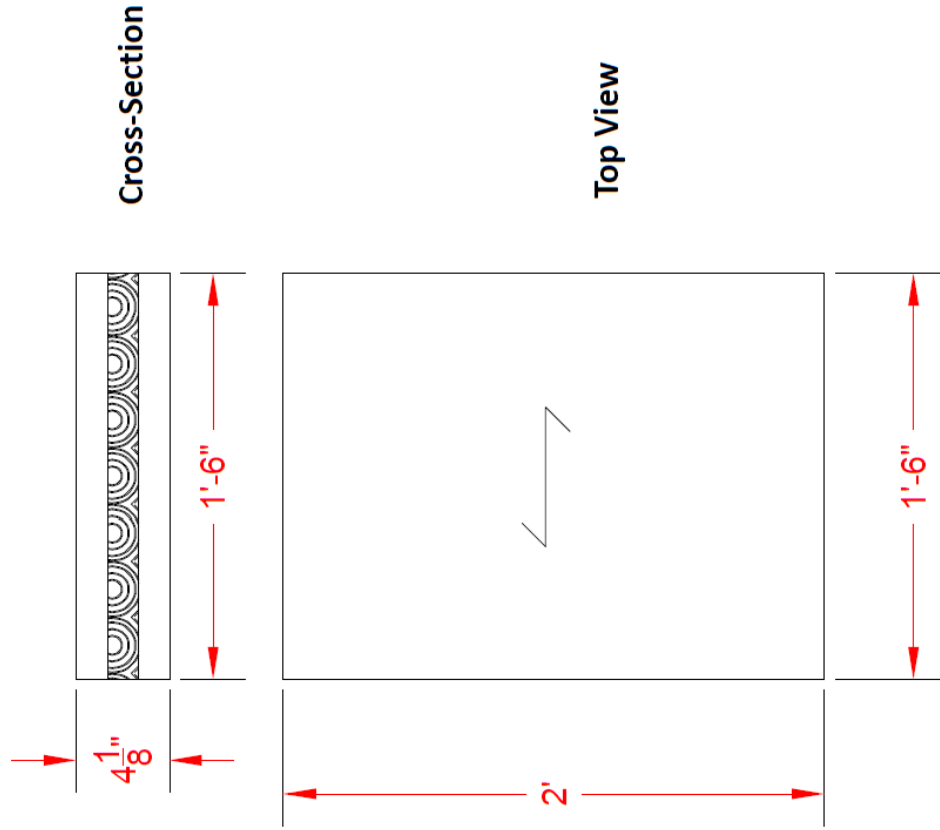
Quantity: **30**

217

CLT Connection Tests: Texas A&M University

Dr. Maria Koliou and Benjamin Hayes

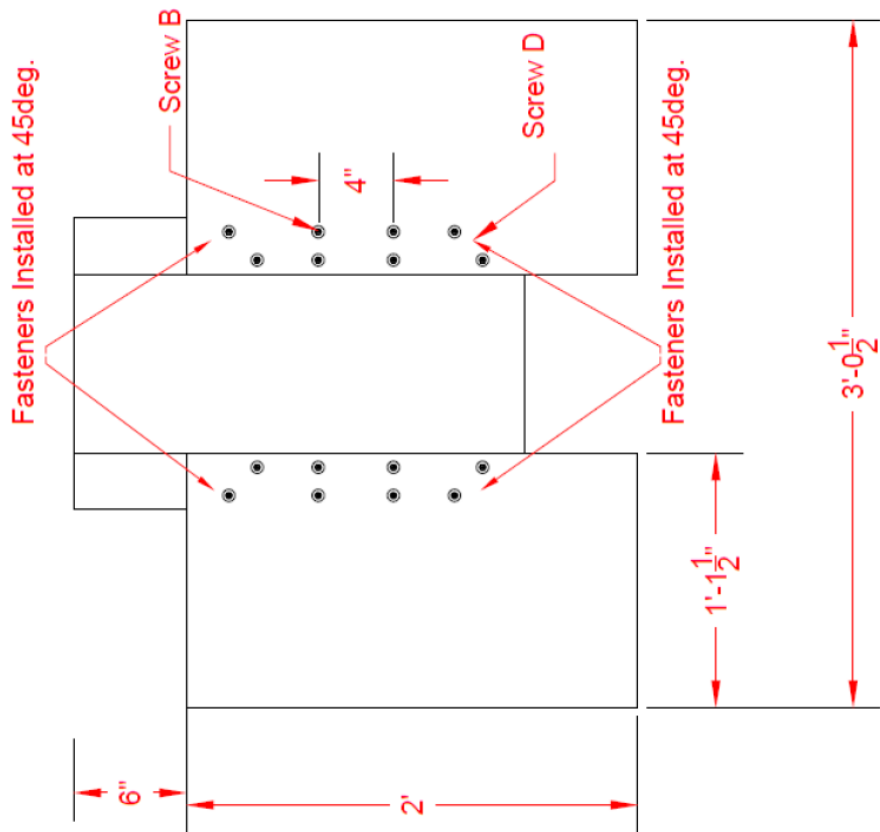| Drawing Number	Configuration
1	Half-Lapped, Screw A
2	Half-Lapped, Screw B
3	Half-Lapped, Screw A and C
4	Half-Lapped, Screw B and D
5	Surface Spline, Screw A
6	Surface Spline, Screw B
7	Load-Bearing Wall-to-Floor, Screw E and F
8	Load-Bearing Wall-to-Floor, Screw G and H
9	Non-Load-Bearing Wall-to-Floor, Screw E and F
10	Non-Load-Bearing Wall-to-Floor, Screw G and H
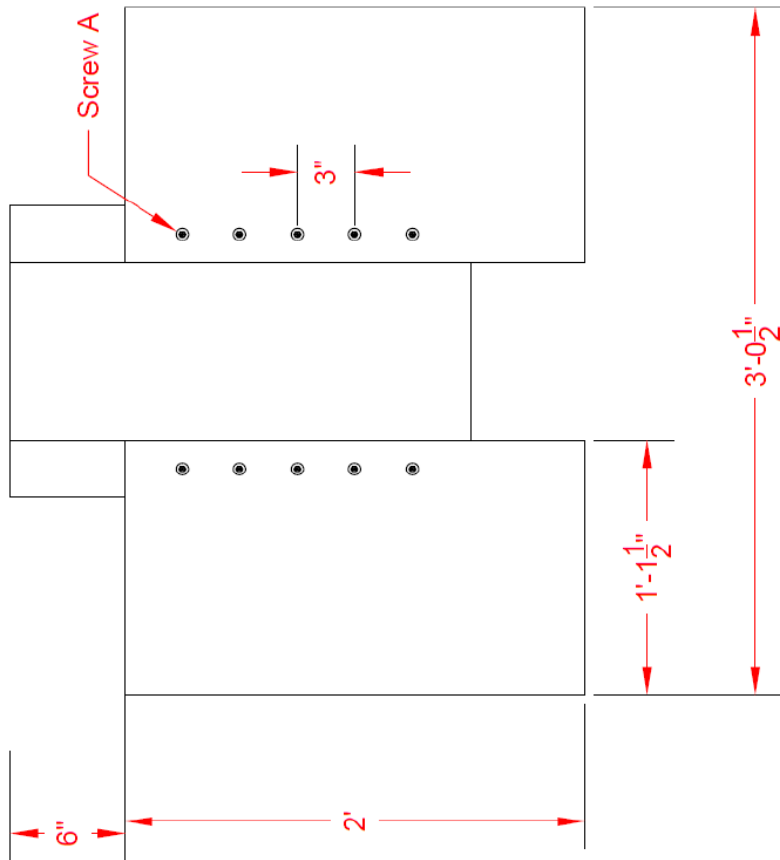
Texas A&M CLT Connection Tests		
Drawing Number		Configuration
1		Half-Lapped, Screw A

Screw A

3"

3'-0½"

1'-1½"

6"

2'

219
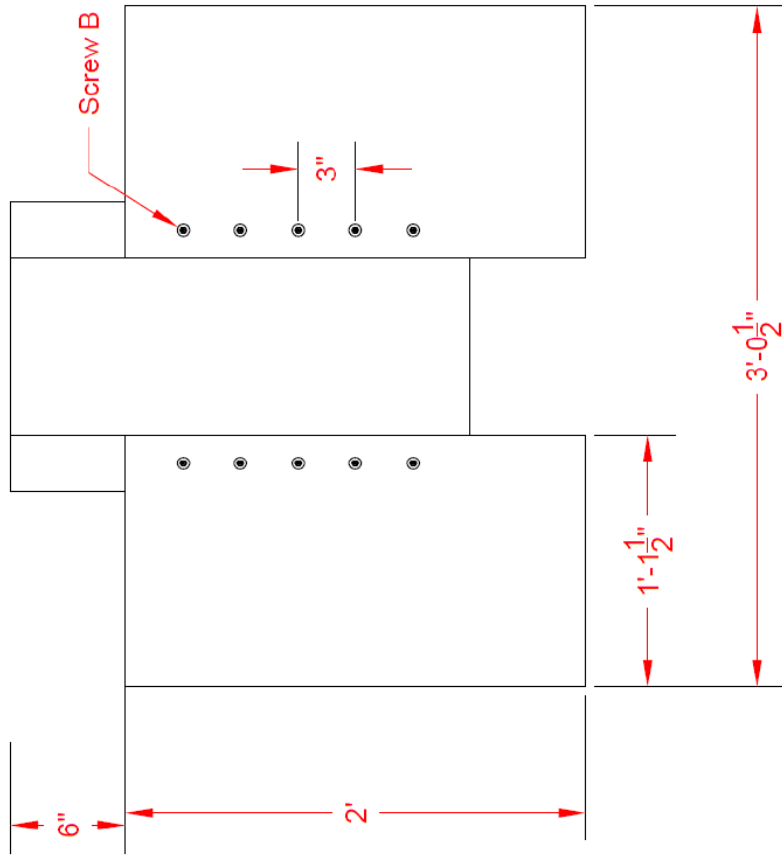
Texas A&M CLT Connection Tests		
Drawing Number	*Configuration*	
2	Half-Lapped, Screw B	

Screw B

3"

3'-0$\frac{1}{2}$"

1'-1$\frac{1}{2}$"

6"

2'
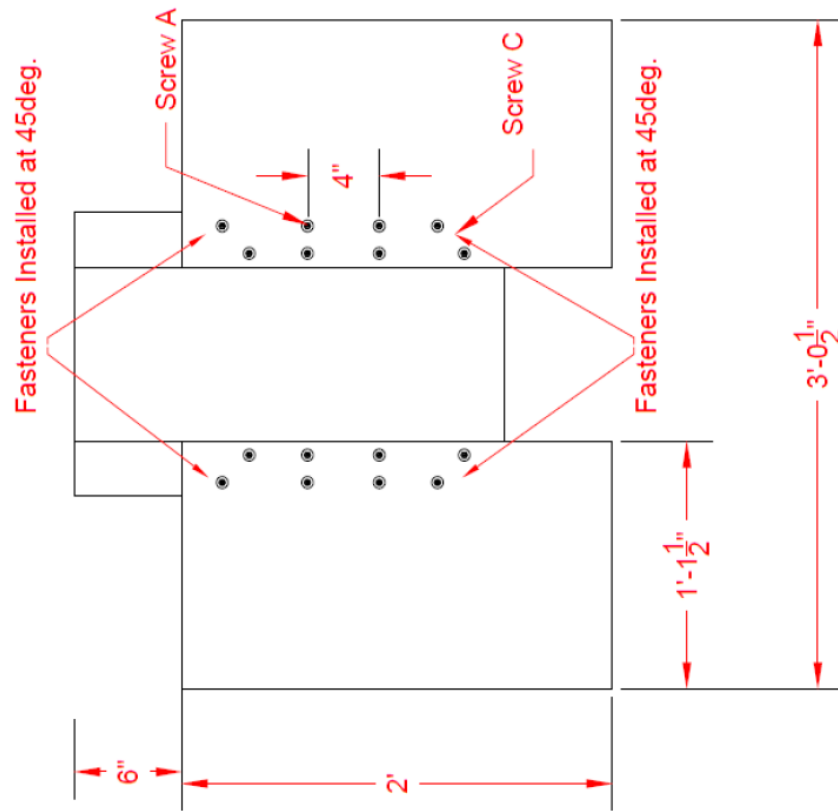
Texas A&M CLT Connection Tests		
Drawing Number		Configuration
3		Half-Lapped, Screw A and C

Texas A&M CLT Connection Tests		
Drawing Number	Configuration	
4	Half-Lapped, Screw B and D	

222
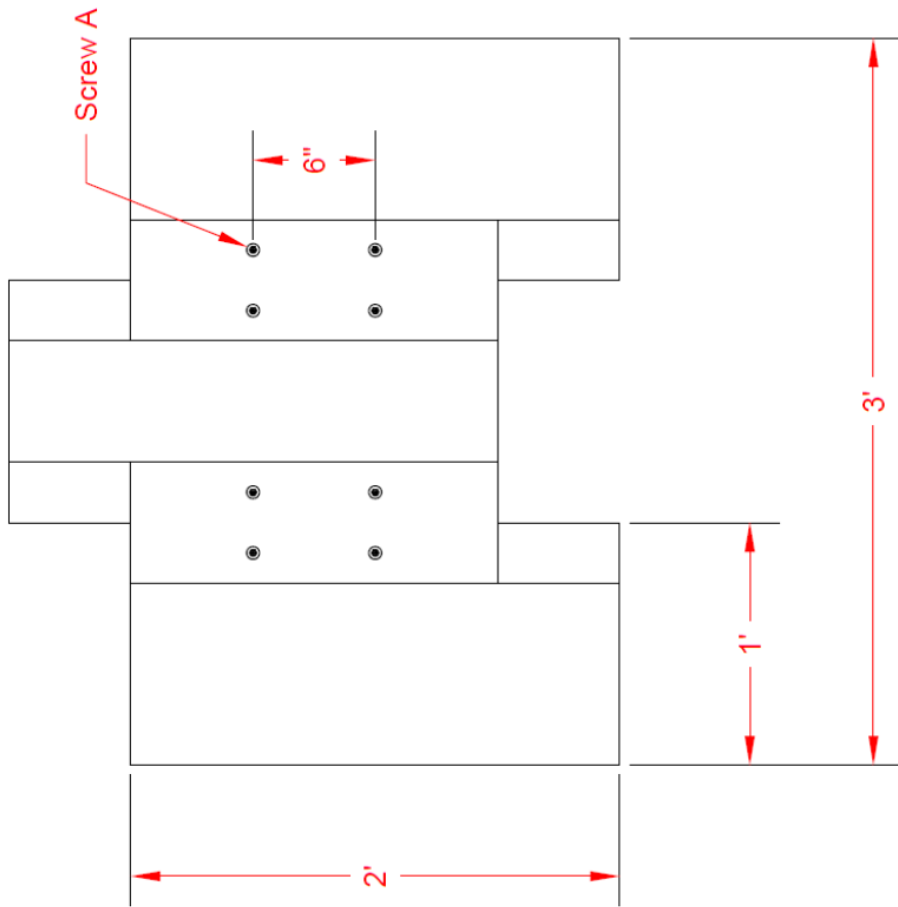
Texas A&M CLT Connection Tests	
Drawing Number	*Configuration*
5	Surface Spline, Screw A
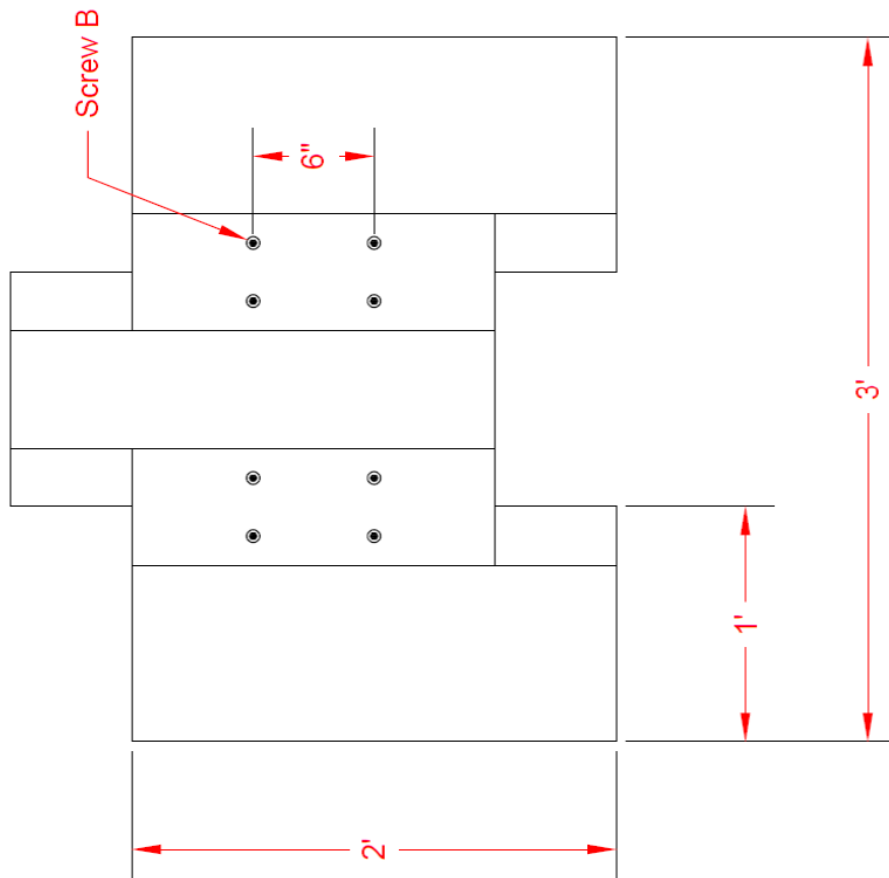
Texas A&M CLT Connection Tests	
Drawing Number	Configuration
6	Surface Spline, Screw B

Screw B

6"

3'

1'

2'

2x4 LVL to mimic bearing
Screw G

Bracket 1
Screw E, F

$4\frac{1}{8}$"

6"

1'-6"

$4\frac{1}{8}$"

6"

1'-6"
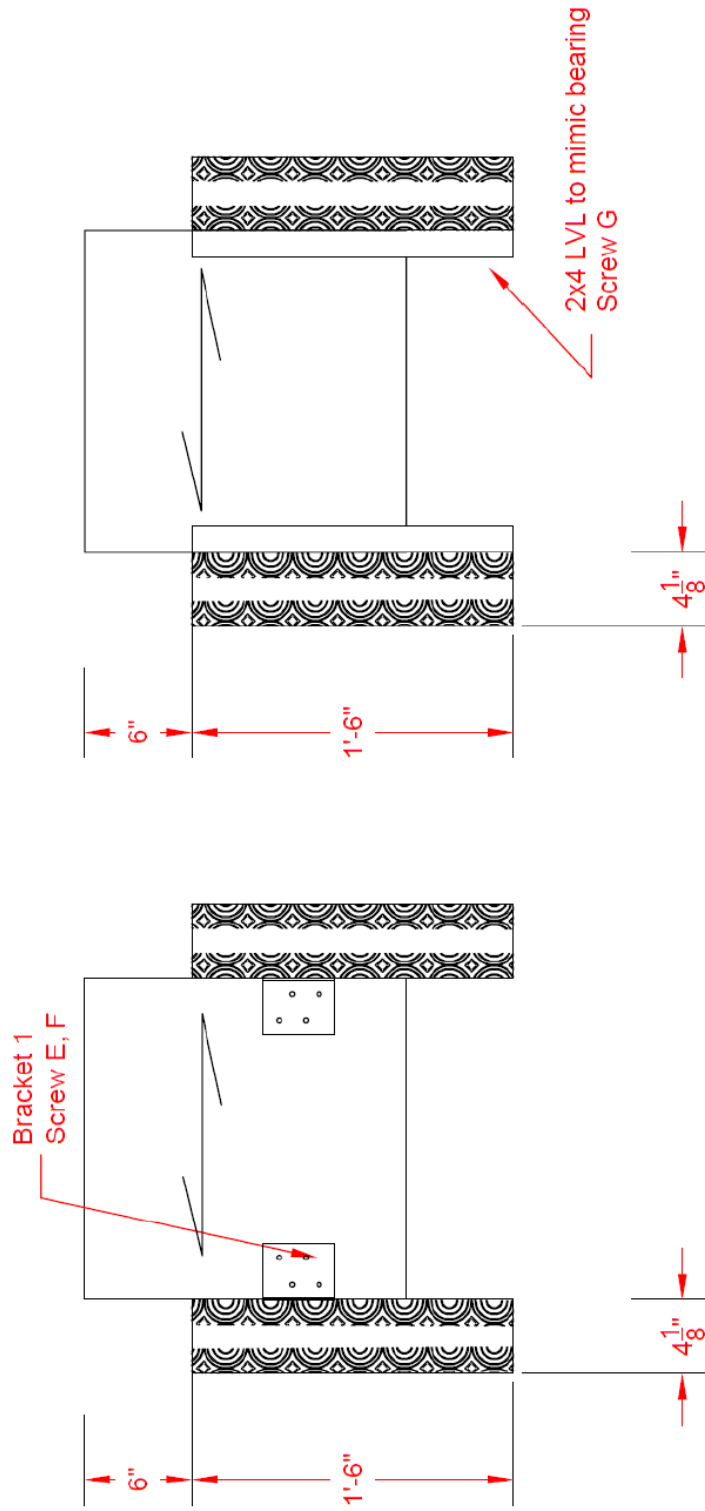
Texas A&M CLT Connection Tests	
Drawing Number	*Configuration*
7	Load-Bearing Wall-to-Floor, Screw E and F

225

Bracket 1
Screw G,H

2x4 LVL to mimic bearing
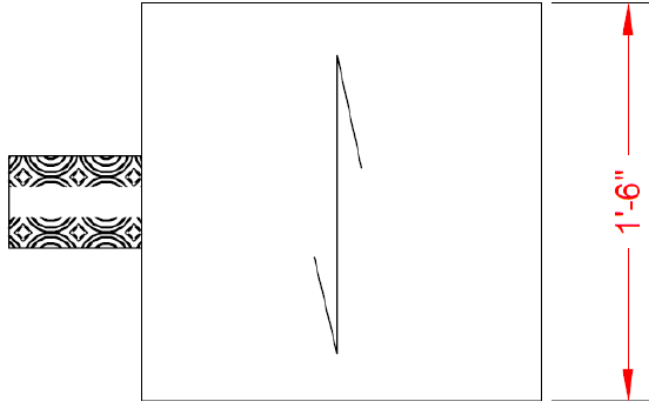Screw G

6"

1'-6"

$4\frac{1}{8}$"
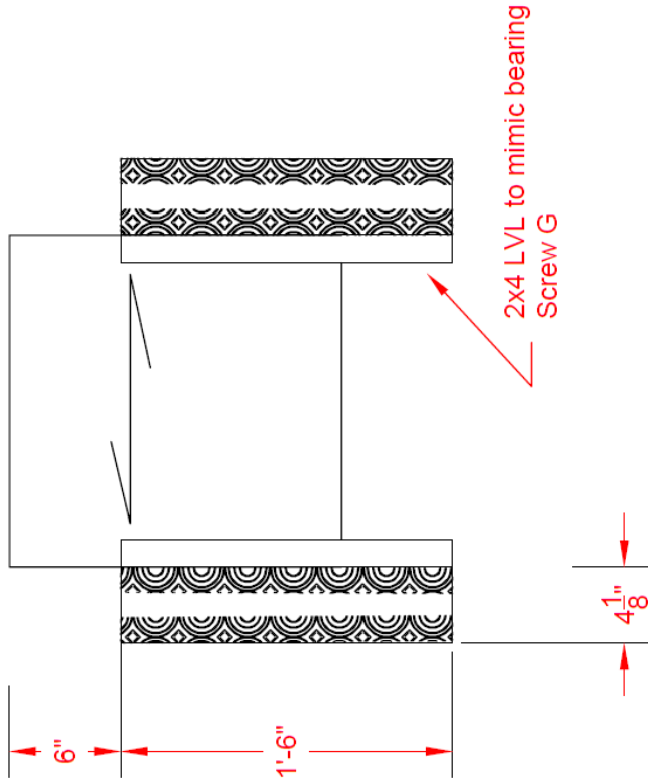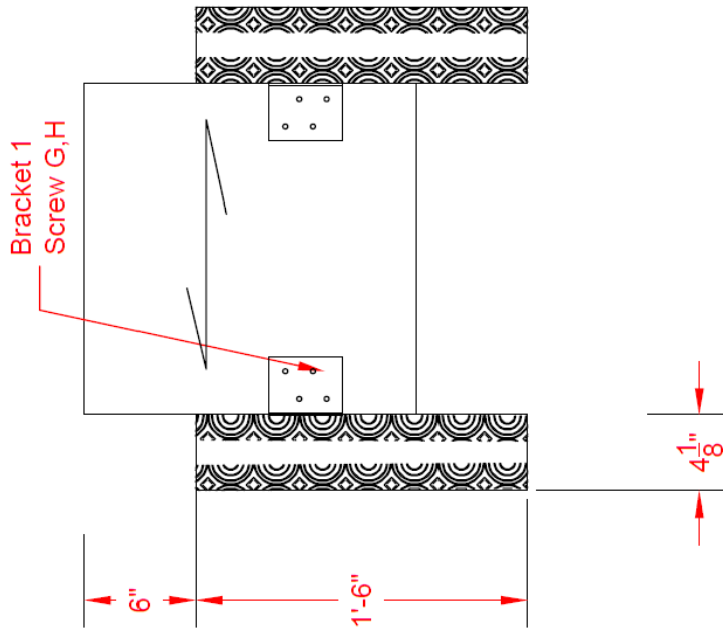
Texas A&M CLT Connection Tests

Drawing Number	Configuration
8	Load-Bearing Wall-to-Floor, Screw G and H
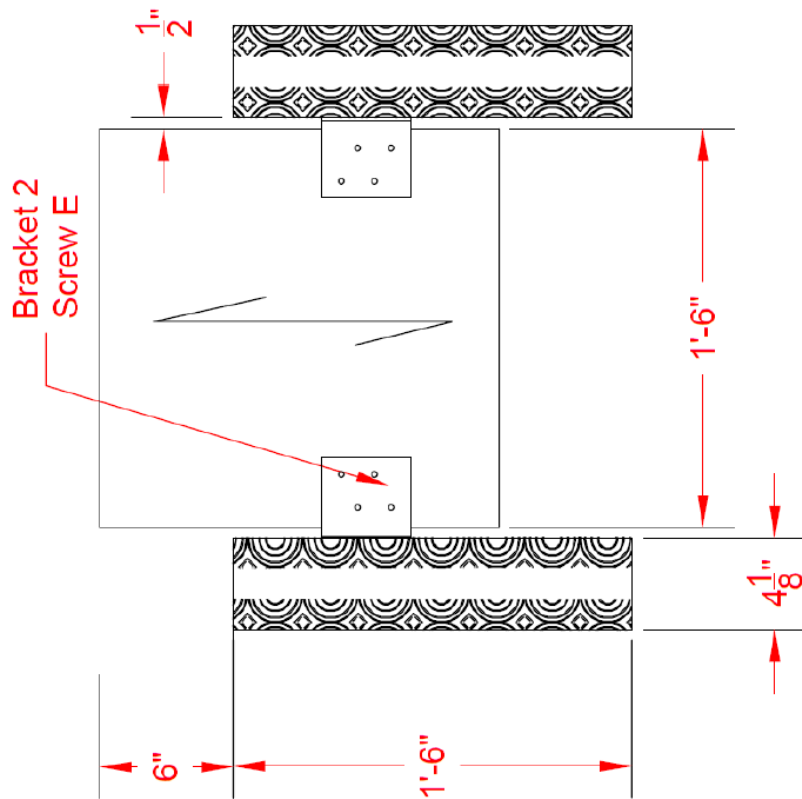
Texas A&M CLT Connection Tests

Drawing Number	Configuration
9	Non-Load Bearing Wall-to-Floor, Screw E

Bracket 2
Screw E

1'-6"

1'-6"

$\frac{1"}{2}$

6"

1'-6"

$4\frac{1}{8}"$
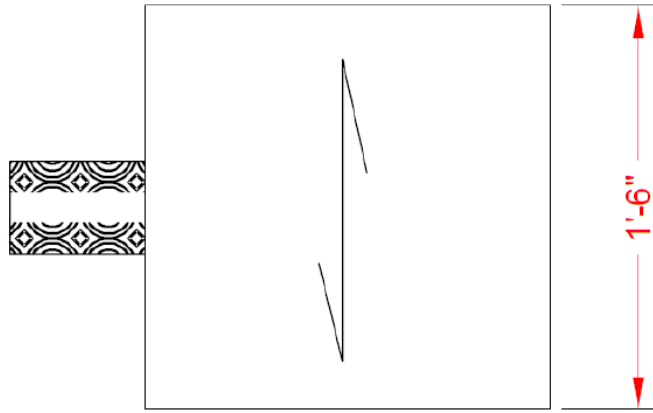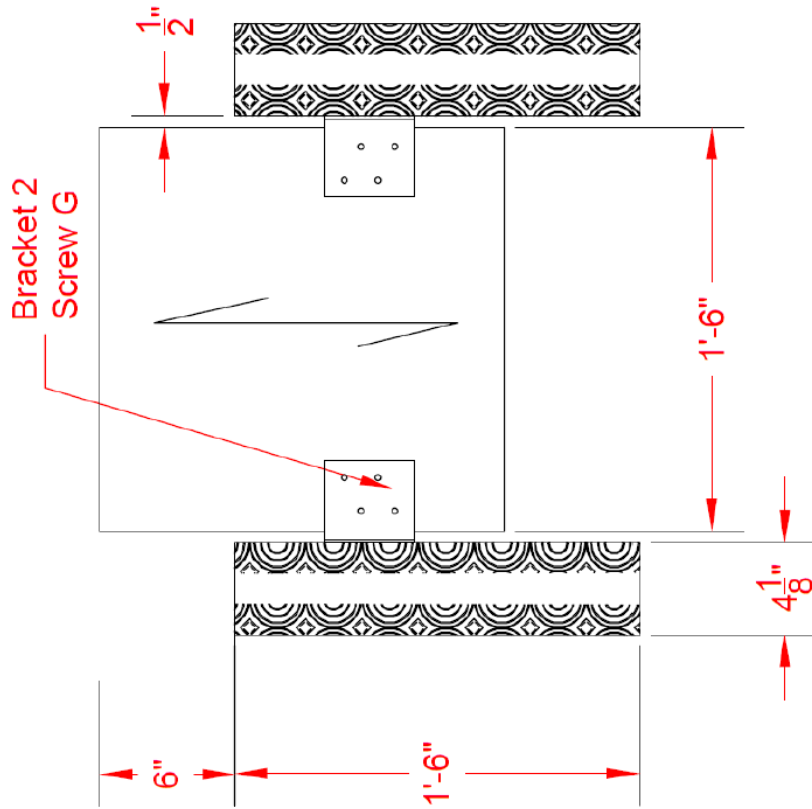
Texas A&M CLT Connection Tests		
Drawing Number	*Configuration*	
10	Non-Load Bearing Wall-to-Floor, Screw G	

Bracket 2
Screw G

$\frac{1}{2}$"

1'-6"

6"

1'-6"

$4\frac{1}{8}$"

1'-6"

228

CLT Connection Tests: Texas A&M University

Dr. Maria Koliou and Benjamin Hayes

Drawing	Application	Quantity
A	Half-Lapped, Side Member	120
B	Half-Lapped, Main Member	60
C	Spline, Side Member	60
D	Spline, Main Member	30
E	Wall-to-Floor Panel 1	150
F	Wall-to-Floor Panel 2	30
G	Biaxial Test, Spline	6
H	Biaxial Test, Half-Lapped	6
I	Biaxial Test, Floor Panel	6

Cross-Section

Top View

1"

3"

3"

4'

4 1/8"

4'

12'

Drawing: G

Application: Biaxial Test, Spline

Quantity: 6

230

Cross-Section

Top View

$4\frac{1}{8}$"   3" $2\frac{1}{16}$"   3"

4'-$1\frac{1}{2}$"

4'-$1\frac{1}{2}$"

12'
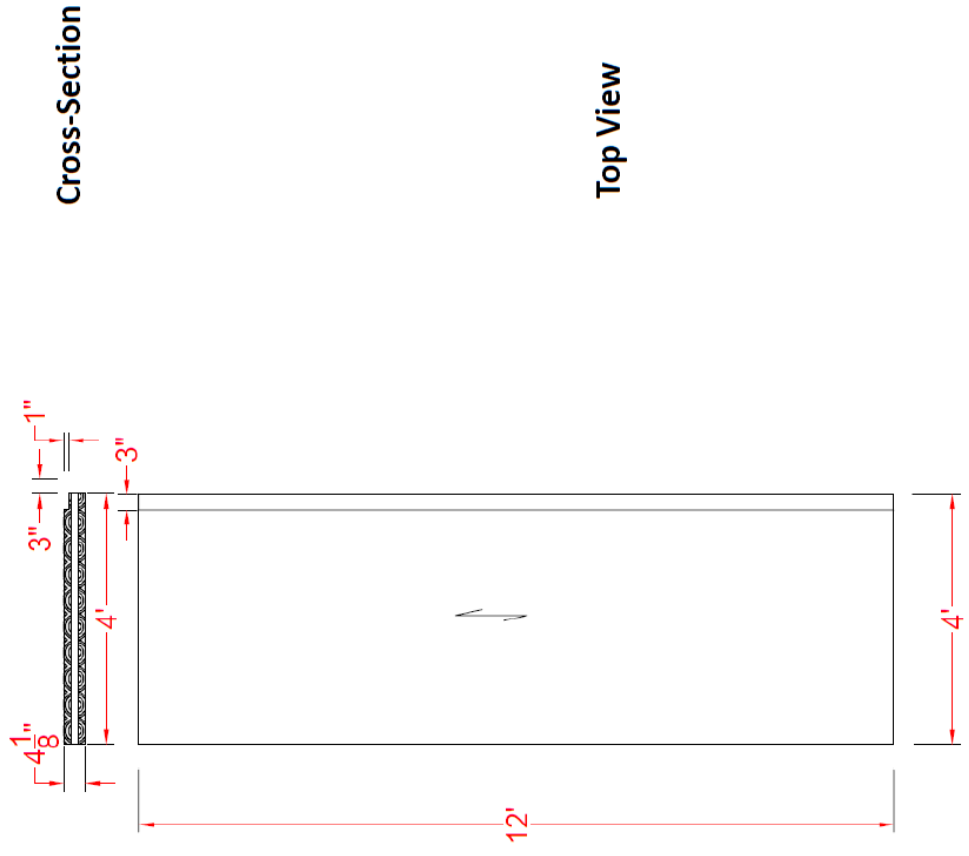
Drawing: H

Application: Biaxial Test, Half-Lapped

Quantity: 6

Drawing: I

Cross-Section

Top View

Application: Biaxial Test, Floor

$4\frac{1}{8}"$

3'

8'

3'

Quantity: **6**

232